SSD

SCIENCE FOR A SUSTAINABLE DEVELOPMENT

FINAL REPORT

ASSESSMENT OF MODELLING UNCERTAINTIES IN LONG-TERM CLIMATE AND SEA LEVEL CHANGE PROJECTIONS « ASTER »

T. FICHEFET, M.F. LOUTRE, H. GOOSSE, P. HUYBRECHTS,
H. GOELZER, A. MOUCHET

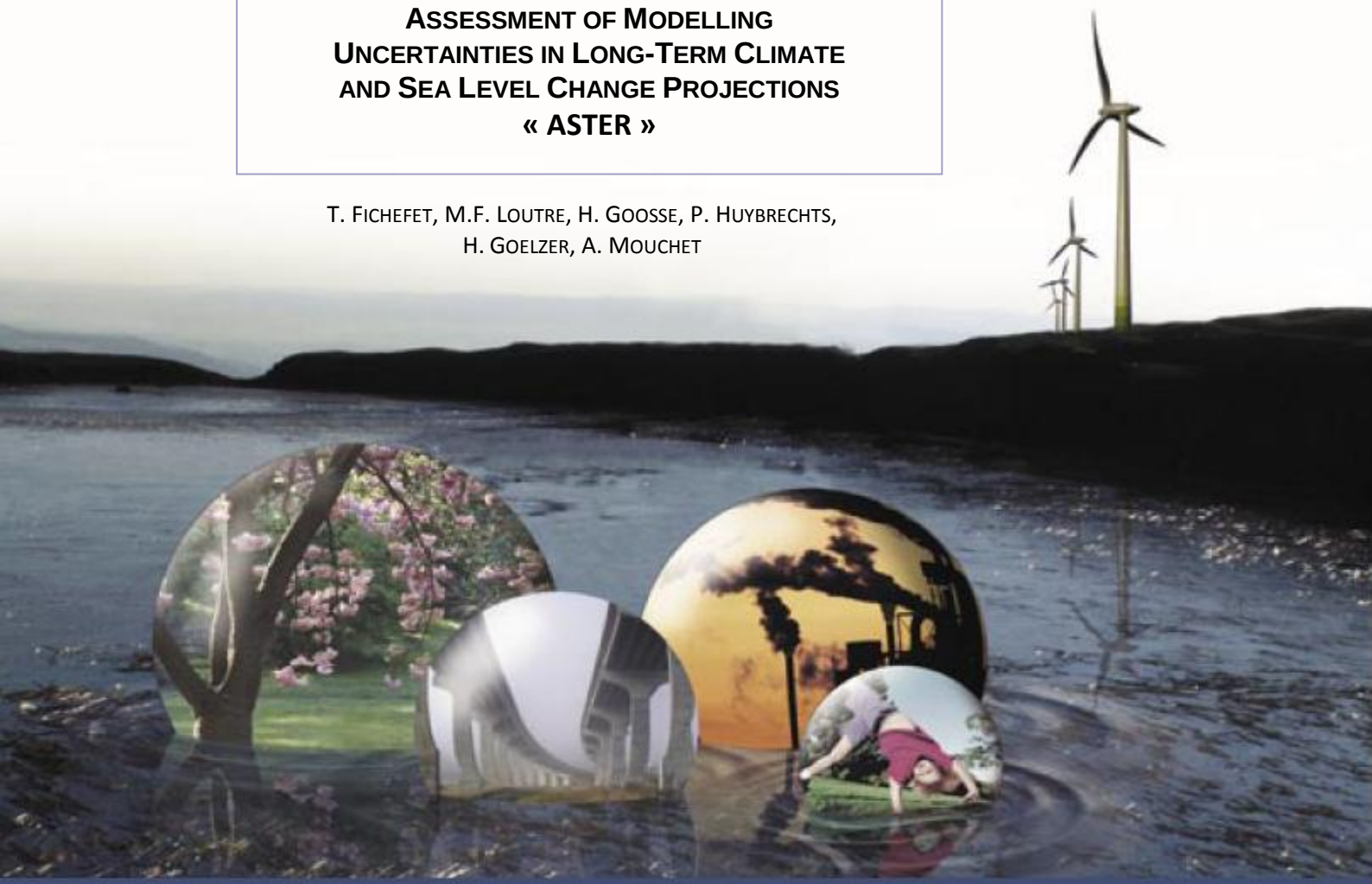

ENERGY

TRANSPORT AND MOBILITY

AGRO-FOOD

HEALTH AND ENVIRONMENT

CLIMATE

BIODIVERSITY

ATMOSPHERE AND TERRESTRIAL AND MARINE ECOSYSTEMS

TRANSVERSAL ACTIONS

.be

SCIENCE FOR A SUSTAINABLE DEVELOPMENT
(SSD)

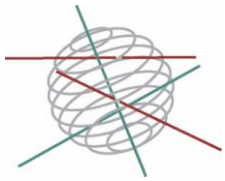

Climate

FINAL REPORT

ASSESSMENT OF MODELLING UNCERTAINTIES IN LONG-TERM CLIMATE AND SEA LEVEL CHANGE PROJECTIONS « ASTER »

SD/CS/01

Promoters

Thierry Fichefet
Université Catholique de Louvain,
Earth and Life Institute,
Georges Lemaître Centre for Earth and Climate Research (TECLIM)
Chemin du Cyclotron, 2
B-1348 Louvain-la-Neuve
Philippe Huybrechts
Vrije Universiteit Brussel
Earth System Sciences & Departement Geografie (VUB-DGGF)
Pleinlaan, 2
B-1050 Brussels
Anne Mouchet
Université de Liège
Département d'Astrophysique, de Géophysique et d'Océanographie
Laboratoire de Physique Atmosphérique et Planétaire (ULg-LPAP)
Allée du 6 août, 17
Bâtiment B5c
B-4000 Liège

Authors

T. Fichefet, M.F. Loutre, H. Goosse
(UCL-TECLIM)
P. Huybrechts, H. Goelzer
(VUB-DGGF)
A. Mouchet
(ULg-LPAP)

D/2012/1191/21
Published in 2012 by the Belgian Science Policy
Avenue Louise 231
Louizalaan 2
B-1050 Brussel
Belgium
Tel: +32 (0)2 238 34 11 – Fax: +32 (0)2 230 59 12
http://www.belspo.be

Contact person: Martine Vanderstraeten
+32 (0)2 238 36 10

T. Fichefet, M.F. Loutre, H. Goosse, P. Huybrechts, H. Goelzer, A. Mouchet - ***Assessment of modelling uncertainties in long-term climate and sea level change projections «ASTER» (SD/CS/01A)***. Brussels : Belgian Science Policy 2012 – 139 p. (Research Programme Science for a Sustainable Development : Final Report)

TABLE OF CONTENT

EXECUTIVE SUMMARY

A. Context

Climate change represents one of the greatest environmental, social and economic threats that the planet is facing. The warming of the climate system is unequivocal, as is now evident from observations of increases in global average air and ocean temperatures, widespread melting of snow and ice, and rising global mean sea level (IPCC, 2007). However, the range of possible future climate change in model projections remains large, mostly because of several sources of uncertainty. A large unknown is how the human activities and, subsequently, the emission of greenhouse gases will evolve in the future. Large uncertainties also arise from the design of the climate models themselves. For example, choice in the approximations and parameterisations must be decided. Another source of uncertainty comes from the physical parameters, which are not perfectly known. As a consequence, policymakers and decision-makers are facing a large range of possible future climate change. Efforts are made to reduce this range or to point towards the most likely realisation.

B. Objectives

We used LOVECLIM, an Earth system model of intermediate complexity to perform simulations of the Holocene, the last millennium and the third millennium climates, as well as sensitivity experiments to identify the behaviour of the model under increased greenhouse gas concentrations and freshwater hosing. Moreover, we identified several parameter sets that yield different responses of the LOVECLIM model to a scenario of doubling of CO_2 concentration and to freshwater hosing, although the simulated present-day climate remains within the range of observations. The parameter values were chosen within their range of uncertainty. There are nine “climatic” parameter sets, three “carbon cycle” parameter sets and three “ice sheet” parameter sets. Past and future climate simulations were performed with all or a subset of these 81 combinations of parameter sets. The model was run either with fixed-prescribed ice sheets or with an interactively coupled Greenland and Antarctic ice sheet model. Simulations of past climates were conducted in order to identify the subset of parameter sets that allow the best reproduction of observations and reconstructions. Simulations of future climate change then provided a range of model responses that were validated against past climate changes.

C. Conclusions

Several improvements have been made to LOVECLIM in the course of the project. The land surface scheme has been adapted to better represent the impact of vegetation on climate change. The bucket depth is now dependent on the vegetation, which has a direct impact on the runoff and soil water availability. Consequently, the transpiration is computed separately for each vegetation type. Moreover, a canopy resistance term has been added, which depends on incident solar radiation, atmospheric humidity and leaf area index. This refined parameterisation induces significant changes in vegetation: e.g., forest area increases over Western Europe and most of North America at the expense of grass and desert extends over most of North Africa and also over Eastern Europe.

When coupling LOCH[1] to CLIO[2], it appeared that the uptake of anthropogenic CO_2 was much too large. The semi-implicit scheme for the computation of the Coriolis term in the equation of motion was then replaced by a totally implicit scheme in order to solve that problem.
The biological module of LOCH has been modified to incorporate a silica dissolution scheme with temperature-dependent rate and depth control. Furthermore, the equation ruling the biomass pool, which export production depends on, includes now a 3-D transport term and allows to consider up to three phytoplankton groups, characterized by their own growth and grazing rates. Finally, the atmospheric module of LOCH now allows for a prognostic computation of carbon isotopes in the atmosphere and the fractionation during soft tissues formation is parameterised to be inversely related to dissolved CO_2 concentration.
The Northern Hemisphere Ice Sheet Model (NHISM) has been interactively coupled to LOVECLIM. NHISM is a three-dimensional thermomechanical ice sheet model that includes an improved scheme for marine calving to better simulate ice sheet expansion and contraction over the shallow marine shelf basins surrounding the Arctic Ocean. In addition, a novel hydrological runoff model was devised to route the meltwater from the ice sheets to the appropriate CLIO oceanic grid boxes. The scheme transports meltwater through the contemporary lake and river system, taking into account isostatic changes of the surface topography, ice-dammed lakes and changes in lake storage. With this new model, the global ice sheets and the climate were simulated during the last deglaciation between the Last Glacial Maximum (LGM) at 21 kyr BP and the beginning of the Holocene at 10 kyr BP. The experiment had prescribed ice sheet configurations and freshwater fluxes from an off-line precursor experiment with NHISM forced by ECBilt[3]-CLIO. It was found that large peaks of continental fresh water released in the Arctic and North Atlantic Oceans at around 17 kyr BP and 14 kyr BP could generate important reductions of the oceanic meridional overturning circulation with ensuing local and global cooling of the climate.
Those improvements had led to making available, for both the project and the scientific community, a new version of the model (LOVECLIM1.2, http://www.climate.be/loveclim).
In order to investigate the parameter uncertainty in LOVECLIM, we varied values of key physical parameters in order to estimate the range of model response for standard sensitivity experiments, to assess the ability of the model to simulate past climates according to the parameter sets and to compute the range of response for climate projections.
More specifically, we selected nine “climatic” parameter sets, three “carbon cycle” parameter sets and three “ice sheets” parameter sets because they yield present-day climate simulations coherent with observations. For the 81 combinations of the parameter sets, we measured the increase in global annual mean surface temperature after 1000 years in a sensitivity experiment in which the atmospheric CO_2 concentration increased by 1% per year from the pre-industrial value until a doubled value was reached and was subsequently held constant (used as an estimate of the climate sensitivity) and the percentage of decrease in the maximum value of the meridional overturning streamfunction below the Ekman layer in the Atlantic Ocean (MOC) after 1000 years in a water hosing experiment in which

[1] LOCH is the oceanic carbon cycle component of LOVECLIM.
[2] CLIO is the ice-ocean component of LOVECLIM.
[3] ECBilt is the atmospheric component of LOVECLIM.

freshwater is added in the North Atlantic (20°-50°N) with a linearly increasing rate of 2×10^{-4} Sv/yr (used as an estimate of the MOC sensitivity to a freshwater perturbation). Sensitivity to doubling of CO_2 concentration ranges from 1.6 to 3.8°C and MOC is reduced by 15 to 75% in the freshwater flux experiments in ECBilt-Clio-VECODE[4] stand-alone (ECV) experiments. In most cases, sensitivities do not exhibit significant changes after the coupling with the carbon cycle model. However, some departure from the values obtained in ECV experiments is shown for the largest climate sensitivity. The reason may be found in different initial conditions; indeed, experiments with interactive carbon cycle departed from the equilibrium state of the corresponding experiment without any carbon cycle. Those various initial states probably explain the large difference in MOC streamfunction reduction with parameter set 51. Furthermore, in fully coupled (LOVECLIM) experiments that considered doubled CO_2 concentrations and/or freshwater hosing of magnitude 0.1-0.2 Sv, we found a significant reduction of the climate sensitivity at the millennial time scale due to the effect of additional freshwater fluxes from the ice sheets. The meltwater induces MOC weakening in the Northern Hemisphere and, subsequently, a local relative cooling, which is amplified by sea ice related feedbacks. A similar mechanism operates in the Southern Hemisphere, but is found to be of smaller magnitude. This mitigation effect increases with ice sheet sensitivity and with the initial climate sensitivity of LOVECLIM itself. It is therefore suggested that it is of great importance to include dynamic ice sheets into global Earth system models.

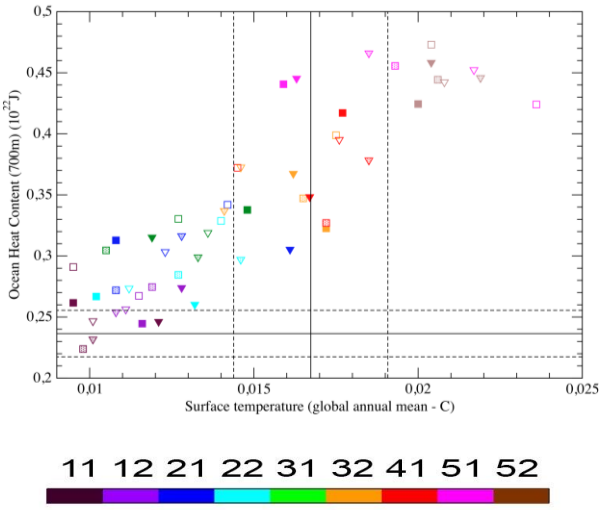

Figure 1: Trend in oceanic heat content in the upper 700 m (10^{22} J.yr^{-1}) (1950 – 2003 AD) wrt trend in global annual mean surface temperature (°C.yr^{-1}) (1979 – 2005 AD). Each dot represents one simulation. Trends are computed as the slope of the regression line through the annual values. Each colour corresponds to one climatic parameter set. Squares (triangles down) correspond to Efor (Conc) simulations; symbols are for carbon cycle parameter sets (1: full; 2: semi-empty; 3: empty) (see description of the parameter sets and of the experiments in the main part of the report). The full black line represents the trend computed from observation (Levitus et al. (2009) for the heat content and Brohan et al. (2006) for surface temperature). The dashed lines represent the uncertainty related with the variability in the data (one standard deviation).

The analysis of global variables representative of the last millennium climate displays relatively similar results for all the parameter sets and thus did not allow us to select

[4] VECODE is the vegetation and continental carbon cycle component of LOVECLIM.

among them the most appropriate one for simulating climate over that time interval. Therefore, we rather focused on the last century. Moreover, we concentrated on global scale model features and on the model ability to reproduce the trend in selected variables over the last few decades. Simulations with the carbon cycle parameter set 3 do not properly reproduce the observed atmospheric CO_2 increase although it does not prevent a reasonable temperature increase. Moreover, no parameter set allows the model simulating simultaneously a correct time evolution of ocean heat content in the upper 700 m, and of Northern Hemisphere sea ice extent or of annual mean surface temperature (Figure 1). This drawback should be investigated in further studies. Generally speaking, simulations with high climate sensitivity have a better global score than simulations with low climate sensitivity. Amongst the best simulations, parameter set[5] 321 performs well for both setup (prognostic or diagnostic CO_2 concentration) and both sulphate aerosol forcing reconstructions considered in our study. Moreover, other parameter sets (322, 511, 512) also display good performance for both setups and for at least one of the sulphate aerosol forcing.

Five parameter sets (112, 212, 312, 412 and 512) were used in transient simulations of the Holocene climate (from 8 kyr BP to 2000 AD). Compared to observations covering the second half of the 20th century, parameter sets 112 and 212 lead to a serious underestimation of the decline in summer Arctic sea ice extent, while parameter set 312 yields only a slight underestimation. Moreover, the model results for the parameter set 512 are in disagreement with the very few reconstructions of the summer Arctic sea ice extent during the early Holocene. However, the agreement with the PMIP2 simulated global pattern of summer temperatures during the mid-Holocene (Braconnot et al., 2007) seems to be the best with parameter set 21. Some equilibrium simulations of the LGM climate were also performed. Only the parameter sets leading to low climate sensitivity (i.e. 11, 12, 21, 22) yield reasonable results. The LGM cooling in high latitudes is too strong for the high climate sensitivity parameter sets. This is a direct consequence of the relatively high polar amplification simulated by LOVECLIM. These results clearly illustrate the difficulty to identify a parameter set that would properly simulate strongly different climates such as the LGM or Holocene one, and the global warming of the last century.

Therefore, in the simulations of future climate, we continued to use several (or all) parameter sets, even if some should be dismissed for their poor ability to simulate climate over one of the past periods considered in this study. Several simulations over the third millennium were performed with LOVECLIM, with the different parameter sets, using SRES greenhouse gas scenarios (B1, A2, A1B) until 2100 AD and greenhouse gas concentrations maintained at their levels as in 2100 AD until the year 3000 AD. According to these simulations, the global mean temperature increases by 1.7 to 3.2°C after 1000 years for scenario A1B with medium carbon and ice sheet sensitivities, depending on the climate sensitivity (Figure 2).

[5] See the main part of the report for a detailed description of the parameter sets

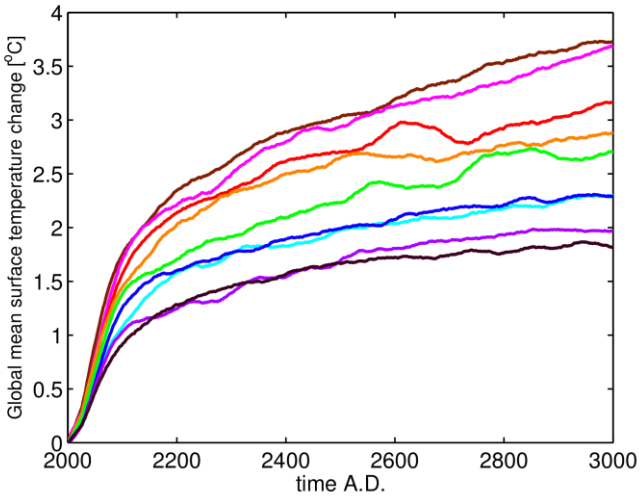

Figure 2: Global mean temperature changes during the third millennium for scenario A1B. Each colour corresponds to one climatic parameter set. Only medium carbon cycle and ice sheet parameter sets (2) are shown.

A large range of ice sheet, glacier, and sea level projections were then performed focusing in particular on the 21st century and the third millennium. The ensemble approach samples the range of uncertainties inherent in crucial ice sheet model parameterisations for basal sliding, flow enhancement, surface ablation and basal melting below Antarctic ice shelves. This is complementary to the usual approach to run model experiments for a wide range of forcing scenarios that were restricted to (prolonged) SRES scenarios B1, A1B and A2. In these experiments, the Greenland ice sheet was found to lose between 15 % (scenario B1, low climate and ice sheet sensitivities) and 95% (scenario A2, high climate and ice sheet sensitivities) of its mass after 1000 years of climate warming (Figure 3). Almost all of the melting occurs by surface ablation, whereas iceberg calving quickly decreases as the ice sheet recedes from the coast. For Antarctica, volume changes varied between slight growth for a low scenario and low climate and ice sheet sensitivities, and a volume loss corresponding to a 6 m sea level rise for the high scenario and high model sensitivities after 1000 years (Figure 3). On the millennial time scale, changes in the Antarctic ice sheet are mainly driven by changes in accumulation and ice shelf melt, with a significant contribution from marginal ablation for the experiments producing the largest warming. For all scenarios and all model sensitivities, virtually all of the ice contained in mountain glaciers and small ice caps has disappeared after 1000 years of climatic warming (Figure 3). For the same range of experiments, sea level rise from oceanic thermal expansion was found to vary between 0.6 and 4 m (Figure 3). We conclude from these experiments that a global eustatic sea level rise of at least 2 m is very likely to occur before the end of the third millennium. For scenario A1B and medium ice sheet and climate sensitivities, the value is ~9 m (Figure 3). The upper bound in excess of 20 m is however considered very unlikely to occur, in part because of the large polar amplification in LOVECLIM.

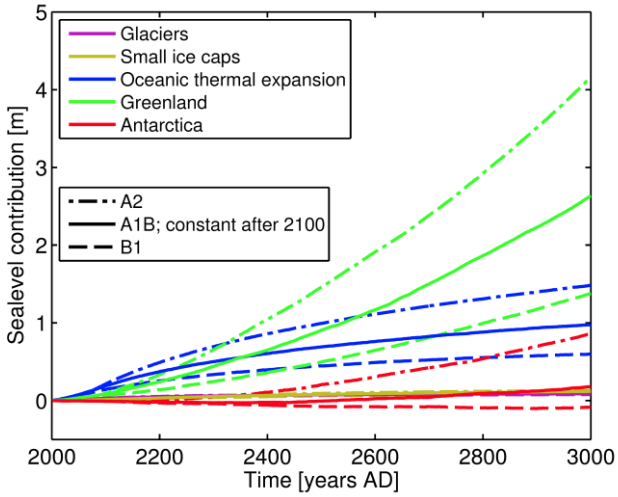

Figure 3: Global sea level contributions from different components for prolonged SRES scenarios B1, A1B and A2. These experiments considered medium ice sheet and low climate sensitivities.

D. Contribution of the project in a context of scientific support to a sustainable development policy

The work made under ASTER is a contribution to the ongoing international scientific effort to better understand climate change and to quantify more accurately the uncertainties related with climate and sea level projections. This is needed in order to provide a sound basis for policies designed to address the challenge of climate change. Identifying and reducing the uncertainties is deeply in line with the recommendation of the scientific community for the coming years, in particular for next IPCC assessment report. Therefore, work performed under ASTER is expected to be included into IPCC AR5.

E. Keywords

Uncertainty on climate change, future climate change, sea level change, ice sheet modelling, ocean circulation, carbon cycle.

1. INTRODUCTION

Policymakers are facing a wide range of possible scenarios for long-term climate and sea level evolutions without knowing precisely why they differ and how reliable they are. Two factors explain this wide estimated range: uncertainties in the future anthropogenic emissions of greenhouse gases and aerosols, and uncertainties in the understanding and modelling of the processes that influence the climate. Moreover, climate policy is a further unknown that is adding uncertainties to the system (Van Vuuren et al., 2008).

The response of the global carbon cycle to human activities is not well constrained and the future levels of atmospheric CO_2 concentration, for given anthropogenic emissions, are still a major cause of uncertainty. Different coupled Earth system models result in very different predictions of the role of the continental biosphere in driving the atmospheric CO_2 amount at the century time scale, the feedbacks ranging from very positive to negative (e.g., Cox et al., 2000; Friedlingstein et al., 2001;Thompson et al., 2004). On the ocean side, modelling and process studies suggest that an enhanced stratification, a reduced oceanic meridional overturning circulation (MOC) and changes in biology are expected to reduce the solubility and biological CO_2 pumps within one or several centuries (e.g., Maier-Reimer et al., 1996; Sarmiento, 1998; Joos et al., 1999; Schmittner, 2005). Furthermore, studies of Zondervan et al. (2001) and Orr et al. (2005) bring concern about the effect of acidification on the marine ecosystems, a fact whose consequences are not known yet. On the one hand, the effect could be a slight increase in oceanic CO_2 uptake (Zondervan et al., 2001; Heinze, 2004), but as $CaCO_3$ shells seem to be very efficient in transferring organic carbon to the deep ocean (e.g., Klaas and Archer, 2002), the longer-term effect could be very different.

For a sustained regional, annual mean warming of more than 3°C, the Greenland ice sheet would eventually completely melt away (Gregory et al., 2004). For warming larger than 10°C, total disintegration could take as little as 1000 years, in which case it would add an average of 7 mm per year to sea level over the period, with wide-ranging implications for climate and mankind. The collapse of the West Antarctic ice sheet in the next few centuries has been largely discussed (Vaughan and Spouge, 2002; Bindschadler, 1998; Oppenheimer, 1998; Vaughan and Arthern, 2007), but its longer-term response remains highly uncertain. Acceleration of ice streams and glaciers as well as the stabilization role of the ice shelves are major concerns that still remain to be established and properly quantified. If fast response mechanisms, such as ice dynamical changes, would still become more widespread and scale with future warming, they would imply greater ice sheet sensitivity to warming than previously considered.

The projected changes in heat fluxes and precipitation over the North Atlantic area as well as interactions with the melting Greenland ice sheet might largely affect the North Atlantic deep water formation and thus the stability of the MOC, with a large potential impact on the climate evolution in the North Atlantic sector and in Europe (e.g. Fichefet et al., 2003). Unfortunately, the magnitude of the MOC response to heat and freshwater perturbations is not very robust among existing models (e.g., Gregory et al., 2005). Moreover, the melting of the Antarctic ice sheet could also release freshwater in the Southern Ocean, with a potential impact on the ocean circulation. Simulations show that freshening or warming in the Southern Ocean acts to increase or stabilize the Atlantic MOC (Rohling et al., 2004; Weaver et al., 2003; Swingedouw et al., 2009)

Under these circumstances, it is difficult to know which decision should be taken to avoid the most dramatic effects of climate change. However, decisions should be taken in a very near future because we could possibly pass some threshold that would lead to irreversible changes. Because of its large impact on sea level and possibly on the MOC, a particularly important issue of large political significance is whether the ice loss would be reversible or whether there exists a point-of-no-return beyond which ice sheet disintegration would continue, even if the climate would revert to present conditions.

The general purpose of the present study is to provide some guidelines on the range of future climate changes and on the causes of the differences between the various projections. In particular, we focus on the stability of the North Atlantic MOC, on the stability of Greenland and Antarctic ice sheets, on biogeochemical feedbacks and on the impact of all these processes on climate (especially in the North Atlantic, European and polar regions) and sea level. Therefore, we use a coupled Earth system model of intermediate complexity, so that the interactions between the various components of the system can be accounted for. However, before studying the future climate, we quantify the ability of our model to reproduce the past. Indeed, future climate scenarios should be checked against the capability of reproducing the past evolution of climate. We focus on the ability of the model to simulate the climate, sea level and atmospheric CO_2 concentration variability and changes.

Different methods have been used to assess uncertainties in modelling past and future climate changes. The most straightforward one is to compare the results from different models under similar conditions. This approach is applied in international model intercomparison exercises such as the Paleoclimate Modelling Intercomparison Project (PMIP) (e.g., Braconnot et al., 2002), the Coupled Model Intercomparison Project (CMIP) (e.g., Covey et al., 2000), the Ocean Carbon Intercomparison Project (OCMIP) (e.g., Dutay et al., 2004) or the Ice Sheet Model Intercomparison Project (ISMIP) (http://homepages.vub.ac.be/~phuybrec/ismip.html). It was also employed in the previous assessment reports of the Intergovernmental Panel on Climate Change (IPCC) (e.g., Houghton et al., 2001; IPCC, 2007) to document the range of climate model responses to a given scenario of greenhouse gas concentration. Nevertheless, this method has two important drawbacks. First, major differences in model conception make it difficult to point at a precise cause for different behaviours. Second, it is not possible to sample all the potential range of responses since, in general, only the standard model configurations are utilized in these studies.

In order to explore in a more systematic way the range of possibilities for future climate evolution, it has been proposed to perform large ensemble of experiments in which some key model parameters are varied within a reasonable range (Murphy et al., 2004; Stainforth et al., 2005). This allows estimating a probability density function of some important climate characteristics like the equilibrium climate sensitivity (the annual mean of the globally averaged surface temperature change resulting from a doubling of the atmospheric CO_2 concentration) or the spatial distribution of temperature and precipitation changes in response to an increase in greenhouse gas concentrations. Such studies were conducted with atmospheric general circulation models coupled to models of the oceanic mixed layer and were limited to the study of the equilibrium response of climate to a doubling of the atmospheric CO_2 concentration.

Here, we focus on the millennial time scale and utilize the fully coupled Earth system model of intermediate complexity LOVECLIM. Compared to coupled general

circulation models (CGCMs), LOVECLIM has the advantage of greatly reduced computer requirements, so that a larger number of sensitivity experiments or climate change and sea level scenarios can be conducted. LOVECLIM is therefore an invaluable tool to explore uncertainties in long-term climate and sea level change projections. First, some components of the model are improved. Then some key parameters of LOVECLIM are varied and parameter sets are selected that lead to very different climate, sea level and atmospheric CO_2 concentration responses to changes in forcing. Eventually, experiments are performed using the improved version of LOVECLIM and several parameter sets. We analyse the response of LOVECLIM to a doubling of the atmospheric CO_2 concentration and to a freshwater perturbation applied over the North Atlantic Ocean (E-experiments). We study the climate simulated over the last millennium (M-experiments). The climate of the Holocene, including the rapid climate change that occurred at 8.2 kyr BP, is also great of interest for this work, although it is only briefly tackled in this report (H-experiments). We simulate climate change over the next millennium under several greenhouse gas forcings (F simulations) with a special emphasis on the evolution of the Greenland ice sheet, as well as its impact on climate, sea level change and ocean circulation. The interaction between climate and carbon cycle is also analysed. All these simulations are performed with the selected parameter sets.

2. METHODOLOGY AND RESULTS

A. Model description

LOVECLIM consists of five major components representing the atmosphere (ECBilt), the ocean and sea ice (CLIO), the terrestrial biosphere (VECODE), the oceanic carbon cycle (LOCH) and the Greenland and Antarctic ice sheets (AGISM). Please refer to http://www.astr.ucl.ac.be/index.php?page=LOVECLIM%40papers for a full list of references on climate change studies carried out with the model.

1. ECBilt

ECBilt is a three-dimensional, spectral, quasi-geostrophic model of the atmosphere developed at the Koninklijk Nederlands Meteorologisch Instituut, De Bilt (Opsteegh et al., 1998). It has a T21 horizontal resolution and 3 levels located at 800, 500 and 200 hPa. The model includes an explicit representation of the hydrological cycle and a dynamically passive stratospheric layer. Cloudiness is prescribed according to present-day climatology. The shortwave radiation scheme accounts for the absorption of solar radiation by atmospheric gases and clouds. Absorption is parameterised as a prescribed fraction of the incoming solar radiation. Reflection of solar radiation takes place at the top of the atmosphere and at the surface. The reflected sunlight from the surface is completely reemitted to space. The longwave radiation scheme follows the approach proposed by Chou and Neelin (1996). To take into consideration clouds, we combine the perturbed fluxes for clear sky conditions with those for cloudy conditions using the actual cloud cover per grid cell.

2. CLIO

CLIO (Coupled Large-scale Ice–Ocean model) is a three-dimensional ocean–sea ice model built at the Université catholique de Louvain (Goosse and Fichefet, 1999).
The oceanic component is a primitive-equation, free-surface ocean general circulation model (Deleersnijder and Campin, 1995; Campin and Goosse, 1999). It contains a sophisticated formulation of the subgrid-scale vertical mixing (Goosse et al., 1999) and a parameterisation of density-driven downslope flows (Campin and Goosse, 1999). An isopycnal diffusion scheme, the Gent and McWilliams' (1990) parameterisation of the tracer transport due to meso-scale eddies, a parameterisation of the large-scale interactions between Antarctic ice shelves and the ocean (Beckmann and Goosse, 2003) and a physically-based representation of the upper boundary condition for the salinity balance (Tartinville et al., 2001) are implemented in this model. Furthermore, a module that computes the contribution of the oceanic thermal expansion and/or haline contraction to global and regional sea level changes is included.
The sea ice component (Fichefet and Morales Maqueda, 1997) accounts for the heat capacity of the snow-ice system, the storage of latent heat in brine pockets trapped inside the ice, the effect of the subgrid-scale snow and ice thickness distributions on sea ice thermodynamics, the formation of snow ice under excessive snow loading and the existence of leads within the ice pack. Ice dynamics are calculated by assuming that sea ice behaves as a two-dimensional viscous-plastic continuum.
The horizontal resolution of CLIO is 3° × 3°, and there are 20 unequally spaced levels in the ocean. The only flux correction applied to CLIO when coupled to ECBilt is an artificial reduction of precipitation over the Atlantic and Arctic Oceans, and a

homogeneous distribution of the removed amount of freshwater over the North Pacific Ocean (Goosse et al., 2001).

3. VECODE

VECODE (VEgetation COntinuous DEscription model) is a reduced-form model of the vegetation dynamics and of the terrestrial carbon cycle (Brovkin et al., 2002).
This model simulates at the same resolution as the one of ECBilt the dynamics of two main terrestrial plant functional types: trees and grassland. The equilibrium tree fraction in a given grid cell is taken as a function of climatic parameters (the positive degree-day (PDD) index and the annual mean precipitation). The equilibrium fraction of desert (i.e. bare soil), either cold or warm, is also obtained from climatic parameters using empirical formulas. The equilibrium grassland fraction is defined as the land covered neither by tree nor by desert. If climate changes, the model simulates vegetation transition from the equilibrium for the previous climate towards an equilibrium for the new climate.
Four carbon compartments are considered in the carbon cycle component of the model. They all have different turnover times: a fast pool of green biomass (leaves), a slow pool of structural biomass (stems, roots), a fast pool of organic matter (litter) and a slow pool of organic matter (woody stems and roots). Carbon isotopes ^{13}C and ^{14}C as well as fractionation processes during their transfer are also modelled. The simulated vegetation changes only affect the land surface albedo in ECBilt and have no influence on other processes such as, for instance, evapotranspiration.

4. LOCH

LOCH (Liège Ocean Carbon Heteronomous model) is a three-dimensional oceanic carbon cycle model developed at Université de Liège (Mouchet and François, 1996). It simulates the fate of dissolved inorganic carbon, total alkalinity, phosphates, dissolved and particulate organic matter, silica, oxygen as well as organic and inorganic ^{13}C and ^{14}C. Physical, chemical and biological processes control the concentration of dissolved CO_2 at the sea surface. A variable rain ratio links the production of carbonate shells to the export production – this ratio is expressed as a function of temperature and silica availability. Since the fate of carbonate shells at depth is fully determined by the water chemistry, LOCH explicitly includes a carbonate compensation mechanism.
LOCH also includes an atmospheric module that simulates the evolution of various gases in the atmosphere (CO_2, $^{13}CO_2$, $^{14}CO_2$ and O_2). The atmosphere is considered to be well mixed in the zonal direction, whereas a diffusive law represents the meridional transport. The concentrations of atmospheric gases are then predicted on the basis of the fluxes to or from the ocean and the terrestrial biosphere, and, if applicable, of any other sources (e.g., anthropogenic emissions).
LOCH is fully coupled to CLIO and runs with the same time step and on the same grid. It is forced by the oceanic temperatures, salinities and velocities, the downsloping currents, the horizontal and vertical diffusivities, the sea ice cover and the surface wind speeds. It should be noted that actual values and not anomalies intervene in the coupling of LOCH to the other LOVECLIM components. VECODE provides LOCH with the annual air-biomass local carbon fluxes that are then zonally integrated in the atmospheric module imbedded in LOCH. Combining the carbon fluxes from the vegetation and the ocean, LOCH then computes the globally averaged annual mean atmospheric CO_2 concentration transmitted to the atmospheric radiative scheme.

The atmospheric module offers two options for the study of the carbon cycle: either the concentrations are prescribed in the atmosphere (diagnostic mode) or the concentrations evolve according to the various exchange processes as described above (prognostic mode).

5. AGISM

AGISM (Antarctic and Greenland Ice Sheet Model) consists of two three-dimensional thermomechanical ice dynamics models for each of the polar ice sheets. Both models are based on the same physics and formulations. They are composed of a three-dimensional thermomechanical model of ice sheet flow, a visco-elastic bedrock model and a model of the mass balance at the ice atmosphere and ice ocean interfaces (Huybrechts, 2002). For both ice sheets, calculations are made on a 10 km $\times$10 km resolution grid with 31 vertical layers in the ice and another 9 layers in the bedrock for the calculation of heat conduction in the crust. The only difference between both ice sheet models is that AISM includes coupled ice shelf flow to enable grounding-line migration, whereas GISM assumes iceberg calving when the ice sheet reaches the prescribed coastline. Interaction with atmosphere and ocean is effectuated by prescribing the climatic input, consisting of the surface mass balance (accumulation minus ablation), surface temperature and the basal melting rate below the ice shelves surrounding the Antarctic continent.
The atmospheric variables needed as an input for AGISM are surface temperature and precipitation. Because the details of the Greenland and Antarctica surface climates are not well captured on the ECBilt coarse grid, these boundary conditions consist of present-day observations as represented on the much finer AGISM grid onto which climate change anomalies from ECBilt are superimposed. Monthly temperature differences and annual precipitation ratios, computed against a reference climate corresponding to the period 1970-2000 AD, are interpolated from the ECBilt grid onto the AGISM grid and added to and multiplied by the observed surface temperatures and precipitation rates, respectively. The oceanic heat flux at the base of Antarctic ice shelves is also calculated in perturbation mode using the parameterisation proposed by Beckmann and Goosse (2003). After performing mass balance and ice dynamics computations, AGISM transmits the calculated changes in land fraction covered by ice and orography to ECBilt and VECODE. In addition, AGISM provides CLIO with the geographical distribution of the annual mean surface freshwater flux resulting from ice sheet runoff, iceberg calving, runoff from ice free land and basal ice melting. All of these sources of freshwater are added to the surface layer of coastal oceanic grid boxes. Some adjustments are regionally applied to the heat and freshwater fluxes to ensure conservation in the coupled system (see Driesschaert (2005) for details).

6. Global glacier melt algorithm

The response of mountain glaciers and ice caps is accounted for by a global glacier melt algorithm (Raper and Braithwaite, 2006). The algorithm is run in off-line mode and consists of a mass balance and a geometric glacier model. A separation is made between melt contributions from mountain glaciers and ice caps, as these have distinctly different geometric characteristics. The algorithm also has an improved treatment of volume shrinkage to take into consideration simultaneous changes in glacier area. This allows glaciers to reach a new equilibrium under a climate warming, contrary to older models which use a time-constant sensitivity for mass balance, so that glaciers would melt away for any warming rather than approaching a

new equilibrium (e.g., Gregory and Oerlemans, 1998; van de Wal and Wild, 2001). The algorithm is forced by applying annual temperature anomalies with respect to the 1961-1990 period. Precipitation changes are not considered in line with conclusions from several studies showing this to be of secondary importance (Braithwaite et al., 2002; van de Wal and Wild, 2001).

B. Methodology

1. Model improvements

Land surface scheme

The land surface scheme included in ECBilt has been improved in order to better represent the impact of vegetation in the frame of climate change. The goal of the new parameterisation is to get a better representation of the feedbacks between vegetation and climate through improvement of the hydrological coupling between them. It takes into account the impact of vegetation on evaporation (transpiration) and on the bucket depth (i.e. the maximum water depth that can be hold in the soil). The variable bucket depth has a direct impact on the runoff.
Originally, evaporation in LOVECLIM was computed as:

$$E = \frac{\rho_a}{r_a} \Delta Q \frac{b_m}{b_{\max}}$$

where the aerodynamic resistance r_a depends on the surface drag coefficient and on the wind speed ; ρ_a is the density of air ; ΔQ is the difference in humidity between the surface and the air layer above ; b_m is the water storage in the soil and $b_{\max}$ is the bucket depth (the maximum possible value of b_m). The reference value of $b_{\max}$ is 0.15 m (bm15). We have performed two sensitivity experiments with this parameter set equal to either 0.10 m (bm10) or 0.20 m (bm20). A smaller value leads to a decrease in the annual mean precipitation over North America and Europe. The evaporation is therefore reduced together with the latent heat flux. Consequently, the annual mean surface temperature increases in these regions (Figure 4).

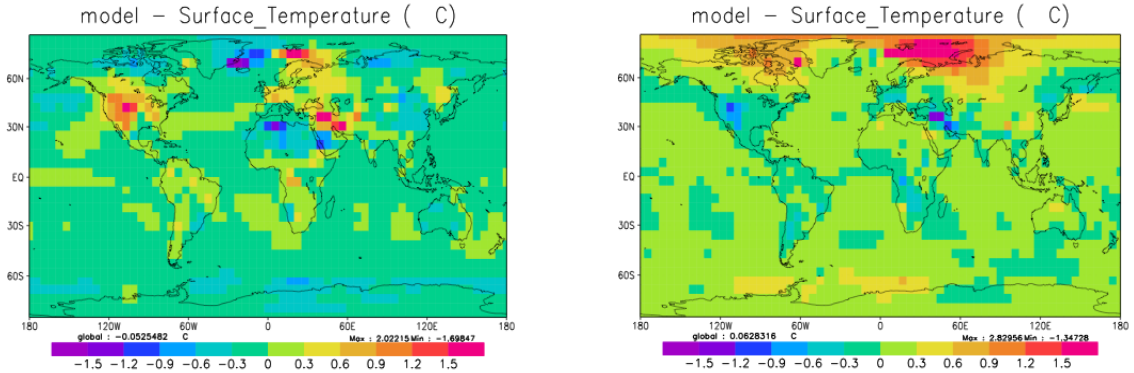

Figure 4: Annual mean surface temperature (°C). Deviation from the reference simulation (bm15) of (left) bm10 and (right) bm20.

This feedback is especially active during summer. The combined changes in precipitation, soil water availability and surface temperature lead to an increase in grass fraction at the expense of the tree fraction. The broad feature is opposite in case of a larger depth active soil. As far as the north of Africa is concerned, a reduced value leads to an increase in desert area there since the soil water content is reduced. The albedo change induces a cooling in this region. The desert fraction

over Sahara is larger for a larger value of this parameter since $b_m / b_{\max}$ decreases in this dry region. The increase in desert area induces a cooling in winter through the albedo increase and the decrease in evaporation implies a warming in summer. Those experiments show that the vegetation is sensitive to the bucket depth.
In order to improve the coupling between climate and vegetation, the bucket depth is made dependent on the vegetation and a canopy resistance term is added. Several parameterisations with increased level of complexity were tested before reaching satisfying results. Only the final formulation of evapotranspiration is presented here. In agreement with Milly and Shmakin (2002), the transpiration is given by the following formula and should be later added to the evaporation:

$$E = \frac{\rho_a}{(r_a + r_s)} \Delta Q \frac{b_m}{b_{\max}}$$

r_s is the canopy resistance and is computed as in SECHIBA (Ducoudré et al., 1993). The canopy resistance includes both bulk stomatal and leaf aerodynamic resistances. It depends on incident solar radiation (R_s) and on the water vapour deficit of the air (δc) simulated above the canopy, and is inversely proportional to the single-sided leaf area index (LAI).

$$r_s = \frac{1}{LAI} \bullet \frac{R_s + R_{s0}}{R_s} \bullet \frac{a + \lambda . \delta c}{k_0}$$

The LAI of trees and grass is assumed to vary linearly according to the surface temperature (Ts) : $LAI = LAI_{\max}(0.2+0.04 \times T_s)$, $LAI_{\max}$ being 6 for trees and 2 for grass. The parameters values are given in Table I.

Table I: Values of the different parameters used for the computation of the canopy resistance.

R_{s0}	125 W m^{-2}
a	23×10^{-3} kg m^{-3}
λ	1.5
k_0(grass)	30×10^{-5} kg m^{-2} s^{-1}
k_0(tree)	25×10^{-5} kg m^{-2} s^{-1}

$b_{\max}$ is a weighted average for the whole grid area. It will be hereafter referred to as $b_{\max\_ave}$. $b_{\max}$ is set to 0.05m for desert, 0.15m for grass and 0.3m for forest. The transpiration term is now computed separately for each vegetation type of the grid cell in order to explicitly account for the fact that the area fraction covered by desert has a shallower rooting depth than the area covered by forest. Therefore, it is corrected in the following way:

$$E_{bare} = \frac{\rho_a}{r_a} \cdot \Delta Q \cdot \frac{b_m}{b_{\max\_ave}} \cdot \frac{b_{\max\_des}}{b_{\max\_tree}}$$

$$E_{tr\_grass} = \frac{\rho_a}{r_a + r_s} \cdot \Delta Q \cdot \frac{b_m}{b_{\max\_ave}} \cdot \frac{b_{\max\_grass}}{b_{\max\_tree}}$$

$$E_{tr\_tree} = \frac{\rho_a}{r_a + r_s} \cdot \Delta Q \cdot \frac{b_m}{b_{\max\_ave}}$$

The evapotranspiration is then computed as the sum of the evaporation (E) and transpiration (Etr):

$$E + E_{tr} = 1 \cdot E_{bare} + F_{grass} \cdot E_{tr\_grass} + F_{tree} \cdot E_{tr\_tree}$$

F is the fraction of the grid cell covered either by grass or trees.

The experiment testing this parameterisation (lbm5) shows as broad feature a strengthening of forests and deserts (Figure 5). There is a cooling over Western North America, Western Europe and South of Africa. This cooling is related to an increase in latent heat flux since the concerned regions are forested areas. There is a warming in the northern part of Africa for the opposite reason. There is also a strong warming over the entire Arctic region, which is due to an increase in tree fraction at high northern latitude decreasing the albedo there in autumn and winter. The impact on vegetation is an increase in forest area over Western Europe and most of North America at the expense of grass. The desert extends over most of North Africa and also over Eastern Europe.

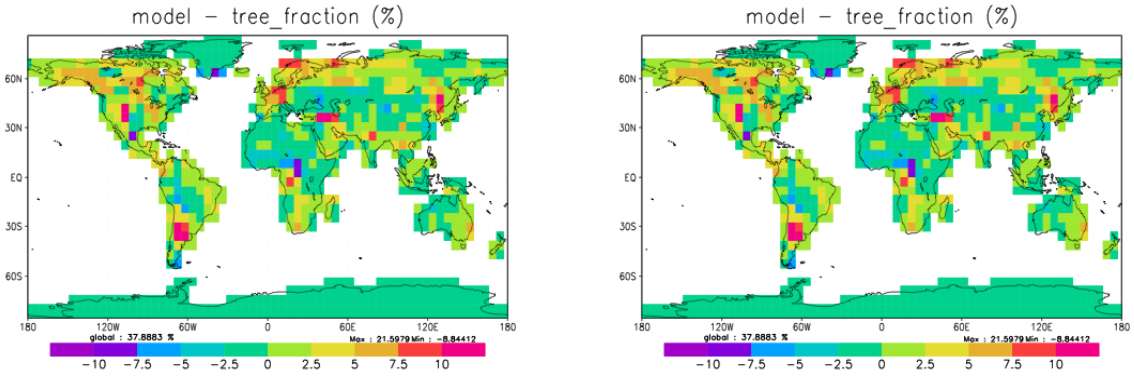

Figure 5: Vegetation change (in lbm5) either forest (left) or desert (right) compared to the reference simulation.

This lbm5 parameterisation was kept in LOVECLIM because it leads to a reasonable response. The feedbacks between vegetation and climate related with climate change between the Holocene and the present time are enhanced. However, further detailed sensitivity experiments should be performed to confirm that result. Some biases of the model could not be reduced by the improvement performed because they result from unrealistic patterns of precipitation in LOVECLIM (e.g., wrong location of deserts in South America and Africa).

The stability of the LOVECLIM model, including this new land surface scheme, has then been tested. Two long equilibrium simulations (2000 years) were performed with the forcing conditions that prevailed during the mid-Holocene (some 6000 years ago) and the pre-industrial times. In both cases, it was checked that the globally averaged, annual mean surface temperature, mean ocean temperature and strength of the Atlantic meridional overturning circulation do not exhibit any long-term drift. The simulated pre-industrial climate is characterized by the globally averaged, annual mean surface temperature of 16.1°C, i.e. 0.3°C higher than with the former land surface scheme. The hydrological cycle is also slightly amplified on a global scale (increase in precipitation and evapotranspiration). Table II, below, provides other characteristics of the simulations.

On an annual average, the zonal mean surface temperature is too high (compared to the data) between 30°N and 60°S (Figure 6). However, the polar regions (Arctic and Antarctic) are cooler than the observations. Annual mean precipitation is in good agreement with observations poleward of 30°. Nevertheless, the model cannot reproduce the large precipitation in the equatorial region and it overestimates the precipitation in the tropical regions (Figure 6). The model including the new land surface scheme simulates more forested area than in the observations over most of the continents, except for the Eurasian boreal forest, which is underestimated compared to observations. However, it has to be mentioned that our pre-industrial

simulation does not take into account the human deforestation, which is present in the observations. The deforestation is estimated to be 30% on a global scale. Taking into account this feature improves considerably the agreement between model and observations. Desert fraction is underestimated over Sahara and Arabia. The Chile desert and the African forest are not well located.

Table II: Some characteristics of the pre-industrial and Holocene simulations with the new land surface scheme.

	Pre-industrial	Holocene
Ts (°C)	16.1	16.4
pp (cm/yr)	107.05	108.32
SST (°C)	19.0	19.1
To (°C)	3.23	3.34
NH sea ice area – max (km^2)	~14×10^6	~14×10^6
NH sea ice area – min (km^2)	~7×10^6	~5×10^6
MOC (in the North Atlantic) (Sv)	~28	~28

Ts : global annual mean surface temperature
pp : global annual mean precipitation rate
SST : global annual mean sea surface temperature
To : global annual mean temperature of the ocean
NH sea ice area – max : maximum of the Northern Hemisphere sea ice area
NH sea ice area – min : minimum of the Northern Hemisphere sea ice area
MOC : maximum value of the North Atlantic meridional overturning streamfunction

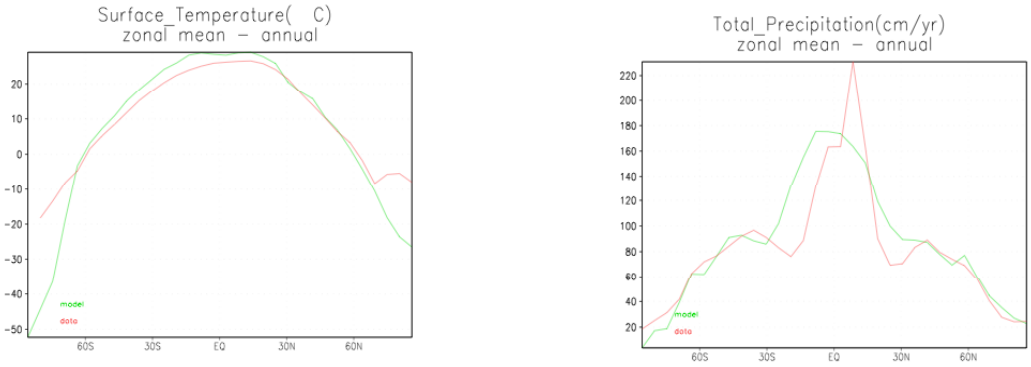

Figure 6: Zonal distribution of the simulated annual mean surface temperature (left) and annual precipitation (right) for the pre-industrial forcings. Model simulation (green) is compared with observations (red).

The major feature of the simulated mid-Holocene climate is a greening of the Sahara desert. The Holocene simulation exhibits indeed a decreased fraction of desert and an increased fraction of grassland over the Sahara region compared to the pre-industrial runs. There is also an increase in the tree fraction over the Sahel region at 6 kyr BP compared to pre-industrial times. This vegetation change is associated with a large precipitation increase over Sahara, as well as over Arabia.

LOCH

In the former LOCH version, rivers compensated for any matter loss to the sediments. The updated version allows the user choosing either automatically adjusting fluxes or prescribed or non-balancing external fluxes. The differences in the outcome of the model are negligible when considering the industrial era and the coming centuries. However, on much longer time scales, this decoupling may be of importance.
The interface coupling LOCH and CLIO was built in order to guarantee that the transports of tracer and salinity are coherent. A hybrid vertical advection scheme was implemented in LOCH to guarantee monotonicity. Off-line tests led to reasonable results. However, when applied in the on-line version, the uptake of anthropogenic CO_2 was much too large (exp. 1hg-1 in Figure 7 and Table III). After analysis, it became clear that numerical noise linked to the inertial term in CLIO caused the vertical velocity in the deep ocean to oscillate with significant amplitude at a high frequency. This translated into a large numerical diffusivity with the hybrid vertical scheme, which resulted in too much mixing of tracers between the surface and the deep ocean. This numerical noise diminished drastically when computing the Coriolis term in the equation of motion in a totally implicit way in replacement of the former semi-implicit scheme. This modification leads to a dramatic decrease of the anthropogenic CO_2 ocean uptake (exp. stdAM-1 in Figure 7 and Table III).

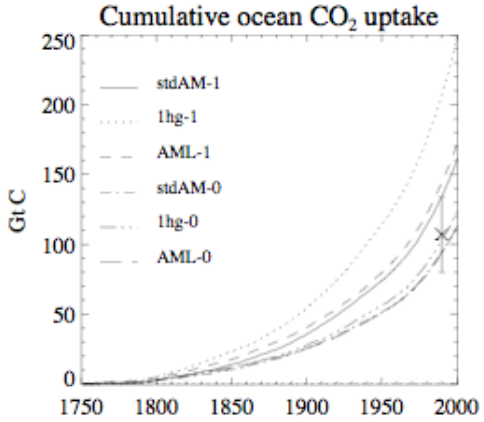

Figure 7: Effect of the implicit factor in the Coriolis term on the ocean anthropogenic CO_2 uptake. This factor is 1.0 for experiment stdAM, 0.75 for exp. AML and 0.5 for exp. 1hg. Two different schemes for the vertical transport of tracers were used: a 2nd order centered scheme (exp. "-0") and the hybrid 1st order scheme (exp. "-1"). The vertical bar represents the data-based estimated ocean uptake of anthropogenic CO_2 (Houghton et al., 2001).

The ocean uptakes of CO_2 during the 80's and 90's are respectively given in rows 4 and 5 of Table III for sensitivity experiments to the numerical scheme. The transport scheme is given in column 2, while column 3 contains the implicit factor for the Coriolis term. The last two lines show the estimates from the OCMIP-2 models and from the IPCC TAR (Houghton et al., 2001).
Up to now, the transport equation of tracers in LOCH did not consider the Gent and McWilliams' parameterisation, as is the case in CLIO. We tested the implications of neglecting this feature in LOCH. Considering it results in marginal changes of tracer distribution. The largest differences between the results obtained with or without the Gent and McWilliams' scheme occur for silica (Figure 8). The reason for such minor changes is probably to be found in the low value of the skew-diffusion coefficient used in CLIO. Including this parameterisation does not improve the distribution of

nutrient concentrations in the Southern Ocean as was suggested elsewhere (Gnanadesikan, 1999).

Table III: Sensitivity of LOCH to the numerical scheme.

Experiment	Vertical scheme	Implicit factor Coriolis term	Air-sea CO_2 flux during the 80's (PgC/yr)	Air-sea CO_2 flux during the 90's (PgC/yr)
1hg-1	hybrid	0.50	3.20	3.93
1hg-0	centered	0.50	1.66	1.99
AML-1	hybrid	0.75	2.33	2.66
AML-0	centered	0.75	1.59	1.80
stdAM-1	hybrid	1.00	2.06	2.54
stdAM-0	centered	1.00	1.51	1.78
OCMIP-2			1.56-2.42	1.80-2.80
IPCC TAR			1.3-2.5	

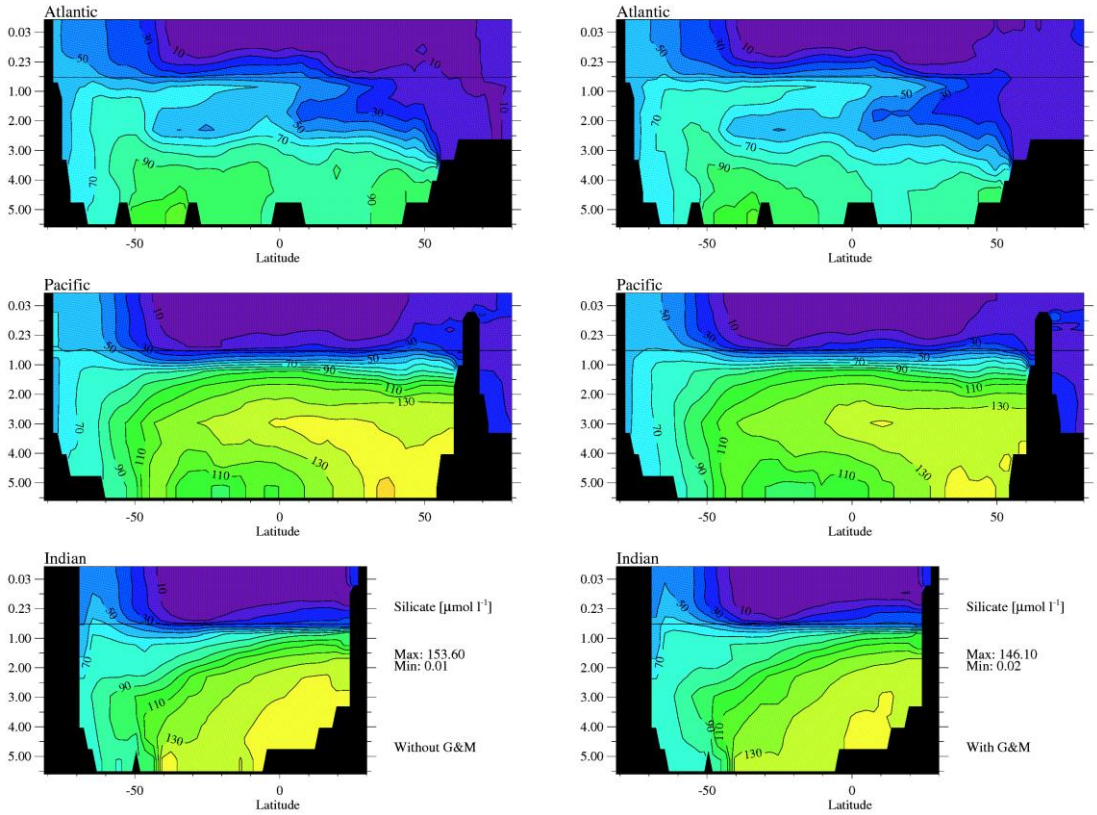

Figure 8: Zonal average of silica concentrations without (left) and with (right) the Gent and McWilliams' parameterisation implemented in LOCH. The vertical scale is depth (km). Note that the scale for the upper 500m is not linear. The same colour scale is used in both panels.

Major adaptations of LOCH are related to the biological module. Silica has the potential to play a significant role in the ocean biochemistry at the long time scales. In climate change experiments performed with LOVECLIM1.0, the main perturbation of the ocean biology was the decrease of silica in the surface ocean at high latitudes (Fichefet et al., 2007). In that version, dissolution of opal is solely allowed in the deepest level (S1 hereafter). We tested other dissolution schemes: one in which opal shells are homogeneously distributed in the water column (S2), then another one

(S3) with temperature-dependent rate and depth control (Bidle et al., 2002; Fuji and Chai, 2005). When examining the global model behaviour (Figure 9), the scheme with bottom dissolution seems to perform slightly better at reproducing the ocean dissolved silica distribution. However, the global opal export rate increases from 75.4 Tmol/yr in S1 to 91.4 Tmol/yr in S3, while field estimates point towards a value less or equal to 120 Tmol/yr (Nelson et al., 1995). The fraction of the export production supported by diatoms in the model also increases from 38% in S1 to 46% in S3. The latter value is very close to the commonly accepted 50% figure (Nelson et al., 1995). The difference between schemes 1 and 3 is that the second allows a refuelling of the euphotic layer consistent with the seasonal time scale. These schemes were also tested with a circulation representing differently the ocean water masses (experiments “A” in Figure 9). The same conclusions may be drawn. Hence the standard version of LOCH now incorporates the temperature-dependent silica dissolution scheme.

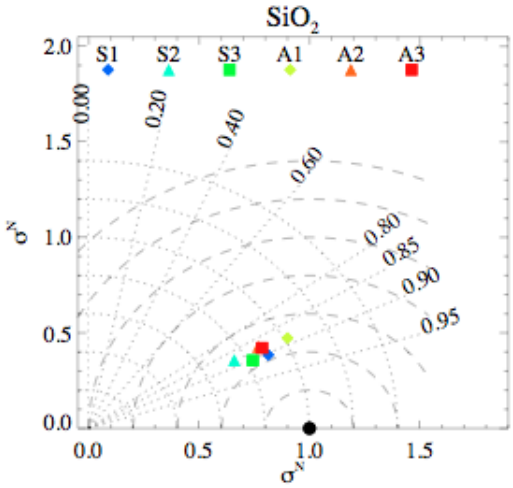

Figure 9: Taylor diagram for the experiments with different silica dissolution schemes. The reference (climatological field (Boyer et al., 2006)) is represented by the filled circle on the abscissa. Each experiment corresponds to a different symbol, which is displayed on the top of the figure for reference. Results correspond to the LOVECLIM circulation (label starting with an “S”) or to another circulation (“A”). The numbers refer to the dissolution scheme: 1 (bottom), 2 (homogeneous) and 3 (temperature). The radial distance from the origin is proportional to the standard deviation of the pattern (σ^N) normalized to that of the data. The centered RMS difference between the test and reference field is proportional to their distance apart. The correlation coefficient between the two fields is given by the cosine of the angle between the abscissa and the line joining the origin to the symbol corresponding to the test field (Taylor, 2001).

Further developments of the biological module in LOCH were carried out in collaboration with the ISMAL (Alger) and GHER (ULg) teams. The biological module in LOCH is based on the computation of the export production (that is the net organic matter flux out of the euphotic zone). This export production is determined in a non-linear way from the availability of nutrients and the growth of a primary producer pool. In the standard LOCH version, this biomass pool is considered as being a standing stock, resulting in a strong geographical link between nutrients and export. In a new LOCH version, the biomass pool is fully submitted to the 3-D transport. This new version also allows considering up to three phytoplankton groups (diatoms, photosynthetic cyanobacteria and other phytplankton species), each group being characterized by its own growth and grazing rates. Nitrogen was also added to the

model; its cycle includes N_2 fixation and denitrification. This model version has been successfully tested with the annual mean circulation fields. This version is not yet part of LOVECLIM. However, in parallel to the ASTER project, the updated LOCH version has been implemented in the 3-D circulation model of the Mediterranean Sea developed by the GHER (Figure 10). Such an application offers a unique opportunity to validate LOCH over an area where the characteristic temporal and spatial scales are much shorter than in the global ocean and where more data are available.

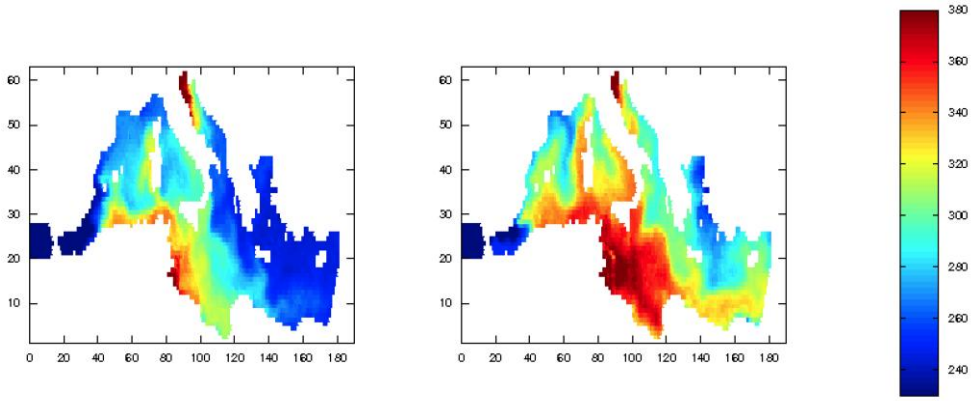

Figure 10: Ocean CO_2 partial pressure (ppmv) from a preliminary simulation with LOCH coupled to the GHER Mediterranean Sea hydrodynamic model. The figure presents the situation in April (left) and October (right). In this simulation the model is constrained with the atmospheric CO_2 as in 1970 A.D. (323 ppmv).

Additional modifications were also brought to the atmospheric module of LOCH in order to allow for a prognostic computation of carbon isotopes in the atmosphere. Two model configurations with respect to the atmospheric isotopic composition (prognostic or constrained) are now available. This feature is useful for simulations over the past.

Several fractionation factors intervene in the exchange of carbon isotopes between reservoirs in LOCH. In the standard version, we take advantage of the formulations of Mook et al. (1974) and Siegenthaler and Münnich (1981) for air-sea exchange: a constant factor is used during soft tissues formation while no fractionation occurs during $CaCO_3$ precipitation. While some fractionation does occur during shell building, its magnitude is higly species-dependent and no clear relationship with the environment has been established yet (Hoefs, 1997). On the contrary, several studies point toward a strong dependency upon water chemistry of the fractionation factor during planktonic growth (e.g. Hinga et al., 1994; Jasper et al., 1994; Rau et al., 1997). We implemented in LOCH the formulation of Jasper et al. (1994), who propose that fractionation during soft tissues formation be inversely related to dissolved CO_2 concentrations.

The impact of this new formulation for the biological fractionation was evaluated with the help of two experiments that only differ by the representation of ^{13}C fractionation during biological assimilation: the fractionation factor is constant in experiment F-CST, while, in experiment F-CO2, it is set according to the formulation of Jasper et al. (1994).

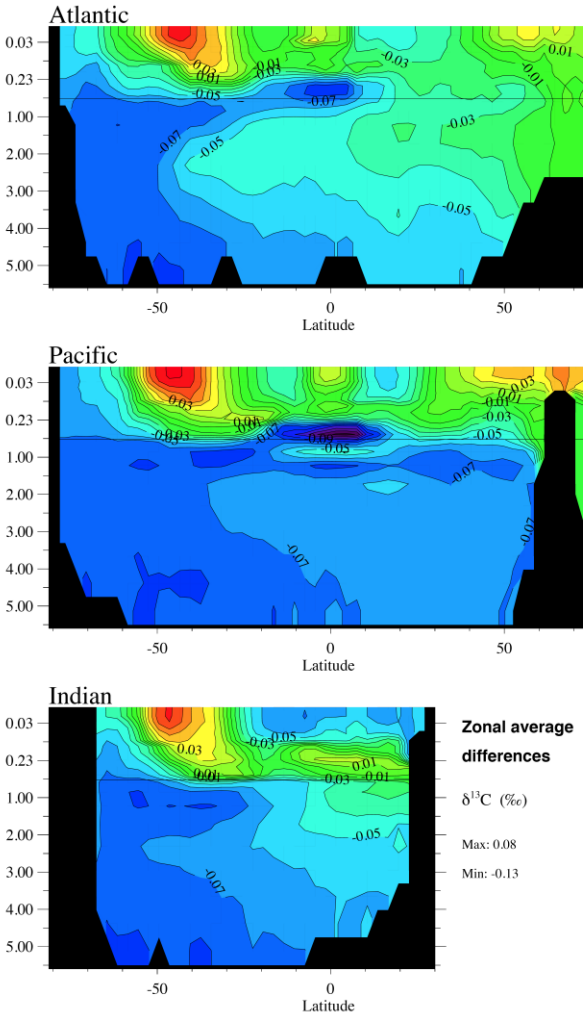

Figure 11: Differences in ocean dissolved inorganic carbon $\delta^{13}C$ between run F-CO2 and F-CST. Positive (negative) values indicate ^{13}C enrichment (depletion) in run F-CO2 with respect to run F-CST.

The global average of the fractionation factor in F-CO2 is 0.9758 (the constant factor in F-CST takes the value 0.9780). On average, the upper ocean (0 to 100m) $\delta^{13}C$ is 2.02 ‰ in F-CO2 and 2.03 ‰ in F-CST. The model runs differ most when comparing the global mean ocean $\delta^{13}C$: the ocean is more depleted with respect to ^{13}C in F-CO2 (0.37 ‰) than in F-CST (0.43 ‰). The largest changes occur in the deep Southern Ocean (Figure 11). The lower $\delta^{13}C$ values at depth in F-CO2 are explained by the larger discrimination against ^{13}C during phytoplankton soft tissue building in deep ocean ventilation areas since such regions are characterized by low temperatures and hence relatively large dissolved CO_2 concentrations. The organic matter sinking to depth hence incorporates less ^{13}C in model run F-CO2 than in F-CST. In turn, this explains the larger values obtained at the surface close to 50°S in F-CO2 (Figure 11). Differences of the order of 0.1‰ should be appreciated in the perspective of $\delta^{13}C$ changes of the order of a few tenths of ‰ since the Last Glacial Maximum (Smith et al., 1999). It should be noted that the global values presented above agree well with field estimates (Broecker and Maier-Reimer, 1992; Hoefs, 1997). In both runs, the continental vegetation $\delta^{13}C$ stabilizes around -24.5 ‰, a value close to that usually quoted for average terrestrial wood (-25 ‰, Hoefs, 1997).

MEDUSA (Munhoven, 2007) is a transient one-dimensional advection-diffusion-reaction model describing the coupled early diagenesis processes of carbonates, organic matter and opal in the surface sediment. A new extended version has been made available to the project. MEDUSA now also includes equations for the ^{13}C isotopic signature of the considered carbon-bearing components (calcite, aragonite, organic matter, CO_2, HCO_3^-, and $CO_3^{=}$).
MEDUSA has been successfully tested in two different setups:
1. in off-line mode with boundary condition datasets generated by LOCH, in the same configuration as the one used with LOVECLIM;
2. in asynchronous coupled mode with the LOCH version that uses the LSG grid.

Steady state simulations as well as glacial-interglacial simulations (120 kyr) were performed.
Some residual problems, typically related to the remineralisation of the organic matter, still need to be solved. The coupling between LOCH and MEDUSA is now completed. The version of LOCH compatible with MEDUSA is totally equivalent to the LOCH version imbedded in LOVECLIM; this was achieved through the development of a “black box” sediment model

Ice sheet model

Most of the ice sheet model development work has concentrated on coupling the Northern Hemisphere Ice Sheet Model (NHISM; Zweck and Huybrechts, 2005) with LOVECLIM. LOVECLIM has been set up to include full two-way coupling. NHISM is a three-dimensional thermomechanical ice sheet model, which includes an improved scheme for marine calving to better simulate ice sheet expansion and contraction over shallow marine basins such as the Arctic Ocean shelf. The model is implemented on a 50 km horizontal resolution, larger than the coarse T21 resolution of ECBilt to sufficiently capture the details of the topography and the width of the ablation zone around the margin. The NHISM resolution, on the other hand, is still coarser than the 10 km resolution of AGISM (Antarctic and Greenland ice sheet model). That is because of the larger model domain and because boundary conditions can be less well specified during glacial times than for the present-day ice sheets. Furthermore, the higher resolution of AGISM is required to better represent the marginal outlet glaciers that are mostly topography-controlled. The apparent discrepancy between the numerical resolution of the ice sheet and the atmospheric components are not at odds with each other as climate changes tend to vary on much larger spatial scales than, e.g., bedrock topography.
The scheme of the coupling between NHISM and LOVECLIM is depicted in Figure 12. The coupling is fully interactive and two-way between the ice sheets, at the one hand, and the ocean and the atmosphere at the other hand. Procedures similar to those employed previously for the coupling of AGISM with ECBilt and CLIO were adopted.

Coupling the NHISM to LOVECLIM

The key parameters needed as input for NHISM are the surface temperature and the precipitation rate. At this stage, climate changes provided by ECBilt are downscaled in the perturbation mode by superimposing temperature anomalies and precipitation ratios (climate changes versus control) from the T21 grid onto the 50 km grid of NHISM. This procedure is implemented because the climate patterns produced by ECBilt differ from observations. Temperature perturbations are applied monthly, but precipitation ratios are imposed annually. Further tests are however needed to

investigate whether precipitation rates from ECBilt could be applied directly; this procedure should provide a better representation of orographic forcing over the former ice sheets. The interpolation of data from the coarse grid relies on interpolation with Lagrange polynomials. Conversely, ECBilt takes into account changes in surface type and surface elevation caused by the evolution of ice sheets on the continents of the Northern Hemisphere. Comparable with the Greenland ice sheet model, there is no influence of changes in the ocean on NHISM.

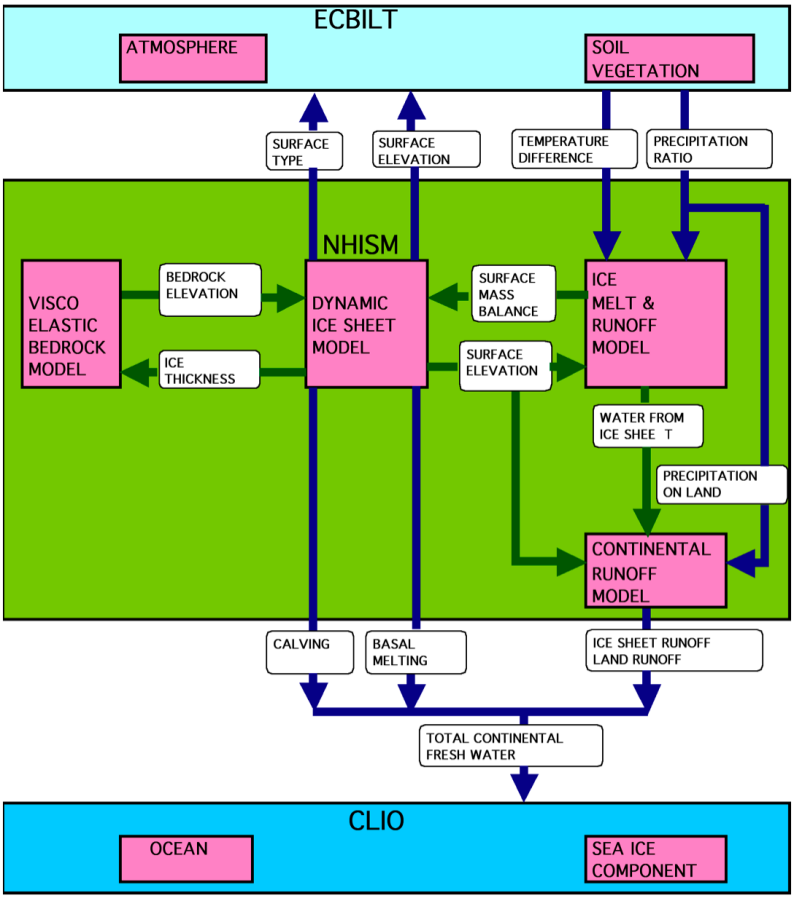

Figure 12: Scheme of the coupling procedure between NHISM and LOVECLIM.

In contrast, the ice sheets provide freshwater fluxes from iceberg calving and meltwater runoff, and to a minor extent from basal melting to the ocean. As long as the ice sheet borders the coastline or is near to it, it can be readily assumed that the freshwater flux will enter the nearest grid cell of CLIO, and a simple allocation scheme suffices. However, most margins of the Northern Hemisphere ice sheets in North America and Eurasia are located far away from the ocean. The produced meltwater therefore needs to be routed through the existing lake and river system. Since the evolution of the ice sheets entails large modifications of the surface orography, both from the weight of the ice mass and from isostatic uplift after retreat, large temporal changes in the runoff routing are expected (e.g., Tarasov and Peltier, 2005). Moreover, the ice sheets are known to be able to create ice-dammed lakes during their retreat, and the associated freshwater release may follow unexpected pathways, including under the ice sheets themselves.
We therefore developed a novel hydrological meltwater routing scheme that takes into account a variable surface relief and is able to determine the discharge pathway the surface water will follow from any continental location to the coast. These can

then be grouped together for any bordering CLIO grid cell. The allocation is unique. A basic assumption is that the meltwater does not evaporate en route, nor infiltrates into the soil. In a first version of the continental runoff model (CRM), it was assumed by the scheme that any depression will entirely fill before spilling over at its lowest margin. In order to account for time-dependent issues related to reservoir filling and emptying, a further development includes treatment of lake water storage changes.
Crucial input to the meltwater routing scheme is a high resolution representation of the surface topography. We used the ETOPO5 (1988) dataset on a 5 x 5 minutes of arc resolution. This corresponds to a resolution of about 9.25 km in latitude and 4.6 km in longitude at 60°N. Although this resolution is still rather coarse to properly resolve all of the narrower valleys, an alternative is not readily available. In recent years, ETOPO5 has been superseded by ETOPO2 (2' resolution) and GTOPO30 (30" resolution), but the latter datasets only show the continental surface and have not been merged with the oceanic bathymetry. They also do not show the bottom topography of the Great Lakes, as does the ETOPO5 dataset. That seriously limits their application in a crucial area of lake formation during ice sheet retreat. The higher resolution datasets would also put too high demands on computer memory and run times.
The continental runoff scheme in NHISM is implemented through the following steps:
1. *Set-up of the interpolation procedure of the NHISM (50 km resolution) onto the ETOPO5 grid.* This is required because changes in NHISM topography are applied to the ETOPO5 topography in anomaly mode to take into account the evolving surface. Use is made of Lagrange polynomials of an order to be selected in the code. The work is performed on a transformed representation of the ETOPO5 data on a 6.25 km x 6.25 km grid for the same stereographic projection as employed in NHISM (called ETOPO5SP). In this way, every 8th grid point in ETOPO5SP coincides with a NHISM grid point.
2. *Inventory of coastal areas and continental depressions.* A mask is first constructed to distinguish between continental and oceanic grid points relative to a variable sea level stand. Using surface gradients, an endpoint is tracked for every ETOPO5SP grid point. An endpoint is the lowest continental surface topography or the first oceanic point that can be reached. If the endpoint is bordering the ocean, the ETOPO5SP grid point belongs to a coastal area. Otherwise, when the endpoint is on land, the continental grid point belongs to a continental depression. The possibility exists to use another contour than sea level to construct the continental mask. Depressions are furthermore defined as consisting of sets of points with the same endpoint. Flat areas are sometimes characterized by a long series of very small depressions.
3. *Grouping of depressions into lakes.* An algorithm is applied to locate adjacent depressions and to find out whether they have a common overflow point, i.e. whether they would merge into a larger lake when filled with water. The procedure is repeated for adjacent depressions until the total number of lakes formed in this way no longer decreases. Convergence is usually reached after applying the search algorithm for about 20 times. The result consists of large depressions or (potential) lakes together with their drainage area.
4. *Documentation of the lakes.* A record is made of the area and volume of the lakes, together with the area of the drainage basin and the coordinates and elevation of the outlet (overflow point). The possibility exists to incorporate evaporation as a control on the lake level but, for now, the scheme assumes that at all times sufficient water is available to fill all depressions.

5. *Grouping of lakes into internal drainage systems.* For all lakes, it is determined into which lower lake it will overflow, i.e. into which contiguous depression having a lower outlet. The process is repeated until the ocean is reached. In this way, all lakes can be grouped for the same 'endlake', i.e. the last lake before the ocean is reached. This defines an internal drainage basin having the same outlet into the ocean, i.e. the outlet of the endlake.
6. *Construction of external drainage systems.* It is now possible to link any continental point to a specific point bordering the ocean (ocean point), be it directly for a point belonging to a coastal area or indirectly for a point belonging to a continental depression. The result is a series of external drainage systems grouping all points draining into the ocean through the same ocean point. Many external drainage systems arise in this way of largely varying size, some of which consist of only one ETOPO5 grid point.
7. *Allocation of any ocean point to a CLIO grid cell.* A search algorithm is applied to group all ocean points draining into the same CLIO grid cell. The procedure is based on the nearest neighbour principle as the CLIO coastline does not exactly coincide with the coastline generated in the ETOPO5SP dataset. In this way, any continental ETOPO5 grid point is linked to a specific CLIO grid cell.
8. *Allocation of NHISM grid points to a CLIO grid cell.* For every NHISM 50 km grid point it is determined what is the corresponding collection of ETOPO5SP grid points where ice sheet runoff is released. In this way, any NHISM grid point not by itself bordering the ocean where calving can take place is linked to a specific CLIO grid cell. The scheme therefore is able to partition runoff in the right proportion into respective CLIO cells.
9. *The additional lake storage module* is mostly a post-processing routine that modifies the output on each CLIO grid cell according to reservoir changes on the runoff pathway. Calculating changes in water storage and redistribution on the high resolution ETOPO5SP grid, although theoretically possible, is too time consuming. We therefore opted for a scheme that only operates on changes in potential water storage and runoff connected to each CLIO grid box at a time, thus dealing with the effective freshwater fluxes that reach the ocean. The routine takes as input the maximum potential volume connected to each CLIO grid box, i.e. the integrated volume of all lakes (4.), and the runoff (8.). Initially, all lakes are assumed as fully loaded and the integrated water storage connected the each CLIO box equals its potential. Modifications of surface orography can then increase or decrease the potential, the latter of which leads to major drainage events at times. Runoff either refills the water storage or is released when the storage reaches its full potential. The time period over which water is released to the ocean cannot be derived from the model itself, but rather has to be defined by the user. A guideline for the choice of this model parameter can be found in paleo evidence of past large-scale drainage events and has to be in line with the capability of the ocean model to deal with huge amounts of localized freshwater input. The above procedure is schematically depicted in Figure 13.

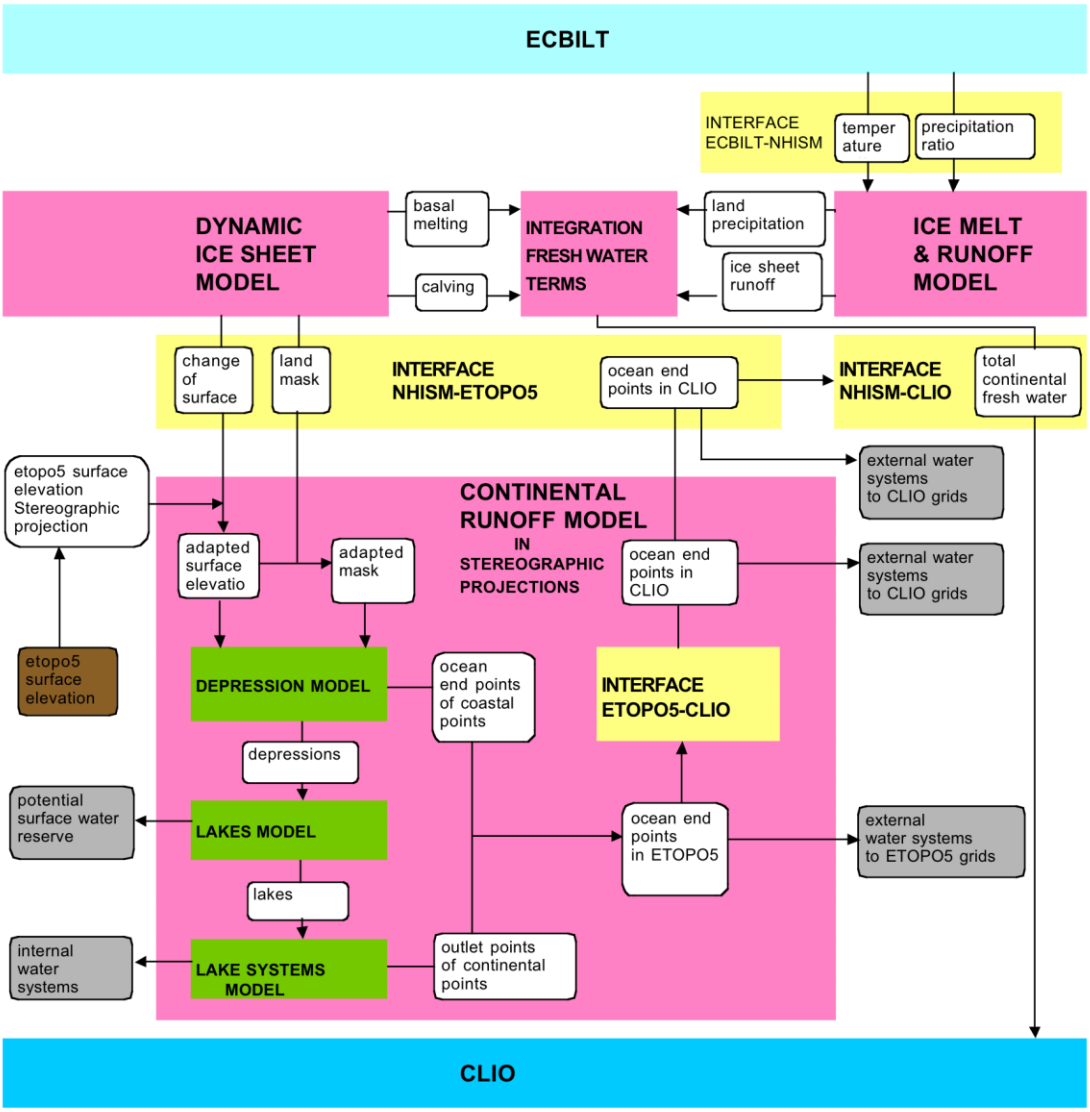

Figure 13: Details of the continental runoff model (CRM).

The hydrological routing scheme can also be used to establish the discharge pathway of continental precipitation. In that case, however, an additional treatment of evaporation is required to conserve the total water fluxes over the continents. An additional complication is the treatment of endoreic regions of interior drainage such as the intermountain southwest of the United States and the arid zones in central Asia. In the hydrological model, such basins will entirely fill before spilling over at their lowest exit. This does not affect ice sheet runoff in North America. However, it means that, e.g., ice sheet runoff destined for the Caspian Sea will ultimately end up in the Mediterranean via the Black Sea and the Bosphorus.

A direct product of the hydrological routing scheme is the delineation of drainage basins. The model determines for every individual continental location the discharge pathway that surface water will follow to reach the ocean. These pathways can then be grouped together to delineate contiguous drainage basins, which drain into the same oceanic grid cell. During the simulations, the procedure needs to be regularly updated to take into account changes of surface topography caused by ice sheet evolution. This is effectuated every 100 years. Figure 14 shows an example of the delineation over the Northern Hemisphere continents. Some artefacts still remain.

These can mostly be explained by the resolution of ETOPO5SP and the slight smoothing produced by the initial map projection transformation. In cases where a major river cuts through a narrow valley, this may cause artificial lakes, which may ultimately drain into another catchment area and CLIO grid cell.

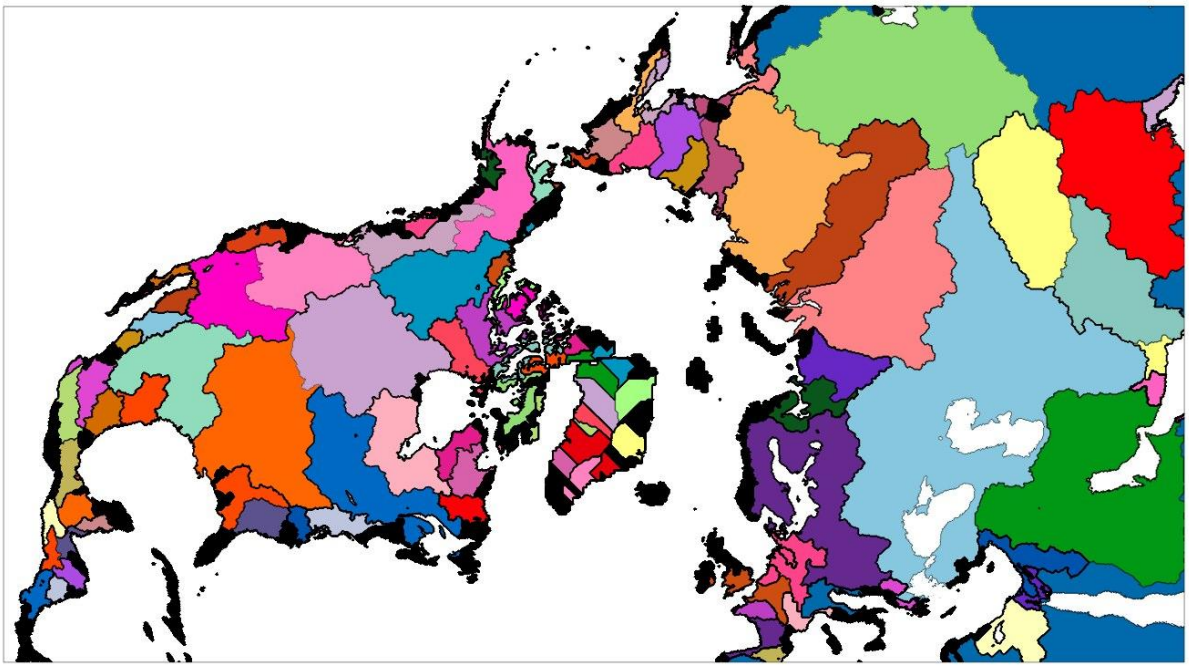

Figure 14: The continental runoff model (CRM) determines for every land point the discharge pathway that surface water will follow to reach the ocean. Each colour represents an area, which drains into the same CLIO oceanic cell. Only the 96 largest catchments areas are distinguished by an own colour. The smaller ones are all shown in black. Large catchment areas in central Asia with no apparent outlet are in fact bordering the NHISM grid; drainage resulting from such areas is routed to the next closest CLIO ocean grid boxes.

Ultimately, a fully coupled transient run from LGM to present day (PD) is envisioned including AGISM and NHISM in order to study the coupled response of climate and ice sheets. Several runs have to be prepared before that, some of which have been performed successfully. These include equilibrium runs for LGM and PD conditions with the same land-ocean mask (Figure 15, left), which is important to guarantee a prescription of temperature and precipitation anomalies that are not affected by applying different masks. An equilibrium simulation for LGM, including a more realistic topography and land-sea mask without interactive ISM, is presented in the next section (evaluation of model performance).
It is worth mentioning here that equilibrium runs for the LGM were originally performed for all nine ASTER climatic parameter sets, but only the four models corresponding to the lowest climate sensitivity (11, 12, 21, 22) yield reasonable results. The cooling when switching the forcing to LGM conditions leads to far too low temperatures in high latitudes for the highest climate sensitivity parameter sets. This is a direct consequence of the relatively high polar amplification in LOVECLIM as discussed further below. Additionally, a quasi-equilibrium spinup experiment for LGM conditions including steady state freshwater fluxes from the ice sheets has been performed (Figure 15, right), which is meant to reduce the coupling drift during transient experiments. Local cooling is visible at different locations of the North Atlantic, where meltwater fluxes have a negative influence on the heat exchange

between atmosphere and ocean, while the South Atlantic and Pacific Oceans are generally warmer in the run including freshwater fluxes.

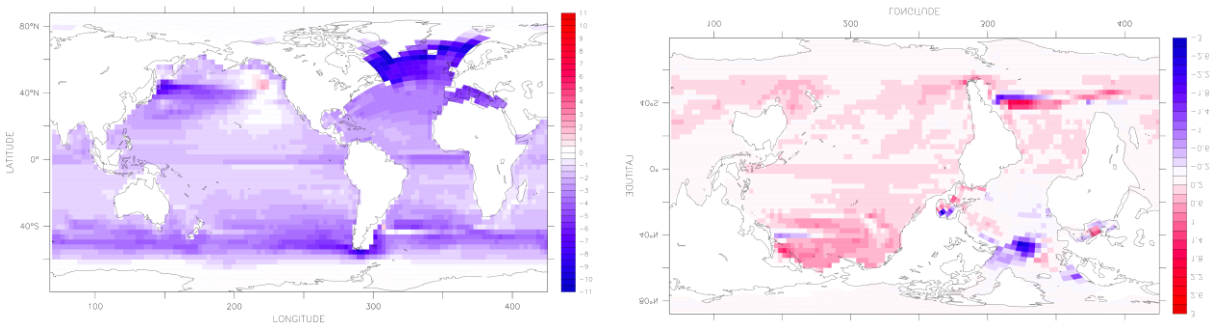

Figure 15: Sea surface temperature difference between LGM and PD with constant LGM land-ocean mask (left) and between LGM equilibrium run and quasi-equilibrium run, which includes freshwater fluxes from the ice sheets (right). The parameter set in use is 1122.

In a further intermediate experiment, we simulate the first part of the deglaciation with LOVECLIM, which is forced with transient freshwater fluxes as calculated by a stand-alone NHISM run (Figure 16, left). The global mean surface temperature (Figure 17, right) shows a response to changes in radiative forcing, which largely arises from variations in the prescribed CO_2 concentration (Figure 16, left). On top of this background variability, the temperature signal responds to changes in the MOC (Figure 17, right), which leads to cooling when the MOC strength is considerably reduced. There are two episodes where the MOC is shut down completely for 400 years, which is related to peaks in the freshwater forcing from the melting ice sheets centred at around 17 kyr PB and 14 kyr BP.

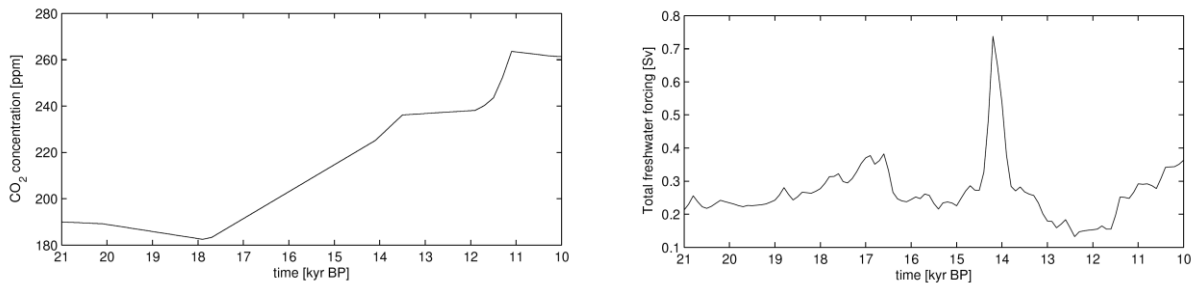

Figure 16: Forcing time series for a transient simulation of the last deglaciation. The CO_2 forcing (left) is derived from ice core records. The freshwater forcing (right) is the output from a transient simulation with the stand-alone NHISM.

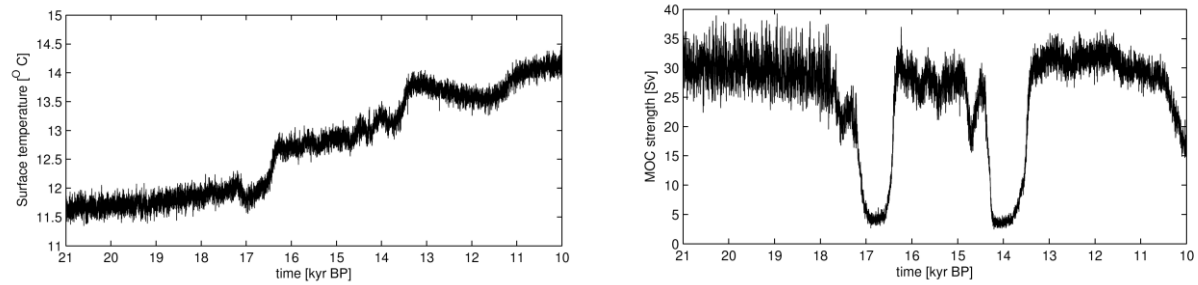

Figure 17: Temperature and MOC response for a transient simulation of the last deglaciation including freshwater forcing from an off-line run of NHISM.

Note that another precursor experiment was carried out in which NHISM had been coupled with ECBilt-CLIO in asynchronous mode for the period since the Last Glacial Maximum (Figure 18). In this experiment, the ice sheet input into ECBilt was prescribed from a gridded representation of ice sheet extent together with a simple parabolic profile to obtain ice sheet elevation at a 200-year resolution. The present-day land-ocean mask was kept constant and feedback between the ice sheets and the global ocean was switched off.
Since unconstrained coupling between NHISM and LOVECLIM may result in unexpected behaviour, it may be necessary to run fully coupled experiments first under controlled conditions, e.g., by setting geomorphological constraints on ice sheet extent.

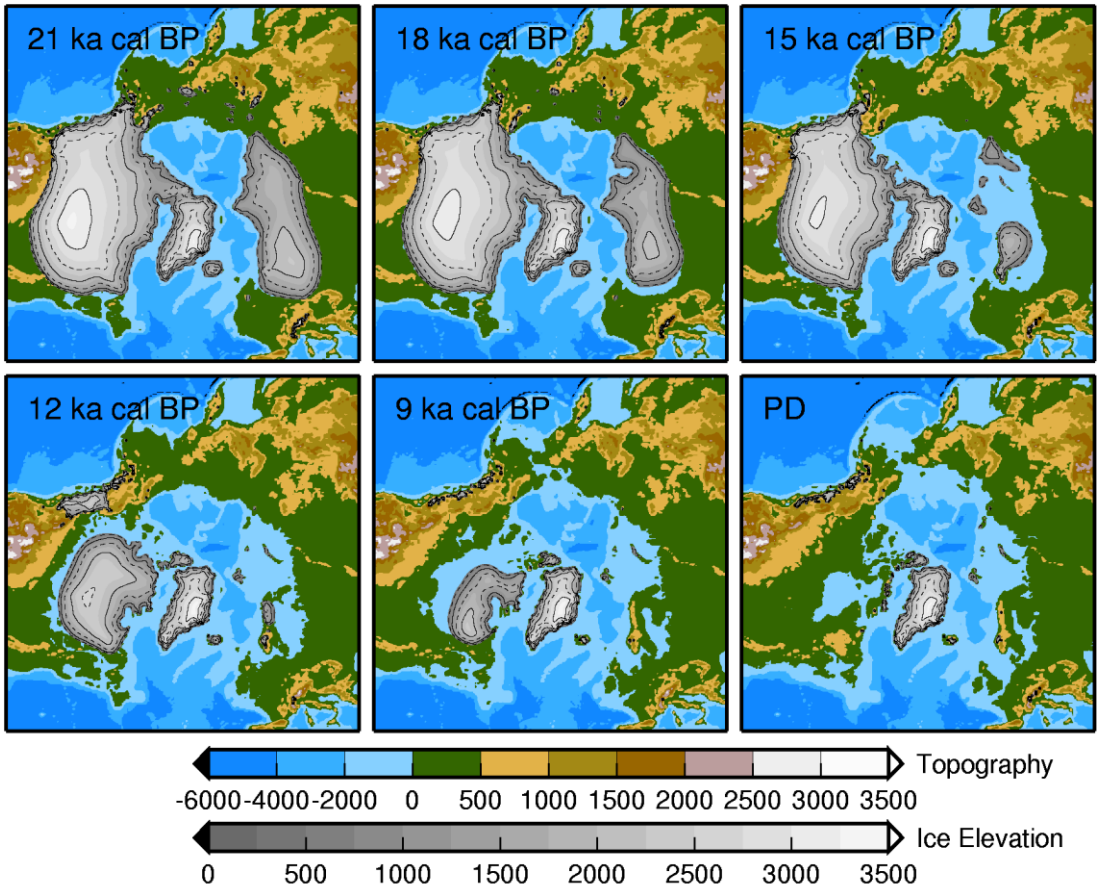

Figure 18: Results from a preliminary off-line simulation of the Northern Hemisphere ice sheets with NHISM forced by ECBilt-CLIO at an asynchronous time step of 200 years.

Results from a stand-alone NHISM run including the CRM can be seen in Figure 19. The total runoff over the last deglaciation adds on average 0.3 Sv to the Northern Hemisphere oceans, with larger peaks connected to the fast disintegration of major parts of the ice sheets. The largest lake drainage events are related to major reorganizations of the runoff pathways with emptying of ice dammed lakes. The rate of freshwater output from lake drainage events is given in Figure 19 under the assumption that all water is released in the year of the event.

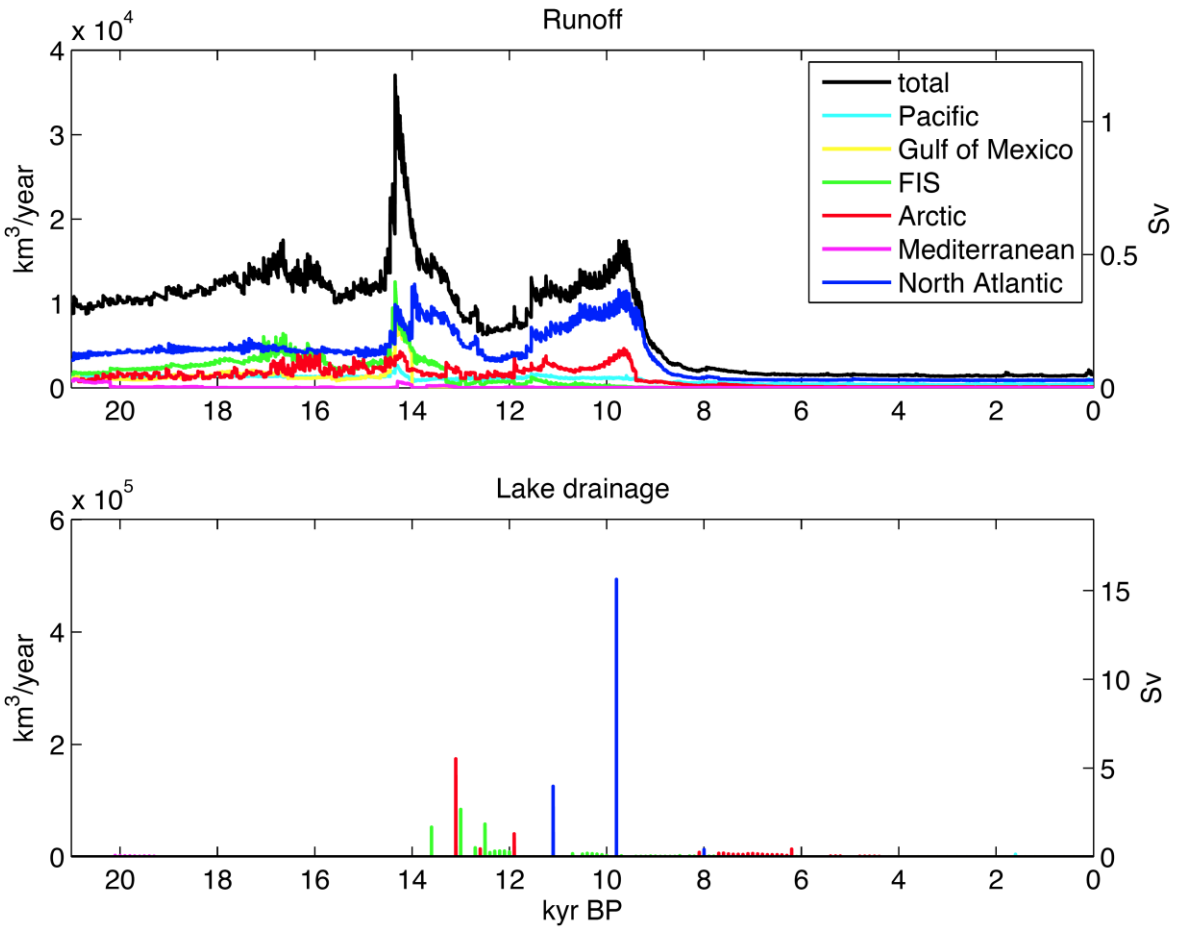

Figure 19: Runoff time series from stand-alone NHISM model run (top) and major lake drainage events (bottom). Runoff to CLIO grid boxes has been grouped into several larger regional areas. The largest lake drainage events are related to major reorganisations of the drainage pathway with emptying of ice dammed lakes.

Evaluation of model performance

As LOVECLIM is a model of intermediate complexity, it cannot be expected to reproduce all the observations with the same skill and the same level of detail as a climate general circulation model (GCM). Indeed, previous studies have underlined some clear and strong model biases in LOVECLIM results. Therefore, we document here the regions (and variables) where the discrepancies are the largest and the ones where the agreement between model results and observations is satisfactory. Therefore, we will describe briefly the mean state of the model for present-day conditions and then discuss the model behaviour for the mid-Holocene (6 kyr BP) and the Last Glacial Maximum (LGM, 21 kyr BP). These two periods are standard ones in the Paleoclimate Modelling Intercomparison Project (PMIP; see, for instance, Braconnot et al., 2007).

Present-day mean climate

A transient simulation has been performed with the fully coupled LOVECLIM model (with the exception of NHISM) over the last 1500 years. The average over the last decades of this simulation is used to evaluate the model behaviour for present-day conditions. The initial conditions for LOCH, VECODE, ECBilt and CLIO come from a quasi-equilibrium run, several thousand years in duration, corresponding to the

forcing applied in 500 AD. For AGISM, as the ice sheets cannot be considered in quasi-equilibrium with the climate at that time, the initial conditions are obtained from a run of AGISM in uncoupled mode covering the last glacial-interglacial cycles and the Holocene up to 500 AD.

During the transient experiment, long-term changes in orbital parameters follow Berger (1978) and the long-term evolutions of non-CO_2 greenhouse gas concentrations are imposed (Houghton et al., 2001). The variations in the carbon emission from fossil fuel burning are derived from Marland et al. (2003). The influence of anthropogenic (1850 AD-2000 AD) sulphate aerosols is represented through a modification of surface albedo (Charlson et al., 1991). Forcing by anthropogenic land-use change (including both surface albedo and surface evaporation and water storage) is applied as in Goosse et al. (2005), following Ramankutty and Foley (1999). Finally, natural external forcings due to changes in solar irradiance and explosive volcanism are prescribed following the reconstructions of Muscheler et al. (2007) and Crowley et al. (2003), respectively. The total solar irradiance changes have been scaled to provide an increase of 1 Wm^{-2} between the Maunder minimum (late 17th century) and the late 20th century (Lean et al., 2002; Foukal et al., 2006).

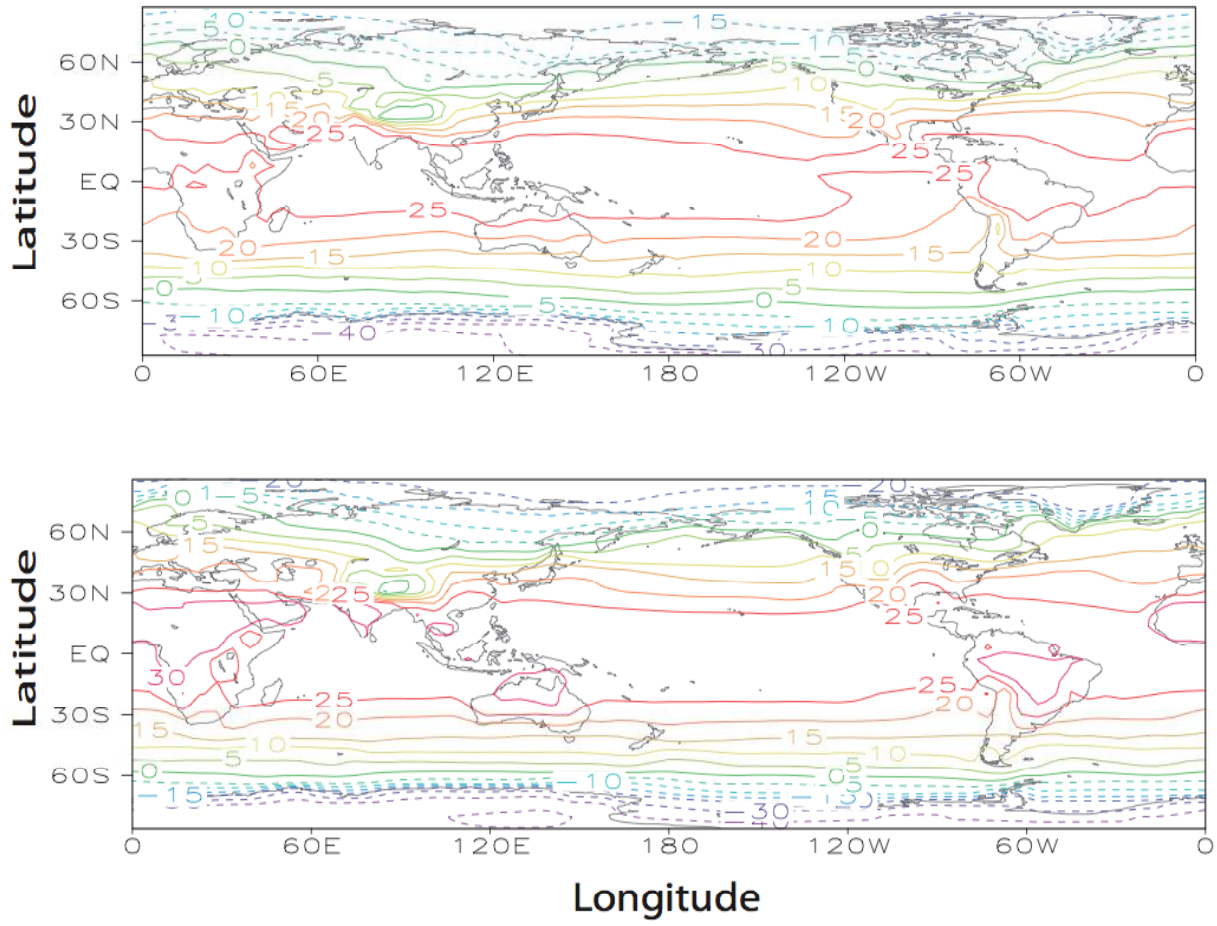

Figure 20: Surface temperature (°C) averaged over the period 1980-2000 in (a) HADCRUT3 dataset (Brohan et al. 2006) and in (b) LOVECLIM.

The comparison between the mean climate over the last decades of this simulation and observations shows that LOVECLIM reproduces reasonably well the main characteristics of the observed surface temperature distribution (Figure 20). For

instance, the zero degree isotherm is quite close to the observed one in both hemispheres, with a more or less constant latitude in the Southern Hemisphere and a wavy structure in the Northern Hemisphere that displays a more northern position on continents than over the oceans. The strong differences at mid-and high latitudes between the cold eastern part of the Atlantic compared to the warmer western part are also clearly seen in both model results and observations. In the tropics, the model is too warm, with a 25°C isotherm located too far away from the equator and an overestimation of the temperature over the continents. Furthermore, the temperature is much too high in the Eastern Pacific.
The simulated zonal mean precipitation has roughly the right magnitude in nearly all the latitude bands (Figure 21). However, the simulated pattern is much too symmetric between the hemispheres. In particular, the model is not able to reproduce the clear and strong absolute maximum observed north of the equator. Furthermore, the precipitation at the observed local minima around 20°S and 30°N is clearly overestimated by the model. At some latitudes, the model error can reach 50% of the precipitation in zonal mean.

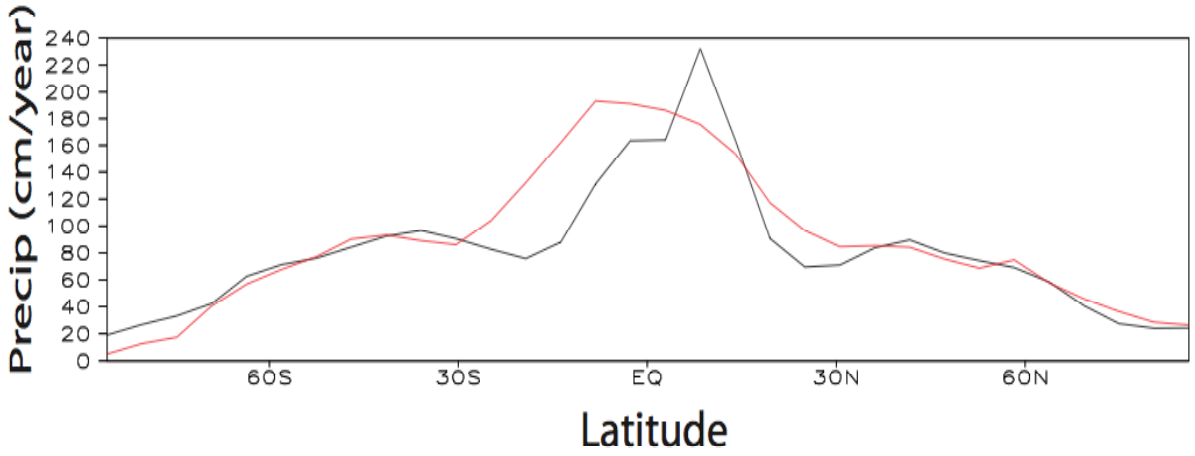

Figure 21: Zonal mean precipitation (cm/year) averaged over the period 1980-2000 in Xie and Arkin (1996 and updates) dataset (black) and in LOVECLIM (red).

During winter in both hemispheres, the large-scale structure of the near-surface atmospheric circulation (Figure 22) is well reproduced by the model with, as expected, a general decrease of the geopotential height with latitudes and local minima in the North Atlantic, the North Pacific and in a belt around 70°S. Except for the Aleutian low, the model underestimates the gradients in both hemispheres, leading to simulated winds weaker than the observed ones. Furthermore, the simulated minimum of the geopotential height in the North Atlantic is located too far eastwards, close to Baffin Bay, while the observations have their minimum near Iceland, inducing a wrong wind direction west of Greenland.

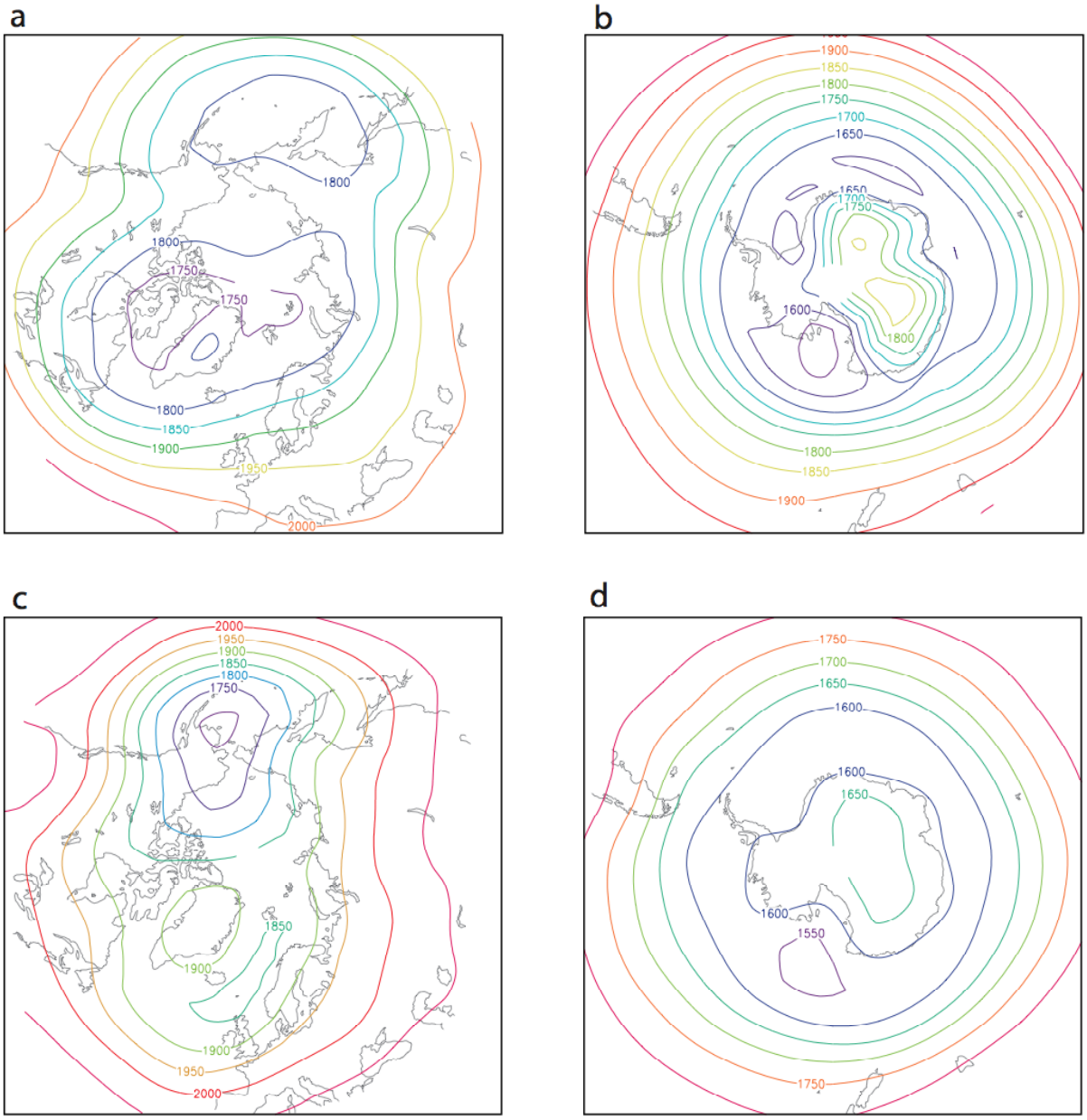

Figure 22: Geopotential height (in m) at 800 hPa in winter averaged over the period 1980- 2000 (DJF in the Northern Hemisphere, JJA in the Southern Hemisphere) in NCEP-NCAR reanalyses (Kalnay et al. 1996, top row) and in LOVECLIM (bottom row).

LOVECLIM is able to simulate reasonably well the sea ice extent in both hemispheres (Figure 23). In the Northern Hemisphere, the sea ice edge is very close to the observed one in the Pacific sector, both during summer and winter. In the Atlantic sector, the simulated sea ice edge is too far northwards in the Baffin Bay and Labrador region in winter, while, in summer, the sea ice extent is too large. The amplitude of the seasonal cycle of the sea ice concentration is thus clearly too weak in this region in the model. In the western part of the North Atlantic, the model tends to slightly overestimate the sea ice concentration, both in summer and winter. The sea ice extent is also slightly overestimated in the Southern Ocean in both seasons. Two exceptions are the regions west of the Antarctic Peninsula in summer and off East Antarctica around 45°E in winter, where the model underestimates the sea ice extent.

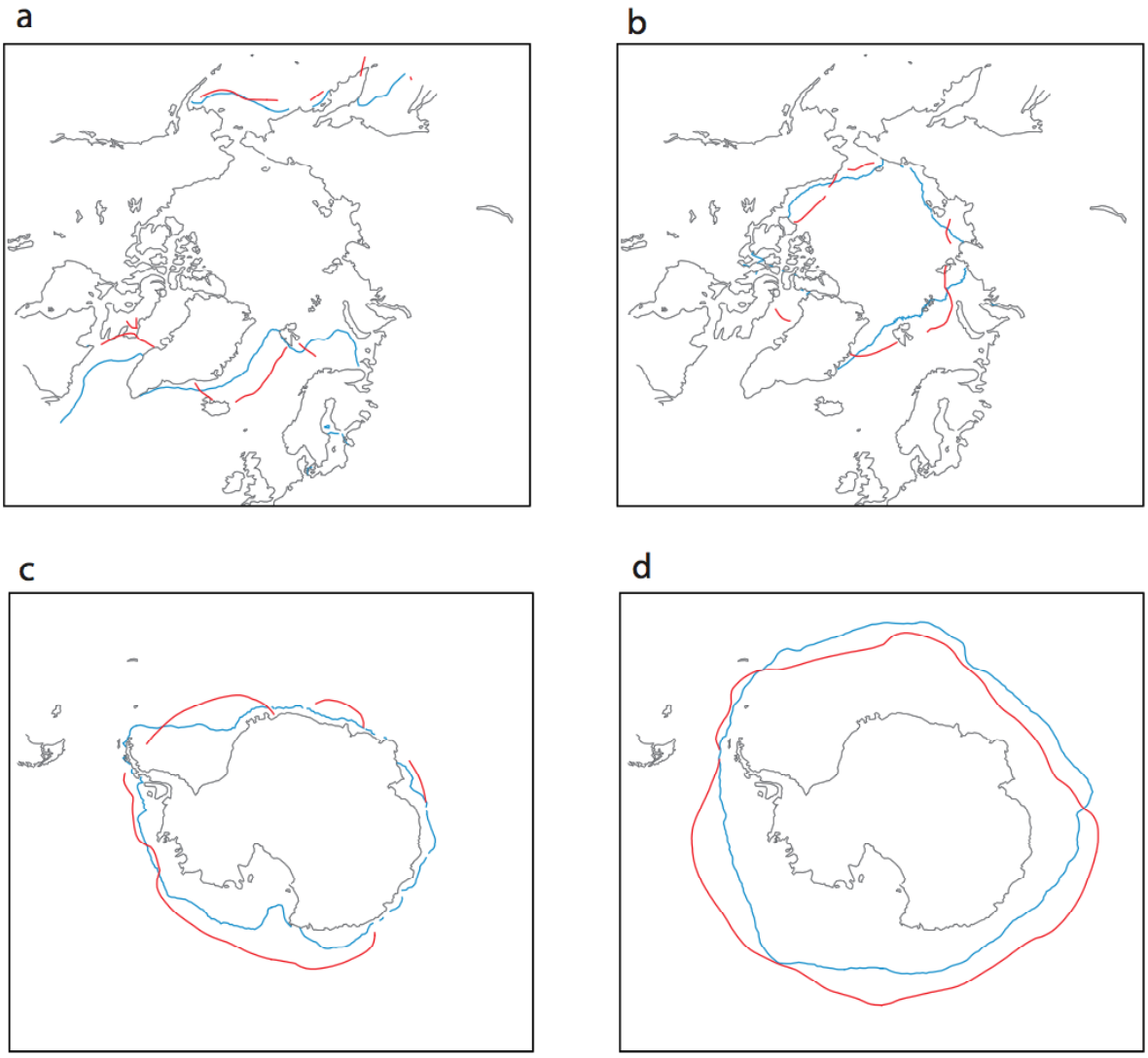

Figure 23: The location of the ice edge averaged over the period 1980-2000, defined by a monthly ice concentration equal to 15%, for (a) March in the Northern Hemisphere, (b) September in the Northern Hemisphere, (c) September in the Southern Hemisphere, (d) March in the Southern Hemisphere. The observations are in blue (Rayner et al., 2003) and LOVECLIM results are in red.

The maximum of the overturning streamfunction in the North Atlantic reaches 22 Sv, with an export towards the Southern Ocean of 13 Sv (Figure 24). Deep convection in the model occurs both in the Greenland-Norwegian Seas as well as in the Labrador Sea, as observed over the last decades. The maximum of the deep cell close to Antarctica has a value of 12 Sv, while 17 Sv are transported northwards close to the bottom in the global ocean. All those values are close to observational estimates and the ones given by other models (Ganachaud and Wunsch, 2000; Gregory et al., 2005; Rahmstorf et al., 2005).
As the model tends to overestimate precipitation in the tropics, the vegetation cover is also overestimated in those regions (Figure 25). The vegetation fraction is also too large at high latitudes, mainly because of an overestimation of the temperature over continents. By contrast, LOVECLIM has a too low vegetation cover in some regions of Australia and Southern America around 30°S.

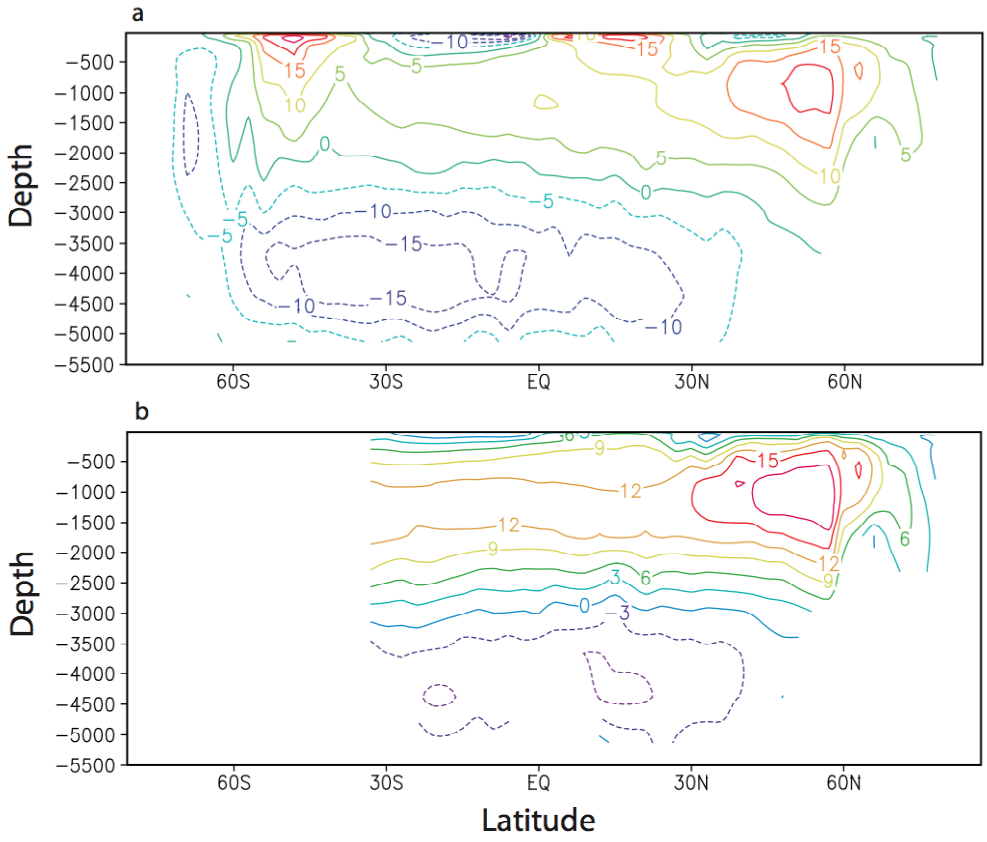

Figure 24: Meridional overturning streamfunction (in Sv) for (a) the whole World Ocean and (b) the Atlantic in LOVECLIM.

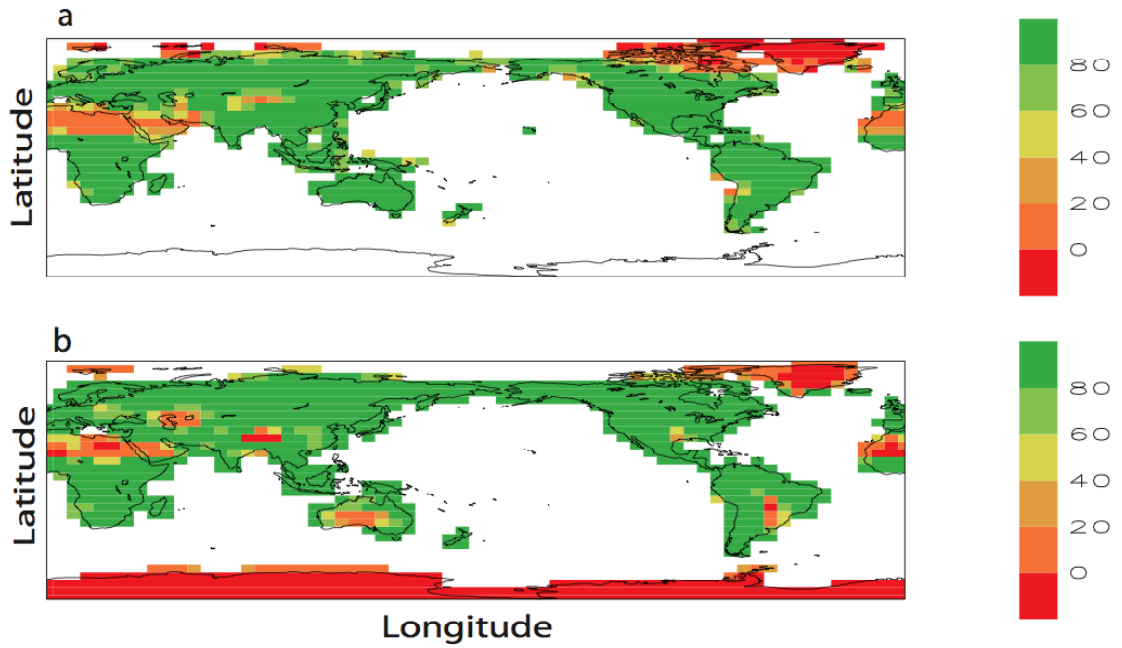

Figure 25: Total vegetation cover in (a) GSWP2 dataset (International GEWEX Project Office, 2002) and in (b) LOVECLIM.

Mid-Holocene conditions

For the mid-Holocene simulation, the orbital parameters are set at the values corresponding to 6 kyr BP and the methane concentration is reduced to 650 ppbv. All

the other conditions are chosen identical to pre-industrial ones and a quasi-equilibrium, multi-millennia run is carried out. For this simulation experiment, LOCH and AGISM are not activated. In response to the larger summer insolation, LOVECLIM simulates an increase of JJAS (June-July-August-September) surface air temperatures at 6 kyr BP over the continents in the Northern Hemisphere and over the Arctic (Figure 26). The Southern Ocean is also warmer, with a local temperature maximum increase of ~4°C between 30°E-40°E. By contrast, some regions experience a slight cooling such as seen in Africa just north of the equator, in the Middle East and west of the Japan coast. The JJAS mean precipitation (Figure 27) produced by LOVECLIM, captures well the mid-Holocene characteristic increase over Northern Africa and in the Middle East, associated with an increase in vegetation there. In the northeast of South America, there is also an increase of ~1mm/day. Just southwards of the equator, there is less precipitation over ocean in the mid-Holocene than today. All those results agree reasonably well with the ones of the other models participating in the PMIP2 intercomparison (Braconnot et al., 2007), albeit tropical ocean feedbacks are relatively weak due to the quasi-geostropic approximation in the atmospheric component ECBilt (Zhao et al, 2005).

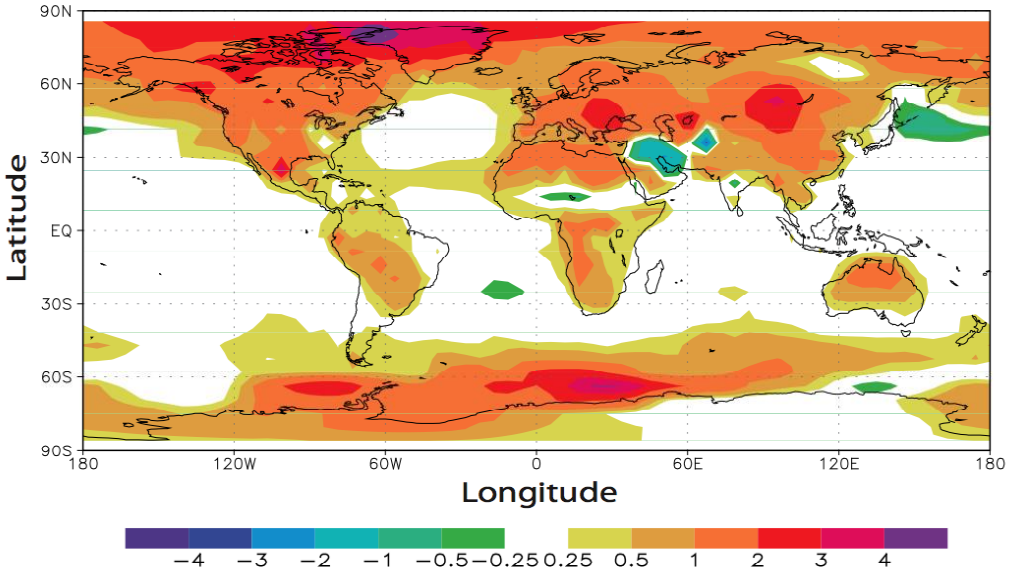

Figure 26: Difference of summer (JJAS) temperatures (in °C) between the mid-Holocene and present-day conditions as simulated by LOVECLIM.

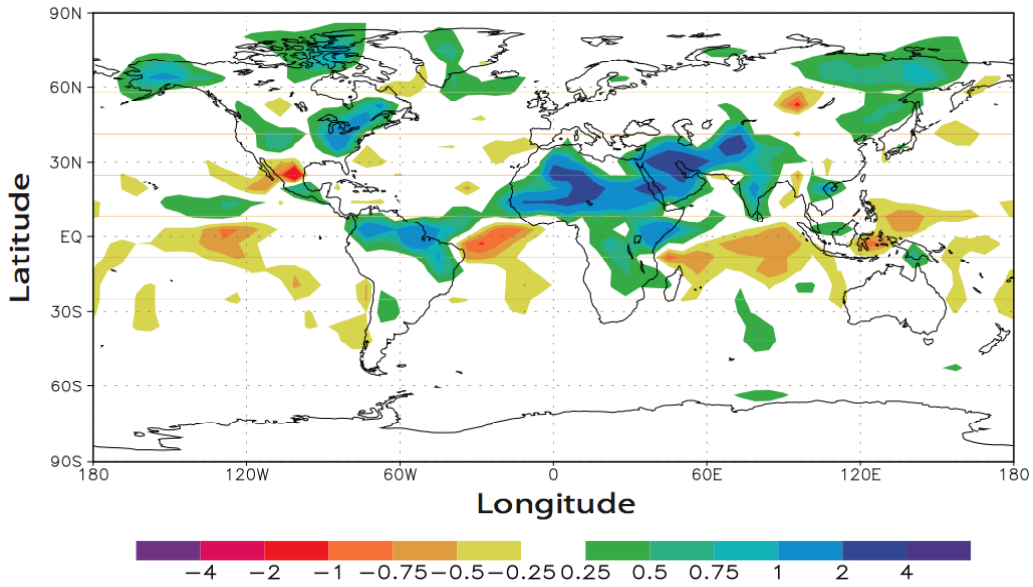

Figure 27: Difference of summer (JJAS) precipitation (in mm per day) between the mid-Holocene and present-day conditions as simulated by LOVECLIM.

The Last Glacial Maximum

In order to simulate the LGM climate, the orbital parameters are modified to the values corresponding to 21 kyr BP and CO_2, methane and N_2O concentrations are set respectively to 185 ppmv, 350 ppbv and 200 ppbv, following the PMIP2 protocol. In addition, the topography of the ice sheets and the geometry of the coastlines are imposed according to the ICE-5G reconstruction (Peltier, 1994). Those boundary conditions were not modified in the LGM simulations presented in the previous section (Coupling the NHISM to LOVECLIM). Moreover, LOCH and AGISM are not activated here. The simulation starts from pre-industrial conditions. After 4000 years, the climate reaches a quasi-equilibrium state characterized by a huge cooling of more than 25°C over the Laurentide and Fennoscandian ice sheets (Figure 28). The model also simulates a large cooling in the Southern Ocean associated with a large increase in sea ice extent. The cooling is stronger over the Atlantic than over the Pacific, in particular northwards of 45°N. In the tropics, the signal is weaker. In some regions, such as North Australia, the changes are very close to zero. Those results are similar to the ones of other simulations performed in the framework of the PMIP2 project (Braconnot et al., 2007), except in the Southern Ocean where the signal obtained in LOVECLIM is larger than the one given by the majority of the other models.

In the North Atlantic, the meridional overturning streamfunction is quite similar to the one simulated for present-day conditions (Figure 29), with a small decrease in magnitude nearly everywhere except between 40° and 60°N in the top 2000m of the water column, while it is generally accepted that the circulation associated with North Atlantic Deep Water was shallower at LGM than at present (Weber et al., 2007; Lynch-Stieglitz et al., 2007). In Figure 29, we also notice a reduction in the inflow of Antarctic Bottom Water in the Atlantic.

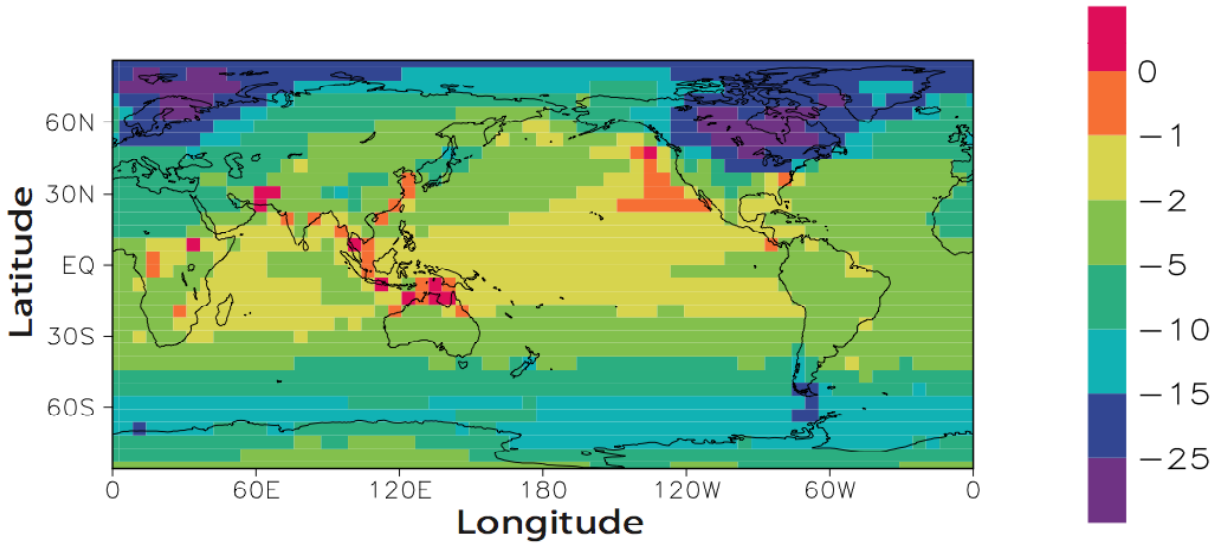

Figure 28: Difference in annual mean surface temperatures (in °C) between the LGM and the present-day conditions as simulated bu LOVECLIM.

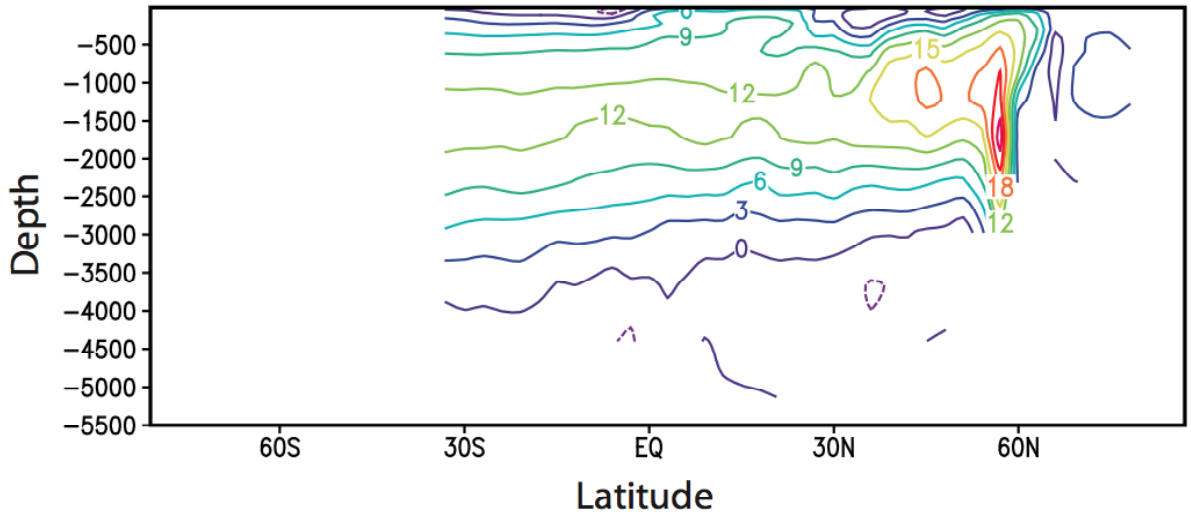

Figure 29: Meridional overturning streamfunction (in Sv) in the Atlantic as simulated buy LOVECLIM at the LGM.

2. Procedure to launch the experiment and to analyse the results

We set up a procedure designed to launch a large number of simulations and to compare them efficiently with observations. An atlas containing the main results of each component of LOVECLIM, i.e. the atmosphere, the ocean–sea ice, the vegetation, the carbon cycle and the ice sheets is automatically created at the end of each simulation. The various atlases contain maps, time evolutions as well as the anomalies with respect to a chosen experiment. In addition, the atlases can contain present-day climatologies. These climatologies are interpolated and plotted onto the corresponding model grid for comparison purposes. The bias, the correlation and the ratio of standard deviations between observations and model results are also

computed. The atlases are made available to the partners on the protected website. Scripts have also been produced to automatically run the off-line glacier melt algorithm (Raper and Braithwaite, 2006) subsequent to each LOVECLIM experiment in order to simulate the evolution of the area and volume of glaciers and small ice caps, and their contribution to sea level change.

3. Choice of the parameters

We select model parameter sets that produce reasonable simulations of the present-day climate and that lead to contrasted simulated responses to a scenario of doubling of CO_2 concentration and to freshwater hosing. Therefore, we identified several sets of **climatic** parameter values chosen within the range of uncertainty of those parameters (Table IV).

Table IV: The nine 'climatic' parameter sets selected for ASTER.

Name (1)	l2 (2)	l4 (2)	amplw (3)	explw (3)	albocef (4)	albice (5)	avkb (6)	CorA (7)
E11	0.125	0.070	1.00	0.3333	1.000	0	1.0 (8)	-0.0850
E21	0.125	0.070	1.00	0.4	0.900	0	1.5	-0.0850
E31	0.131	0.071	1.00	0.5	0.950	0	2.5	-0,0850
E41	0.131	0.071	1.10	0.5	0.900	0	2.5	-0.0850
E51	0.131	0.071	1.30	0.5	1.050	0.02	2.0	-0.0850
E12	0.120	0.067	1.00	0.4	0.900	0	2.0	0.0000
E22	0.125	0.070	1.00	0.4	0.900	0	1.5	-0.0425
E32	0.125	0.070	1.05	0.5	0.900	0	1.5	-0.0425
E52	0.125	0.070	1.30	0.5	1.000	0.02	1.5	-0.0425

(1) The names of the experiments have been designed to provide a quick overview of their main characteristics:
The first digit is related to the quasi-equilibrium response of the global mean surface temperature to a doubling of CO_2 concentration in the atmosphere, as obtained in a 1000-yr experiment:

1 corresponds to a climate sensitivity lower than 2.0°C;
2 corresponds to a climate sensitivity between 2.0 and 2.5°C;
3 corresponds to a climate sensitivity between 2.5 and 3.0°C;
4 corresponds to a climate sensitivity between 3.0 and 3.5°C;
5 corresponds to a climate sensitivity between 3.5 and 4.0°C.

The second digit is related to the response of the model to freshwater perturbation applied in the North Atlantic, which linearly increases at a rate of 0.1 Sv per 500 years (reaching thus a flux of 0.2 Sv after 1000 years);

1 corresponds to a decrease of less than 50% of the maximum of the MOC streamfunction after 1000 yr;
2 corresponds to a decrease of more than 50% of the maximum of the MOC streamfunction after 1000 yr.

The third and fourth digits are related to the response of the carbon cycle and the ice sheets to temperature perturbations, respectively.
(2) l2 and l4 are two parameters applied in the Rayleigh damping term of the equation of the quasi-geostrophic potential vorticity. l2 corresponds to the 500-800 hPa layer of the model, while l4 corresponds 200-500 hPa layer (see equation 1 of Opsteegh et al. (1998) and equation 11 of Haarsma et al. (1996)).
(3) The simple longwave radiative scheme of LOVECLIM is based on an approach termed the Green's function method (Chou and Neelin, 1996; Schaeffer et al., 1998). The scheme could be briefly represented for clear-sky conditions by the following formula for all the model levels:

Flw= Fref + FG(T',GHG')+ G1 * amplw*(q')**explw
where Flw is the longwave flux, Fref a reference value of the flux when temperature, humidity and the concentration of greenhouse gases are equal to the reference values, FG a function, not explicitly described here, allowing to compute the contribution associated with the anomalies compared to this reference in the vertical profile of temperature (T') and in the concentrations of the various greenhouse gases in the atmosphere (GHG'). The last term represents the anomaly in the longwave flux due to the anomaly in humidity q'. The coefficients Fref, G1 and those included in the function FG are spatially dependent. All the terms have been calibrated to follow as closely as possible a complex general circulation model longwave scheme (Schaeffer et al., 1998), but large uncertainties are of course related to this parameterisation, in particular as the model only computes one mean relative humidity between the surface and 500 hPa, the atmosphere above 500 hPa being supposed to be completely dry.
(4) The albedo of the ocean in LOVECLIM depends on the season and on the location. At each time step, it is multiplied by albcoef in the experiments analysed here. For a typical albedo of the ocean of 0.06, using a value of 1.05 for albcoef increases the value of the albedo to 0.063.
(5) The albedo of sea ice (albice) is based on the scheme of Shine and Henderson-Sellers (1985), which uses different values for the albedo of snow, melting snow, bare ice and melting ice. For thin ice, the albedo is also dependent on the ice thickness. If albice is different from zero in the experiments discussed here, the value of the albedo in the model is increased by albice for all the snow and ice types.
(6) As explained in detail in Goosse et al. (1999), the minimum vertical diffusion coefficient in the ocean follows a vertical profile similar to the one proposed by Bryan and Lewis (1979). The coefficient avkb is a scaling factor that multiplies the minimum values of the vertical diffusion at all depths. A value of avkb of 1 (1.5, 2, 2.5) corresponds to a minimum background vertical diffusivity in the thermocline of 10^{-5} m^2/s (1.5×10^{-5}, 2.0×10^{-5}, 2.5×10^{-5} m^2/s).
(7) As ECBilt systematically overestimates precipitation over the Atlantic and Arctic Oceans, it has been necessary to artificially reduce the precipitation rate over the Atlantic and Arctic basins (defined here as the oceanic area north of 68°N). The corresponding water is dumped into the North Pacific, a region where the model precipitation is too weak (Goosse et al., 2001). CorA corresponds to the percentage of reduction of the precipitation in the Atlantic.
(8) The Coriolis term in the equation of motion is computed in a totally implicit way because the semi-implicit scheme used for this term in Driesschaert et al. (2007) induced too much numerical noise. The older scheme has been kept here in experiment E11 only, in order to have an easier comparison with the former version of LOVECLIM (Driesschaert et al., 2007). Because of the larger implicit diffusion associated with this scheme, a lower value of the explicit diffusion is applied in E11.

For each parameter set, three initial experiments are carried out with LOVECLIM without interactive coupling with the ice sheet (AGISM) and oceanic carbon cycle (LOCH) models. A control run under pre-industrial conditions is performed until equilibrium to check that the present-day climate simulated with each selected model parameter set is in relatively good agreement with observations. The equilibrium state is then used as initial state for the next two experiments. Second, a simulation is performed in which the atmospheric CO_2 concentration is doubled, with an increase of 1% per year from the pre-industrial value (277.5 ppm), and is held constant thereafter (Figure 30, left). Third, an experiment is conducted in which the amount of freshwater added in the North Atlantic (20°-50°N) linearly increases from 0 to 0.1 Sv in 500 yr (i.e. a rate of 0.0002 Sv/yr) (Figure 30, right). Two main indices are selected to characterize the response of the model to the prescribed perturbation: the increase in global annual mean surface temperature after 1000 years in the

doubling CO_2 experiment from the equilibrium value and the percentage of decrease in the maximum value of the MOC streamfunction below the Ekman layer in the Atlantic Ocean after 1000 years in the water hosing experiment. For the nine climatic parameter sets, the model sensitivity to a CO_2 doubling ranges from 1.6 to 3.8°C (Table V). Figure 31 shows that the phase space (temperature, MOC) is rather homogeneously covered. For comparison, the GCMs used in the IPCC AR4 (Randall et al., 2007) have an equilibrium climate sensitivity ranging from 2.1°C to 4.4°C, with a mean value of 3.2°C. Our parameter sets almost cover this range, except for the largest climate sensitivities. On the other hand, in an intercomparison of Earth system models of intermediate complexity, Rahmstorf et al. (2005) showed that the width of the hysteresis curve, corresponding to changes in freshwater input, varies between 0.2 and 0.5 Sv. Amongst the models used in this intercomparison, those with three-dimensional ocean models (including ECBilt-CLIO, a former version of LOVECLIM, with general features similar to those of parameter set E11) display a sharp weakening of the North Atlantic MOC for a freshwater input of less than 0.3 Sv. In our sensitivity experiment, which uses a slightly different setup, the meridional overturning streamfunction displays a very strong reduction for freshwater input ranging from 0.2 Sv to 0.4 Sv.

It is reminded that the name of the experiments (Table IV and Table V) has been designed to provide a quick overview of their main features, i.e. response to a doubling of CO_2 concentration in the atmosphere (first digit) and the response to freshwater forcing in the North Atlantic (second digit). The third and fourth digits are related to the response to a perturbation of the carbon cycle and to the ice sheet, respectively.

It must also be underlined that the model parameter sets lead to different equilibrium states with respect to the MOC streamfunction (Table V). Moreover, the time decrease of the MOC streamfunction (in the water hosing experiment) shows several different patterns according to the model parameter sets (Figure 32, right). Indeed, for some model parameter sets (e.g., E11), the MOC streamfunction decreases almost linearly, while others (e.g., E12) exhibit a more abrupt reduction of the circulation. This should be kept in mind for the interpretation of future simulations.

Table V: Main features of the model parameter sets selected for ASTER.

Name	Climate sensitivity (1) (°C)	MOC sensitivity (2) (%)	Equilibrium MOC (3) (Sv)
E11	1.6	-20	28.2
E21	2.1	-32	25.9
E31	2.6	-20	25.2
E41	3.2	-17	24.7
E51	3.8	-38	23.5
E12	1.7	-55	17.5
E22	2.1	-62	23.3
E32	2.7	-55	20.5
E52	3.6	-58	20.0

(1) the increase in global annual mean surface temperature after 1000 years in the doubling CO2 experiment from the equilibrium value;
(2) the percentage of decrease in the MOC streamfunction after 1000 years in the water hosing experiment;
(3) equilibrium strength of the MOC streamfunction in the North Atlantic (Sv).

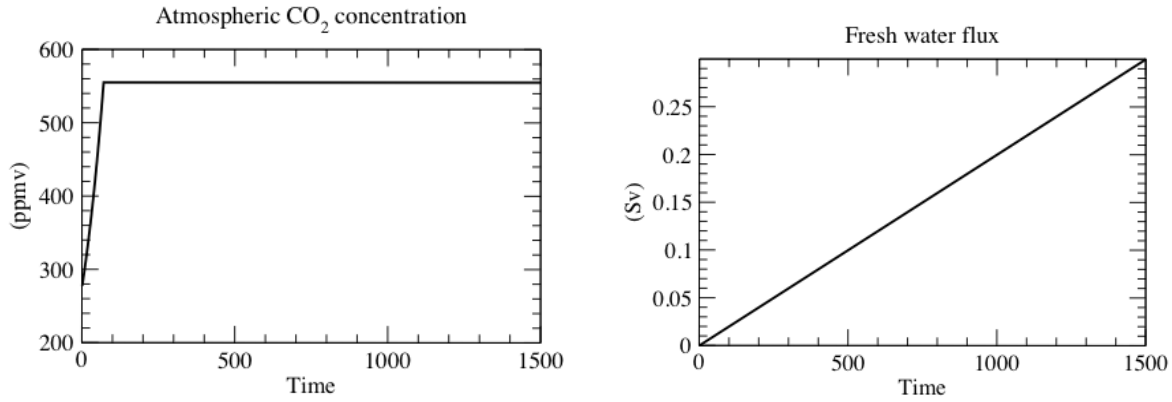

Figure 30: Perturbation scenarios. (Left): atmospheric CO_2 concentration; (right): freshwater forcing in the North Atlantic.

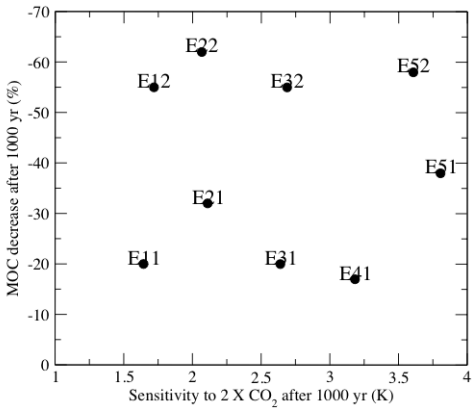

Figure 31: Distribution of the model parameter sets in the phase space (temperature, MOC).

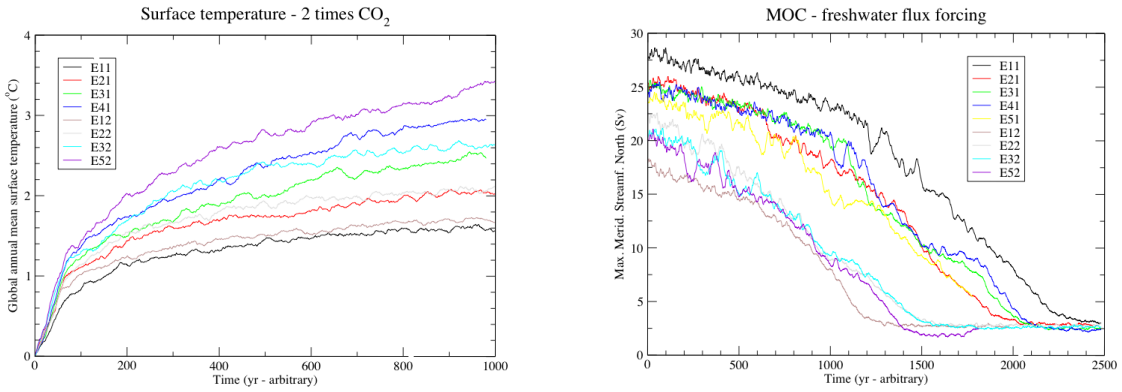

Figure 32: Time evolution of the model response according to the selected model parameter sets to the perturbation experiments. (Left): doubling of CO_2 concentration; (right): freshwater forcing. Temperature is presented as deviation from the initial value and MOC is the absolute value.

The key parameters for the **carbon cycle** are chosen among those with strong impact on the marine biogeochemical cycle and on the response of atmospheric CO_2 to emission scenario. The sensitivity experiments deal with the rain ratio and the vertical flux of POM in the ocean, on the one hand, and the continental vegetation fertilization effect, on the other hand. We review these three themes in the following,

present the choice of the parameter sets that are specified for the project experiments and conclude with an analysis of the carbon-climate feedback factor for some of the climatic parameter sets.

a) Ocean carbon cycle

The vertical flux of POM is one factor controlling the sequestration of CO_2 in the deep ocean. It is represented in the model by a power law z^{α}, with z the depth (Martin et al., 1987). Several distributions were proposed (Figure 33), which correspond to different ocean provinces or different estimation methods. The spread in the vertical POM flux profile could also be explained by differences in ecosystems (e.g., Klaas and Archer, 2002)

A shallow profile leads to a large export production by making nutrients more readily available in the upper ocean. But this may be accompanied by a less effective carbon sequestration in the deep ocean. We varied the α factor from -0.950 to -0.648 in LOCH and obtained the export production change summarized in Table VI. A variant of this formulation is found by associating different factors to different foodwebs. In this case, the flux of POM is modelled by associating a deep POM profile (less negative α) to the production supported by diatoms. The remaining of the production is due to organisms characterized by smaller sinking velocities, hence experiencing a shallower remineralization. With such a parameterisation the effect of a potential ecosystem change on the global carbon cycle is fully accounted for.

Table VI: Export productions (GtC/yr) obtained with different POM distribution profiles. Columns 6 and 7 correspond to the mixed formulation in which we differentiate between the flux law for diatoms (α = -0.750 and -0.500, respectively) and for other species (α =-0.950).

α	-0.950	-0.858	-0.750	-0.648	-0.750/ -0.950	-0.500/ -0.950
export pr. (GtC/yr)	6.5	6.2	5.7	5.3	6.2	5.5

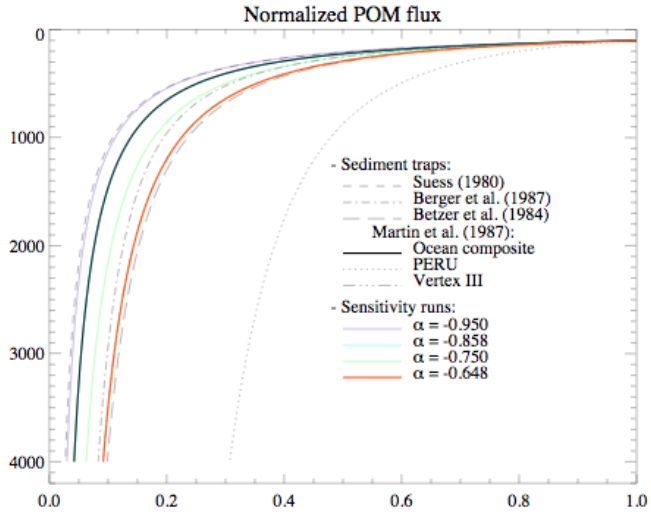

Figure 33: Illustration of POM flux with depth as from the literature. These fluxes have been normalized to their value at 100 m. The sensitivity experiments performed with LOCH correspond to the colour curves.

The buildup of calcium carbonate shells in the surface ocean results in a CO_2 source to the atmosphere, while dissolution constitutes a sink. The global value of the

calcium carbonate flux to the deep ocean is not well constrained. The rain ratio (defined as the ratio of inorganic carbon content over that of organic carbon in biogenic particles sinking to depth) exhibits a large range of values. The canonical global value of 0.25 has been revised downward as present-day estimates point towards a value around 0.1 (Archer, 2003; Najjar et al., 2007). Smaller values of this rain ratio are observed in more productive area where diatoms usually dominate the foodweb (Tsunogai and Noriki, 1991). At the phytoplankton level, the rain ratio in LOCH is mainly controlled by the assimilation of silica. Hence we modified the Ψ_{zoo} parameter, which represents the contribution of zooplankton in the precipitation of biogenic CaCO3. A larger value of this parameter implies a larger rain ratio. Two sets of parameters were determined (Table VII). With the first set, a global rain ratio of 0.07 is obtained, while the second set results in a value of 0.12. As LOCH contains a carbonate compensation mechanism, any rain ratio change also impacts the dissolution of calcium carbonate in the deep ocean. With the larger rain ratio, we obtain a downward calcium carbonate flux of 66 TmolC/yr, while dissolution amounts to 48 TmolC/yr. The lower rain ratio results in the precipitation of 38 TmolC/yr, with the dissolution of most of it (32 TmolC/yr).

Table VII: Model parameter sets for the carbon cycle. These parameters influence the continental vegetation fertilization effect (βg and βt; columns 2 and 3), the vertical flux of POM (α_{diatom} and α_{others}, columns 4 and 5) and the buildup of calcium carbonate shells (Ψ_{zoo}, column 6).

Carbon cycle parameter set	βg	βt	α_{diatom}	α_{others}	Ψ_{zoo}
1	0.14	0.50	-0.750	-0.950	0.10
2	0.36	0.36	-0.858	-0.858	0.22
3	0.14	0.22	-0.648	-0.648	0.22

The different parameters related to the ocean carbon cycle were tested interactively with the climate over the historical period as well as over the next centuries by forcing the model as described in the next section. The response of the atmospheric CO_2 remained well within that obtained with previous versions of the model. On short time scales, changes in the rain ratio or in the export production have a negligible impact on the atmospheric CO_2. For example, the atmospheric CO_2 partial pressure in 2100 AD changes by at most 7 ppmv across experiments performed with the different parameters for the rain ratio and the POM flux. This change is within the variability produced by the model and can't be ascertained yet.

b) Terrestrial biosphere

Previous works showed that in experiments performed over the 21st century, LOVECLIM predicts a larger atmospheric carbon uptake by the continental biosphere under climate warming than in experiments in which the radiative effect of the increasing concentrations of greenhouse gases is not accounted for (Plattner et al., 2008). This response is in contrast to other studies (Friedlingstein et al., 2006). Under climate warming, up to 70% of the response of the vegetation in LOVECLIM may be attributed to the fertilization effect, while the climate is responsible for the remaining 30% (Fichefet et al., 2007).

The effect of CO_2 on continental vegetation uptake is parameterised with the following formula:

npp=npp0 (1+ β ln (pCO2/pCO2ref)), where npp is the net primary production, pCO2 the CO_2 atmospheric pressure and npp0 and pCO2ref the npp and pCO2 for a

reference state, respectively. The fertilization effect constitutes a negative feedback on CO_2. Under ideal conditions, this effect may be quite large for some ecosystems (e.g., +25% to 60% for young trees under CO_2 doubling; +14% for a mixture of grassland and crops; Houghton et al., 2001). For natural forest ecosystems, the magnitude of the effect is poorly known and might be low or negligible. It appears that limitations including nutrients and water constrain the ecosystem response to CO_2 (Reich et al., 2006; Pitman and Stouffer, 2006). The standard value for β in VECODE is 0.36, i.e. the npp increases by 25% for CO_2 doubling. As there are different fertilization responses according to the ecosystem, we separated the fertilization effect in two terms: one for grass (βg) and one for forests (βt). In addition to the standard case (β = 0.36), two sets of parameters were determined that lead to a lower fertilization effect.

The impact of a change in the fertilization response may only be assessed under transient simulations with increasing atmospheric CO_2 concentration. In this purpose, we performed a transient experiment for each couple of β parameters starting from a pre-industrial equilibrium run and forcing the model with CO_2 emission pathway SP1000EC2100 (Plattner et al., 2008). Under this scenario, CO_2 emissions keep on increasing up to around 2050 AD, then stabilize and finally stop in 2100 AD. There were no other radiative forcings than CO_2 and no deforestation. The experiment started in 1749 AD and was carried on over 1000 yr, a control run with same duration being performed in parallel. The magnitude of the sensitivity of the model to CO_2 fertilization may be evaluated from Table VIII and

Table IX as well as from Figure 34.

Table VIII: Sensitivity of the CO_2 response to fertilization. Atmospheric CO_2 concentration in 2100 AD (column 4) and 2749 AD (column 5) as obtained from sensitivity experiments of the vegetation response to CO_2 under the emission scenario SP1000EC2100. The values of the fertilization factors for grass (βg) and for trees (βt) corresponding to each experiment are given in column 2 and 3, respectively.

βg	βt	Atm. CO_2 (ppmv)	
		2100 AD	2749 A.D
0.36	0.36	690	453
0.50	0.14	716	464
0.22	0.14	752	489

Table IX: Maximum value of the annual mean atmospheric CO_2 concentration and carbon-climate feedback factor *f* for the 3 carbon cycle parameter sets and climatic parameter sets 11 (columns 2 and 3), 31 (columns 4 and 5) and 52 (columns 6 and 7). Results from the transient simulations with atmospheric CO_2 forcing as in Figure 34. The maximum atmospheric CO_2 is from the experiment with climate change.

Climatic parameter set	11		31		52	
Carbon cycle parameter set	Max CO_2 (ppmv)	*f*	Max CO_2 (ppmv)	*f*	Max CO_2 (ppmv)	*f*
1	1146	0.92	1153	0.90	1146	0.91
2	1202	0.94	1221	0.92	1195	0.92
3	1315	0.95	1348	0.94	1318	0.93

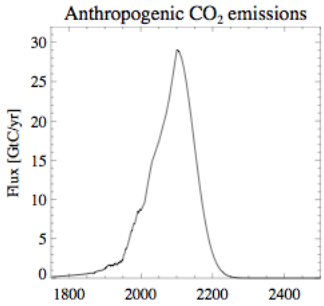

Figure 34: CO_2 emission scenario used to assess the sensitivity of the carbon cycle to the different carbon cycle parameter sets (see description of the scenario in the text). It includes both fossil fuel emission and fluxes related to land use changes.

c) Carbon cycle parameter sets and climate-carbon feedback

Table VII summarizes the combination of parameters in the global carbon cycle with low to high impacts on atmospheric CO_2. The parameters in set number 2 are identical to the standard version of LOCH used in former versions of LOVECLIM. The three parameter sets in Table VII are those used for the project experiments. The third digit in the experiment name refers to the carbon cycle parameter set, with relatively low (1), medium (2) or high (3) changes in atmospheric CO_2 in response to the same emission scenario.

We assess the sensitivity of the atmospheric CO_2 level to the carbon cycle parameter sets by performing a prognostic CO_2 experiment for each of these sets. This transient simulation starts from an equilibrium state corresponding to the conditions prevailing in 1750. It runs until 3000 and is constrained by changes in the Earth's orbital parameters (Berger, 1978) and in concentrations of greenhouse gases (GHGs) except CO_2. In addition, the model is forced by anthropogenic emissions of CO_2, including both fossil fuel and deforestation fluxes. Over the historical period (1750-2000), the GHG concentrations (except for CO_2) (Houghton et al., 2001) and carbon emissions (Marland et al., 2003; Houghton, 2003) follow the historical records. From 2000 to 2100, we use the SRES A2 scenario (Houghton et al., 2001) for both carbon emissions and GHG concentrations. After 2100, concentrations of all GHGs (except CO_2) are kept fixed to their 2100 values, while CO_2 emissions from land use are set to zero and fossil fuel emissions decrease according to a bell-shaped curve so that they reach zero a few decades after 2200 (Figure 34). In parallel, each experiment is accompanied with a control simulation in which all the forcings are maintained at their 1750 values with no anthropogenic CO_2 emission.

The three carbon cycle parameter sets lead to contrasted responses of the atmospheric CO_2 concentration to the identical forcing (Figure 35, left, and

Table IX). Maximal values of the atmospheric CO_2 concentration differ by up to 169 ppmv between carbon sets 1 and 3 (

Table IX). By year 2500, they still differ by 133 ppmv, i.e. a relative difference of about 11%. With parameter sets 1 and 2, the land CO_2 uptake outpaces the ocean uptake (Figure 35, middle), while the reverse happens with carbon set 3.

The parameters related to the continental vegetation processes explain up to 87% of the difference in atmospheric CO_2 response between the various experiments. On such time scales, changes in the rain ratio or in the export production have a much smaller impact on the atmospheric CO_2 level. The contribution of the rain ratio to the

maximum value of the atmospheric CO_2 concentration range is about 10%, while changes in remineralization depth explain about three percents. All together, the three parameter sets allow us to obtain a change in the carbon climate sensitivity (Frank et al., 2010) of the order of 7% (Figure 35, right).

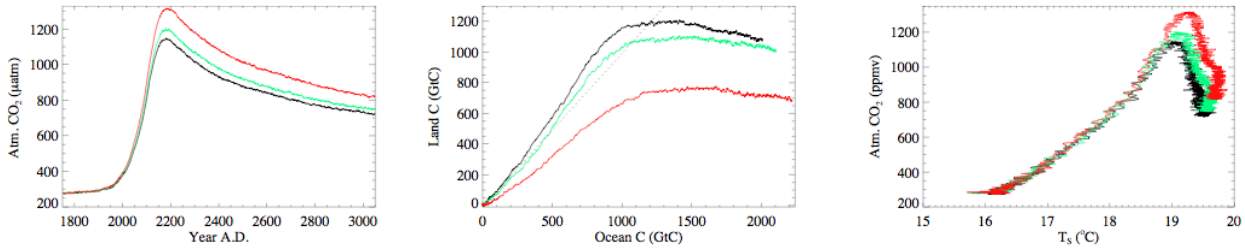

Figure 35: Evolution of the annual mean atmospheric CO_2 concentration (ppmv) with time (left), terrestrial carbon inventory versus ocean carbon inventory (both in GtC) (middle) and atmospheric CO_2 versus the global annual mean surface temperature (right) for the different carbon cycle parameter sets. The dashed line in the middle panel represents the 1:1 slope. Inventories are presented as anomalies with respect to the control run. The same color code is used in each panel, i.e. black for carbon cycle parameter set 1, green for set 2 and red for set 3. Climatic parameter set 11 is used here.

We further analysed the impact of different climatic parameter sets on the global carbon cycle by repeating the transient experiment with climatic parameter sets 31 and 52. In order to be able to evaluate the carbon cycle–climate feedback factor, that is a measure of the influence of climate change on the CO_2 uptake by the ocean and the terrestrial biosphere, we performed the experiment with exactly the same CO_2 emission scenario but in uncoupled mode, that is by switching off any radiative effect from greenhouse gases. Therefore, the coupled experiment includes the full climate and CO_2 interactions, while the uncoupled experiment represents the response of the system to increasing CO_2 levels in an unpertubed climate state (with the exception of the CO_2 fertilisation effect on the terrestrial vegetation).
The feedback factor *f* (Friedlingstein et al., 2001) is determined from the ratio of coupled to uncoupled atmospheric CO_2 concentrations. *f* is greater than 1 (positive carbon cycle–climate feedback) if the climate change leads to a reduced CO_2 uptake by the ocean and/or the terrestrial biosphere under climate change. The factor is less than 1 for a negative carbon cycle–climate feedback. In that case, lower atmospheric CO_2 levels are obtained in the coupled experiment for a given emission scenario.

The maximum value of the annual mean atmospheric CO_2 concentration does not change much among climatic parameter sets (

Table IX); larger changes are obtained with different carbon cycle parameter sets for the same set of climate parameter. The carbon cycle–climate feedback factor (

Table IX) increases with carbon sensitivity, decreases with climate sensitivity and remains lower than 1 in all cases. This negative feedback is explained by the increased carbon uptake of the terrestrial biosphere under climate change for high climate sensitivity (Figure 36, left). This increase compensates for the slower uptake by the ocean (Figure 36, middle) resulting from a reduced solubility under warming. The different responses from the terrestrial biosphere and the ocean are fully evidenced in Figure 36 (right). Larger climate sensitivities lead to larger carbon uptake by the terrestrial vegetation under climate change.

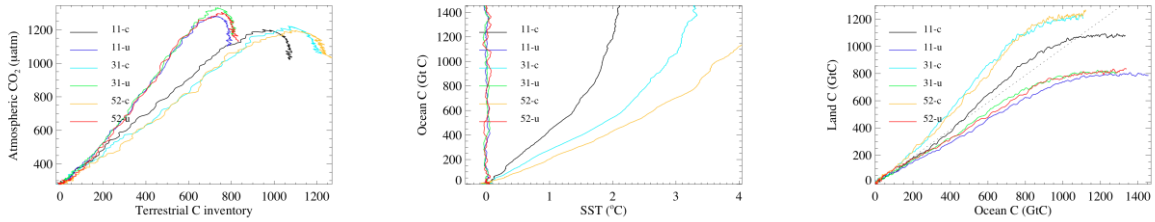

Figure 36: Evolution of the annual mean atmospheric CO_2 concentration (ppmv) with terrestrial carbon inventory (left), ocean carbon inventory versus the global annual mean sea surface temperature (SST) (middle) and terrestrial carbon inventory versus ocean carbon inventory (right) for the different climatic parameter sets in coupled (-c) and uncoupled (-u) modes. The dashed line in the right panel represents the 1:1 slope. Inventories are presented as anomalies with respect to the control run. The same color code is used in each panel. Carbon cycle parameter set 2 is used here. Results are presented for the period 1750 AD to 2350 AD.

For the **Antarctic and Greenland ice sheets**, we define three different parameter sets that control ice sheet sensitivity along the 'melting axis'. These three model versions of AGISM are referred to as 'low', 'mid', and 'high', expressed by the fourth digit in the experiment name respectively equal to 1, 2 or 3. The 'mid' model versions are identical to the standard version of AGISM used so far in LOVECLIM (Driesschaert et al., 2007; Swingedouw et al, 2008), which was tuned to best reproduce the current ice sheets and their assumed sensitivity to climate change. Table X gives an overview of the parameter values selected to this effect.
Surface melting and runoff in AGISM are linked to surface temperature through the positive degree-day factors and the standard deviation 'SIGMA' of temperature variations around the monthly mean in the degree-day model (Janssens and Huybrechts, 2000). In GISM, these parameters also influence the shape of the present-day ice sheet as surface runoff is an important ingredient of today's mass balance. The melting strength controls mainly the area of the ice sheet but not its central thickness. To compensate for the associated volume change in the reference state, it is therefore necessary to make adjustments for the ice stiffness and the ability to slide by making concomitant changes in the flow enhancement factor and the basal sliding parameter. The latter parameters mainly control the height-to-width ratio, and thus ice thickness, but hardly affect surface area. It is not possible to find a parameter set that satisfies present-day constraints on both ice thickness and surface area when the melting strength is modified. For the LOVECLIM sensitivity runs, the parameter sets were chosen in order to obtain the same Greenland ice volume for the present day. Likewise, the smaller ice sheet corresponding to the higher melting parameters also has the highest central ice thickness. The effect of the parameter choices for the three GISM runs is illustrated in Figure 37.

Table X: Parameter selection for three versions of AGISM along the melting axis.

Parameter	'low' sensitivity	'mid' sensitivity standard version	'high' sensitivity
AISM			
Basal melting below ice shelves [m/yr]	Constant at 0.25	According to net heat input below the cavity	Triple the amount of the 'mid' run
SIGMA (standard deviation melt model) [°C]	4.0	4.5	5.0
DDFS (positive-degree-day factor for snow melting) [m/yr/PDD]	0.75*0.003	0.003	1.25*0.003
DDFI (positive-degree-day factor for ice melting) [m/yr/PDD]	0.75*0.008	0.008	1.25*0.008
GISM			
ANEWG (enhancement factor/ multiplier for the rate factor in the flow law)	1.25*3.5	3.5	0.5*3.5
ASL (basal sliding parameter) [N^{-3} $year^{-1}$ m^{8}]	$1.25*10^{-10}$	$1.00*10^{-10}$	$0.5*10^{-10}$
SIGMA (standard deviation melt model) [°C]	4.0	4.5	5.0
DDFS (positive-degree-day factor for snow melting) [m/yr/PDD]	0.75*0.003/0.91	0.003/0.91	1.25*0.003/0.91
DDFI (positive-degree-day factor for ice melting) [m/yr/PDD]	0.75*0.008/0.91	0.008/0.91	1.25*0.008/0.91

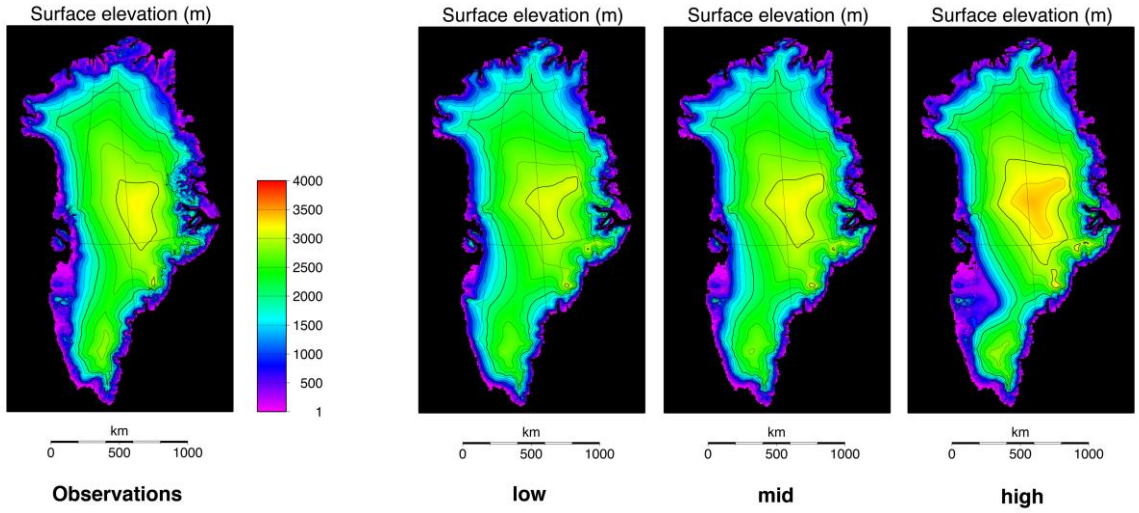

Figure 37: Modelled present-day geometries of the Greenland ice sheet corresponding to the 3 parameter sets chosen for the ASTER sensitivity runs. These all have the same ice volume at the present time. The picture at the left shows the observed surface elevation for comparison.

The complication of present-day reference state is absent from AISM as surface runoff is negligible under the current climate. Instead, code and parameter modifications that involve basal melting below ice shelves were chosen to only influence changes with respect to the present-day reference run. This enables to use the same initial start-up files for all three sensitivity versions of AISM. The basal melting rate below the ice shelves arguably constitutes the most important environmental forcing for the Antarctic ice sheet in case of moderate warming. However, its sensitivity to oceanic conditions is subject to very large uncertainties, as is its spatial distribution below the respective ice shelves (e.g., Rignot and Jacobs, 2002). Therefore, our 3 runs vary from a case with constant basal melting ('low') to a case in which the oceanic heat input is tripled ('high'), cf. Table X.

To assess the influence of the 3 parameter sets on the behaviour of AGISM, schematic off-line experiments were performed under prescribed forcings, which mimic 4xCO_2 conditions from earlier runs with LOVECLIM for a duration of 3000 years (Driesschaert et al., 2007). The main outcome of those experiments are summarized in Figure 38 to Figure 40 and set the stage for the parameter variation runs over the third millennium.

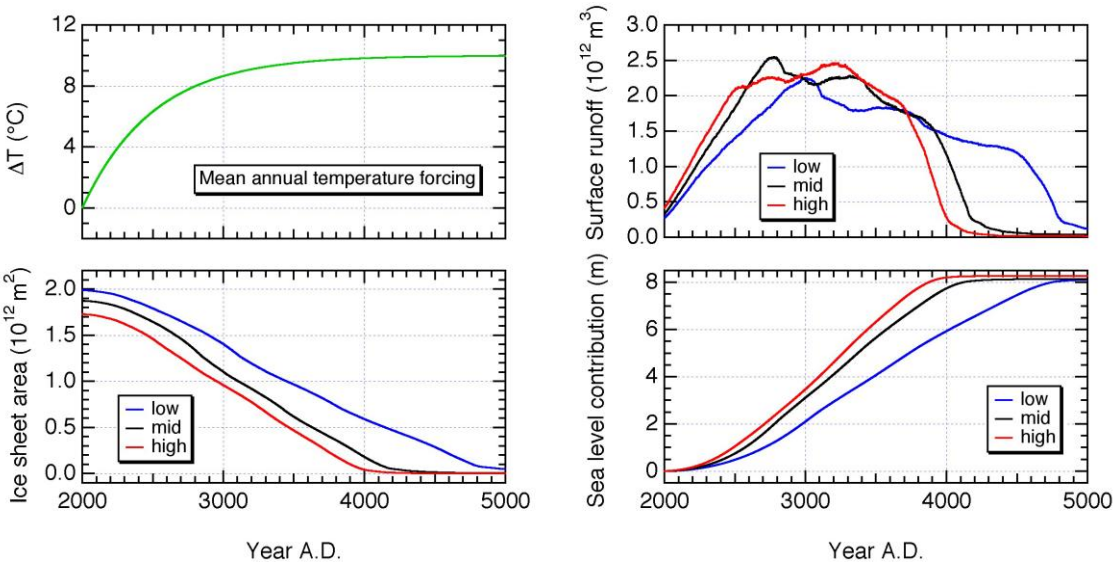

Figure 38: Evolution of several large-scale variables of the Greenland ice sheet in the 3 parameter sensitivity runs over the next 3 millennia.

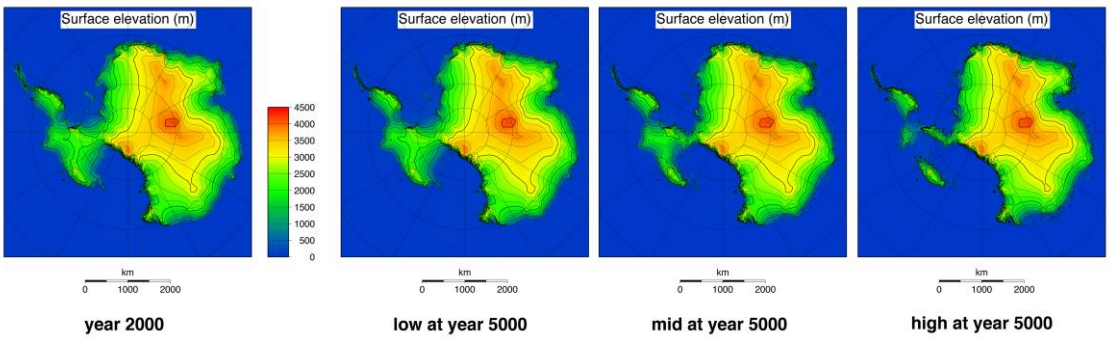

Figure 39: Antarctic ice sheet geometries after 3000 years of 4xCO_2 conditions under the low, mid and high parameter sets. For comparison at the left is the initial condition at the year 2000.

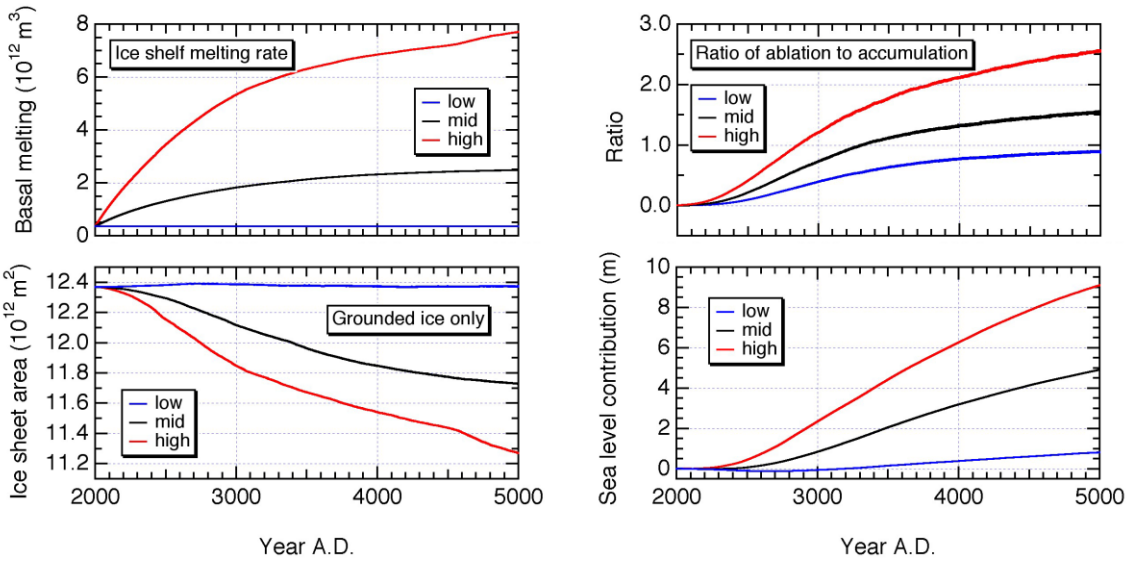

Figure 40: Evolution of several large-scale variables of the Antarctic ice sheet for the 3 parameter sensitivity runs over the next 3 millennia.

For a warming reaching 10°C over Greenland, the ice sheet is found to entirely waste away over a period of between 2000 and 3000 years, in accordance with previous results (Huybrechts and de Wolde, 1999). The melting is entirely driven by surface runoff of up to 10 times larger than the current amount peaking at about 0.08 Sv between 800 and 1200 years after the warming started. The total sea level rise is near to 8 m, with maximum rates of between 40 cm per century (low sensitivity) and 65 cm per century (high sensitivity).
Under similar 4xCO_2 conditions over Antarctica, ice sheet retreat is first controlled by increased basal melting rates up to an average of 3 m/year in the high sensitivity experiment. Eventually, surface runoff takes over as the main wastage mechanism. After about 800 years of sustained warming in the high sensitivity experiment, a negative surface mass balance causes continued ice sheet retreat, which is further strengthened by the elevation-mass balance feedback. In that case, the West Antarctic ice sheet disintegrates entirely and the East Antarctic ice sheet starts to retreat on land after 3 millennia, causing a total sea level rise in excess of 9 m. A stable evolution towards a new steady state under a 4xCO_2 scenario seems only possible for the low sensitivity parameter set.

4. Description of the experiments

So far (section B.3), several parameter sets were identified that yield different responses of the LOVECLIM model, although the present day simulated climate remains within the range of observations. We distinguish (1) nine parameter sets inducing different sensitivities of the climate to changes in atmospheric CO_2 concentration and different responses to changes in freshwater flux in the North Atlantic [climatic parameters], (2) three parameter sets inducing different responses of the carbon cycle model [carbon parameters] and (3) three parameter sets inducing different responses of the ice sheets (Greenland and Antarctica) to temperature changes [ice sheet parameters]. All experiments that are described in this section are performed with a sub-set of the 81 possible combinations of these parameter sets.
The characteristics of the model with each parameter set and, in particular, its ability to simulate past climates are studied with several experiments. A letter indicating the

type of the simulation (e.g., "M" for last millennium simulations) differentiates the experiments. Since LOVECLIM is run in two different model configurations (excluding and including the dynamically coupled ice sheet model AGISM), we use the convention to double the experiment type letter in the latter case (e.g., "FF" for future experiments including the ice sheets).
Each experiment type consists of a series of simulations with different forcings that are named with a four letter word. Two control experiments are routinely performed with either constant CO_2 concentration (CCTL) or prognostic CO_2 concentration (ECTL) and otherwise constant forcing. In other experiments, the variations of atmospheric CO_2 concentration or emission of CO_2 may be prescribed.

Sensitivity experiments (types E and EE)

First, a series of schematic sensitivity experiments are performed starting from a pre-industrial control climate. The sensitivity of the climate model to changes in atmospheric CO_2 concentration is evaluated with simulations where the atmospheric CO_2 concentration is doubled with a 1% increase per year, reaching twice the pre-industrial value of 277.5 ppmv after 70 years and held constant thereafter (2CO2, Figure 30, left). The sensitivity of the MOC streamfunction to changes in freshwater flux is tested with experiments where an anomalous freshwater flux of 0.1 Sv and 0.2 Sv (FW01, FW02) is instantaneously added in the North Atlantic (20-50°N) in addition to experiments with linearly increasing freshwater input from 0 to 0.2 Sv in 1000 years (HYST). Control simulations (CCTL and ECTL) are performed in both cases. The initial conditions for these simulations are obtained from equilibrium simulations under pre-industrial forcing (insolation and CO_2 concentration).
In the case of the fully coupled LOVECLIM simulations (EE), a 500-yr spinup is run before the sensitivity experiments themselves in order to reduce the model coupling drift. The initial state of the ice sheet model for the pre-industrial climate is set according to stand-alone AGISM simulations. Since AGISM needs present-day reference climate states for the computation of anomalies in temperature and precipitation over the ice sheets, an ensemble of three members of simulations including the years 1970-2000 is performed. These simulations are similar to the last millennium experiments (MM, Conc) as described below, but because reference climate states are also needed for these runs, they are updated in an iterative procedure.

Last millennium experiments (types M and MM)

The climate of the last millennium is simulated for each of the 27 combinations of parameter sets involving climatic and carbon cycle parameters. All the simulations start at 500 AD from an equilibrium state at that time. They are run in transient mode until 2000 AD (the procedure described here is similar to the one used for the evaluation of the model performance for present-day conditions; see section B.1). The variations of the atmospheric CO_2 concentration as reconstructed over the historical period are prescribed for the Conc simulations. These simulations also take into account land use changes related to human activities (percentage of crops; Ramankutty and Foley, 1999). On the contrary, the atmospheric CO_2 concentration is modelled (prognostic) in the simulations with prescribed emissions of CO_2 from fossil fuel burning (Efor). Moreover, in those simulations, land use changes are prescribed, which induce changes in CO_2 emission. A second prognostic CO_2 experiment (EMIS) is also realised with fossil fuel emissions as in Efor but in which emissions from deforestation are prescribed after Houghton and Hackler (2002). In the EMIS

experiments there is no land use change scenario. At last, two control runs, with constant forcings as in 500 AD, are also performed with either constant CO_2 concentration (CCTL) or prognostic CO_2 concentration (ECTL). In addition to the atmospheric CO_2 concentration, either prescribed or computed by the model, the transient simulations are forced by the volcanic activity (Crowley, 2000), the solar activity (Muscheler et al., 2007) and greenhouse gas (except CO_2) concentrations (Houghton et al., 2001). The initial conditions for LOCH, VECODE, ECBilt and CLIO are obtained from a 1500-yr long equilibrium simulation with prescribed present-day ice sheets under forcings at 500 AD. In case of MM simulations, the initial conditions for the Greenland and Antarctic ice sheets are obtained from a run of AGISM in uncoupled mode covering the last glacial-interglacial cycles and the Holocene. The Greenland and Antarctic ice sheets are fixed to their present-day values in M simulations (i.e. AGISM is not coupled with LOVECLIM).
The scenario of historical changes in global land cover developed by Ramankutty and Foley (1999) starts only in 1700. We hypothesize that the land cover changes evolved linearly from its natural state in 500 AD to the estimated values in 1700 AD. Moreover, we assume that croplands replace only forests as long as there is a forest fraction. Deserts and forests (except for the part replaced by crops) are keeping their original (500 AD) extents. Recently, Pongratz et al (2008) estimated the extent of cropland and pasture from 800 AD to 1700 AD. We decided to keep our linear scenario of land use changes, which is actually not too much different from the Pongratz et al (2008) scenario.
The MM simulations (simulations of the last millennium climate with the fully coupled LOVECLIM) are only performed for the Conc and CCTL experiments in order to provide initial state for the FF-experiments (simulation of the future climate) as described below. They start with the same initial conditions as the M simulations for the ocean, the atmosphere and the carbon cycle and include initial conditions for the ice sheets that are obtained from the AGISM stand-alone simulation.

Holocene experiments (type H)

The purpose of the Holocene experiments is to study the ability of the model to simulate the climate of the last part of the last deglaciation, which is characterized by changes in vegetation cover, mostly in the tropical regions, and by considerable changes in the freshwater forcing. Several simulations are conducted over the Holocene.
In a first set of experiments, a transient simulation is run from 8 kyr BP to year 2100 AD, starting from a quasi-equilibrium obtained for 8 kyr BP. In these simulations, LOCH and AGISM are not interactively coupled. The quasi-equilibrium simulation is carried out with orbital parameters and greenhouse gas concentrations corresponding to the 8 kyr BP conditions. The CO_2, CH_4 and N_2O concentrations are maintained constant at values of 260.6 ppmv, 701.5 ppbv, 267.4 ppbv, respectively. Between 8 kyr BP and 1 AD of the transient simulations, the only forcings applied are the insolation and greenhouse gas ones as in Renssen et al. (2005). After 1 AD, in addition to those forcings, the variations in the total solar irradiance, the impact of big volcanic eruptions as well as the role of land use changes (starting in 1000 AD) and of the increase in aerosol load (starting in 1850 AD) are taken into account as in the last millennium (Conc) experiments described here above. For the 21st century, the forcing follows the scenario IPCC Special Report on Emissions Scenarios (SRES) B1, in which the CO_2 concentration reaches 540 ppmv in 2100 AD. In all those experiments, the ice sheet topography is kept the same as today. For the early

Holocene, sensitivity experiments performed with an earlier version of the model (Renssen et al., 2005) have shown that neglecting the influence of the remnant of the Laurentide ice sheet has only a marginal, regional impact at that time and this approximation should thus not strongly influence our results.
In a second set of experiments, the importance of freshwater fluxes in the North Atlantic during the early Holocene, in particular the runoff of meltwater from the Laurentide ice sheet that accumulated in huge proglacial lakes south of the ice sheet is investigated (in line Wiersma and Renssen (2006)) by studying the response of LOVECLIM to freshwater fluxes into the Labrador Sea. These simulations refer to a cooling event, mostly recorded in the Northern Hemisphere that occurred approximately 8.2 kyr BP. The strongest evidence for the event comes from the North Atlantic region. A large temperature anomaly is recorded in the Greenland ice cores. It is also present in sedimentary records in the North Atlantic as well as over the adjacent continents (Alley et al., 1997; Alley and Ágústsdóttir, 2005). The estimated cooling over Europe is about 0.5-1°C. Moreover, there is evidence for a wetter climate over Europe during that event, related with the southward shift of the wetter westerlies (see Wiersma and Renssen (2006) for a review). Simultaneously, the collapse of the remnant Laurentide ice sheet and the drainage of large proglacial lakes that collected meltwater delivered huge amount of meltwater into the Hudson Bay (e.g., Clarke et al., 2004).
The simulations start from an early Holocene equilibrium state, i.e. the boundary conditions are adjusted to their 8.5 kyr BP values. The atmospheric greenhouse gas concentrations are taken from Raynaud et al. (2000) (CO_2 = 261 ppbv, CH_4 = 650 ppbv and N_2O = 270 ppbv) and the orbital parameters and insolation are computed as in Berger (1978). LOVECLIM is not coupled with the ice sheet model (AGISM) but we account for the remnant Laurentide ice sheet by lowering surface albedo and increasing elevation of the concerned grid cells (Peltier, 1994), following Wiersma et al. (2006). The model is first run until quasi-equilibrium with these boundary conditions (EH simulations). Then, we perturb this simulation by releasing an additional freshwater pulse into the Labrador Sea (ECBilt grid cell centred around 53.5°N and 50.5°W) (EHF simulations). In our simulations, a total amount of $1.63\times10^{14}m^3$ of water is released over two years and the simulation is then continued with no additional freshwater flux. It must be noted that there is a large uncertainty in the amount of freshwater involved in the 8.2 kyr event. It varies from less than 1 up to $5\times10^{14}m^3$ (see Wiersma et al (2006) for a review). Moreover, the drainage duration is not precisely known. All these experiments are performed with six parameter sets, i.e. 112, 122, 312, 322, 512 and 522.

Third millennium experiments (type FF)

The major goal of this project is to provide a range of plausible scenarios for future climate and sea level evolution. Therefore, simulations are performed over the next 1000 years (2000 AD to 3000 AD) with a wide range of model sensitivities (parameter sets) and three commonly used SRES scenarios (B1, A1B, A2) that have been prolonged after 2100 AD. Two configurations are used: constrained atmospheric CO_2 concentrations (Figure 41, left) and prescribed fossil fuel emissions (Figure 41, right). In both cases greenhouse gas concentrations other than CO_2 are maintained at their levels as in 2100 AD until the year 3000 AD. Similarly, we use a scenario until 2100 AD and then the value at 2100 AD until the year 3000 AD for the sulphate radiative forcing. Land use changes and associated carbon fluxes are computed with respect to the crop-area fraction as defined in the forcing file for 1992

AD. These simulations are the continuation of the M and MM simulations over the last millennium. Only the Conc, Efor, ECTL and CCTL simulations are performed for the future climate.

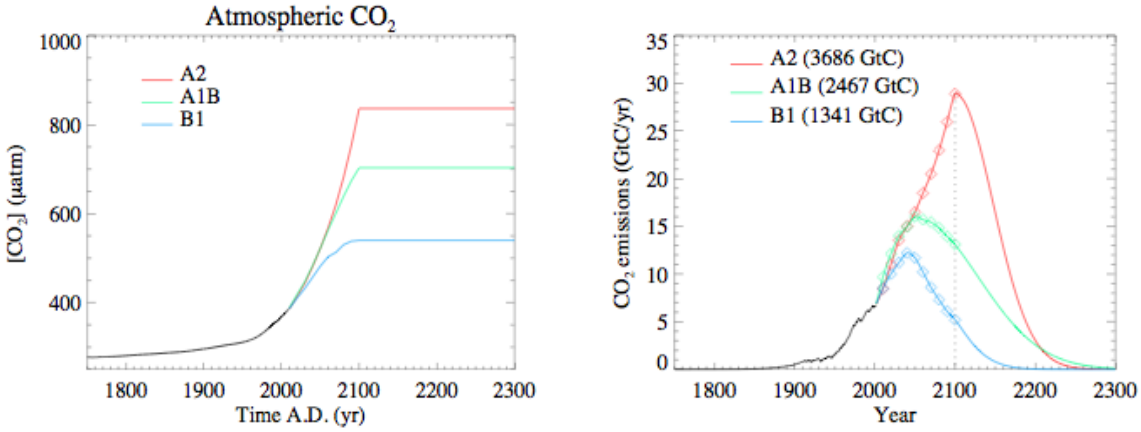

Figure 41: CO_2 concentrations (left) and CO_2 emission (right) scenarios used to perform experiments over the next millennium. In the case of Conc simulations, CO_2 concentration after 2300 AD is maintained at its value in 2100 AD. The emissions scenarios (Efor simulations) follow the fossil fuel emission scenarios from the IPCC TAR (SRES-marker; Annex 2, IPCC, 2002) up to the year 2100 AD. After this date, they were prolonged with the help of a logistic function constrained with the total amount of fossil fuel burned (number in parenthesis to the right of scenario labels). Emissions cease after 2300 AD.

C. Results

1. The pre-industrial climate

An equilibrium experiment under pre-industrial conditions is performed using each of the nine selected climatic parameter sets. For these simulations, LOVECLIM is coupled neither with the ice sheet model (AGISM) nor the oceanic carbon cycle model (LOCH). The various forcings are kept constant. No volcanic eruption is considered. The greenhouse gas concentrations are kept to their 1750 AD values. Simulated climatic variables are compared to recent observations. The model-data comparison mostly puts forward the systematic biases of the model that are present with almost all parameter sets (e.g., Figure 42) as well as in other versions of the model (Goosse et al., 2001) rather than the slight differences between pre-industrial and present-day climates. The purpose of this comparison is to demonstrate that all the parameter sets lead to reasonable mean states but not to analyse in detail model performance for the mean climate. The differences between recent and pre-industrial climates are thus of minor importance here.

For all the parameter sets, the globally averaged, annual mean surface temperature is slightly too high, varying between 15.8 and 16.4°C, the main overestimation being observed at low latitudes (Figure 42a). LOVECLIM underestimates precipitation in the equatorial regions and overestimates it around 20°S and 30°N (Figure 42b). This model feature is a consequence of the quasi-geostrophic approximation, which induces difficulties to simulate a correct Hadley cell (Renssen et al., 2002); it is not significantly modified by any parameter set. Mid- and high latitude precipitation is more properly represented than equatorial precipitation, independent of the parameter set. The model overestimates the tree fraction (Figure 42c) at all latitudes, whatever the parameter set. This overestimation is mostly at the expanses

of the grass fraction, except in the mid-to-high southern latitudes (southern South America), where the cold desert area is underestimated. This feature of the model is related with the overestimation of temperature over land and overestimation of precipitation in the tropics. The maximum of the strength of North Atlantic MOC (i.e. the annual mean value of the maximum of the North Atlantic meridional overturning streamfunction below the Ekman layer) varies between 17 and 28 Sv. These values lie within the range given by GCMs (e.g., Dixon and Lanzante, 1999; Gent, 2001). The sea ice extent in the Northern Hemisphere varies seasonally from a maximum between 14.3 and 15.1×10^6 km^2 in March to a minimum between 6.7 and 9.3×10^6 km^2 in September, while observations (average value between 1979 and 2000; Comiso and Nishio, 2008) give a maximum of less than 16×10^6 km^2 and a minimum of 6.9×10^6 km^2.

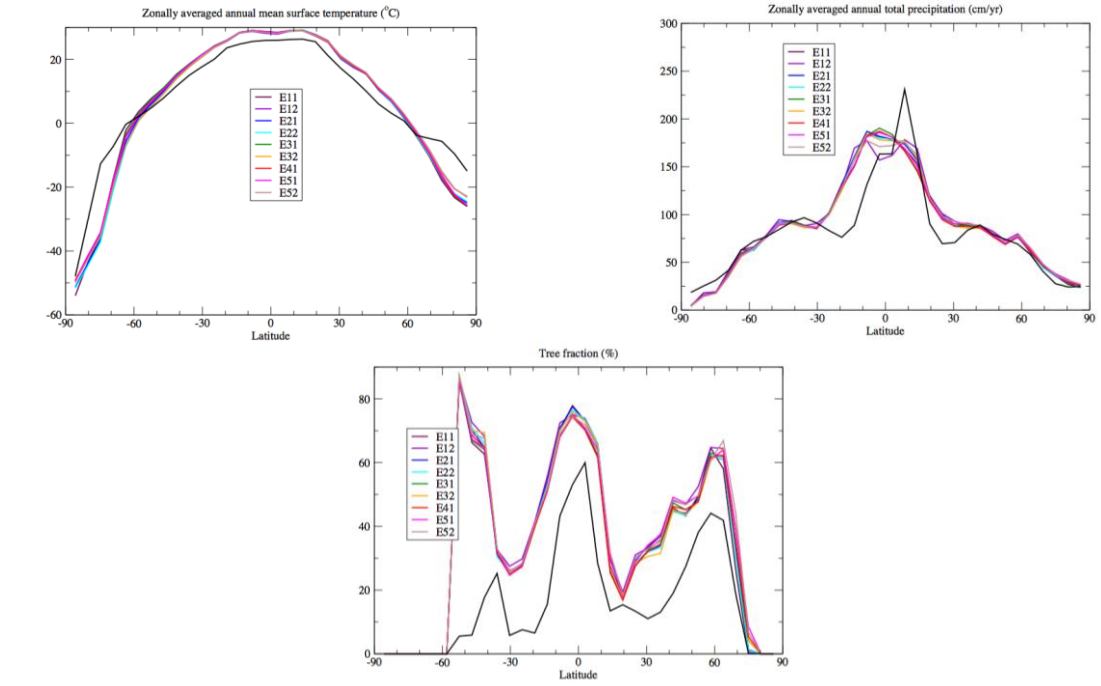

Figure 42: Zonally averaged surface temperature (°C), annual mean precipitation (cm/yr), and tree fraction (%) simulated for the pre-industrial time according to the nine climatic parameter sets (colour lines). Observations are in black (Brohan et al. (2006) for temperature; Xie and Arkin (1996, 1997) for precipitation ; http://www.monsoondata.org:9090/dods/gswp/grid/fixed/classfrac_igbp for tree fraction). Carbon cycle parameter set 2 is used here.

2. Changes in the coupled model state when including the ice sheets

Climate sensitivity

To characterise the response of the model to the prescribed CO_2 forcing, we define the index CS_{eff}^{1000} as 'effective climate sensitivity' (Murphy, 1995; Cubasch et al., 2001) after 1000 years in experiment 2CO2. This definition runs in parallel with the IPCC AR4 definition (Randall et al., 2007), taking into account a specific cryospheric time scale of 1000 years, when both major ice sheets are still present and contribute to climate feedbacks. This choice is guided by the fact that the two other IPCC AR4 definitions of 'equilibrium climate sensitivity' (ECS) and 'transient climate response' (TCR) (Cubasch et al., 2001; Randall et al., 2007) are not well suited either for our

models including dynamic ice sheets (ECS) or for the time scale under consideration here (TCR). We compute CS_{eff}^{1000} following the notation of Gregory et al. (2002):

$$CS_{eff}^{1000} = Q_{2x} / \lambda,$$

(6)

where $Q_{2x} = 3.78 Wm^{-2}$ is the radiative forcing that results from a doubling of the CO_2 concentration in our model and λ can be calculated as

$$\lambda = \frac{Q_{2x} - F^{1000}}{\Delta T^{1000}}.$$

(7)

F^{1000} and ΔT^{1000} are the ocean heat uptake in Wm^{-2} and the surface temperature change at year 1000 of our model experiments, respectively. The resulting CS_{eff}^{1000} is consequently a measure of the strength of the feedbacks active on millennial time scales, which is the desired outcome. Note that the latent heat transfer associated with ice sheet melting is an order of magnitude lower than the ocean heat uptake and is not taken into account here.

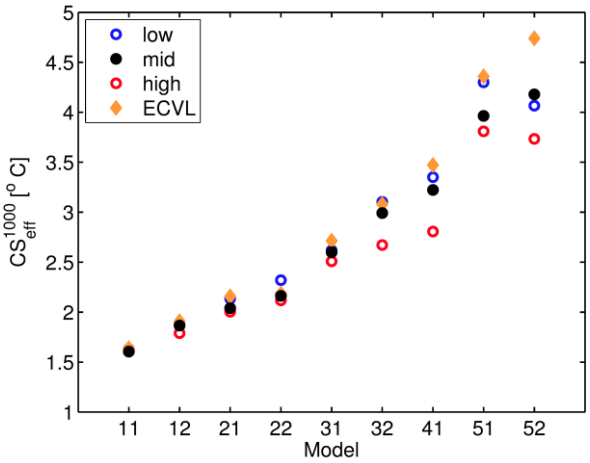

Figure 43: Effective climate sensitivity after 1000 years (CS_{eff}^{1000}) of ECVL with fixed ice sheets (orange diamonds) and LOVECLIM with fully interactive Greenland and Antarctic ice sheet models (circles) with high (red), medium (black) and low (blue) ice sheet sensitivity.

The equal spread of climate sensitivities of the models over a wide range was originally designed by adjustment of parameters of the uncoupled climate model. An important new finding is that the 'effective climate sensitivity' CS_{eff}^{1000} is generally lower when the ice sheets are included (Figure 43). The strength of this mitigation effect scales with the effective climate sensitivity and furthermore depends on the ice sheet sensitivity: all high ice sheet sensitivity models show the lowest CS_{eff}^{1000} of the three ice sheet parameter sets. The mitigation of temperature changes in LOVECLIM is ultimately a negative feedback effect due to increasing freshwater fluxes from the melting ice sheets that affect the heat exchange in the ocean and at the sea-air interface. Stronger temperature response and stronger melting of the ice sheets both lead to stronger freshwater fluxes to the ocean and therefore increase the strength of the mitigation effect. In the Northern Hemisphere, freshwater fluxes from the melting Greenland ice sheet cause a weakened MOC, which in turn leads to lower temperatures in the northern North Atlantic. The lower temperatures allow for a larger sea ice cover with higher albedo and reduced ventilation, which feeds back on the relative cooling. For Antarctica, freshwater fluxes cause a shallow halocline,

weakening of deep water formation, reduction of vertical heat exchange in the ocean and a larger sea ice cover (Swingedouw et al., 2008). The effect is relatively strong in model versions with high climate sensitivity due to the relatively large polar amplification of LOVECLIM. We suggest that it is of great importance to be aware of this dynamical effect when including ice sheet models into global Earth system models, and also when using models where interactions with the ice sheets are not considered.
Including the ice sheets in our model leads to ice-climate interactions that are otherwise not present, and this already in the control runs without greenhouse warming. One example is a stronger MOC streamfunction variability due to feedback with freshwater fluxes from the Greenland ice sheet (Figure 44). When the ice sheet model is first coupled, additional freshwater fluxes from the Greenland ice sheet lead to a MOC streamfunction reduction, with consequences for the meridional heat transport and heat exchange between atmosphere and ocean. As a result, a local cooling over the northern North Atlantic develops which feeds back on Greenland temperatures and ultimately on the melting rate.

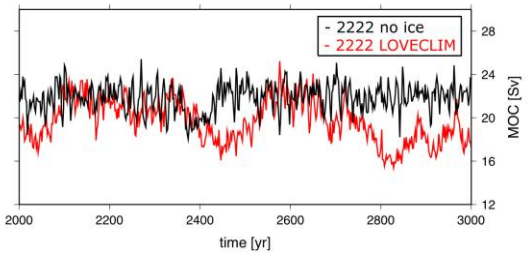

Figure 44: MOC variability in unforced control runs without (black) and with (red) coupled ice sheets. Including the ice sheets introduces variability on centennial time scales due to interactions between Greenland ice sheet melting and the MOC.

Because freshwater fluxes from the ice sheets to the ocean play an important role for the evolution of climate, we analyse the response of the model to artificial freshwater fluxes in the northern North Atlantic in the fully coupled model. As mentioned in the experiment description, we add instantaneously freshwater fluxes of 0.1 Sv and 0.2 Sv (FW01 and FW02) and analyse the maximum of the MOC streamfunction after 1000 years. This guarantees a more stable response compared to transient increasing freshwater forcing. These experiments have also been carried out for the model including and excluding the ice sheets, for comparison.
In all experiments, the MOC is weaker after 1000 years of freshwater forcing compared to the initial state (Figure 45). The reduction in overturning strength depends on the model MOC sensitivity and the amplitude of the forcing, with 0.2 Sv (FW02) yielding a considerably stronger response than 0.1 Sv (FW01). Two important differences can be observed when the ice sheets are included in the model than when they are excluded (filled symbols in Figure 45, left). First, the initial MOC streamfunction strength at year 0 of the experiments is weaker in models including the ice sheets. This is readily explained by meltwater fluxes from the ice sheets, which already influence the overturning throughout the 500 years spinup experiment before. Second, the total MOC streamfunction response after 1000 years is in most FW02 experiments up to 10% lower when the ice sheets are included (Figure 45, right). The reason for this reduction of MOC sensitivity lies within a negative feedback of MOC streamfunction weakening on Greenland meltwater fluxes. Local cooling over the Greenland ice sheet of several degrees in response to a reduction of MOC

streamfunction strength considerably weakens the melting and freshwater fluxes to the ocean. For weak anomalous freshwater forcing (FW01), the additional meltwater fluxes from the ice sheet are in some cases (models 12, 21, 41, 51) just enough to cross a threshold and lead to considerably higher MOC streamfunction reduction than without ice sheets.

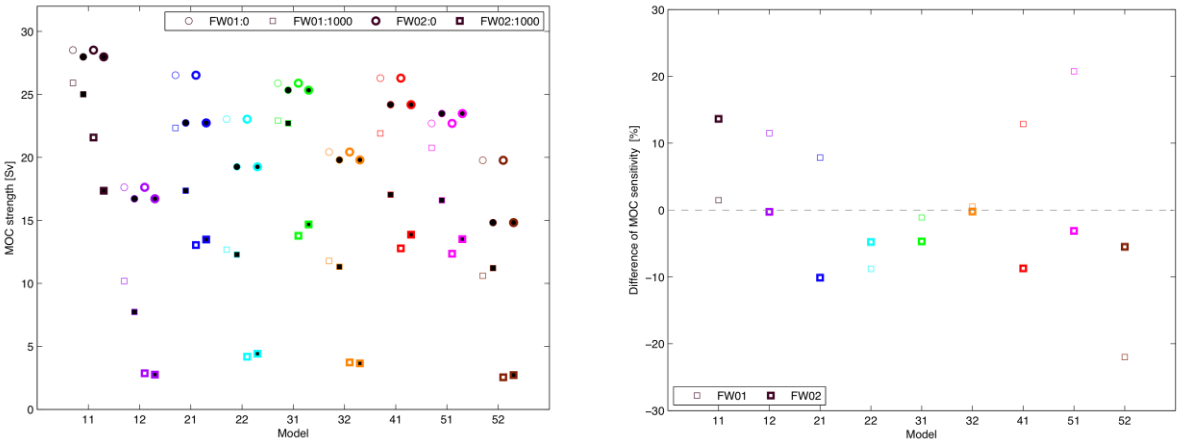

Figure 45: MOC streamfunction strength changes in response to anomalous constant freshwater forcing in the North Atlantic of 0.1 Sv and 0.2 Sv (left panel). Filled and empty symbols indicate experiments including and excluding the ice sheets, respectively, circles stand for the initial state and squares for the state after 1000 years. Differences in MOC changes after 1000 years between models including and excluding the ice sheets are shown on the right, with negative values indicating a lower MOC sensitivity of the fully coupled model.

Response of the ice sheets in the idealized 2xCO_2 scenario

Experiments with idealized greenhouse warming scenarios (2CO2) give a first idea about the expected response of the ice sheets in the runs over the third millennium. The climate sensitivity of the model directly translates into a respective change in global mean surface temperature and, more important for Greenland and Antarctica, temperature changes over the ice sheets. For the model version with highest climate sensitivity, the Greenland ice sheet loses more than half of its volume throughout the 1000-yr experiment (Figure 46), which leads to a sea level rise of ~5 meters, associated with a considerable amount of additional freshwater for the North Atlantic. The parameter sets with lower climate sensitivity yield lower volume changes mainly following the weaker temperature changes imposed on the ice sheets.
For the Antarctic ice sheet, grounded ice volume changes over the 1000 years remain positive or become only slightly negative for all experiments except for the two parameter sets with highest climate sensitivity (Figure 47). The accumulation rate in these runs stabilizes after around 400 and 600 years, while surface melting at the margins and flux across the grounding line both keep increasing beyond that point. The contribution to global sea level rise from Antarctica, of less than 90 cm, remains well below the contribution from Greenland for the highest sensitivity model throughout the 1000-yr experiment.

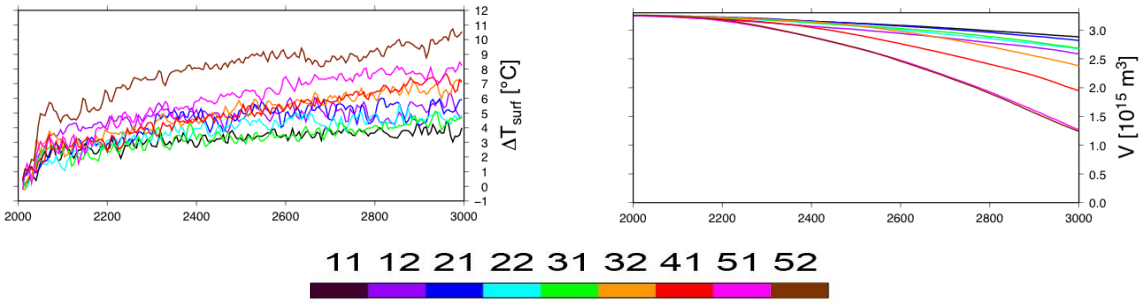

Figure 46: Time evolution of annual mean temperature over Greenland (left) and Greenland ice volume (right) in response to a stabilized 2xCO_2 scenario for models of different climate sensitivities. For these simulations, the medium carbon cycle and ice sheet parameter sets (2) are used. Note that the same colour code for the experiments will be used in all the figures.

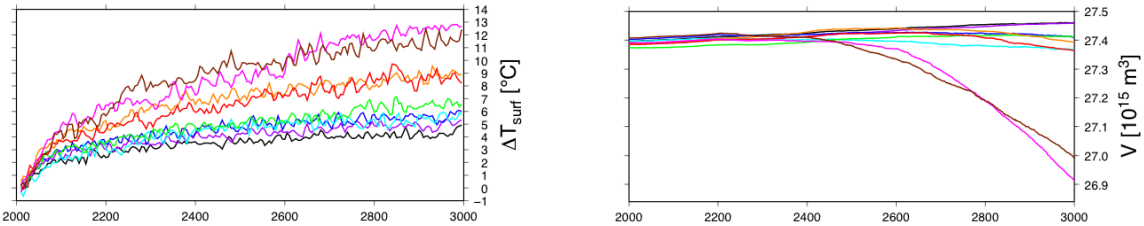

Figure 47: Mean temperature change over Antarctica (left) and Antarctic volume changes (right) in response to a stabilized 2xCO_2 scenario for models of different climate sensitivities. See colour code in Figure 46.

Different response for different ice sheet sensitivities

Comparable to the other model components, three different parameter sets were defined (low=xxx1, medium=xxx2 and high=xxx3), which determine the ice sheet sensitivity in response to temperature changes. As intended in the experimental setup, the surface melting rates (and the shelf melting rates for Antarctica) in response to rising temperatures is increasing with model ice sheet sensitivity. Accordingly, the Greenland ice volume losses in response to an idealized 2xCO_2 warming scenario are increasing with model sensitivity (Figure 48). For Antarctica, surface ablation rates and the flux across the grounding line increase with model sensitivity, while the accumulation rate is similar for the three different runs. The Antarctic grounded ice volume at the end of the experiment is therefore decreasing with increasing ice sheet sensitivity.

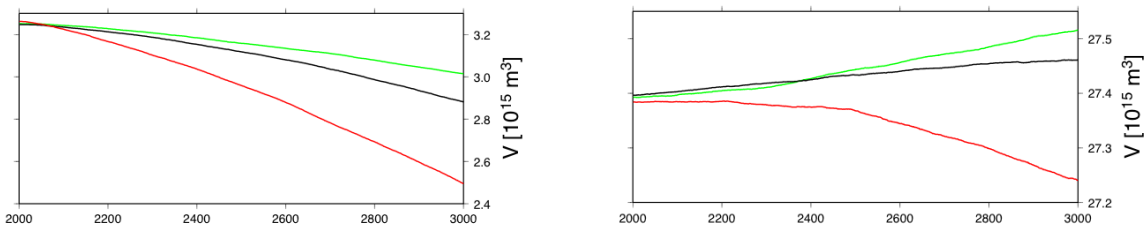

Figure 48: Volume changes for different ice sheet sensitivities in response to a stabilized 2xCO_2 scenario (model version E11). The grounded ice volume at the end of the experiment increases with ice sheet sensitivity (green=low, black=medium, red=high) for both Greenland (left) and Antarctica (right).

Polar amplification

LOVECLIM exhibits a polar amplification in the Arctic (Figure 49) that is relatively strong compared to other coupled Earth system models (Holland and Bitz, 2003). We adopt the definition of polar amplification of Holland and Bitz (2003) as the ratio between mean polar temperature change (70°-90°) and global mean temperature change at the time of CO_2 doubling in experiment 2CO2 (average over the years 60-80).

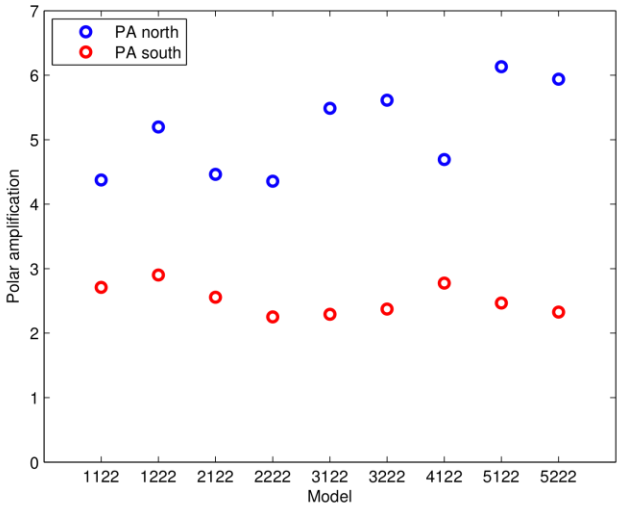

Figure 49: Polar amplification of LOVECLIM for the 9 different climatic parameter sets. LOVECLIM exhibits a relatively strong polar amplification in the Northern Hemisphere (blue circles) and a weaker one in the Southern Hemisphere (red circles).

The representation of positive feedbacks in tropical and equatorial regions is quite poor in LOVECLIM, in particular the water vapour feedback. As a consequence, LOVECLIM underestimates the response to a perturbation at low latitudes and thus overestimates the polar amplification. This relation becomes evident when looking at the polar amplification in the Southern Hemisphere of a factor 2 to 3 in LOVECLIM, which is small in most other models (Holland and Bitz, 2003). The polar amplification in LOVECLIM varies for different parameter sets but with no clear relation to climate or MOC sensitivities.
Overall, the relatively large polar amplification of LOVECLIM combines with low climate sensitivity versions (E11, E12, E21, E22) to yield polar temperature changes for a given radiative forcing that are in line with more comprehensive GCMs, while models with high climate sensitivity show a relatively stronger polar response. This has to be taken into account when interpreting climate change and sea level projections with LOVECLIM.

3. Carbon cycle and climate sensitivities

Model sensitivity with interactive carbon cycle

A particular attention was drawn at examining the impact of the interactive carbon cycle on climate sensitivities. In this purpose, experiments HYST and 2CO2 were repeated with the interactive carbon cycle. CO_2 is prognostic for the HYST simulations. The impact on climate sensitivities, as defined in section B.3, is illustrated in Figure 50 (left).

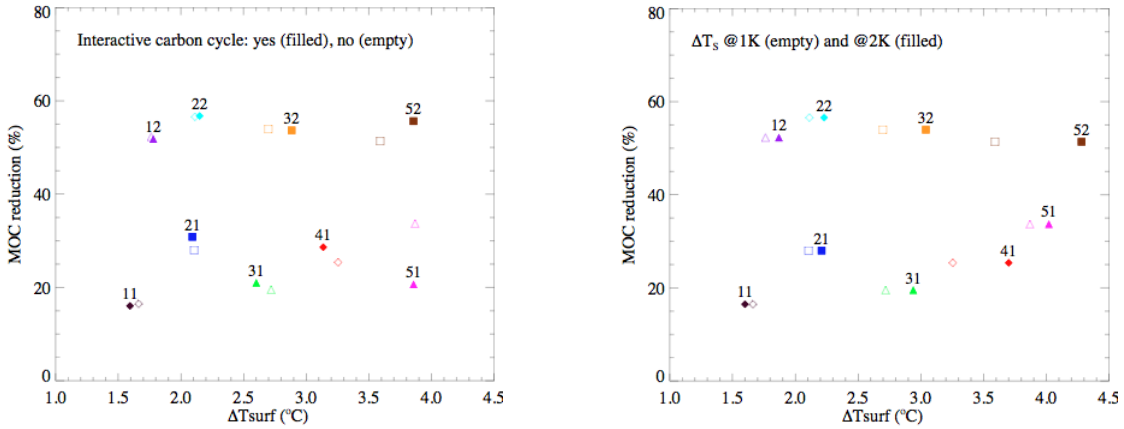

Figure 50: Climate sensitivities with (filled) and without (empty) the interactive carbon cycle (left). These results are obtained with carbon cycle parameter set 2 and no interactive ice sheets. In the right panel, the surface temperature change in 2CO2 experiments is computed after 2 kyr (filled) and compared to that obtained after 1 kyr (empty) – these results are obtained in experiments without interactive carbon cycle or ice sheets.

In most cases, sensitivities do not exhibit significant changes after the coupling with the carbon cycle model. Parameter sets with largest climate sensitivity (51 and 52) show some departure from the values obtained in ECBilt-CLIO-VECODE stand-alone experiments. The reason may be found in different initial conditions; indeed, experiments with interactive carbon cycle departed from the equilibrium state of the corresponding experiment without any carbon cycle. The internal model variability probably explains the large difference in MOC streamfunction reduction with parameter set 51 (Figure 50, left).
The temporal evolution of MOC streamfunction and global annual mean surface temperature are illustrated in Figure 51 for three climatic parameter sets. The evolutions of those variables over a long period are very close, with and without interactive carbon cycle. The surface temperature difference observed at the end of experiment HYST for parameter set 51 is however a direct consequence of the inclusion of an interactive carbon cycle. The atmospheric CO_2 concentration increase in the coupled run, consecutive to a significant reduction of the terrestrial biosphere carbon, results in a warmer state (Figure 51, right). In additional experiments, we tested the sensitivity to the initial conditions, which proved to be weak when using a sufficiently equilibrated initial state.

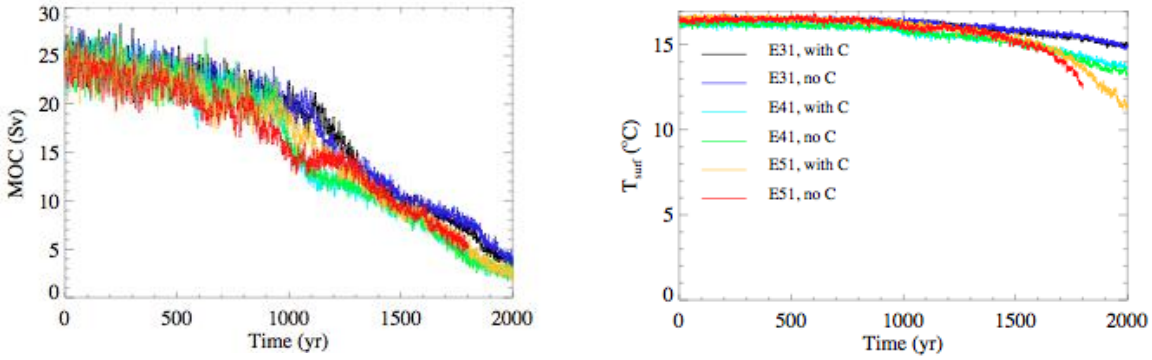

Figure 51: Temporal evolution of the MOC (left) and of the global annual mean surface temperature (right) in HYST experiments for 3 climatic parameter sets without (blue, green and red) and with (black, cyan and yellow) the interactive carbon cycle.

Equilibrium climate sensitivity is usually defined as the equilibrium temperature increase under a $2xCO_2$ forcing. We prolonged the 2CO2 experiments such as to reach an equilibrium state (total run duration of 2 kyr). The equilibrium climate sensitivity (Figure 51, right) is still larger for parameter sets associated with large climate sensitivity. Hence it is important to consider the equilibration time when comparing models.

Freshwater experiments: the carbon cycle feedbacks

Atmospheric CO_2 partial pressure at the end of the freshwater experiments varies significantly among model versions (Figure 52, left panel): from 0 (E11) up to 60 μatm (E52). This CO_2 increase results from the decrease of continental vegetation (Figure 52, right panel).

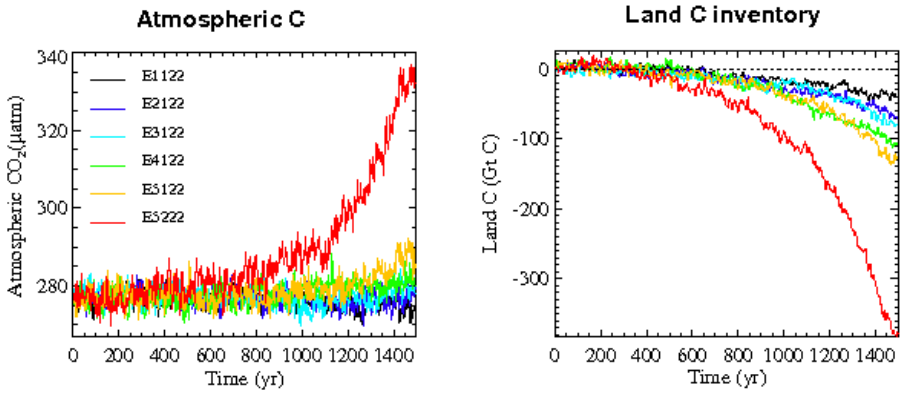

Figure 52: Atmospheric CO_2 partial pressure (left) and land carbon inventory (right) evolution under freshwater forcing for several parameter sets.

Models with larger climate sensitivities lead to a larger cooling consecutive to the MOC slowdown. This cooling results in an expansion of desert areas (Figure 53). This effect is amplified for climatic parameter sets with larger sea ice and ocean albedo values (sets 51 and 52).

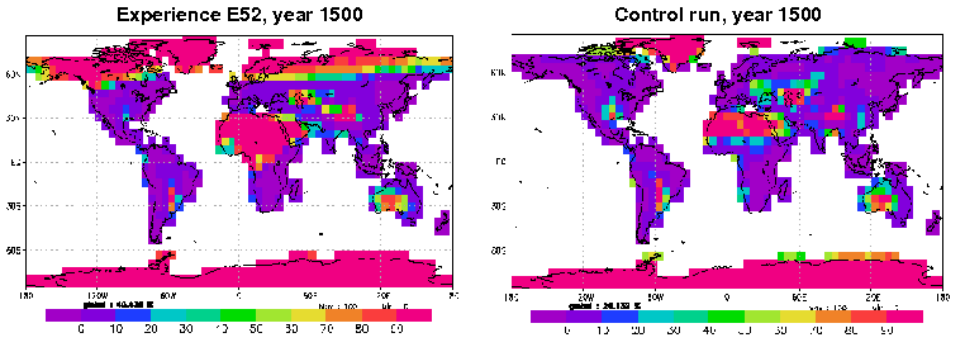

Figure 53: Desert fraction distribution with climatic parameter set 52 at the end of the freshwater experiment (left) and in the control run (right).

Very similar results are obtained with climatic parameter set 51 when allowing the freshwater flux experiment to run for 500 more years. The robustness of these results has been ascertained by repeating the experiments with different initial conditions. Since extremely close results were obtained, we may be confident that the predicted changes result from different model sensitivities.

4. Freshwater experiments – Export production

A significant reduction of the export production occurs in experiments E12, E22 and E32 (Figure 54). This reduction occurs in parallel with the MOC streamfunction decrease. The MOC weakening is associated with lower upwelling rates, hence lower nutrient availability in the upper ocean layers. In contrast, experiment E52 exhibits a moderate decrease in export production. With climatic parameter set 52, the amount of nutrients trapped at depth appears to be lower than with the other parameter sets.

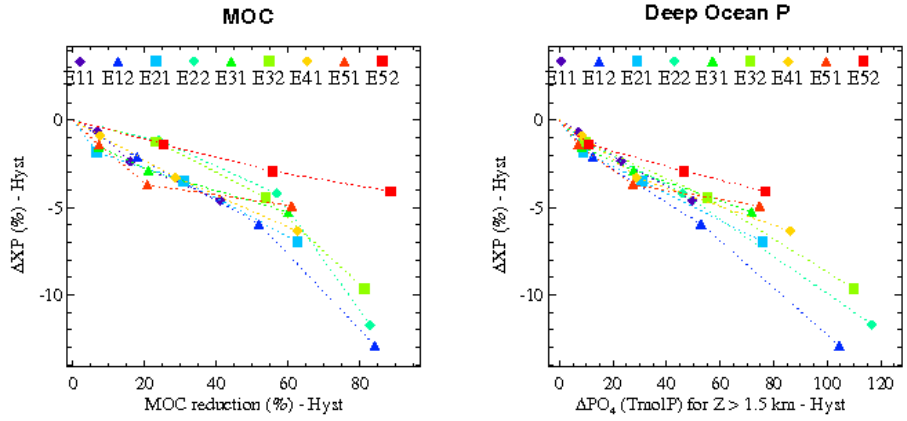

Figure 54: Export production anomaly versus MOC reduction (left) and versus deep ocean phosphate inventory anomaly (right). The symbols on the different curves represent the state every 500 years. The situation at the end of a given experiment (1500 yr) corresponds to the value at the far right of the individual curve. Phosphates inventories are evaluated for depth larger than 1.5 km.

The reasons for the different evolutions of export production may be evidenced with the help of a water age tracer. The age, constrained to be zero at the surface, is a measure of the time needed by a water mass to reach a particular location at depth (England, 1995).

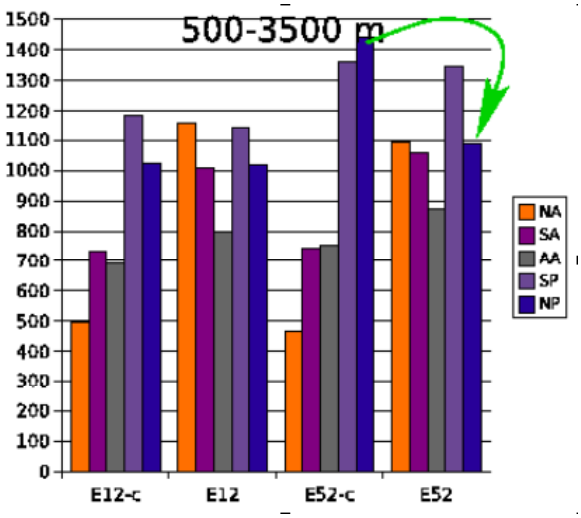

Figure 55: Basin averages of water age for depths located between 500 and 3500m in year 1500 of the control run and the experiment for parameter sets 12 and 52. Values for the control correspond to the columns labelled E12-c and E52-c. Five ocean basins are considered: North Atlantic (NA, Eq.-70°N), South Atlantic (SA, 50°S-Eq), Southern Ocean (AA, south of 50°S), South Pacific (SP, 50°S-Eq.) and North Pacific (NP, Eq.-70°N). Ages are expressed in years.

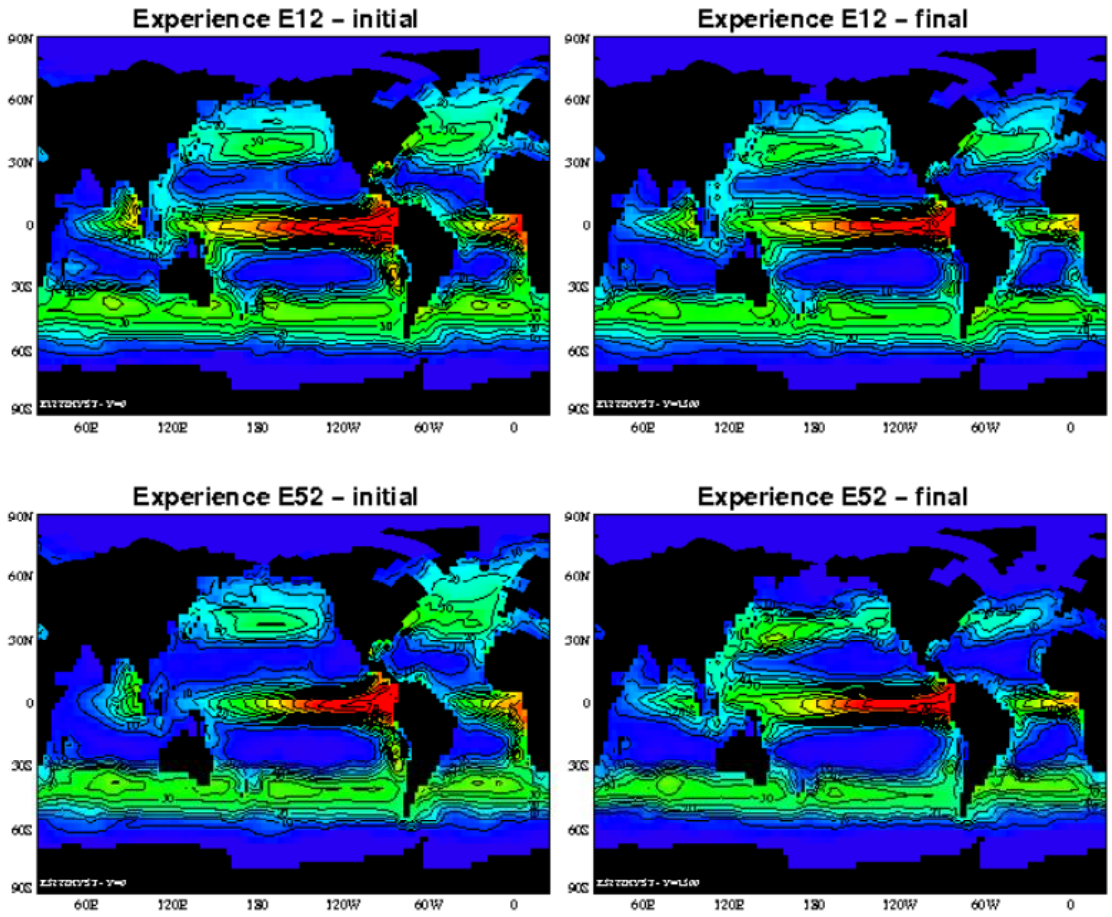

Figure 56: Geographical distribution of export production for the initial (left panels) and final (right panels) years of experiments E12 (top) and E52 (bottom). Values are in (gC/m^2).

The ventilation rate of intermediate layers (500-3500m) in the North Pacific evolves differently for versions E12 and E52 (Figure 55). The North Pacific intermediate waters at the end of the freshwater experiment E52 exhibit a smaller age than in the corresponding control experiment (E52-c). This is in contrast to the evolution obtained with model version E12 where no such change is observed. A similar behaviour to that obtained with parameter set 52 was observed in an uncoupled -D OGCM experiment (Mikolajewicz et al., 1997). Several field studies evidence an anti-phased pattern of changes in the North Atlantic (NA) and the North Pacific (NP) since the Last Glacial Maximum (e.g., van Geen et al., 1996; Zheng et al., 2000).
The increase in ventilation in the North Pacific explains the modest change in export production obtained with parameter set 52. The MOC streamfunction decrease leads to a dramatic lowering of the export production in the North Atlantic Ocean for all model versions (Figure 56). In the case of parameter set E52, this decrease is compensated for by a local increase in export production in the North Pacific area. This increase is driven by the larger rate of supply of nutrients to the surface resulting from the enhanced ventilation of deep waters.

5. M simulations

The analysis of global variables representative of the climate evolution over the last millennium makes it clear that such a strategy will not allow us to rank the parameter sets according to their ability to properly simulate the past climate. Indeed the

uncertainties on the climate reconstructions may be large, especially when going further in the past. Moreover, the variability of the model also prevents an accurate comparison. Additional uncertainties stem from the CO_2 emission reconstructions. Carbon fluxes associated to deforestation over the historical period are not constrained enough. Net emissions from the vegetation predicted by the model (Efor) are lower than the best available estimates as used in EMIS (Fichefet et al., 2007).

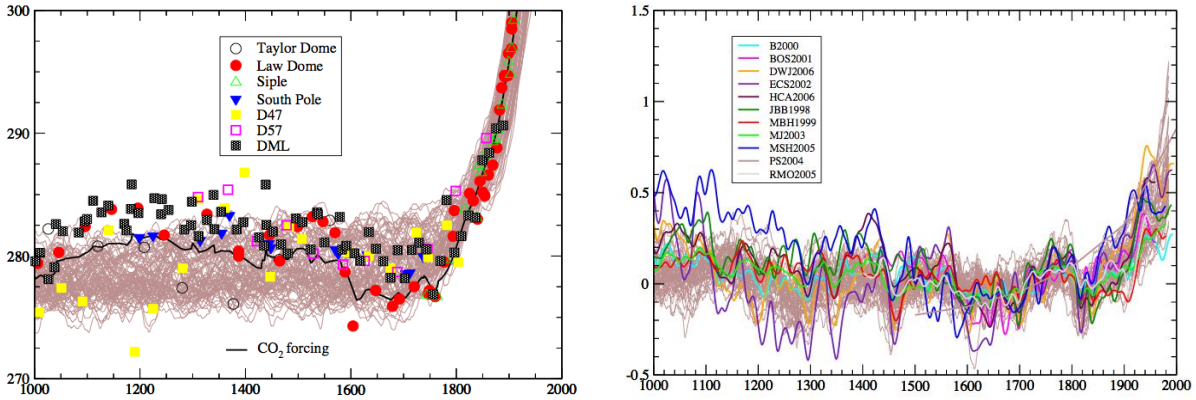

Figure 57: Evolution over the last millennium of the atmospheric CO_2 concentration (ppmv) (left) and the Northern Hemisphere annual mean surface temperature (°C) (right) simulated by LOVECLIM according to the 27 parameter sets (brown). Results are displayed for Efor simulations in the case of the atmospheric CO_2 concentration and for Conc simulations in the case of temperature. CO_2 concentration measured in Antarctic ice cores is shown for comparison. Temperatures are expressed as anomalies from their 1500 to 1899 means. They are smoothed with a 31-yr window. Colour lines in the right panel correspond to temperature reconstructions using multiple climate proxy records (See IPCC (2007) for more details) (see Table XI for the references for the CO_2 concentration and the proxy records).

Table XI: References for the atmospheric CO_2 concentration (left) and temperature reconstructions (right) presented in Figure 57.

CO_2 data	References	Temperature data	References
Taylor Dome	Indermühle et al., 1999	B2000	Briffa, 2000; calibrated by Briffa et al., 2004
Law Dome	Etheridge et al., 1998	BOS2001	Briffa et al., 2001
Siple	Neftel et al., 1994	DWJ2006	D'Arrigo et al., 2006
South Pole	Siegenthaler et al., 2005.	ECS2002	Esper et al., 2002; recalibrated by Cook et al., 2004
D47	Barnola et al., 1995.	HCA2006	Hergel et al., 2006
D57	Barnola et al., 1995	JBB1998	Jones et al., 1998; calibrated by Jones et al., 2001
DML	Siegenthaler et al., 2005.	MBH1999	Mann et al., 1999
		MJ2003	Mann and Jones, 2003
		MSH2005	Moberg et al., 2005
		PS2004	Pollack and Smerdon, 2004; reference level adjusted following Moberg et al., 2005.
		RMO2005	Rutherford et al., 2005

As an illustration to show the difficulty to assess the quality of the simulations over the last millennium, we display here the simulated Northern Hemisphere annual mean surface temperature in Conc and the atmospheric CO_2 concentration simulated in Efor (Figure 57).
At this stage, although none of the simulations is perfect, none of them is in complete disagreement with available climate observations (or reconstructions). Therefore, we decided to focus on the most recent part of these simulations (i.e. the last century) for which some accurate measurements of climate variables are available.

The last century

Five ensemble members are performed over the last century (1900 AD to 2010 AD) in order to account for the internal variability. The members of one ensemble differ only in their initial conditions. To do so, we introduce a very small perturbation on the quasi-geostrophic potential vorticity the first day of the simulation. Each simulation started in 1900 AD from the state of the corresponding millennial simulation at that time. The average of the members is analysed and discussed.
The radiative forcing computed by LOVECLIM for the present day with respect to the pre-industrial era related to sulphate aerosol load is -0.4 Wm^{-2} in the reference situation (E11). However, there is a large uncertainty in this quantity. IPCC-AR4 (Forster et al., 2007) reported a direct radiative forcing due to sulphate aerosols of $–0.40 \pm 0.2$ Wm^{-2}. The overall aerosol direct radiative forcing (i.e. radiative forcing values associated with several aerosol components) was estimated to $–0.50 \pm 0.40$ Wm^{-2}. In addition to a direct effect, aerosol particles also affect the formation and properties of clouds. IPCC AR4 gives a median value of –0.70 Wm^{-2} for the cloud albedo radiative forcing due to aerosol influence on clouds. Due to this large uncertainty, we decide to perform a second set of simulations for which the radiative forcing related to sulphates is doubled (S2).
This study concentrates on global-scale climate features. Moreover, we focus on the behaviour of variables that potentially have a direct or indirect impact on the future evolution of sea level and the climate of polar regions. Therefore, in addition to atmospheric CO_2 concentration and surface temperature, we consider sea ice extent, ocean heat content and ocean circulation.
Here, we investigate the model ability to reproduce the trend in selected variables over the last few decades. Other criteria could be used. For example, Reifen and Toumi (2009) studied the model ability to replicate a mean anomaly over a historic time period. They show that an accurate response of a model over one period does not imply the accuracy of the same model over another period.

CO_2 concentration

The comparison of the simulated time evolution of the atmospheric CO_2 concentration over the last century with data shows that some parameter sets display a poorer agreement than others (Figure 58). In particular, the simulated increase in CO_2 concentration obtained with carbon cycle parameter set 3 is of the order of 10 ppmv larger than in the corresponding observations over the 20^{th} century. By contrast, the simulated increase in atmospheric CO_2 concentration remains close to the measured one for carbon cycle parameter sets 1 and 2.
Similar conclusions can be reached by analysing the rate of increase in CO_2 concentration over different periods. Between 1959 and 2008, it varies between 1.35 and 1.47 ppmv/yr, for carbon cycle parameter sets 1 and 2, with the nominal (S1) sulphate forcing. Furthermore, the rate is higher with the carbon cycle parameter set

3 (~1.58 ppmv/yr) as well as when the S2 sulphate forcing is applied (by about 0.03 ppmv/yr). This is in reasonable agreement with the corresponding value in the Mauna Loa record (NOAA ESRL, 2009) of 1.44 ppmv/yr. A comparison with another observation series (Enting et al., 1994; GLOBALVIEW-CO2, 2006) over the time interval 1979-2005 yields similar conclusions. For this period, the rate of increase in CO_2 concentration varies between 1.48 and 1.62 ppmv/yr for carbon cycle parameter sets 1 and 2, with the S1 sulphate forcing. It is higher with the carbon cycle parameter set 3 (between 1.71 and 1.79 ppmv/yr). Here we obtain a larger CO_2 increase for a smaller temperature increase, which can be considered as a negative CO_2-climate feedback. In other words, the net feedback (Friedlingstein et al., 2003), which is the global warming amplification, is slightly smaller than one.

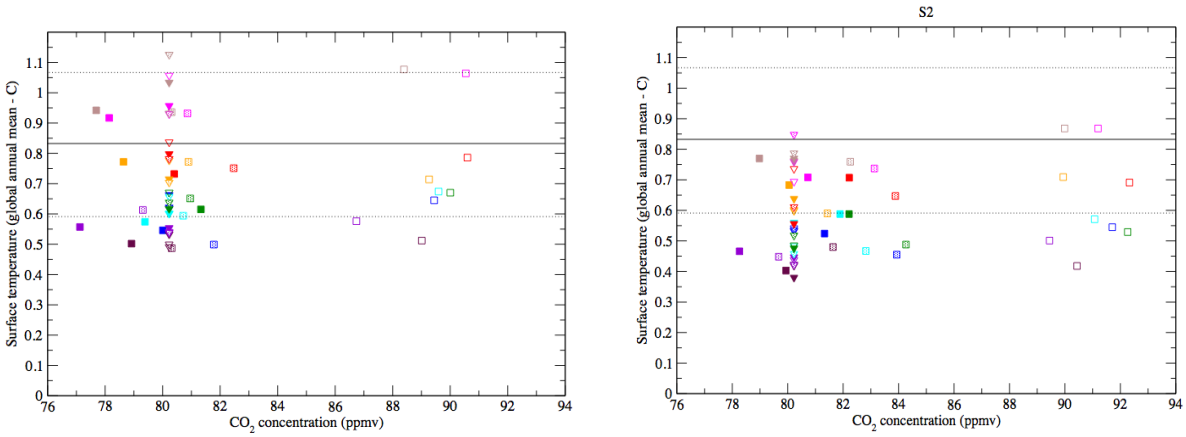

Figure 58: Global annual mean surface temperature increase with respect to increase in atmospheric CO_2 concentration. The increase is computed between the beginning of the 20th century (mean value over 1901-1910) and the beginning of the 21st century (2000-2009). Values are averaged over the five members of an ensemble. The left (right) panel displays results for S1 (S2) sulphate forcing. Each colour corresponds to one set of climatic parameter sets (see colour code in Figure 46). Squares (triangles down) correspond to Efor (Conc) simulations; full symbols are for carbon cycle parameter set 1, semi-empty symbols are for carbon cycle parameter set 2 and empty symbols are for carbon cycle parameter set 3. The full black line indicates the similar temperature increase as reconstructed by Brohan et al. (2009) (i.e. 0.8324°C). The dashed lines are the upper and lower 95% uncertainty ranges.

On the other hand, compared to the Mauna Loa record (NOAA ESRL, 2009), the absolute values of atmospheric CO_2 concentration between 1959 and 2008 are the best reproduced with carbon cycle parameter set 3 when using the S1 sulphate forcing, and with carbon cycle parameter sets 2 or 3, depending on the climatic parameter set, when a higher sulphate forcing reconstruction is used.

Surface temperature

The increasing trend in global annual mean surface temperature, computed from HadCRUT3 time series (Brohan et al., 2006), is 0.0168 °C/yr over the last 35 years (1979-2005) and 0.0071 °C/yr over the last century (1901-2005). Some parameter sets lead to an underestimate of this increasing trend. This is for example the case for 11, 21 and 22, especially with the S2 sulphate forcing , while other parameter sets yield overestimate of this trend, e.g., 51 and 52, especially with the S1 sulphate forcing. This behaviour was mostly expected due to differences in climate sensitivity. Indeed, the parameter sets corresponding to the lowest climate sensitivity (such as 11, 21 and 22) lead to small temperature changes over the last century and those with the largest climate sensitivities (e.g., 51 and 52) lead to a large temperature

increase over the last century. Moreover, using a larger sulphate aerosol forcing tends to shift the simulated temperature increase over the last century towards smaller values because of the radiative cooling effect of those aerosols. Still, the discrepancy between simulated global annual mean surface temperature and observations remains small (within one standard deviation) for many configurations. Moreover, although the deviation from observations of the simulated atmospheric CO_2 concentration is of the order of 10 ppmv over the 20th century (Figure 58) for carbon cycle parameter set 3, this discrepancy is not large enough to drive the surface temperature towards larger values than for carbon cycle parameter set 1 or 2.

Northern Hemisphere minimum sea ice extent

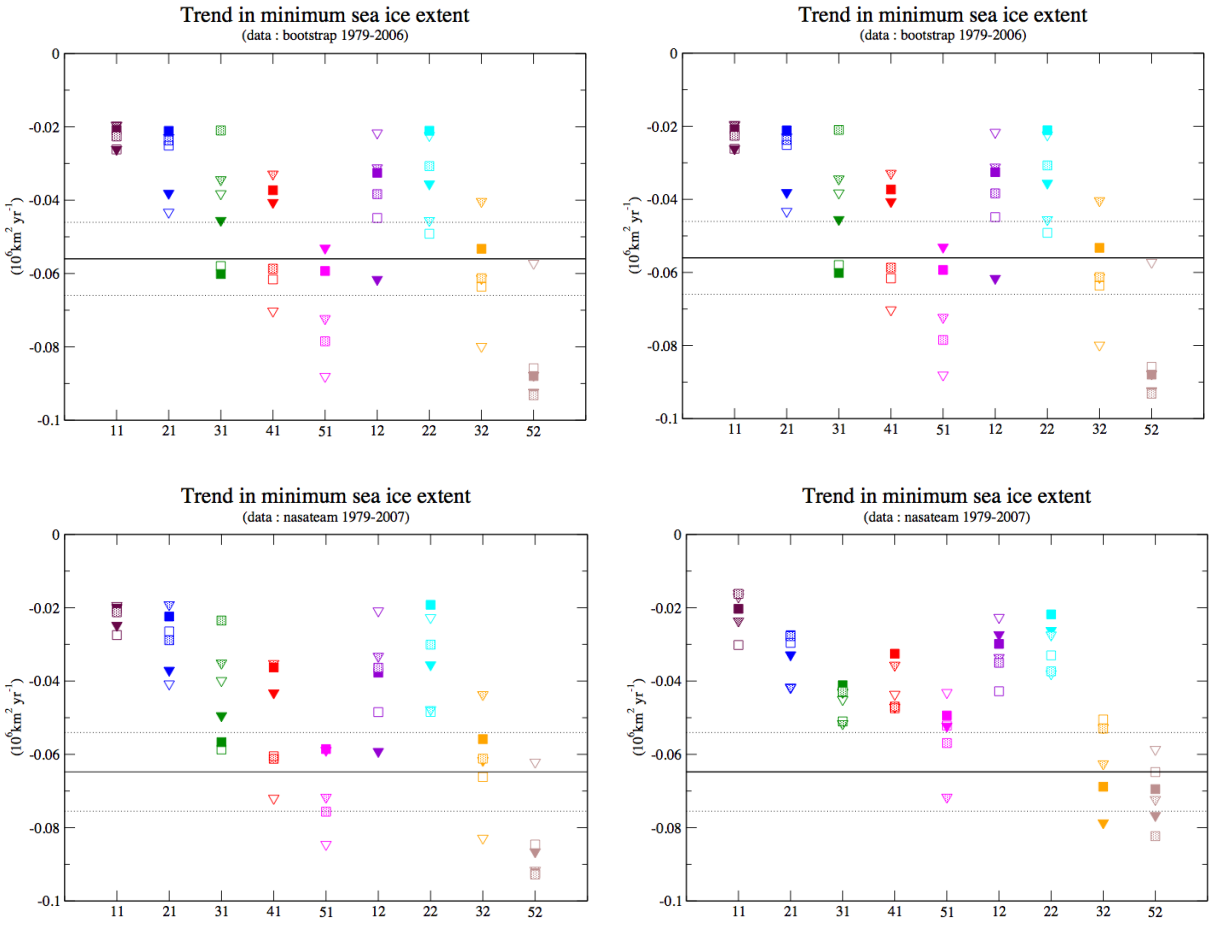

Figure 59: Trend in Northern Hemisphere minimum sea ice extent between 1979 and 2006 (upper part) or 2007 (lower part). X-axis is for the climate sensitivity, either for S1 (left) or S2 (right) sulphate forcing. Each colour corresponds to one set of climatic parameter sets (see colour code in Figure 46). Squares (triangles down) correspond to Efor (Conc) simulations; full symbols are for carbon sensitivity set to 1, semi-empty symbols are for carbon sensitivity set to 2 and empty symbols are for carbon sensitivity set to 3. The full black line indicates the trend in minimum sea ice extent as reconstructed by Comiso and Nishio (2008) (http://nsidc.org/data/smmr_ssmi_ancillary/area_extent.html; last visit August 19, 2009). The dashed lines represent one standard deviation of the data. Two algorithms were used for this reconstruction (top and bottom parts) with slightly different time range.

Most of the simulations, either with S1 or S2 sulphate forcing, experience a too small trend in Northern Hemisphere minimum sea ice extent between 1979 and 2006/2007 compared to the observations (Figure 59). This is especially the case for those simulations with low climate sensitivity (11, 12, 21 22). For higher sensitivities, the type of simulation (Efor or Conc) and the sulphate radiative forcing may have a significant impact on the simulated trend. However, S2 sulphate forcing do not necessarily lead to lower or higher trend in Northern Hemisphere minimum sea ice extent.

Ocean features

The modelled ocean circulation does not experience major changes during the last century. All the simulations exhibit a reduction of less than 4 Sv in the strength of North Atlantic MOC for S1 sulphate aerosol forcing [3 Sv; S2 sulphate aerosol forcing] over this period (Figure 60). It must be reminded that there is a large spread in the mean intensity of the MOC depending on the parameter sets. For example, this strength varies between 28 and 17 Sv in 1900 depending on the parameter set used. In a model intercomparison, Gregory et al. (2005) used several GCMs and EMICs (including LOVECLIM) to study the response of the North Atlantic MOC to an increase in atmospheric CO_2 concentration. In this context, partially coupled integrations were performed to evaluate the influence of heat and freshwater in each of the models. They pointed out that heat flux changes contribute more than freshwater flux changes to weakening the MOC for all models.

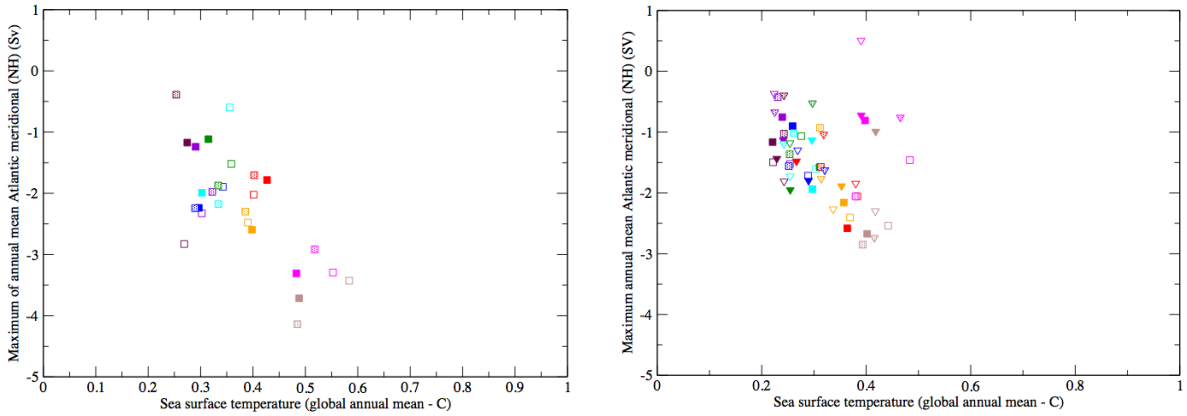

Figure 60: Change in the maximum of the North Atlantic meridional overturning streamfunction (Sv) wrt change in the global annual mean sea surface temperature (°C). Each colour corresponds to one set of climatic parameter sets (see colour code in Figure 46). Squares (triangles down) correspond to Efor (Conc) simulations; full symbols are for carbon cycle parameter set 1, semi-empty symbols are for carbon cycle parameter set 2 and empty symbols are for carbon cycle parameter set 3.

The simulations performed here display an approximately linear relationship between the increase in the upper ocean heat content and the increase in sea surface temperature (Figure 62), i.e. when temperature increases, in particular sea surface temperature, the ocean captures more heat. There is also an approximately linear relationship between the sea surface temperature and the North Atlantic MOC intensity (Figure 60). In contrast, there is no clear change in the upper ocean heat content related with the MOC sensitivity (Figure 61). Therefore, the climate sensitivity has a stronger effect on the ocean behaviour than the MOC sensitivity. In other words, even though we selected parameter sets in a large phase space, the ocean is

responding more to the atmospheric forcing than to its intrinsic characteristics. The initial states of the ocean, that are different depending on the parameter sets, do not induce large changes in the upper ocean heat content neither.

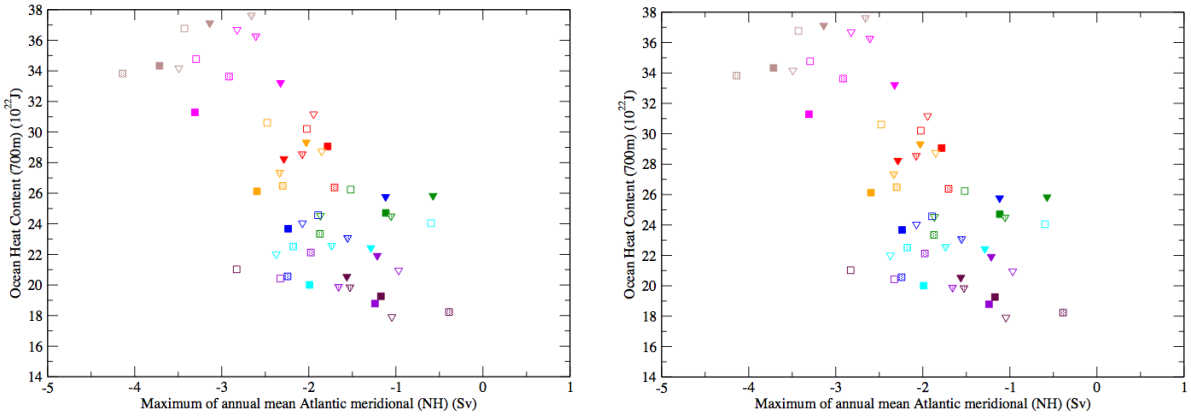

Figure 61: Change in ocean heat content (upper 700 m) (10^{22} J.yr^{-1}) wrt changes in the maximum of the North Atlantic meridional overturning streamfunction (Sv). The increase is computed between the beginning of the 20th century (mean value over 1901-1910) and the beginning of the 21st century (2000-2009) for the average of the five members of an ensemble. Each colour corresponds to one set of climatic parameter sets (see colour code in Figure 46). Squares (triangles down) correspond to Efor (Conc) simulations; full symbols are for carbon cycle parameter set 1, semi-empty symbols are for carbon cycle parameter set 2 and empty symbols are for carbon cycle parameter set 3.

Although none of the selected parameter sets is able to provide a perfect balance that would yield climate simulation in the range of observations for all the variables examined, some parameter sets are performing better. The purpose of the next section is to identify the parameter sets that lead to the best simulation of the climate trend over the last century.

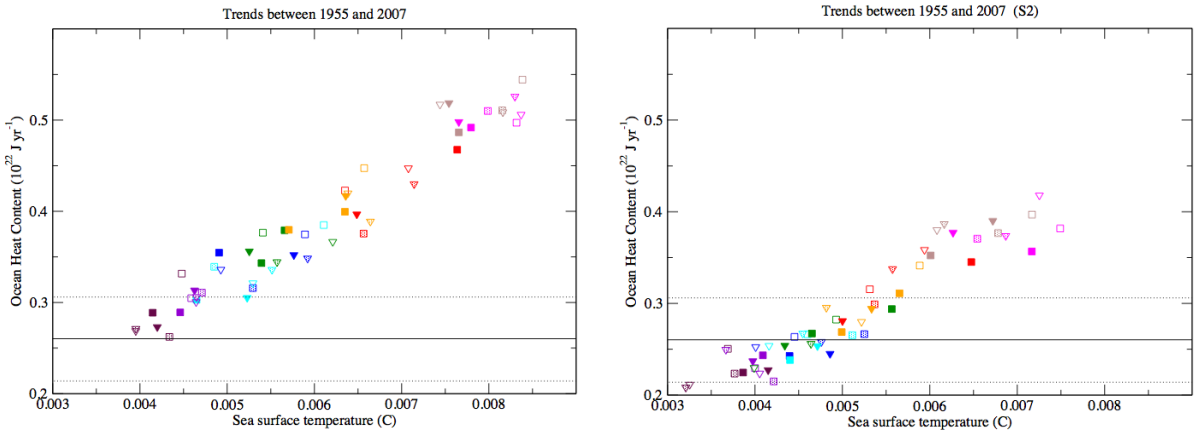

Figure 62: The trend in oceanic heat content in the upper 700 m (10^{22} J.yr^{-1}) wrt trend in global mean sea surface temperature (°C.yr^{-1}). Each dot represents one simulation. Trends are computed as the slope of the regression line through the annual values between 1955 and 2007. Each colour corresponds to one set of climatic parameter sets (see colour code in Figure 46). Squares (triangles down) correspond to Efor (Conc) simulations; full symbols are for carbon cycle parameter set 1, semi-empty symbols are for carbon cycle parameter set 2 and empty symbols are for carbon cycle parameter set 3. The full black line represents the trend computed from observation (Levitus et al., 2009). The dashed line represents the uncertainty related with the variability in the data (one standard deviation).

Performance of the parameter sets : design of a metric

In this section, we focus on the design of a metric that quantifies the ability of a simulation (i.e. a given parameter set and a given configuration) to simulate the observed climate change over the last century (Loutre et al., 2010). This metric is a measure of the adequacy between the simulated and observationally-based trends of several climatic indicators during the 20th century. Specifically, the selected variables are those already discussed hereabove, i.e. the global annual mean surface temperature, atmospheric CO_2 concentration, minimum sea ice extent in the Northern Hemisphere and ocean heat content of the upper 700 m of the global ocean. Trends are computed over several decades of the last century according to the length of the dataset available for comparison (Table XII). For model results, trend is defined as the slope of the straight line fitted by linear regression through the mean of the five members of an ensemble corresponding to the same parameter set and the same configuration. Table XII summarizes for each variable the considered time interval and the reference for the observational dataset. Similarly, the trend in the data is computed as the slope of the straight line fitted by linear regression through this dataset. Two datasets for minimum sea ice extent and ocean heat content are used for the metric. It should be noted that, for the most part, the sea ice extent data rely on the same observations. The end product only differs in the analysis systems and methodology used.

Table XII: Column 2 gives the references of the different datasets used for comparison of the simulated time evolution for the variables given in column 1. The trend of the observations (column 4) is computed over the time interval given in column 3. cy stands for century.

variable	Reference		
Global annual mean surface temperature	Brohan et al., 2006	1901-2005	0.71°C/cy
Global annual mean surface temperature	Brohan et al., 2006	1979-2005	1.68°C/cy
Atmospheric CO_2 concentration	Enting et al., 1994; GLOBALVIEW-CO2, 2006.	1901-2005	70 ppmv/cy
Atmospheric CO_2 concentration	Enting et al., 1994; GLOBALVIEW-CO2, 2006.	1979-2005	162 ppmv/cy
Sea ice extent	Bootstrap algorithm; Comiso and Nishio, 2008	1979-2006	-5.63×10^6 km^2/cy
Sea ice extent	Nasateam algorithm; Comiso and Nishio, 2008	1979-2007	-6.52×10^6 km^2/cy
Ocean heat content (upper 700 m)	Levitus et al., 2009	1955-2007	26 10^{22} J/cy
Ocean heat content (upper 700 m)	Domingues et al., 2008	1950-2003	24 10^{22} J/cy

For given a variable (b_i) and corresponding reference (b_{obs}), we define the ratio (R_i) of their difference to the median (M) of the deviation from observations for all the simulations (i.e. all the parameter sets) of a given setup (either Conc or Efor). Actually, M is the median of abs(b_i-b_{obs}). Following Gleckler et al. (2008), we define a

'typical' error as the median rather than the mean value to reduce the weight of outliers (simulations with unusually large error). The metric is thus defined as follows:

$$R_i = \frac{abs(b_i - b_{obs})}{M}$$

The index i stands for each of the 54 experiments with combinations of the nine climatic parameter sets, the three carbon cycle parameter sets and both S1 and S2 sulphate forcings. The procedure is conducted separately for the Conc and Efor setups. The value of R yields a measure of how well a given set of parameters (i), with a given experimental setup, compared with a typical simulation. For example, if R_i equals one, then the difference between the simulation (mean over five members) and the observations is the same as the median error for all simulations. If $R_i < 1$ ($R_i > 1$), the simulation performs better (worse) than the median. If the trend in the simulation and in the observations is the same, R_i is zero.

The performance of each simulation for each variable is assessed with a threshold value for R_i, set here to 0.66. One point is attributed to a particular parameter set and configuration if R_i is less than 0.66 and no point otherwise. One point is attributed for the ocean heat content or the sea ice extent if the simulation performs well with respect to at least one of the observational datasets. The total score (the metric) is computed as the total number of good performances for each variable. None of the simulations received the maximum score of four (Conc) or six (Efor) points. The best simulations received a total score of three (Conc) and four (Efor) points (Figure 63).

It appears that no simulation is perfect. In particular, none can simulate simultaneously a correct time evolution for the Northern Hemisphere sea ice extent and for the ocean heat content in the upper 700 m. Simulations with the carbon cycle parameter set 3 do not properly reproduce the observed atmospheric CO_2 increase. Still it must be underlined that the deviation from observations remains less than 10 ppmv over the last 50 years. Moreover, this does not prevent to simulate a temperature increase in agreement with observations. The aerosol forcing scenario (S1 or S2) has also a strong impact on the skill of a parameter set to reproduce the climate change for a given variable.

Amongst the simulations ranking the highest (i.e. a final mark of three for Conc and four for Efor), configuration 321, 322, 511 and 512 display good performance for both Conc and Efor, either for S1 or S2 sulphate aerosol forcing. The 321-parameter set is performing particularly well. Its major weakness is the simulation of the evolution of the upper ocean heat content in the case of S1 sulphate forcing and long-term temperature (and CO_2) in case of S2 sulphate aerosol forcing. Simulating an increase of the upper ocean heat content in line with observations is also a major problem for the other 'good' parameter sets (except for 322 under Conc- configuration with S2 sulphate aerosol forcing).

At this stage, we should also remind the reader that the skill of the parameter sets is computed on a small set of variables. Therefore, another set of variables, for example giving more weight to the ocean component of the system, could give rise to a slightly different conclusion about the skill of the parameter sets.

The raw R-values can take rather large values, meaning a strong discrepancy between the simulated and observed trends. This is even true for parameter sets that exhibit a good overall skill. For example, the 321-parameter set (under Conc-setup) yields large R-values for the upper ocean heat content with S1 sulphate aerosol forcing. Conversely, some parameter sets, which yield a low skill, actually display too large individual R-values. The mean R-value of 211 for all the variables is less than 1 under Conc-setup; however, it is lower than the selected threshold for

only one variable and larger than one for several of them. This also highlights how critical is the choice of the threshold value that separates between 'good' and 'poor' agreement.

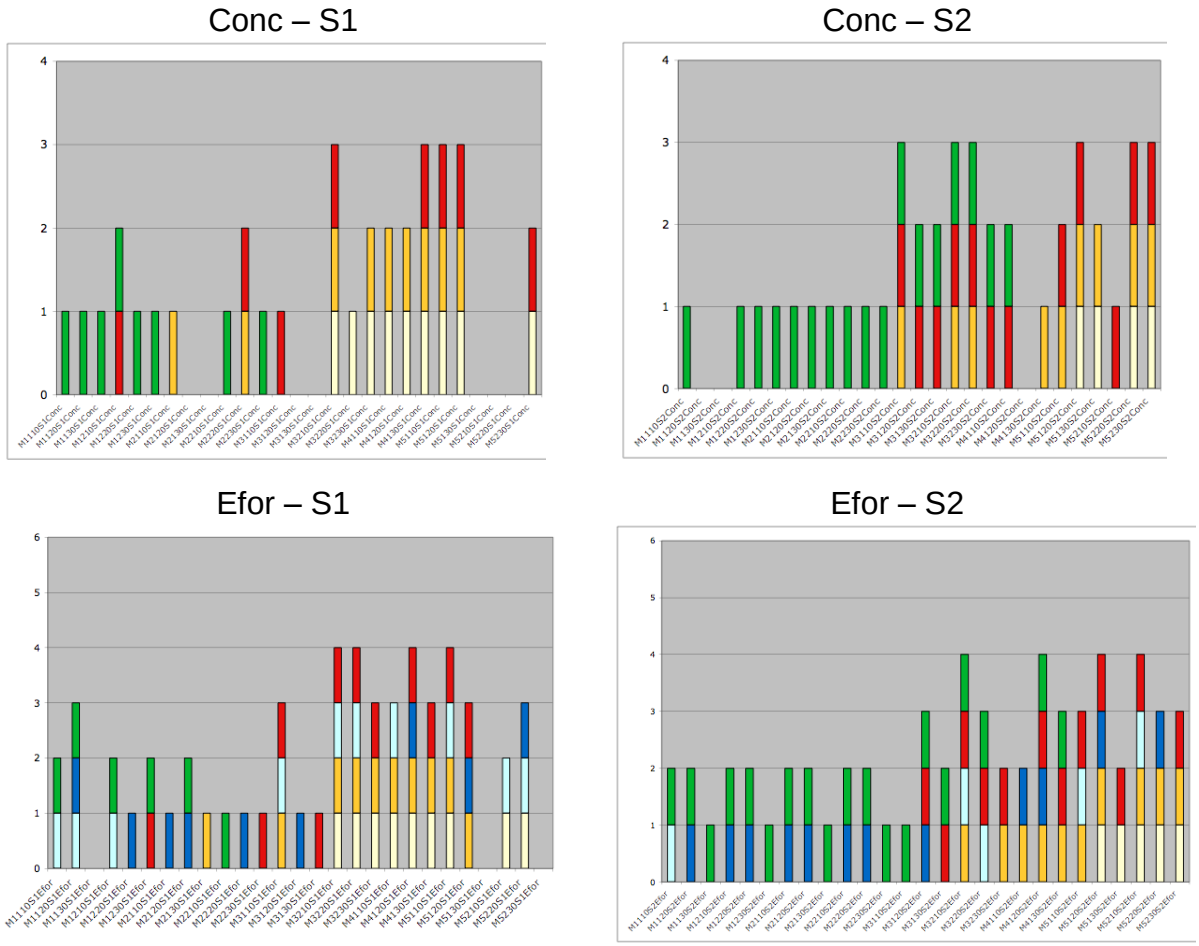

Figure 63: Summary of the performance of the Conc (top) and Efor (bottom) simulations to reproduce the observed trend of the time evolution for different climate variables for each parameter set under S1 (left) and S2 (right) sulphate aerosol forcings. The variables and the time intervals are described in Table XII. The x-axis lists all the parameter sets. Colour bars indicate the variables simulated with a good skill (according to our metric), i.e. R above the threshold (see text). A single colour bar is used for sea ice and upper ocean heat content. Ts stands for global annual mean surface temperature either over the interval 1901-2005 (light yellow) or 1979-2005 (dark yellow). CO2 is for atmospheric CO_2 concentration either over the time interval 1901-2005 (dark blue) or 1979-2005 (light blue). Sea ice extent trend (red) is computed either between 1979 and 2006 or 1979 and 2007. Trend in ocean heat content in the upper 700 m (green) is computed over either the time interval 1955-2007 or 1950-2003. See also Table VI for references.

Carbon isotope and atmospheric CO_2 over the last centuries

In order to resolve uncertainties associated with the CO_2 fluxes associated to deforestation over the historical period, we repeated the M experiments over the last centuries with prognostic carbon isotope. The response is analysed for some of the parameter sets over two periods during which the temporal evolution of atmospheric $\delta^{13}C$ is nearly linear (Figure 64): 1850-1960 AD and 1955-2000 AD.

For each parameter set, we ran 3 experiments: Efor, EMIS and ECTL. The initial state for each experiment is a long equilibrium corresponding to conditions prevailing

in 1700 AD. Transient experiments were then performed from 1700 AD until 2000 AD in prognostic CO_2 and ^{13}C mode. All forcings are identical to those used for the M experiments. The ^{13}C-to-^{12}C ratio of the fossil-fuel source is taken from Andres et al. (2009). The ^{13}C flux from deforestation in EMIS is computed by assuming a constant isotopic ratio, $\delta^{13}C$=-24.5 permil. This value corresponds to the average terrestrial biosphere isotopic composition predicted by VECODE for pre-industrial conditions. The predicted atmospheric $\delta^{13}C$ is then compared to the data from Francey et al. (1999) up to 1978 AD and from Francey et al. (1999) and Keeling et al. (2010) onwards.

The increase rate in atmospheric CO_2 concentration in Efor is lower than in the reconstruction for all parameter sets during the first epoch (1850-1960 AD) while, in the second time period (1955-2000 AD), the atmospheric CO_2 concentration in EMIS systematically increases faster than as observed (Figure 65). This contrasted behaviour arises from the fact that net emissions from the vegetation predicted by the model (Efor) are lower than the best available estimates as used in EMIS (Fichefet et al., 2007). The bias in atmospheric $\delta^{13}C$ trend does however not exhibit such a systematic behaviour (Figure 66), with several parameter sets falling within the 99% confidence interval for both periods and both experiment types.

With the help of the metric presented earlier (M experiments over the last century), we may classify the 6 parameter sets under study in this section according to their performance. The maximum score reached for each experimental configuration is 4 (*R* less than 0.66 simultaneously for CO_2 and $\delta^{13}C$ trends for both time periods). The individual scores are presented in Table XIII. It can be seen from this table that climatic parameter set 32 with carbon cycle parameter set 1 performs best both in Efor and EMIS. Parameter sets 3220, 3230 and 4120 satisfy half of the criteria in the Efor run. Those results do not contradict the classification obtained by evaluating the model over the 20th century.

Table XIII: Performance of several parameter sets (column 1) in reproducing the atmospheric CO_2 and $\delta^{13}C$ trends over two periods: 1850-1960 AD (T1) and 1955-2000 AD (T2). The score (columns 6 and 11) is the sum of the individual performances in the Efor (columns 2 to 5) or EMIS (columns 7 to 10) experiments.

Parameter set	Efor					EMIS				
	Atm. CO_2		Atm. $\delta^{13}C$		Score	Atm. CO_2		Atm. $\delta^{13}C$		Score
	T1	T2	T1	T2		T1	T2	T1	T2	
3120	0	0	0	0	**1**	0	0	0	0	**1**
3210	1	1	1	0	**3**	1	1	1	0	**3**
3220	0	1	1	0	**2**	0	1	0	0	**1**
3230	1	0	0	1	**2**	0	0	0	1	**1**
4120	0	0	1	1	**2**	0	0	0	0	**0**
5220	0	0	0	1	**1**	1	0	0	1	**2**

However, further analysis is needed in order to obtain a more precise evaluation. These results are preliminary and should not be compared directly to the M analysis. The model performance is indeed sensitive to the chosen time period for evaluation. Ensemble runs would probably help resolving this sensitivity. We may nevertheless conclude that $\delta^{13}C$ is a good candidate for constraining the model.

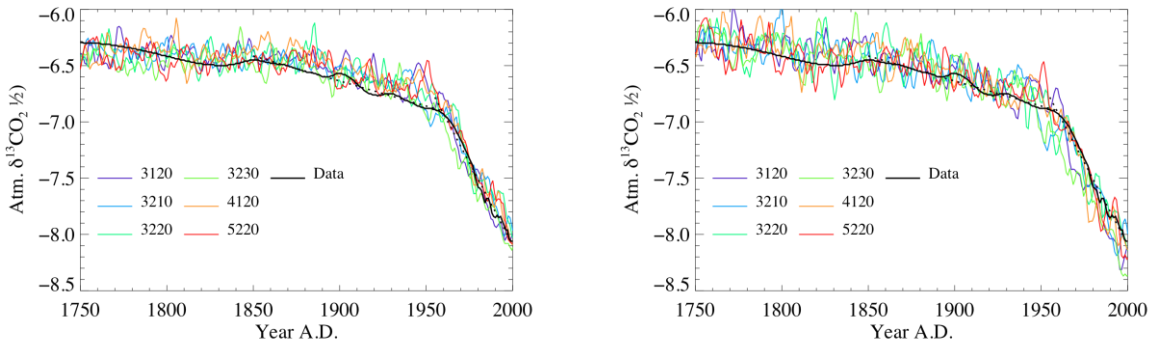

Figure 64: Temporal evolution of atmospheric $\delta^{13}C$ during industrial era as obtained in Efor (left) and EMIS (right) experiments. The dotted lines represent the linear trend in the data over the periods 1850-1960 AD and 1955-2000 AD, respectively. The data (solid black) are from Francey et al. (1999) up to 1978 AD and from Francey et al. (1999) and Keeling et al. (2010) onwards.

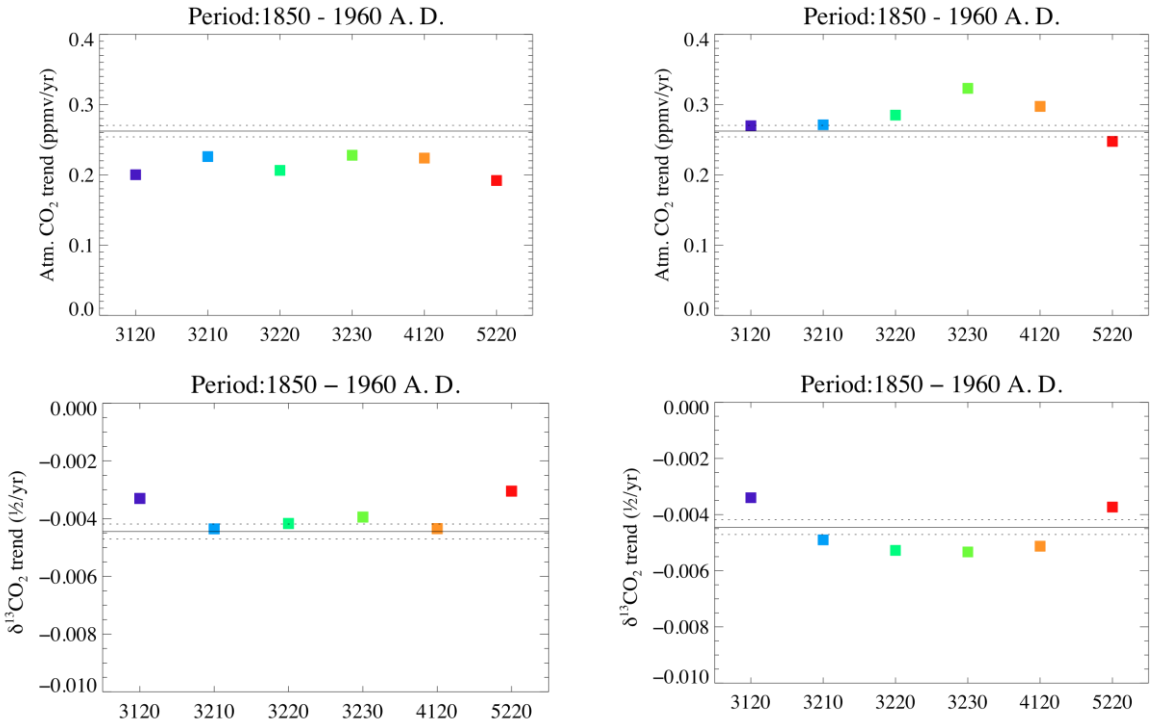

Figure 65: Trends in atmospheric CO_2 concentration (top) and $\delta^{13}C$ (bottom) over the period 1850-1960 AD in Efor (left) and EMIS (right) experiments. The dotted lines delineate the 99% confidence interval in the data trend.

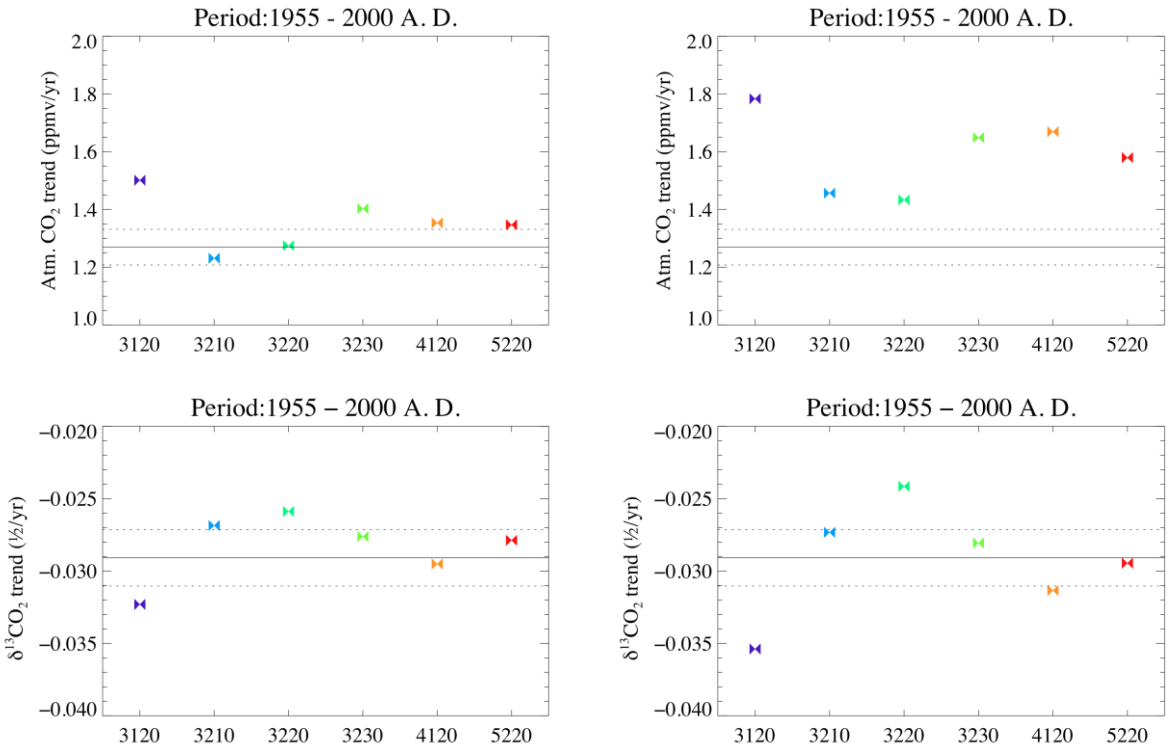

Figure 66: Trends in atmospheric CO_2 concentration (top) and $\delta^{13}C$ (bottom) over the period 1955-2000 AD in Efor (left) and EMIS (right) experiments. The dotted lines delineate the 99% confidence interval in the data trend.

6. The Holocene simulations

The Mid-Holocene (6 kyr BP)

Transient simulations are performed from 8 kyr BP to year 2100 AD, starting from a quasi-equilibrium state obtained under 8 kyr BP forcing conditions (Goosse et al., 2007) with five climatic parameter sets (11, 21, 31, 41, 51). Here, simulations are performed with ECBilt-CLIO-VECODE (i.e. the LOCH and AGISM components are not activated). Between 8 kyr BP and 1 AD, the only forcings applied are insolation and greenhouse gas concentration changes (see full description above, section B.4).
First, the simulated climate at the mid-Holocene (6 kyr BP) is compared with the modelled present-day climate (mean climate over a reference period, 1980-2000 AD). The mean climate over the reference period is computed from the transient simulations carried out over the last millennium, as described in the previous section. For mid-Holocene, the mean climate is computed over 100 years (at 6 kyr BP) of the transient simulations starting at 8 kyr BP.
The different simulations are sharing common features. Summer temperature (June-July-August-September (JJAS); Figure 67) is higher at 6 kyr BP than at present over Siberia, Southern and Central Europe, northern North America and northern North Africa. Temperature is also larger over part of the continents of the Southern Hemisphere but the difference is smaller than in the Northern Hemisphere. India, Middle East, Arabian Peninsula and Sahel region experience a cooling during the mid-Holocene compared to the present. However, some features are not the same for all the parameter sets. According to parameter sets 11, 31 and 41, Antarctica was cooler at 6 kyr BP, although the Southern Ocean was warmer with parameter

sets 31 and 41, and cooler with parameter set 11. The mid-Holocene Southern Ocean was much warmer than at present according to simulation 51. Higher temperatures are also simulated over Antarctica. According to PMIP2 (Braconnot et al., 2007), summer surface air temperature increased over NH continents, reaching a maximum of about 2°C in Central Eurasia and over the Tibetan Plateau. This feature is well reproduced with all the parameter sets, especially over Eurasia. The warming of the Arctic simulated with all the parameter sets is in agreement with the larger temperatures suggested by the ensemble mean of PMIP2 simulations. However, the warming of the North Pacific and North Atlantic Oceans, suggested by PMIP2, is less well reproduced (except with parameter set 51). A cooling is even observed over the Northern Hemisphere ocean with parameter set 31. In the Southern Hemisphere, the ocean is colder than or similar to today in PMIP2 simulations as well as in our simulations. A slight warming depicted off the Antarctic continent with PMIP2 is also

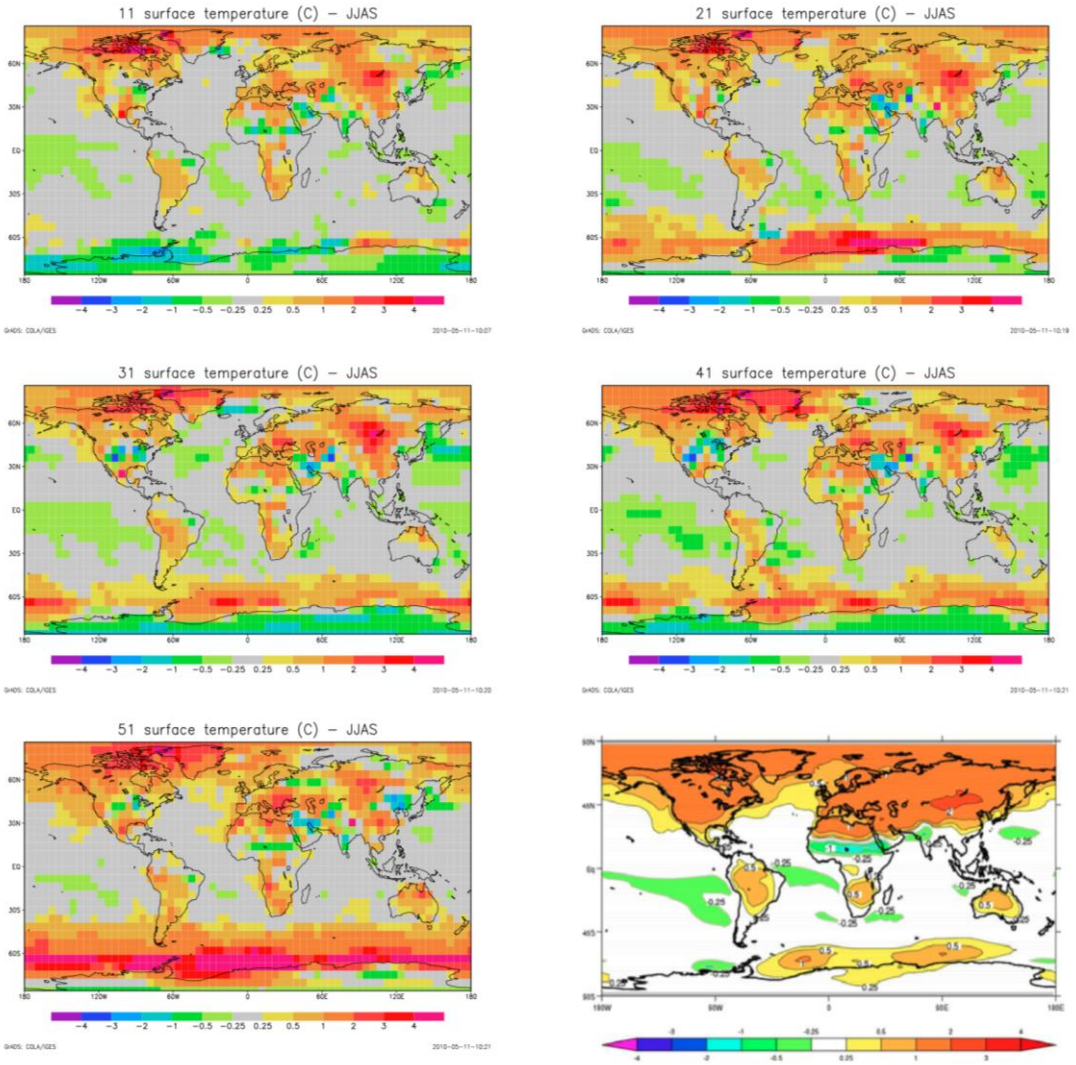

Figure 67: June-July-August-September (JJAS) surface temperature changes according to the five climatic parameters sets (11 - 21 - 31 - 41 - 51). Maps are showing the differences between 6 kyr BP and the present day (present day means the time interval 1980-2000 AD in the corresponding millennium experiments). The lower right panel displays the JJAS mean surface air temperature differences (°C) between mid-Holocene (6 kyr BP) and pre-industrial (0 kyr) for the ensemble mean PMIP2 simulations (Braconnot et al., 2007).

simulated with parameter sets 21, 31 and 41, although PMIP2 did not show temperature changes over Antarctica (as it is the case with 31 and 41). Parameter set 21 offers a good compromise between the temperature features that are correctly simulated by the model and those that are less well simulated.
The major feature of the changes in JJAS precipitation pattern (Figure 68), for the five parameter sets as well as for the ensemble mean PMIP2 simulations, is an enhanced monsoon over North Africa, Arabian Peninsula and India. The decrease in JJAS precipitation over the tropical oceans, present in PMIP2 simulations is also simulated with all the parameter sets, although the magnitude of the change varies according to the parameter set. Our simulations show three additional regions of increased summer precipitation that are not displayed in the ensemble mean PMIP2 simulations, i.e. the centre of North America, the south of Africa and the northeast of South America.

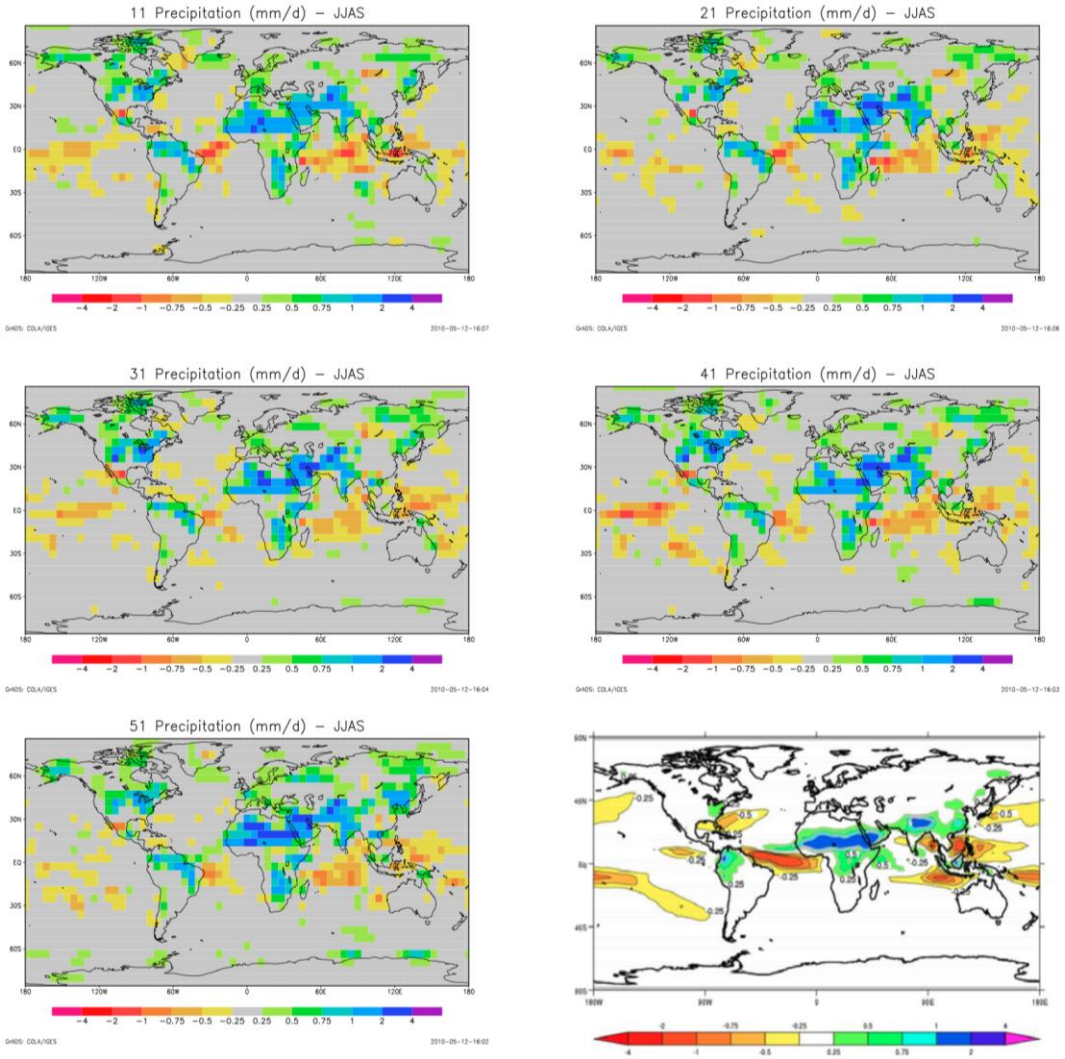

Figure 68: JJAS precipitation (mm/day) differences between mid-Holocene and present day for the five parameter sets and the ensemble mean of PMIP2 simulations (bottom-right).

All the parameter sets lead to a 'greening' of the Sahara at 6 kyr BP (Figure 69). The desert (Sahara and Arabian Peninsula) regressed at 6 kyr BP compared to present day, mostly at the expense of grass, in relationship with the increase in precipitation. This is in agreement with fossil pollen (Jolly et al., 1998) showing that the Saharan

desert was almost completely covered by annual grasses and low shrubs during the mid-Holocene. There is also evidence suggesting that it was then wetter than today (Petit-Maire and Guo, 1996).

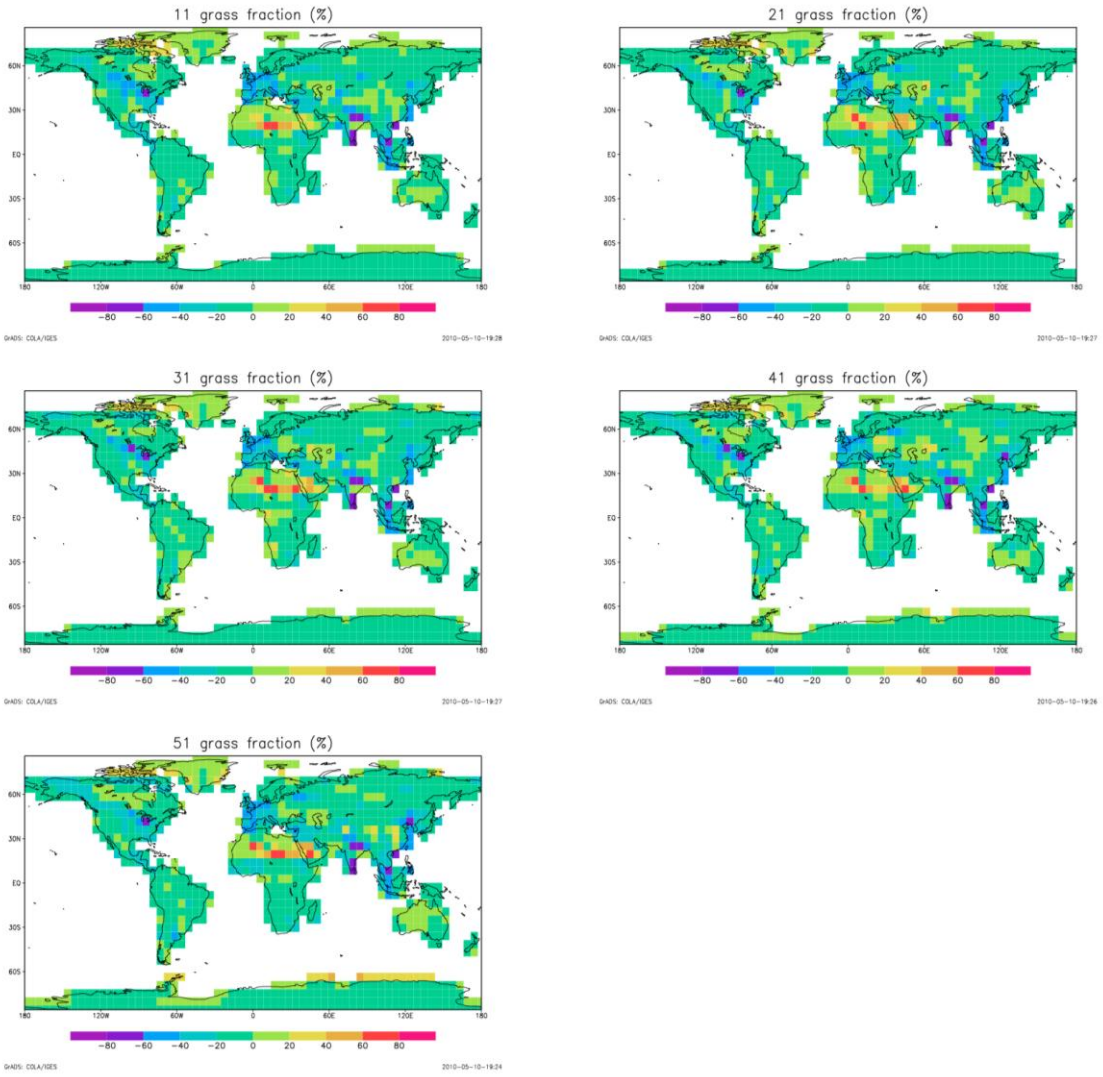

Figure 69: Grass fraction at 6 kyr BP according to the five selected parameters sets. Maps are showing the deviation from the mean value computed over the time interval 1980-2000 AD in the corresponding millennium experiments.

The early Holocene

The simulated early Holocene climates (quasi-equilibrium simulations at 8 kyr BP) for the same parameter sets (11, 21, 31, 41, 51) are then compared the 21st century climates obtained in the transient simulations from 8 kyr BP to 2100 AD. We find a surprisingly strong relationship between the Arctic summer sea ice extent simulated for the two periods (Figure 70) (Goosse et al., 2007).

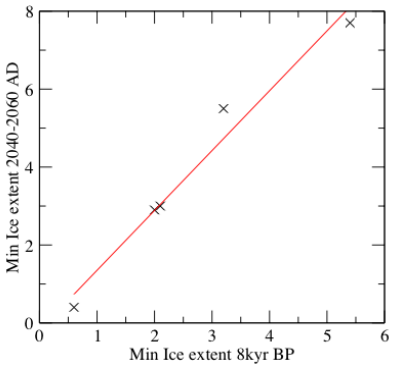

Figure 70: Link between the Arctic summer sea ice extent (in 10^6 km^2) for the early Holocene and the period 2040-2060 AD. Simulations corresponding to different parameter sets (E11, E21, E31, E41, E51) are represented by a cross. The red line is a regression line for those five points.

In particular, the summer ice extent averaged over the period 2040-2060 is very close to 1.5 times the one simulated for 8 kyr BP, for all the model simulations. This strong relationship between the simulated decrease in the summer ice extent in the future and for 8 kyr BP is obtained for a wide range of model responses despite the very different forcings during the two periods. Indeed, the forcing is slowly varying for the early Holocene and has a very strong seasonal cycle. By contrast, the forcing is changing rapidly over the 20th and 21st centuries, the climate system being clearly in a transient state, and the forcing is more widely distributed for the different seasons. Information about the state of the climate system during the early Holocene can thus help us to estimate the strength of those feedbacks and thus to reduce our uncertainties on future changes. Information on the observed ice extent during the early Holocene is quite fragmentary. In the framework of the International Polar Year, new oceanic cores have been collected in the Arctic, providing new information on the summer ice extent during the early Holocene. Such observations and similar ones, in particular north of the Siberian shelves, could provide strong constrains on model behaviour, complementary to the ones obtained from recent observations. This will then allow to select the parameter sets that are the most realistic and to reduce our uncertainties on the future decline of the ice cover.

The 8.2 kyr BP event

Here we pertub the 8.5 kyr BP equilibrium simulations by releasing additional fresh water into the Labrador sea (see description of the experiments, section B.4) in order to mimick the 8.2 kyr BP event. With all the six parameter sets used, the maximum value of the North Atlantic meridional overturning streamfunction weakens sharply after the introduction of the freshwater pulse. The MOC is reduced by 27 to 46% within 15 years. The reduction is the smallest with parameter sets 122 (27%) and 322 (32%) for which the initial value of the MOC is smaller than with the other parameter sets. The weakening phase is followed by a rapid acceleration back to the initial state. Then, the MOC returns back to a state close to the pre-perturbation one in less than 30 years. The MOC has completely recovered around less than 100 years after the perturbation for 112, 312 and 512 (i.e. parameter sets with the lowest MOC sensitivity). It takes a few decades more for the other parameter sets.

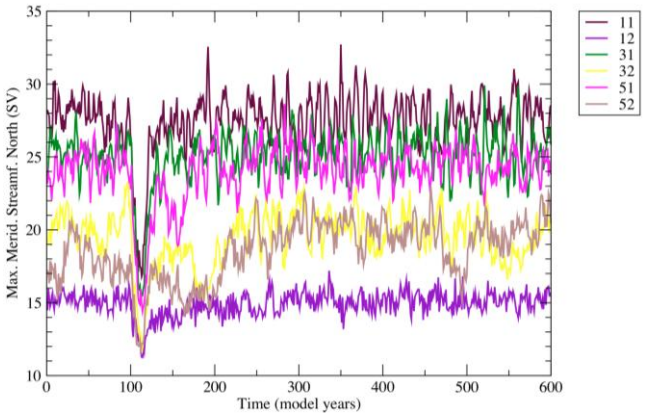

Figure 71: The maximum of the MOC (Sv) in the 8.2 kyr BP simulations without baseline flow for the different parameter sets. The freshwater pulse is introduced at time 100 (EH simulations before the year 100 and EHF simulations after).

Table XIV: The annual mean value of the maximum of the North Atlantic meridional overturning streamfunction below the Ekman layer (column 2) for the EH experiments and (column 3) for the EHF experiment. For EH the mean value of the last 100 years of the simulation is given. For EHF, the minimum value over the 20 years following the input of freshwater is given.

	EH	EHF
E112	27.7	16.8
E122	15.2	11.3
E312	25.3	15.1
E322	20.2	11.9
E512	24.4	14.4
E522	17.8	11.7

7. F simulations

The simulations covering the third millennium were performed for all nine climatic parameter sets in combination with three different ice sheet parameter sets and medium carbon cycle parameter set. We first show the general model response for medium ice sheet sensitivity and include the two other ice sheet parameter sets when discussing ice-climate interactions.

Temperature and climate change over the third millennium

The climate sensitivity of the model directly translates into a respective change of global mean surface temperature (Figure 72). Temperature changes over the Greenland and Antarctic ice sheets show a relatively strong polar amplification in both hemispheres, as discussed above. Local differences of the average temperature over the ice sheets compared to the global trend are visible.

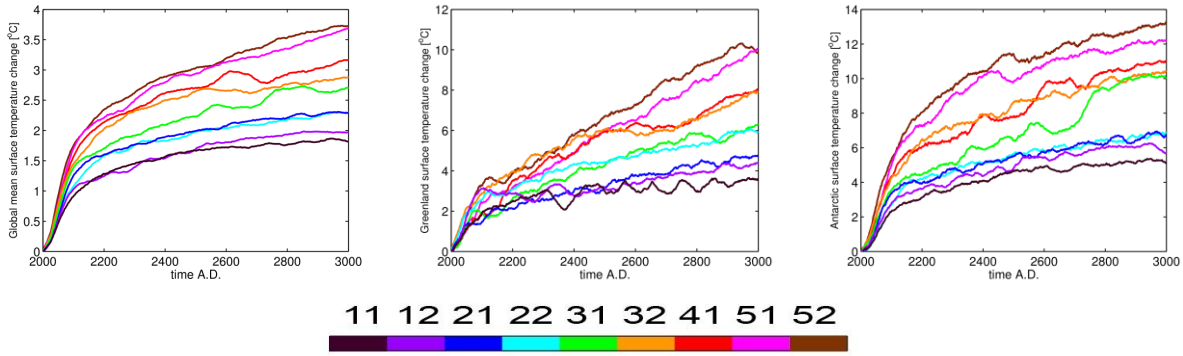

Figure 72: Global mean temperature changes during the third millennium for scenario A1B (left) and over the Greenland and Antarctic ice sheets (middle and right, respectively). Only medium carbon and ice sheet parameters (2) are shown.

Carbon and climate change over the third millennium

Experiments performed with the emission scenario A1B exhibit a large atmospheric CO_2 increase up to the year 2200 AD when emissions cease (Figure 73, left). All model versions predict a long lasting atmospheric perturbation. The perturbation here is larger than that in Plattner et al. (2008) since, in the present work, emissions do not abruptly end in 2100 AD but slowly decline after that date. In 3000 AD, the atmospheric CO_2 content is approximately reduced by half with respect to its maximum value in most cases. The climatic parameter set 11 exhibits a faster decrease, due to a larger ocean ventilation rate. With each of the climatic parameter set, the land uptake of CO_2 drastically diminishes shortly after the end of emissions; from then on, the ocean is driving the atmospheric CO_2 level. For the same climate sensitivity no significant differences among simulations performed with different ice sheet parameters are observed.

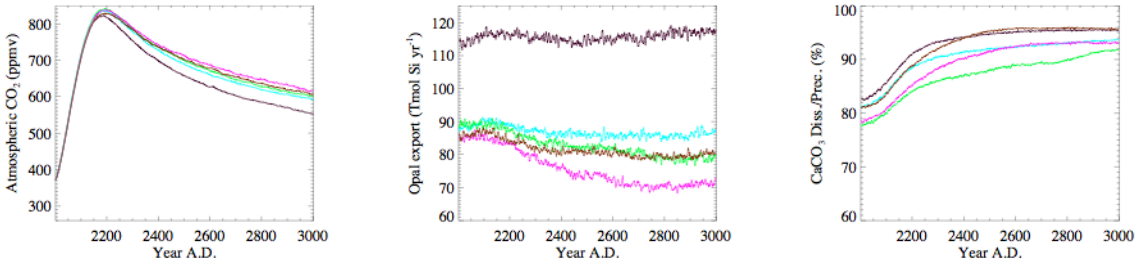

Figure 73: Temporal evolution of atmospheric CO_2 concentration (left), opal export (middle) and ratio of dissolved over precipitated $CaCO_3$ shells (right) over the next millennium. The same colour code as in previous figures is used. The five experiments illustrated were performed under emission scenario A1B with carbon sensitivity 2 and ice sheet sensitivity 2.

The main changes occurring in the ocean biogeochemical cycles are related to the opal export and to the CO_2 invasion at depth. The opal export exhibits different fates under different climatic parameter sets (Figure 73, middle). While there is a modest increase in the 21st century in some cases (climatic parameter sets 11, 22 and 52), the general tendency is a steady decrease over the following centuries with the exception of climatic parameter set 11. The decrease is significant with climatic parameter set 51, since, at the end of the experiment, the opal export decreases by about 17% with respect to its value in 2000 AD. The behaviour of simulation “11” is

explained by the low MOC streamfunction decrease and the faster overturning of ocean waters observed with this parameter set. On the contrary, the MOC streamfunction decrease for set “51” is proportionally larger than with any other parameter set. The slower ocean ventilation results in a trapping of silica at depth, and a reduced availability in surface waters for opal shell buiding.
Significant changes in deep ocean chemistry occur in each of these experiments. CO_2 invasion at depth leads to an increase in the dissolution rate of calcium carbonate ($CaCO_3$) shells. $CaCO_3$ shell preservation over production drops from around 20% to much less than 10% at the end of the millennium (Figure 73, right). In the end, this constitutes a negative, though small, feedback on atmospheric CO_2 level. The rate of change of the dissolved fraction reflects the CO_2 invasion rate, which is directly related to the deep ocean ventilation rate.

Dynamic response of the ice sheets in simulations over the third millennium

The results for the continental cryosphere and sea level are similar for similar warming and scale well with the rate and amount of radiative forcing. In first order, changing model climate sensitivity or changing the forcing scenario for future atmospheric greenhouse gas concentrations influences the ice sheet response in similar ways. We therefore focus our physical analysis on the A1B scenario and include estimates for total sea level rise at the end of this section for all three scenarios (B1, A1B, A2).

Greenland

The response of the ablation ratio (mean ablation to mean accumulation) is dominated by a steep increase in mean ablation and remains above one in all experiments (Figure 74a). Ablation starts to decrease only when most of the ice is already removed in high sensitivity models. For low sensitivity models, the ablation fraction is still increasing at the end of the third millennium, despite the fact that the greenhouse gas forcing has long been stabilized. In the process, calving shows a steep decrease in the first 100 to 200 years as the ice sheet retreats from the coast (Figure 74b). Volume and area of the Greenland ice sheet are consequently decreasing for all experiments (Figure 74c), with a rate relative to the climate sensitivity of the models. The ice is almost completely removed in high sensitivity experiments at the year 3000, which causes freshwater fluxes to decrease in the last part of the simulation, while runoff over land increases accordingly (Figure 74d). It is noteworthy that none of the model versions shows a slowing of volume losses for the A1B scenario over the course of the third millennium unless if the ice sheet is already mostly removed.

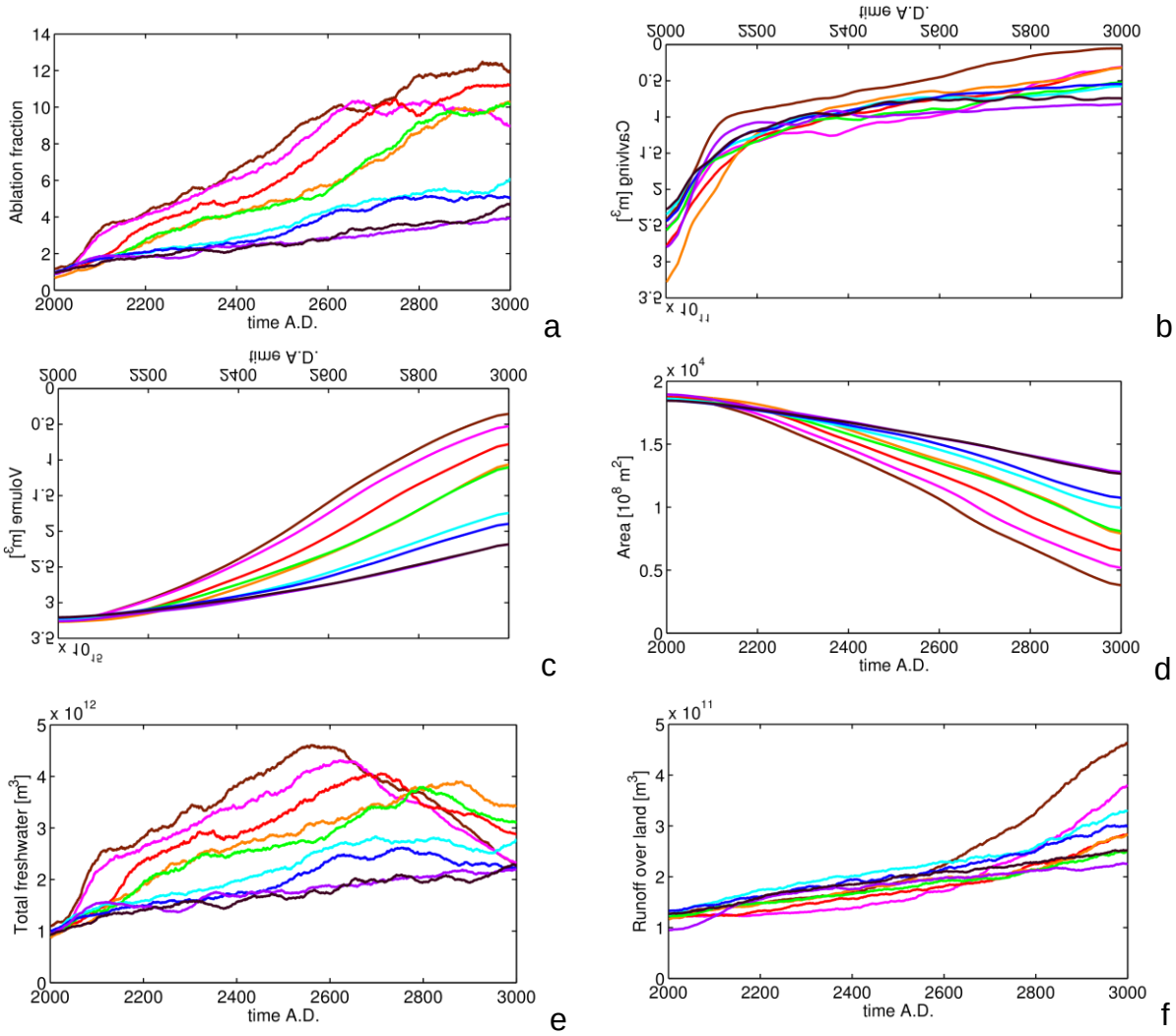

Figure 74: Evolution of major variables of the Greenland ice sheet: ratio of mean ablation to mean accumulation: (a), calving (b), volume (c) and area (d). Total freshwater fluxes (e) and runoff over land (f) are given in m^3/year (same colour code as in Figure 72). Note that 10^{12} m^3/year equals approximately 0.03 Sv.

Figure 75 gives snapshots of the melting Greenland ice sheet for three different model versions. While small differences in regional response patterns are apparent between different parameter sets, the total rate of change scales with climate sensitivity of the model. The ice sheet retreat first occurs in the southwest, where already today a 300-km wide band of tundra is present. After several centuries of retreat, the Greenland ice sheet becomes fully land-based. The central dome survives longest at an almost constant elevation of around 3000 m. The ice sheet ultimately retreats to the eastern mountains, gradually exposing bare land, which can heat up much more during the summer than the ice cover because of a lower albedo.

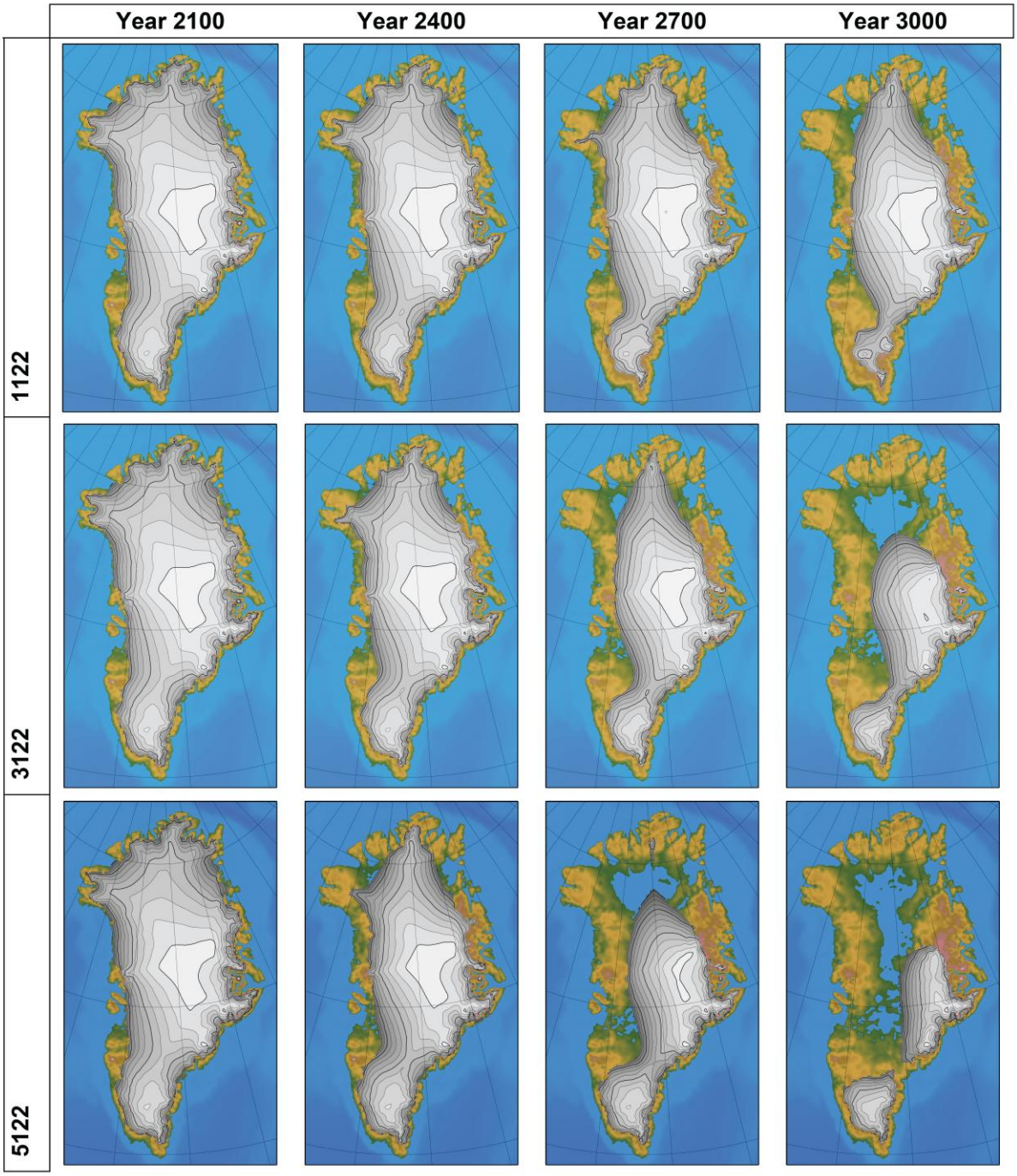

Figure 75: Evolution of the Greenland ice sheet in different experiments. The background field is for surface elevation. Ice sheet cover is shaded grey and contoured every 250 m, ice-free areas range from green to red and blue colours depict the ocean. Thick contour lines over the ice are for every 1000.

Antarctica

The grounded ice volume of the Antarctic ice sheet (Figure 76a) increases slightly before decreasing in all but the highest sensitivity experiment (5222). Volume changes after 2400 AD are negative for all runs. Changes in grounded ice area (Figure 76b) are related to grounding line retreat mainly in West Antarctica.

Grounded ice accumulation volume shows a weak increase of 10-25% over the course of the third millennium largely unrelated to the model climate sensitivity (Figure 76c). For high sensitivities, surface conditions along the margin of Antarctica take on characteristics of the present-day Greenland, and surface melting (Figure 76d) becomes a dominant factor for the mass balance of the ice sheet. Note that at the year 3000, ablation exceeds accumulation and the surface mass balance is negative for the four models with highest climate sensitivity. Furthermore, accumulation has mostly stabilized at that point, while ablation increases further at an almost constant rate. Since the climate forcing has long stabilized at this point, the melting of the Antarctic ice sheet can be expected to continue for a long time thereafter.

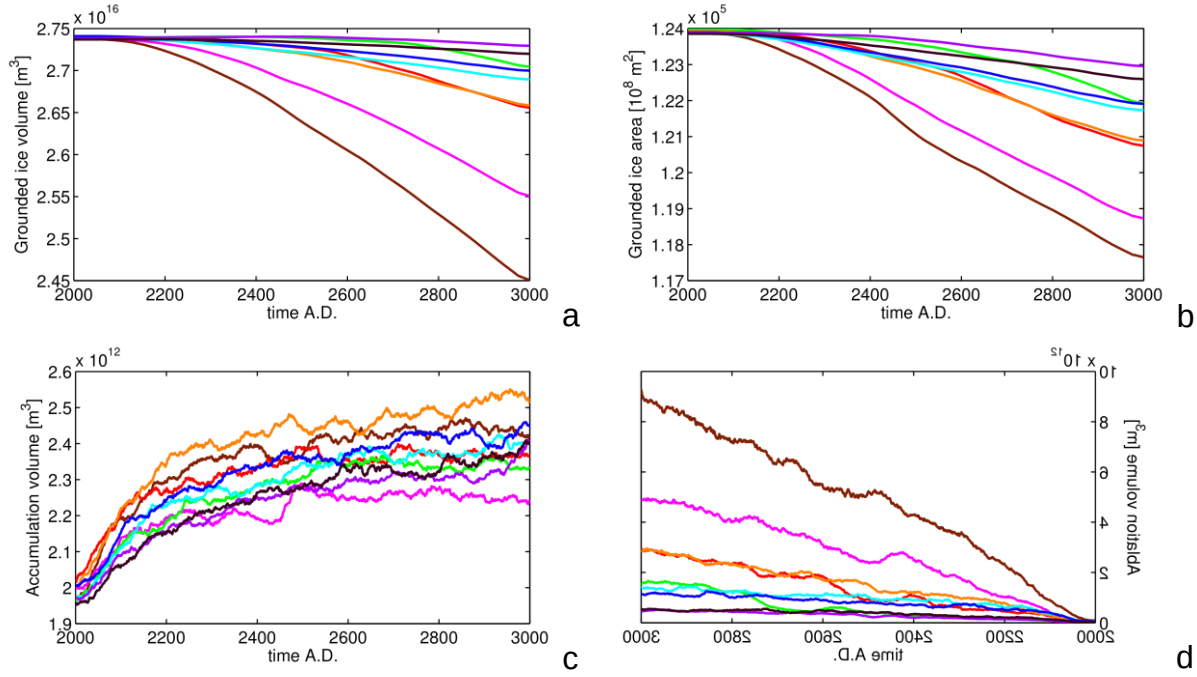

Figure 76: Grounded ice volume (a), grounded ice area (b), grounded ice accumulation volume (c) and ablation volume (d) of the Antarctic ice sheet for scenario A1B. See colour code in Figure 72.

The mean basal shelf melt rate (Figure 77) increases during the third millennium proportional to the heat input under the Antarctic ice shelves by up to a factor of 6 and 16 for ice sheet sensitivity 'mid' and 'high', respectively. Basal melting reduces the thickness of the ice shelves and the buttresing effect, which causes an increase in ice velocities on the shelves and at the grounding line. This in turn increases losses from the grounded ice volume. In addition to increases in marginal ablation, basal ice shelf melting is the main reason for substantial Antarctic sea level contributions. A positive contribution to sea level rise at an increasing rate at the year 3000 indicates that the Antarctic ice sheet is still far from equilibrium with the imposed climate change. In effect, very long time scales of the order of 10^4 years are required before the Antarctic ice sheet eventually reaches a new steady state with less or almost no ice. The observed response for the high sensitivity models is probably an underestimate in case the large ice shelves would break up and calving could take place at grounding lines. These effects are not well represented in the current model, which was developed for generally colder conditions with ice shelves present. For high basal melt rates below the ice shelves as observed for the high

sensitivity models, it seems unlikely that the large ice shelves can be sustained, and they may well disintegrate after 500 to 1000 years (Warner and Budd, 1998).

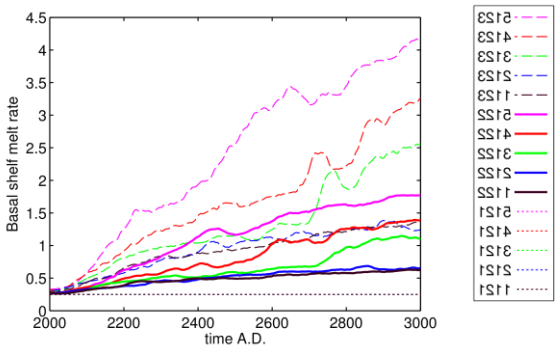

Figure 77: Mean basal shelf melt rate under the Antarctic ice shelves.

Figure 78 gives snapshots of the retreating Antarctic ice sheet for the highest climate sensitivity model. The most important change is grounding-line retreat for the West Antarctic ice sheet and along overdeepened glaciers of the East Antarctic ice sheet. At the millennial time scale considered here, ice thickness in central East Antarctica remains largely unaffected. For less sensitive model versions, the response is weaker, but follows the same geographical pattern. The grounded Antarctic ice volume is reduced at the end of the third millennium even for the lowest climate sensitivity model.

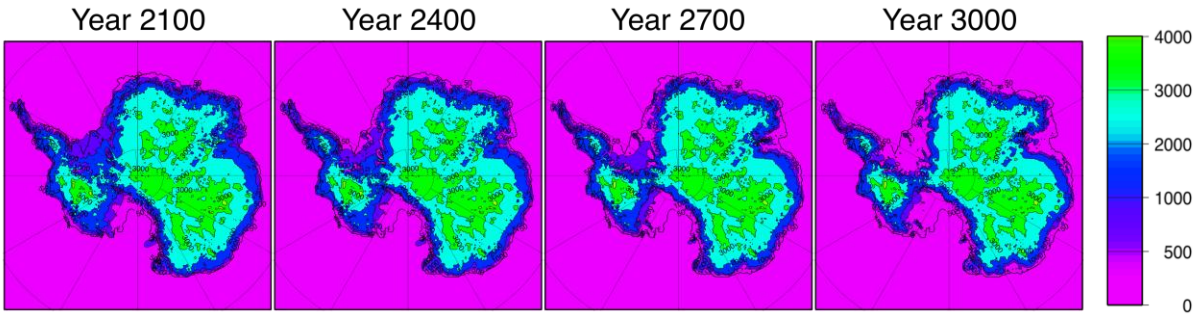

Figure 78: Evolution of Antarctic ice thickness in experiment 5122 for scenario A1B.

Ice-climate interactions

Dynamic coupling of the Greenland and Antarctic ice sheet models in LOVECLIM reveals a number of ice-climate interactions that are strong enough to have to be taken into account for transient climate simulations. Freshwater fluxes from the melting Greenland and Antarctic ice sheets have a potential influence on the heat exchange between atmosphere and ocean. For Greenland, meltwater fluxes to the ocean cause a weakening of the MOC streamfunction in all experiments (Figure 79a). In some of the simulations presented here, we even observe an almost complete shut down of the ocean thermohaline circulation. The associated reduction in meridional heat transport leads to a local relative cooling in the northern North Atlantic, which is further amplified by the sea ice-related feedbacks. For Antarctica, freshwater fluxes cause a shallow halocline, weakening of deep water formation, reduction of vertical heat exchange in the ocean and a larger sea ice cover (Swingedouw et al, 2008). Again, sea ice-related feedbacks amplify the local relative cooling to a degree that the combined effect of the Northern and Southern

Hemisphere signals becomes visible in the global mean surface temperature evolution (Figure 79b). The models with the lowest ice sheet sensitivities and thus with the lowest freshwater fluxes therefore show the highest global surface temperature rise. This is consistent with another mechanism that links lower ice sheet sensitivities to a lower oceanic thermal expansion (Figure 79c). Less freshwater input from the ice sheets yields a stronger heat release from ocean to atmosphere. This reduces the oceanic heat content, which ultimately leads to a small reduction of sea level rise due to thermal expansion compared to models with higher ice sheet sensitivity.

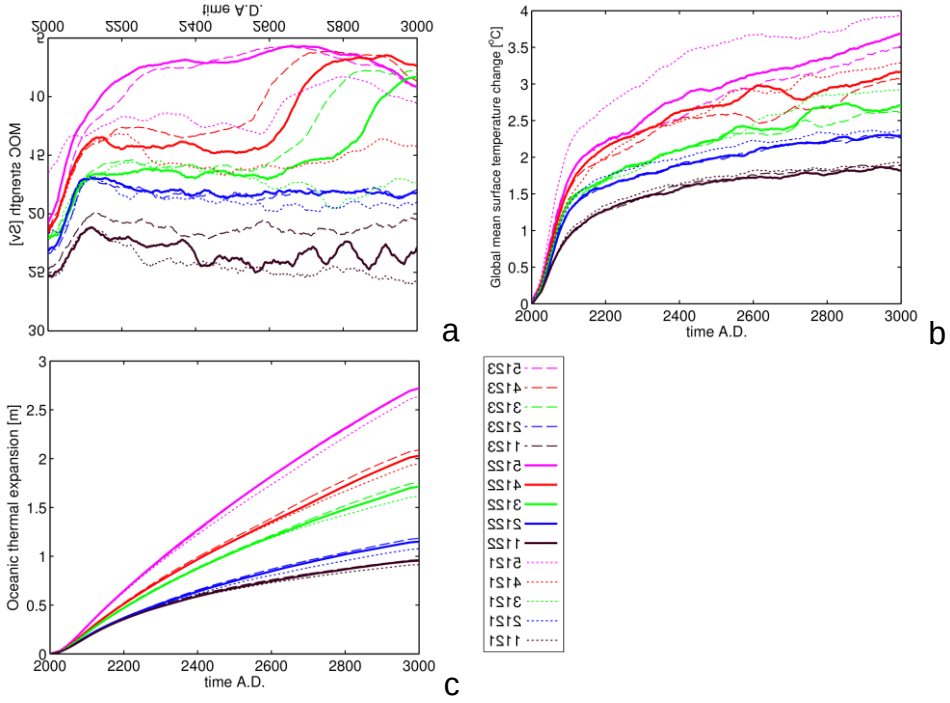

Figure 79: MOC strength (a), global mean surface temperature change (b) and sea level rise due to thermal expansion (c), all depend on ice sheet sensitivity.

Total sea level estimates

In the following, we give total sea level rise projections for the third millennium including contributions from oceanic thermal expansion, the Greenland and Antarctic ice sheets, small ice caps and glaciers. Melting of glaciers and small ice caps is calculated in an off-line procedure based on the temperature evolution of the whole model run (Raper and Braithwaite, 2006). With this component, the global sea level budget (except for changes in water storage on land) is closed.

Glaciers and small ice caps combined have the potential to contribute only 21.8 cm to sea level rise. For scenario A1B, most glaciers disappear after already 400 years, dependent on the model sensitivity, while small ice caps largely disappear before the end of the third millennium (Figure 80).

Oceanic thermal expansion is steadily increasing in all experiments, as more heat is stored in the oceans (Figure 81). Since the deep ocean has a relatively long response time scale, the sea level contribution is still increasing at the end of the 1000-yr experiments at an almost linear rate.

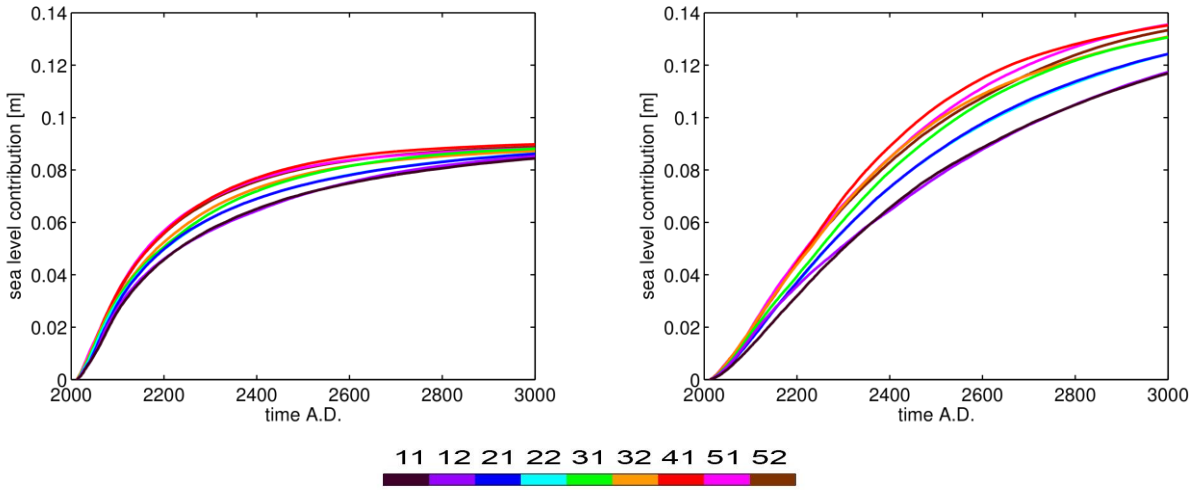

Figure 80: Sea level contributions from glaciers and small ice caps for scenario A1B. For clarity only models with medium ice sheet and carbon sensitivities are displayed.

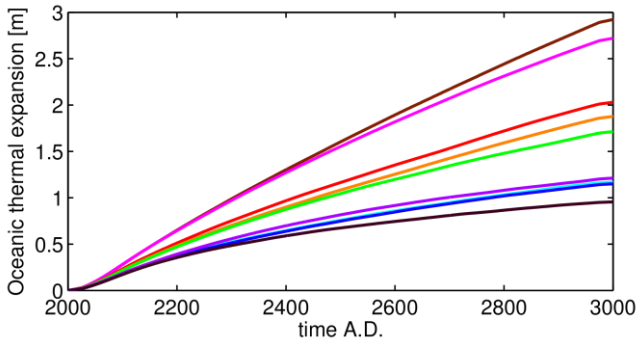

Figure 81: Sea level contribution from oceanic thermal expansion for scenario A1B. See colour code in Figure 80. For clarity, only models with medium ice sheet and carbon sensitivities are displayed.

In addition to the observed warming in the atmosphere, the amount of sea level rise due to thermal expansion also depends on the heat exchange between atmosphere and ocean. It can be affected e.g. by changes in oceanic circulation and sea ice cover. An alternative display of the model results is therefore shown in Figure 83, which includes information about different scenarios and climate and ice sheet sensitivities. All models align quasi-linearly in this plot, which shows the sea level contribution from oceanic thermal expansion as a function of the temporal average global mean temperate change wrt. 2000 AD. Changing ice sheet sensitivity (different symbols) leads to a different temperature response, due to the influence of meltwater fluxes on the climate sensitivity of the models (see discussion above). Furthermore, the sea level contribution for a given average warming is lower for low ice sheet sensitivity models. In these cases, less meltwater input to the ocean compared to the standard models means stronger ventilation and exchange of heat between ocean and atmosphere. This effect is amplified by sea ice-related feedbacks and causes more heat release from the ocean and consequently lower thermal expansion.

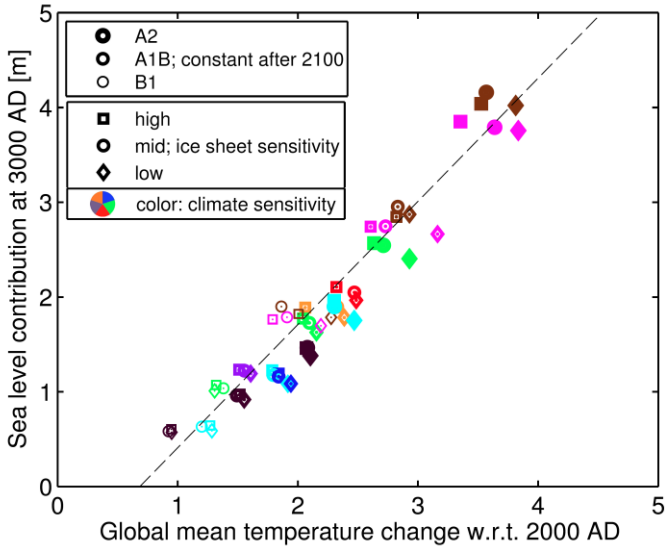

Figure 82: Sea level contribution from oceanic thermal expansion in the year 3000 AD as a function of temporal average global mean temperature change wrt 2000 AD.

The sea level contribution from the Greenland ice sheet directly scales with ice volume changes in our model because all ice is assumed to be land-based (Figure 83, left). That is distinct for the Antarctic ice sheet where marine ice removed below floatation is replaced by ocean water, as is accounted for in our model (Figure 83, right).

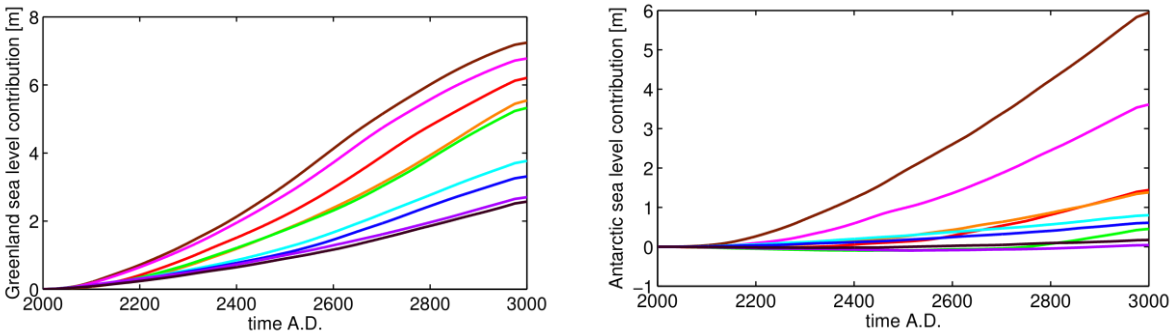

Figure 83: Sea level contributions from Greenland (left) and Antarctica (right) for scenario A1B. See colour code in Figure 80. For clarity only models with medium ice sheet and carbon sensitivities are displayed.

Looking at the sea level contribution as a function of temporal average ice sheet wide mean temperature change reveals that changing scenario (thickness of symbols) and changing model climate sensitivity (colour of symbols) have a similar impact on the Greenland ice sheet (Figure 84, left). All experiments align around a curve that is limited for cases of extreme warming by the total available ice volume of the GIS of around eight meter sea level equivalent.
The ice shelf melt parameterisation in the Antarctic model has a strong influence on the sea level response of the Antarctic ice sheet (Figure 84, right). For model E11 as an example, the lowest ice sheet sensitivity models show no or even a negative contribution to sea level change depending on the applied scenario. This is due to an

increase in accumulation over Antarctica for all warming scenarios that cannot be balanced by increases in ablation or grounding-line retreat in these experiments.

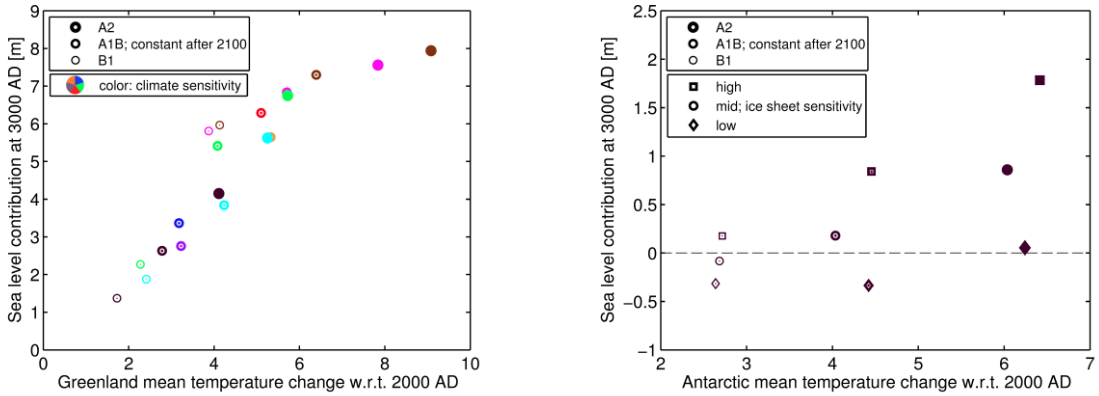

Figure 84: Sea level contribution from the Greenland (left) and Antarctic (right, model E11) ice sheets in the year 3000 AD as a function of temporal average ice sheet wide mean temperature change wrt 2000 AD.

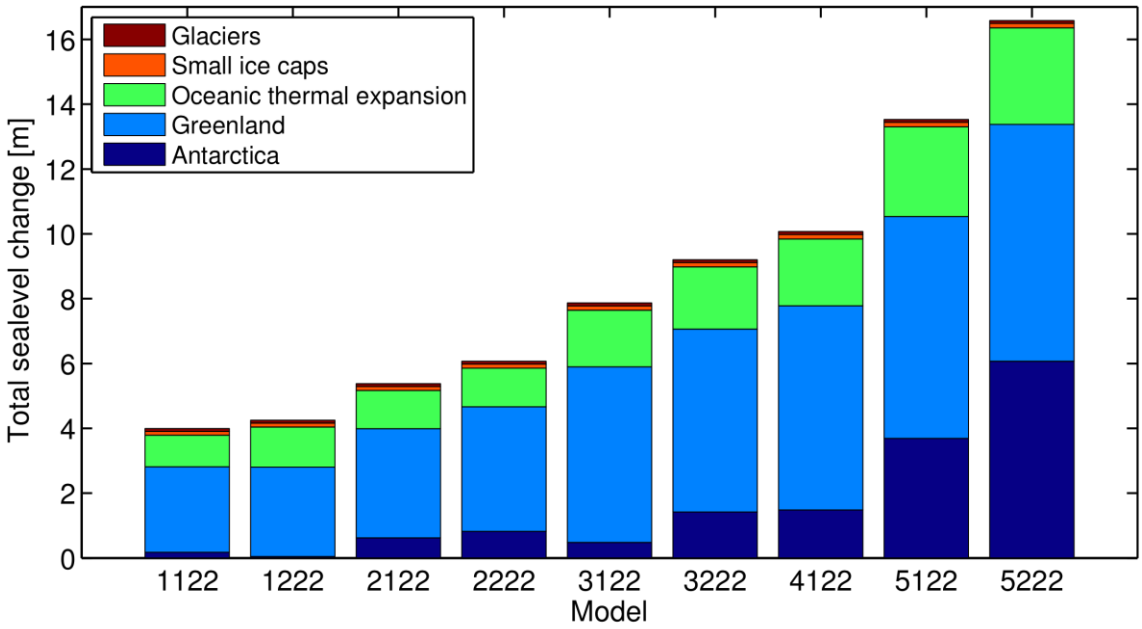

Figure 85: Total sea level change in the year 3000 AD and its components for scenario A1B. For clarity only models with medium ice sheet and carbon sensitivities are displayed.

Contributions of Greenland, Antarctica and thermal expansion and their relative importance depend strongly on climate model sensitivity (Figure 85). The Greenland ice sheet almost completely disappears in high sensitivity models before the end of the third millennium, adding a maximum possible amount of ~8m to sea level rise. The response of the Antarctic ice sheet is more dependent on the choice of model parameters than the Greenland ice sheet, with low climate sensitivity models switching to an overall negative mass balance of the Antarctic ice sheet only in the last half of the third millennium. For scenario A1B, all models of different climate sensitivity project a sea level rise of more than four meters over the third millennium.

Taking into account the relatively high polar amplification of LOVECLIM, sea level projections of the high climate sensitivity models of up to 16 meters have to be considered with caution.

8. Bistability and regrowth of the Greenland ice sheet

One of the open questions for long-term future ice sheet evolution revolves around the two connected problems of the stability of the Greenland ice sheet and the reversibility of Greenland ice sheet melting. It is of great interest to establish whether there exists a 'threshold of reversibility' beyond which Greenland melting becomes self-sustained due to the feedbacks in the coupled ice sheet–climate system (e.g., Gregory et al., 2004; Gregory and Huybrechts, 2006; Ridley et al., 20010) for present-day climate conditions. Connected to this issue is the question under which conditions the Greenland ice sheet would regrow, once it has been completely removed (e.g., Lunt et al., 2004; Toniazzo et al., 2004).
We tackled these questions with idealized experiments in which the CO_2 concentration is raised to four times its pre-industrial value for 3000 years and reset to lower values thereafter. In a first set of experiments we tested the effect of imposing lower levels of CO_2 concentration (200, 280, 380 ppmv) when the ice sheet has completely disintegrated after ~3000 years (Figure 86). We observe a very slow regrowth for 200 ppmv and 280 ppmv with a linear trend that indicates growth times between 350 kyr (200 ppmv) and 1000 kyr (280 ppmv). No regrowth of the Greenland ice sheet could be established for 380 ppmv.

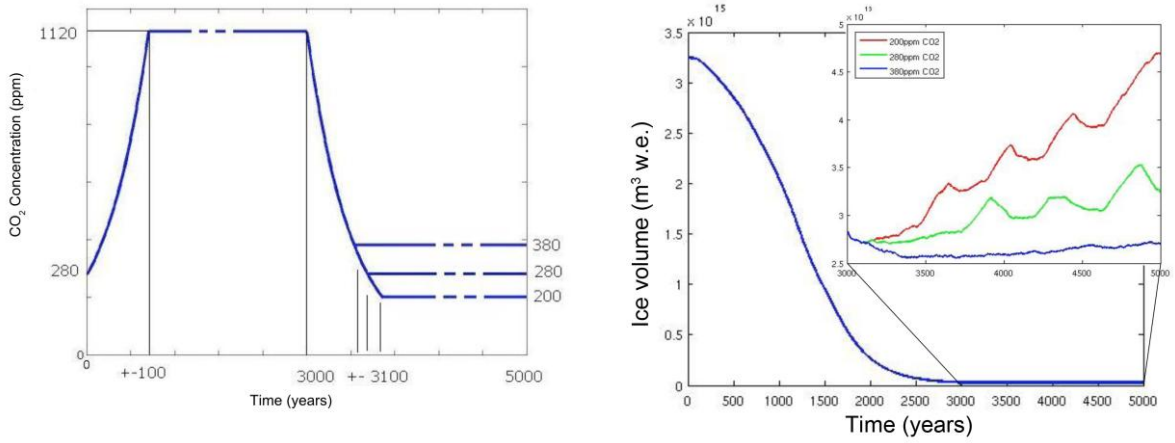

Figure 86: Idealized CO_2 scenarios for testing reversibility of Greenland ice sheet growth (left). The atmospheric CO_2 is increased to four times the pre-industrial value of 280 ppmv and then held constant in order to provide a warm enough climate to completely melt the ice sheet. After 3000 years the CO_2 concentration is reduced to 200 ppmv, 280 ppmv and 380 ppmv corresponding to glacial, pre-industrial and current CO_2 levels, respectively. Greenland ice sheet volume evolution (right). The inset in the right panel zooms in on the last 2000 years of the integrations and shows the responses to three different equilibration levels of CO_2 in more detail.

In a second set of experiments, we therefore reset the CO_2 concentration to glacial conditions (200 ppmv) after 500 years, 1500 years and 3000 years during disintegration of the ice sheet (Figure 87, left). The ice sheet disintegration halts for a large initial ice sheet after 500 years (Figure 87, right) when ~85% of the present-day volume is still remaining. The ice sheet continues to melt away for a small initial ice sheet (~15% of present-day volume) after 1500 years. No regrowth of the Greenland ice sheet is observed for any of these three experiments.

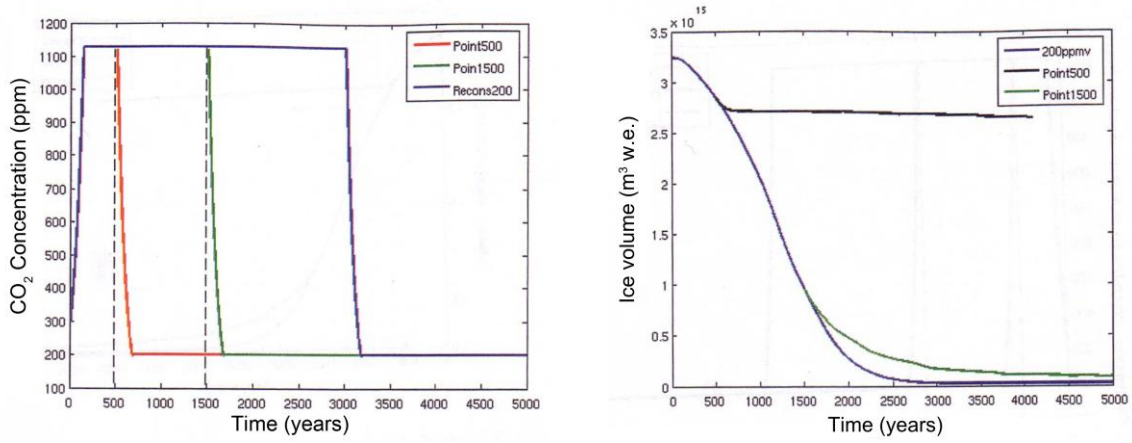

Figure 87: Ice volume evolution for the idealized CO_2 scenario.

Although these experiments indicate a bistability of the Greenland ice sheet in LOVECLIM, the reasons have to be further investigated and analysed. It may be necessary to run the experiments for much longer times than 2000 years, since a gradual cooling in response to lowering CO_2 concentration is still ongoing after 2000 years. This could be done with asynchronous coupling between climate and ice sheet in order to reduce the computing time. Delayed rebound of the bedrock furthermore makes the surface temperatures initially too high, which inhibits the regrowth. The effect of orbital parameters has not been considered in the presented experiments, which could have an effect on the results. The coupling procedure between atmosphere and ice sheet should also be carefully revised, since the lapse rate for elevation corrections may introduce unwanted biases. Finally, the relatively coarse resolution of climatic input to the ice sheet model may play a crucial role in preventing the regrowth of an ice sheet. All these caveats considered, an in depth investigation of all aspects of the GIS bistability problem with LOVECLIM could be undertaken, but has not been done in this project.

9. Concluding remarks

This ASTER project allowed us developing and improving the LOVECLIM model. It is a very important and valuable tool to study climate changes, both in the past (for assessment of the model) and in the future (for climate projection). Its high computational efficiency allows performing a large number of experiments of long duration. The new version of the model (LOVECLIM1.2) released during and thanks to the ASTER project is available on http://www.climate.be/loveclim, for both the project partners and the whole scientific community.

In order to investigate the parameter uncertainty in LOVECLIM, we varied values of key physical parameters in order to estimate the range of model response for standard sensitivity experiments, to assess the ability of the model to simulate past climates according to the parameter sets and to compute the range of response for climate projections. Therefore, we selected nine “climatic” parameter sets, three “carbon cycle” parameter sets and three “ice sheet” parameter sets because they yield present-day climate simulations coherent with observations. Combination of those parameter sets lead to a sensitivity to CO_2 doubling ranging from 1.6 to 3.8°C and a reduction in the MOC intensity from 15 to 75% in response to a freshwater

hosing. Note that those numbers are obtained without interactive carbon cycle and ice sheet components[6].

Equilibrium simulations of the LGM climate show that only the parameter sets leading to low climate sensitivity (i.e. 11, 12, 21, 22) yield reasonable results, the cooling in high latitudes being too strong for the high climate sensitivity parameter sets. This is a direct consequence of the relatively high polar amplification simulated by LOVECLIM. According to transient simulations carried out over the Holocene without carbon cycle and ice sheet components, it appears that, among the parameter sets used (i.e. 11, 21, 31, 41 and 51), 51 is clearly in disagreement with the very few reconstructions of the summer sea ice extent during the early Holocene. Moreover, the broad features of the mid-Holocene climate do not differ much according to the parameter sets. Nevertheless, climatic parameter set 51 is the only one that yields an annual mean surface warming in the North Pacific and North Atlantic Oceans that is in agreement with PMIP2 (Braconnot et al, 2007), while the simultaneous cooling off the Antarctic continent and the unchanged temperature over that continent suggested by PMIP2 (Braconnot et al., 2007) is only reproduced with climatic parameter set 21. These results clearly point towards the impossibility to find 'the perfect' parameter sets among those selected for this study.

Our sudy of the climate evolution over the last few decades of the 20th century reinforces this conclusion. Indeed, only a few parameter sets are able to reproduce the observed trends of key climatic variables over the last few decades (such as global annual mean surface temperature, Northern Hemisphere minimum sea ice extent or oceanic heat content). For example, carbon cycle parameter set 3 overestimates the increase in atmospheric CO_2 concentration over the last 50 years. Climatic parameter sets with low climate sensitivity (simulations 1x, 2x) are 'scoring' low when assessing the model ability to reproduce recent climatic trends. Amongst the 'best' simulations configurations 321, 322, 511 and 512 display good performances for both Conc and Efor, either for S1 or S2 sulphate forcing. Moreover, no parameter set allows the model simulating simultaneously a correct time evolution of upper ocean heat content and of Northern Hemisphere summer sea ice extent or of annual mean surface temperature. This drawback should be investigated in further studies.

Several simulations over the third millennium were performed with LOVECLIM, with the different parameter sets, using SRES greenhouse gas scenarios (B1, A2, A1B) until 2100 AD and greenhouse gas concentrations maintained at their levels as in 2100 AD until the year 3000 AD. According to these simulations, the global annual mean surface temperature increases by 1.7 to 3.2°C after 1000 years for scenario A1B with medium carbon and ice sheet sensitivities, depending on the climate sensitivity. The Greenland ice sheet does not completely disappear before 3000 AD, according to the range of parameter sets and forcings used here, although it loses 95% of its present-day volume in the most extreme case (mostly related with high climate sensitivity). Moreover, the same parameter sets also induce an important melting of the Antarctic ice sheet. We conclude from all our experiments that a global eustatic sea level rise of at least 2 m is very likely to occur before the end of the third millennium. For scenario A1B and medium ice sheet and climate sensitivities, the value is ~9 m. The upper bound in excess of 20 m is however considered very unlikely to occur, in part because of the large polar amplification in LOVECLIM.

[6] see the detailed description of these sensitivity experiments in section B.4.

Another major question related to global warming is related with change in the ocean circulation. From our sensitivity experiments, it appears that only massive input of freshwater and highly sensitive parameter sets could lead to a strong reduction (even an almost complete shut down) of the ocean thermohaline circulation. Such massive input of freshwater is unlikely to occur.

3. POLICY SUPPORT

The work made within ASTER is a contribution to the ongoing international scientific effort to better understand climate change and to assess more accurately the uncertainties associated with climate and sea level projections. This is needed in order to provide a sound basis for policies designed to address the challenge of climate change. The problem is most likely to become more and more important. This is why each Party to the United Nations Framework Convention on Climate Change (UNFCC) has committed itself to "promote and cooperate in scientific (...) research (...) related to the climate system and intended to further understand and reduce the remaining uncertainties (...)" (UNFCC Article 4.1 (g)).

The specific objective of ASTER, i.e. assessing model uncertainties in long-term climate and sea level change projections, fully meets one of the major goals of the IPCC for its next assessment report (AR5). The ASTER outcomes are therefore expected to be part of this report, which will be an invaluable tool for the policymakers. Finally, the ASTER project has allowed Belgian teams to keep a global climate modelling potential operational. The expertise build up in these teams has been solicited by policy makers at both the national and international level, for instance for risk analysis assessments on future sea level rise. Two of the ASTER promotors (TF and PH) have been nominated as key contributors of the IPCC AR5 due in 2013, and therefore will contribute directly in the underpinning of the scientific basis of climate change.

4. DISSEMINATION AND VALORISATION

Scientists involved in ASTER disseminated the results of this project through international research programmes on and assessments of climate change such as the European Union's Sixth and Seventh Framework Programme, WCRP (CliC, CLIVAR, COPES), IGBP (SOLAS) and SCAR (ACE) and IPCC.

Dissemination took place via the training of Master students, PhD students and postdoctoral researchers, participation in working groups, presentations at national and international scientific workshops and meetings (see list below), and publication of results in international, peer-reviewed scientific journals (see section 5).

ASTER results were also transferred to the Belgian Science Policy through annual reports and meetings with the follow-up committee. These meetings allowed constructive discussion between scientists of slightly different horizons: those who model the global and regional climate, and those who have expertise in impact studies. The discussion between these two groups led to a better tuning between offer and demand of model outputs.

In addition, a web site devoted to ASTER was created (http://www.astr.ucl.ac.be/ASTER/). This web site provides full information about the objectives, the model, the progress of the project and some important findings. Furthermore, it includes a database with the relevant model outputs (mostly as atlases). The numerical results themselves, because of their size, are stored on a mass storage repository. This database (atlases and numerical values) is accessible to the whole scientific community upon request.

Members of ASTER also took part in dissemination activities intended for the general public. In particular, the ASTER results were presented to students in primary and secondary schools during the "Atelier Scienceinfuse", "Festival Scienceinfuse – Printemps des Sciences" and "Journée des Rhétos". Some results were also forwarded to the PolarFoundation for a climate exhibition. The researchers also gave numerous interviews on the issue of global change to the international and local press (TV, radio and newspapers), presentations for several organisations as part of university outreach programmes and lectures for different societies as well as intended for the general public.

Networking

The ASTER project has fostered and strengthened collaborations with other research groups using the same modelling tool. The improvements made within the project and the results obtained have helped to launch new collaboration with foreign researchers, e.g., University of Hawaii. Furthermore, we could count on help from colleagues abroad to address some weaknesses of the model and thus to produce an improved version (e.g., MIT). These improvements allowed us making available to the scientific community a new version of LOVECLIM. The ongoing close collaboration with the Vrije Universiteit Amsterdam (The Netherlands) was also made possible through the work done within ASTER. More than ten research groups in the world are now using LOVECLIM, e.g., ETH (Switzerland), Universidade de Vigo (Spain), University of Hawaii (USA), Rutgers University (USA), Yokohama Institute for Earth Sciences (Japan), Vrije Universiteit Amsterdam (The Netherlands), University of Tulan (USA), Deferal Univseriyr if Viçosa (Brazil), University of Kiel (Germany), Penn State University (USA) and University of Bremen (Germany). The ASTER project has allow to establish or reinforce such collaborations.

The expertise gained through this project allows us taking part in several research programmes. PMIP2 and PMIP3 study the role of climate feedbacks arising for the different climate subsystems (atmosphere, ocean, land surface, sea ice and land ice) and evaluate the capability of the climate models to reproduce climate states that are radically different from those of today. The scientific goal of The Global Carbon Project is to develop a complete picture of the global carbon cycle including both its biophysical and human dimensions together with the interactions between them. Past4Future is a Collaborative Project under the 7th Framework Programme (FP7) of the European Commission. It investigates the climate and environment of past warm periods (interglacials) to inform on future climate and possible abrupt changes. Ice2sea, funded by FP7 aims at improving projections of the contribution of ice to future sea-level rise.

Scientific missions with communication involving ASTER members

BE-POLES Workshop, Brussels (Belgium), 23-25 March 2006.

1. Goosse, H., O. Arzel, A. De Montety, E. Driesschaert, T. Fichefet, W. Lefebvre, and H. Renssen: Climate change and climate variability in polar regions. Royal Museum of Natural History.
2. Driesschaert, E., V. Brovkin, T. Fichefet, H. Goosse, P. Huybrechts, I. Janssens, A. Mouchet, and G. Munhoven: Impact of a Greenland deglaciation on climate during the next millennia.
3. Pattyn F., J.L. Tison, P. Huybrechts, D. Samyn, and R. Lorrain: Antarctic subglacial processes and interactions: the role of transition zones in ice sheet stability.

AGU Ocean Sciences Meeting, Honolulu (USA), 20-24 February 2006.

4. Mouchet, A., E. Driesschaert, V. Brovkin, T. Fichefet, H. Goosse, P. Huybrechts, and G. Munhoven: Future ocean carbon cycle: a study of feedbacks with the LOVECLIM model, Eos Transactions AGU, 87(36), Ocean Sci. Meet. Suppl., Abstract OS45B-13.

European Geosciences Union General Assembly, Vienna (Austria), 2-7 April 2006.

5. Goosse, H., H. Renssen, A. Timmermann, R.S. Bradley, and M.E. Mann: Using paleoclimate proxy-data to select optimal realisations in an ensemble of simulations of the climate of the past millennium, Geophysical Research Abstracts, vol. 8, 00527 (CD-ROM).
6. Goosse, H., O. Arzel, J. Luterbacher, M.E. Mann, H. Renssen, N. Riedwyl, A. Timmermann, E. Xoplaki, and H .Wanner: Origins of seasonally-variable temperature changes in Europe over the past millennia, Geophysical Research Abstracts, vol. 8, 00524 (CD-ROM).
7. Driesschaert, E., V. Brovkin, T. Fichefet, H. Goosse, P. Huybrechts, I. Janssens, A. Mouchet, and G. Munhoven: Impact of a Greenland deglaciation on climate during the next millennia, Geophysical Research Abstracts, vol. 8, 01485 (CD-ROM).
8. Driesschaert, E., T. Fichefet, H. Goosse, P. Huybrechts, I. Janssens, A. Mouchet, and G. Munhoven: On the warming asymmetry between Europe and North America in climate change projections, Geophysical Research Abstracts, vol. 8, 01487 (CD-ROM).

9. Driesschaert E., M.F. Loutre, H. Renssen, and T. Fichefet: Assessing the vegetation feedbacks at 6 kyr BP with ECBilt-CLIO-VECODE, Geophysical Research Abstracts, vol. 8, 03633 (CD-ROM).
10. Huyghe, A., F. Pattyn, and P. Huybrechts: Testing numerical techniques to solve the mass continuity equation in a coupled ice-sheet / ice-shelf model, Geophysical Research Abstracts, vol. 8, 05520 (CD-ROM).
11. Grosfeld, K., G. Lohmann, M. Butzin, P. Huybrechts, and C. Zweck: The response of the glacial ocean circulation to spatio-temporal freshwater discharges derived from an ice sheet model for the glacial period, Geophysical Research Abstracts, vol. 8, 07467 (CD-ROM).
12. Huybrechts, P., O. Rybak, F. Pattyn, and D. Steinhage: Non-climatic biases and chronology of the EDML ice core derived from a nested Antarctic ice sheet model, Geophysical Research Abstracts, vol. 8, 09803 (CD-ROM).
13. Janssens, I., P. Huybrechts, S. Raper, E. Driesschaert, T. Fichefet, H. Goosse, A. Mouchet, and G. Munhoven: Projections of ice sheet and sea level changes over the next millennia with the LOVECLIM Earth System Model, Geophysical Research Abstracts, vol. 8, 09822 (CD-ROM).
14. Huybrechts, P.: ISMIP - POLICE: a new intercomparison exercise to assess model uncertainties in polar ice sheet simulations under future climate warming conditions, Geophysical Research Abstracts, vol. 8, 09834 (CD-ROM).
15. Plattner, G.-K., R. Knutti, F. Joos, T. F. Stocker, and IPCC-AR4 EMIC Contributors: Long-term projections of climate change commitment. Geophysical Research Abstract , 8, 04594 (CD-ROM).
16. Renssen, H., H. Goosse, and T. Fichefet: Contrasting trends in North Atlantic deep-water formation in the Labrador Sea and Nordic Seas during the Holocene. Geophysical Research Abstract, 8, 04737 (CD-ROM).
17. Renssen, H., H. Goosse, T. Fichefet, V. Masson-Delmotte, and N. Koç: The Holocene climate evolution in the high-latitude Southern Hemisphere simulated by a coupled atmosphere–sea ice–ocean–vegetation model. Geophysical Research Abstract, 8, 04766 CD-ROM.
18. Wilhelms, F., J. Freitag, S.H. Faria, H. Oerter, H. Miller, S. Kipfstuhl, U. Ruth, P. Huybrechts, I. Hamman, D. Fritzsche, G. Lawer, A. Frenzel, D. Dick, T. Karlin, P. Kaufmann, A. Lambrecht, O. Rybak, B. Twarloh, F. Valero-Delgado: Both EPICA cores completed: Is the little sister the elder one?

WCRP/COPES International Conference on 'Understanding sea-level rise and variability, Paris (France), 6-9 June 2006.

19. Huybrechts, P.: Ice sheet modeling: current status and needed improvements.

PAGES/CLIVAR Workshop on 'Past millennia climate variability: proxy based reconstructions, modelling and methodology -synthesis and outlook', Wengen (Switzerland), 7-10 June 2006.

20. Goosse, H.: How can we optimally combine the information provided by proxy records and model results.

HOLIVAR2006 Natural Climate Variability and Global Warming, London (UK), 12-15 June 2006.

21. Goosse, H.: Simulating the climate of the last millennia: the role of internal and forced variability.

Ocean Carbon and Biogeochemistry (OCB) Summer Workshop, Woods Hole Oceanographic Institution (USA), July 23-26, 2007.

22. Mouchet A., E. Driesschaert, and T. Fichefet: Future Ocean Biogeochemical Cycles Sensitivity with an Earth System Model.

International Symposium on Cryospheric Indicators of Global Climate Change, Cambridge (UK), 21–25 August 2006.

23. Janssens, I., and P. Huybrechts: A monthly positive degree-day melt and runoff model of the Greenland ice sheet.
24. Huybrechts, P., I. Janssens, S.C.B. Raper, E. Driesschaert, T. Fichefet, H. Goosse, A. Mouchet, and G. Munhoven: Projections of ice sheet and sea level changes over the next millennia with the LOVECLIM Earth system model.
25. Hanna, E., K. Steffen, P. Huybrechts, R. Huff, J. Cappelen, and A. Stephens: Record Greenland melt and runoff in 2005 attributed to global warming.

Max Planck Institute for Meteorology, Hambourg (Germany), 14-15 September 2006.

26. Goosse, H.: Simulating the climate of the last millennium: the role of internal and forced variability.

Laboratoire de Sciences du Climat et de l'Environnement, Gif-sur-Yvette (France), 21 September 2006.

27. Goosse, H.: Simulating the climate of the last millennium: the role of internal and forced variability.

PAGES/CLIVAR Intersection Workshop on ‘the 8.2 Kyr Event’, Birmingham (UK), 23 October 2006.

28. Fichefet, T., H. Renssen, and A. Wiersma: Evaluation of different freshwater forcing scenarios for the 8.2 ka BP event in a coupled climate model.

EPICA Science Meeting, Il Ciocco (Italy), 16-19 October 2006.

29. Rybak, O., and P. Huybrechts: Sensitivity of ice-core dating to the varying geothermal heat flux.

Rapid Climate Change International Science Conference, Birmingham (UK), 24-27 October 2006:

30. Fichefet, T., E. Driesschaert, H. Goosse, P. Huybrechts, I. Janssens, A. Mouchet, G. Munhoven, V. Brovkin, and S.L. Weber: Modeling the interactions between the Greenland ice sheet and climate during the next millennia.

The Fourth CLIVAR/CliC/SCAR Southern Ocean Region Panel Meeting, Buenos Aires (Argentina), 14-17 November 2006.

31. Goosse, H.: IPCC models in Southern Ocean region.

Bern University, Bern (Switzerland), 22 January 2007.

32. Goosse, H.: Simulating the climate of the last millennium: the role of internal and forced variability.

11th Alpine Glaciology Meeting 2007, Zürich (Switzerland), 1-2 March 2007.

33. Nemec, J., P. Huybrechts, and J. Oerlemans: Reconstruction of the surface mass balance of Morteratschgletscher since the Little Ice Age.

Polar Environment and Climate: the Challenges, Brussels (Belgium), 5-6 March 2007.

34. Goosse, H.: Modelling climate variability and climate change in the Southern Ocean.

Kick-off Meeting of the Programme "Science for a Sustainable Development", Brussels (Belgium), 26–27 March 2007.

35. Fichefet, T.: Assessment of modelling uncertainties in long-term climate and sea level change projections.

European Geosciences Union General Assembly, Vienna (Austria), 15–20 April 2007.

36. Fichefet, T., E. Driesschaert, H. Goosse, P. Huybrechts, I. Janssens, A. Mouchet, G. Munhoven, V. Brovkin, and S.L. Weber: Modeling the influence of Greenland ice sheet melting on the Atlantic meridional overturning circulation during the next millennia. Geophysical Research Abstracts, vol. 9, (CD-ROM).
37. Loutre, M.F., X. Boës, N. Fagel, and M. De Batist: Climate control of varve thickness in Chilean lacustrine sediments during the deglaciation. Geophysical Research Abstracts, vol. 9 (CD-ROM).
38. Goosse, H.: Using paleoclimate proxy-data to select optimal realisations in an ensemble of simulations of the climate of the past millennium. Geophysical Research Abstracts, vol. 9 (CD-ROM).
39. Rybak, O., P. Huybrechts, F. Pattyn, and D. Steinhage: Model-derived ice core chronology and non-climatic biases in the lower part of the EDML ice core, Geophysical Research Abstracts, vol. 9(CD-ROM).
40. Mouchet, A., E. Driesschaert, and T. Fichefet: Future ocean biogeochemical cycles sensitivity and robustness with an Earth system model, Geophysical Research Abstracts, vol. 9, 10522 (CD-ROM).
41. Calov, R., R. Greve, P. Huybrechts, E. Bueler, D. Pollard, F. Pattyn, and L. Tarasov: First results of the ISMIP-HEINO model intercomparison project, Geophysical Research Abstracts, vol. 9 (CD-ROM).
42. Cristini, L., K. Grosfeld, G. Lohmann, and P. Huybrechts: The evolution of the Antarctic Ice Sheet under different climate boundary conditions, Geophysical Research Abstracts, vol. 9 (CD-ROM).
43. Gregory, J. M., P. Huybrechts, and R.B. Alley: Ice-sheet contributions to future sea-level change, Geophysical Research Abstracts, vol. 9 (CD-ROM).
44. Wake, L.M., P. Huybrechts, I. Janssens, E. Hanna, and J. Box: Surface mass balance history of the Greenland Ice Sheet (1868-2005), Geophysical Research Abstracts, vol. 9 (CD-ROM).
45. Grosfeld, K., G. Lohmann, M. Butzin, P. Huybrechts, and C. Zweck: Glacial ocean circulation in response to spatio-temporal freshwater discharges derived from an ice sheet model, Geophysical Research Abstracts, vol. 9 (CD-ROM).
46. Bintanja, R., and R. van de Wal: A 3-million-year reconstruction of climate, ice volume and sea level; identifying mechanisms behind the inception of Northern-Hemisphere glaciation and the mid-Pleistocene transition, Geophysical Research Abstracts, vol. 9 (CD-ROM).
47. Renssen, H., A. P. Wiersma, H. Goosse, and T. Fichefet: The impact of catastrophic meltwater drainage on the early Holocene climate: Model simulations of the 8.2 kyr BP event, Geophysical Research Abstract, 9 (CD-ROM).

NICE Kick-off meeting, Gif-sur-Yvette (France), 14 May 2007:

48. Huybrechts, P.: Simulations with LOVECLIM during the third millennium and beyond concenting the cryosphere and sea level changes.

General Assembly of the International Union of Geodesy and Geophysics IUGG 2007, Perugia (Italy), 2-13 July 2007:

49. Wen, J., Y. Wang, J. Liu, K. Jezek, P. Huybrechts, B. Csatho, and K. Farness: Mass budget of the grounded ice in Lambert Glacier-Amery Ice

Shelf system. Symposium on Cryosphere: Observations, Processes, and Future Evolution.

50. Fichefet, T., E. Driesschaert, H. Goosse, P. Huybrechts, I. Janssens, A. Mouchet, G. Munhoven, V. Brovkin, and S.L. Weber: Influence of the Greenland ice sheet melting on the Atlantic meridional overturning circulation during the next millennia. Symposium on Cryosphere: Observations, Processes, and Future Evolution.
51. Menviel, L., A. Timmermann, A. Mouchet and O.Timm: Meridional reorganizations of tropical marine and terrestrial productivity during Heinrich events. IAPSO Symposium on Abrupt Climate Change.

XVII INQUA Congress, Cairns (Australia), 27 July-3 August 2007.

52. Loutre, M.F.: Glacial inception at the end of MIS11: sensitivity tests.

Second International Conference on Earth System Modelling, Hamburg (Germany), 27-31 August 2007.

53. Goosse, H., J.F.Gonzalez Rouco , H. Beltrami , M.F. Loutre, and T. Fichefet: Is it possible to constrain climate sensitivity by comparing simulated and observed borehole temperature profiles?
54. Goosse, H., M.E. Mann, H. Renssen, and A. Timmermann: Reconstructing temperature changes over the past millennium using both model results and observations.
55. Goosse, H. : Impact of a Greenland deglaciation on climate during the next millennia.
56. Driesschaert, E., T. Fichefet, H. Goosse, P. Huybrechts, I. Janssens, A. Mouchet, G. Munhoven, V. Brovkin, and S.L. Weber: Influence of the Greenland ice sheet melting on the Atlantic meridional overturning circulation during the next millennia.

Ninth International Conference on Paleoceanography (ICP9), Shanghai (China), 3-7 September 2007.

57. Loutre M.F.: Climate evolution during the Holocene: modelling studies.

Workshop on Assessing the Mass Balance of the Polar Ice Sheets, Dresden (Germany), 10 september 2007:

58. Huybrechts, P., K. Haasemann, and S. Linow: Mass signal separation from a combination of observational data and modeling.

Fall Conference of the Western Canadian Cryospheric Network, Banff (Canada), 28-29 September 2007.

59. Adhikari, S., and P. Huybrechts: Numerical modelling of historical front variations and the 21st century evolution of Glacier AX010, Nepal Himalaya.

Workshop on the WCRP/CliC Global Prediction of the Cryosphere (GPC) Project, British Antarctic Survey, Cambridge (UK), 8-9 october 2007.

60. Fichefet, T.: On the ability of current atmosphere–ocean general circulation models to predict the evolution of sea ice.

Joint International Symposium of the GRACE Science Team and DFG SPP Symposium, Potsdam (Germany), 15-17 October 2007.

61. Huybrechts, P., K. Haasemann, R. Dietrich, and M. Baessler: Progress towards assessing the contemporary evolution of the Greenland ice sheet.
62. Horwath, M., R. Dietrich, P. Huybrechts, and S. Linow: Antarctic ice mass change estimates from GRACE: Results, uncertainties, and the combination with complementary information.

AGU Fall Meeting, San Francisco (USA), 10-14 December 2007.

63. Goosse, H.: Information on the early Holocene climate constrains the summer sea ice projections for the 21st century.
64. Goosse, H.: Data assimilation over the last millennium using a large ensemble of simulations.
65. Menviel, L., A. Timmermann, A. Mouchet, and O. Timm: Meridional reorganizations of marine and terrestrial productivity during Heinrich events.
66. Milne, G., A. Long, M. Simpson, L. Wake, S. Woodroffe, P. Huybrechts, and D. Roberts: Constraining the response of the Greenland ice sheet to climate change during the past 150 years using measurements of sea-level change.

NICE first annual meeting, Murten (Switzerland), 17-18 January 2008.

67. Huybrechts, P.: Numerical modelling of ice-sheet/ climate interactions with comprehensive Earth System Models applied to the last glacial-interglacial transition and the next millennia.

ASTER first scientific meeting, Louvain-la-Neuve (B), 21 January 2008:

68. Huybrechts, P.: Progress on the cryospheric component of LOVECLIM.
69. Fichefet, T., H. Goosse, and M.F. Loutre: Response of LOVECLIM to CO_2 forcing and freshwater perturbations.

38th International Arctic Workshop 2008, Program and Abstracts, Institute of Arctic and Alpine Research, University of Colorado at Boulder, Boulder (USA), 5-7 March 2008.

70. Crespin, E., H. Goosse, T. Fichefet, and M.E. Mann: Simulating the climate of the Arctic during the last millennium in a coupled climate model including data assimilation.

Leverhulme Climate Symposium, Cambridge (UK), 10-12 March 2008.

71. Menviel, L., A. Timmermann, A. Mouchet, and O. Timm: Climate and carbon cycle dynamics on millenial and orbital timescales

23. Internationale Polartagung, Münster (Germany), 10-14 March 2008.

72. Cristini, L., P. Huybrechts, K. Grosfeld, and G. Lohmann: Simulating the Antarctic ice sheet with a coupled atmosphere-ice sheet model approach.

International Workshop on Mass Balance Measurements and Modeling, Skeikampen (Norway), 26-28 March 2008.

73. Nemec, J., P. Huybrechts, O. Rybak, and J. Oerlemans: Reconstruction of the surface mass balance of Morteratschgletscher since 1865.
74. Wake, L., P. Huybrechts, J.E. Box, E. Hanna, I. Janssens, and G. Milne: Surface mass balance changes of the Greenland ice shet since 1866.

Second SPP 1257 Workshop on Mass Transport and Mass Distribution in the Earth System, Herrsching bei München (Germany), 31 March-2 April 2008.

75. Haasemann, K., P. Huybrechts, R. Dietrich, and M. Baessler: Progress towards assessing the contemporary evolution of the Greenland ice sheet.

Second International Conference APEX (Arctic Palaeoclimate and its Extremes) - Recent Advances, Durham (UK), 1-4 April 2008.

76. Simpson, M., G. Milne, A. Long, and P. Huybrechts: Constraining a glaciological model of the Greenland ice sheet using relative sea level data.

European Geosciences Union General Assembly, Vienna (Austria), 13-18 April 2008.

77. Belounis, M., A. Mouchet, and J. M Beckers: Modelling the carbon cycle in the Mediterranean sea. Geophysical Research Abstracts, Vol. 10, 2-2-2008
78. Crespin, E., H. Goosse, T. Fichefet, and M.E. Mann: Simulating the climate of the Arctic during the last millennium in a coupled climate model including data assimilation. Geophysical Research Abstract, 10, CD-ROM.

79. Goosse, H., E. Driesschaert, T. Fichefet, and M.F. Loutre: Information on early Holocene climate constrains the summer sea ice projections for the 21st century, Geophysical Research Abstract, 10, CD-ROM.
80. Haasemann, K., and P. Huybrechts: The effect of surface runoff on enhancing basal sliding and ice-sheet sensitivity in a three-dimensional Greenland ice sheet. Geophysical Research Abstract, 10, CD-ROM.
81. Loutre, M. F., T. Fichefet, H. Goosse, P. Huybrechts, A. Mouchet, and D. Swingedouw: How do ice sheets impact on climate sensitivity and ocean meridional overturning circulation? Geophysical Research Abstract, 10, CD-ROM.
82. Menviel, L., A. Timmermann, A. Mouchet, and O. Timm: Climate and marine carbon cycle response to changes in the strength of the southern hemispheric westerlies, Geophysical Research Abstract, 10, CD-ROM.
83. Mouchet, A., M.F. Loutre, T. Fichefet, H. Goosse, and P. Huybrechts: Ocean biogeochemical cycles and climate sensitivity in an Earth system model, Geophysical Research Abstract, 10, CD-ROM.
84. Mouchet, A.: Oxygen, a tool for assessing ocean tracer transport models, Geophysical Research Abstract, 10, CD-ROM.
85. Renssen, H., D.M. Roche, H. Goosse, and T. Fichefet: Modelling the impact of the Laurentide ice sheet on the timing of the Holocene thermal maximum, Geophysical Research Abstract, 10, CD-ROM.
86. Renssen, H., D.M. Roche, H. Goosse, and T. Fichefet: Modelling the impact of the Laurentide ice sheet on the timing of the Holocene thermal maximum, Geophysical Research Abstract, 10, CD-ROM.
87. Swingedouw, D., T. Fichefet, H. Goosse, and M.F. Loutre: Impact of transient freshwater release in the Southern Ocean on the AMOC and climate, Geophysical Research Abstract, 10, CD-ROM.
88. Swingedouw, D., T. Fichefet, P. Huybrechts, H. Goosse, E. Driesschaert, and M.F. Loutre: Antarctic ice-sheet melting provides negative feedbacks on future climate warming, Geophysical Research Abstract, 10, CD-ROM.

NATO-Russian Advanced Research Workshop and 40th International Liège Colloquium on Ocean Dynamics on Influence of Climatic Change on Arctic, Université de Liège, Liège (Belgium), 2-7 mai 2008.

89. Crespin E.: Simulating the climate of the Arctic during the last millennium in a coupled climate model including data assimilation.
90. Goosse, H.: Information on the early Holocene climate constrains the summer sea ice projections for the 21st century.

Workshop on Holocene Climate Variability at High-Southern Latitudes: An Integrated Perspective, organized by the French Embassy in London. London (UK), 14-15 May 2008.

91. Goosse, H.: Climate during the last millennium in the Southern Hemisphere.

Climate Change, From the Geologic Past to the Uncertain Future, A symposium Honouring André Berger, Université catholique de Louvain, Institut d'astronomie et de géophysique Georges Lemaître, Louvain-la-Neuve (Belgium), 26-29 May 2008.

92. Crespin, E., H. Goosse, T. Fichefet, and M.E. Mann: Simulating the climate of the Arctic during the last millennium in a coupled climate model including data assimilation.
93. Goosse, H., E. Driesschaert, T. Fichefet, and M.F. Loutre: Information on early Holocene climate constrains the summer sea ice projections for the 21st century.

94. Huybrechts, P.: Modeling late-Quaternary continental glaciation.
95. Loutre, M.F.: The astronomical forcing.

American Quaternary Association Biennial Meeting, State College, Pennsylvania (USA), 5-7 June 2008.

96. Simpson, M., G. Milne, A. Long, and P. Huybrechts: Constraining a glaciological model of the Greenland ice sheet using relative sea-level data.
97. Wake, L.M., G.A. Milne, A.J. Long, S.A. Woodroffe, M.J. R. Simpson, P. Huybrechts, and D.H. Roberts: Constraining the response of the Greenland ice sheet during the past 150 years using measurements of sea level change.

Astrophysics, Geophysics and Oceanography Department, Université de Liège, Liège (Belgium), 12 June 2008.

98. Mouchet, A: Cycle du carbone et sensibilités climatiques dans un modèle de complexité intermédiaire du système Terre.

Global Atmospheric Circulation During the Past 100 Years, Monte Verità (Switzerland), 15-20 June 2008.

99. Goosse, H.: Consistent past half-century trends in the atmosphere, the sea ice and the ocean at high southern latitudes.

SCAR/IASC IPY Open Science Conference, Sankt Peterburg (Russia), 8-11 July 2008.

100. Rybak, O., P. Huybrechts, F. Pattyn, and D. Steinhage: Mathematical modeling in support of the interpretation of the EDML ice core.

William Smith meeting 2008: Observations and Causes of Sea-Level Changes on Millennial to Decadal Timescales, Geological Society, London (UK), 1-2 September 2008.

101. Wake, L.M., G. A. Milne, A. J. Long, S. A. Woodroffe, M.J.R. Simpson, P. Huybrechts, and D.H. Roberts: Constraining the response of the Greenland ice sheet during the past 150 years using measurements of sea level change.

SPP1257 Kolloquium ‘Massentransporte und Massenverteilungen im System Erde’, München (Germany), 6-8 October 2008.

102. Linow, S. and P. Huybrechts: The Antarctic ice sheet mass balance from modeling and radar remote sensing.
103. Linow, S., K. Haasemann, and P. Huybrechts: The Antarctic ice sheet evolution from modeling and radar remote sensing.

NICE Autumn School ‘Methods of quantitative palaeoenvironmental reconstructions, Poznan (Poland), 11 October 2008.

104. Huybrechts, P.: Modeling late-Quaternary continental glaciation.

Derde Belgische Dagen van de Geografie, Brussel (Belgium), 24-25 oktober 2008.

105. Huybrechts, P.: Global warming, ice sheets, and sea level.
106. Gölzer, H., P. Huybrechts, M.F. Loutre, and A. Mouchet: Assessement of modeling uncertainties for long-term climate ice sheet interactions
107. Rybak, O., P. Huybrechts, and F. Pattyn: Application of mathematical modeling for interpretation of an Antarctic ice core.

Congrès International "Impacts Anthropiques sur le Milieu Marin" CIEM 2008, Alger (Algeria), 27-28 octobre 2008.

108. Mouchet, A., M.F. Loutre, T. Fichefet, H. Goosse and P. Huybrechts: Ocean biogeochemical cycles and climate sensitivity in an Earth System Model.

New Methodologies and Interdisciplinary Approaches in Global Change Research, Porquerolles (France), 5-10 November 2008.

109. Goosse, H.: Modelling forced and internal climate variability during the last millennium.

2008 AGU Fall meeting, San Francisco (USA), 15-19 December 2008.

110. Crespin, E., H. Goosse, T. Fichefet, and M.E. Mann: Causes of 15th century warming event in the Arctic in a coupled climate model including data assimilation, EOS Trans. Amer. Geophys. Union, 89(53).
111. Hanna, E., J. Cappelen, X. Fettweis, P. Huybrechts, A. Luckman, and M.H. Ribergaard: Hydrologic response of the Greenland ice sheet: the role of oceanographic warming.
112. Loutre, M.F., A. Mouchet, T. Fichefet, H. Goosse, and P. Huybrechts: Modelling uncertainties in the climate of the last millennium : The ASTER project, EOS Trans. Amer. Geophys. Union, 89(53).
113. Milne, G.A., L.M. Wake, M.J.R. Simpson, P. Huybrechts, A.J. Long, and S.L. Woodroffe: Modelling the glacial isostatic adjustment of Greenland on millennial to decadal timescales.
114. Mouchet, A., M.F. Loutre, T. Fichefet, H. Goosse, and P. Huybrechts: Carbon cycle and climate sensitivity in an Earth system model, EOS Trans. Amer. Geophys. Union, 89(53).
115. Renssen, H., H. Seppa, D.M. Roche, H. Goosse, and T. Fichefet: The Holocene thermal maximum in transient coupled climate model simulations. EOS Trans. Amer. Geophys. Union, 89(53).
116. Simpson, M.J., G.A. Milne, P. Huybrechts, and A.J. Long: Calibrating a glaciological model of the greenland ice sheet from the Last Glacial m
Maximum to present-day using field observations of relative sea level and ice extent.
117. Wake, L.M., G.A. Milne, P. Huybrechts, M.J. Simpson, A.J. Long, and S.A. Woodroffe: Interpreting century-to-decadal scale sea-level records from greenland.

MARE General Assembly, Université de Liège, Liège (Belgium),12 December 2008.

118. Mouchet A., M.F. Loutre, T. Fichefet, H. Goosse, and P. Huybrechts: Ocean biogeochemical cycles and climate sensitivity in an Earth System Model

Meteoclim PhD Symposium 2009, Louvain-la-Neuve (Belgium), 28 January 2009.

119. Nemec, J., I. Janssens, H. Goelzer, and P. Huybrechts: Freshwater fluxes from the Northern Hemisphere ice sheets during the Last Deglaciation.

2009 BELQUA Annual Scientific Meeting, Brussels (Belgium), 3 March 2009.

120. Nemec, J., I. Janssens, H. Goelzer, and P. Huybrechts: Freshwater fluxes from the Northern Hemisphere ice sheets during the Last Deglaciation.

Third International Conference APEX (Arctic Palaeoclimate and its Extremes) – Beyond the Frontier, Copenhagen (Denmark), 31 March-3 April 2009.

121. Simpson, M.J., G.A. Milne, P. Huybrechts, and A.J. Long: Calibrating a glaciological model of the Greenland ice sheet from the Last Glacial Maximum to present-day using field observations of relative sea level and ice extent.

European Geosciences Union General Assembly, Vienna (Austria), 19-24 April 2009.

122. Crespin, E. H. Goosse, T. Fichefet, and M.E. Mann: Did fluctuations of the thermohaline circulation in the North Atlantic play a role during Arctic warm episodes of the past millennium?, Geophysical Research Abstract, 11, USB.
123. Crespin, E., H. Goosse, T. Fichefet, and M.E. Mann: Potential causes of 15th century Arctic warming using coupled model simulations with data assimilation, Geophysical Research Abstract, 11, USB.

124. Gonzalez-Rouco, J.F., M. B. Stevens, H. Beltrami, H. Goosse, V. Rath, E. Zorita, and J. Smerdon: Comparison of climate model simulated and observed borehole temperature profiles, Geophysical Research Abstract, 11, USB.
125. Goosse, H. E. Crespin, M.E. Mann, H. Renssen, and A. Timmermann: A dynamically consistent reconstruction of surface temperature changes during the last 600 years based on climate model simulations using data assimilation, Geophysical Research Abstract, 11, USB.
126. Goosse H., W. Lefebvre, A. de Montety, and A. Orsi: Consistent past half-century trends in the atmosphere, the sea ice and the ocean at high southern latitudes, Geophysical Research Abstract, 11, USB.
127. Loutre, M.F., A. Mouchet, T. Fichefet, H. Goosse, H. Goelzer, and P. Huybrechts: Modelling uncertainties in the climate of the last millennium: the ASTER project, Geophysical Research Abstract, 11, USB.
128. Mann, M.E., R.S. Bradley, E. Crespin, H. Goosse, M.K. Hughes, S. Rutherford, D. Shindell, and Z. Zhang: Towards understanding patterns of climate change in past centuries, Geophysical Research Abstract, 11, USB.
129. Murray, T., K. Scharrer, T.D. James, S.R. Dye, E. Hanna, A.D. Booth, N. Selmes: A. Luckman, A.L.C. Hughes, and P. Huybrechts: Has dynamic thinning switched off in south-east Greenland?
130. Nemec, J., I. Janssens, H. Goelzer, and P. Huybrechts: Freshwater fluxes from the Northern Hemisphere ice sheets during the Last Deglaciation, Geophysical Research Abstract, 11, USB.
131. Renssen, H., H. Seppä, O. Heiri, D.M. Roche, H. Goosse, and T. Fichefet: The global nature of the Holocene thermal maximum in transient coupled climate model simulations, Geophysical Research Abstract, 11, USB.
132. Sundal, A.V., A. Shepherd, P. Nienow, E. Hanna, S. Palmer, and P. Huybrechts: Evolution of supra-glacial lakes across the Greenland ice sheet, Geophysical Research Abstract, 11, USB.

ASTER final workshop on 'Assessment of modelling uncertainties in long-term climate and sea level change projections', Brussels (Belgium), 19 May 2009.

133. Fichefet, T., Goosse, H., Loutre, M.F.: Last millennium.
134. Goelzer, H. and P. Huybrechts: Ice sheet-climate interactions during the third millennium in LOVECLIM.
135. Nemec, J., H. Goelzer, I. Janssens and P. Huybrechts: Coupling a northern hemisphere ice sheet model to LOVECLIM.

Japan Geoscience Union (JpGU), Tokyo (Japan), 16-21 May 2009.

136. Menviel, L., A. Timmermann, O. Timm, and A. Mouchet: Biogeochemical changes in the North Pacific in response to a shut down of the Atlantic meridional overturning.

NICE Second Annual Meeting, Potsdam (Germany), 4-5 June.

137. Nemec, J., J, I. Janssens, H. Goelzer, and P. Huybrechts: The response of LOVECLIM to freshwater fluxes from the Northern Hemisphere ice sheets since the Last Glacial Maximum: first results.

Mechanisms of Quaternary Climate Change: Stability of Warm Phases in the Past and in the Future. ESF-FWF Conference, Universitätszentrum Obergurgl (Austria), 6-11 June 2009.

138. Huybrechts, P., and O. Rybak: Dependence of Antarctic basal conditions on the geothermal heat flux: the example of basal temperature and basal ice age.

139. Loutre, M.F.: When will the next glacial inception take place?

5th SALE Meeting, Brussels (Belgium), 10-11 June 2009.

MOCA-09, Our Warming Planet. IAMAS-IAPSO-IACS, Montreal (Canada), 19-29 July 2009.

140. Fichefet, T., D. Swingedouw, P. Huybrechts, H. Goosse, E. Driesschaert, and M.F. Loutre: Antarctic ice sheet melting provides negative feedbacks on future climate warming, Abtracts, CD-ROM.

Nuuk Climate Days 2009. International Symposium on Changes of the Greenland Cryosphere, Nuuk (Greenland), 25-27 August 2009.

141. Hanna, E., R. Bales, J. Cappelen, P. Huybrechts, I. Janssens, J. Jones, J. McConnell, J. Scheidegger, K. Steffen, and R. Thomas: Greenland Ice Sheet mass balance in a changing climate 1908-2008.

SOEST, University of Hawaii, Hawaii, 15 october 2009.

142. Mouchet, A.: Model e and carbon cycle – climate feedbacks: a study with an Earth System Model.

Cryospheric Science Workshop, University of Sheffield, 4-6 November 2009:

143. Simpson, M., G. Milne, and P. Huybrechts: The influence of non-Greenland ice mass loss on sea-level change around Greenland over the last deglaciation: Implications for Greenland ice sheet (GrIS) evolution.

SOLAS Open Science Conference, Barcelona (Spain), 16-19 November 2009.

144. Mouchet, A., M.F. Loutre, H. Goelzer, T. Fichefet, H. Goosse and P. Huybrechts: Model sensitivities and carbon cycle - climate feedbacks: a study with an Earth System Model.

ETH Zurich (Switzerland), 23-24 November 2010.

145. Goosse, H. : Reconstructing the climate of the past centuries using model simulations with data assimilation (invited seminar).

AGU Fall Meeting, San Francisco (USA), 14-18 December 2009.

146. Goelzer, H., M.F. Loutre, A. Mouchet, P. Huybrechts, T. Fichefet, and H. Goosse, 2009 : Impact of including fully interactive Greenland and Antarctic ice sheets on the climate sensitivity of an Earth system model of intermediate complexity. EOS Trans. Amer. Geophys. Union, 90(52), Fall Meet. Suppl., Abstract A31A-0077.

147. Murray, T., K. Scharrer, T. D. James, S. Dye, E. Hanna, A. Booth, N. Selmes, A. J. Luckman, A. L. Hughes, and S. Cook, P. Huybrechts: Ocean regulation of glacier dynamics in south-east Greenland and implication for ice sheet mass changes. EOS Trans. Amer. Geophys. Union, 90(52), Fall Meet. Suppl., Abstract C11A-03.

Sea Level Changes: the Science of a Changing World, Quaternary Research Association (QRA) - Annual Discussion Meeting, Durham (UK), 5-8 January 2010:

148. Ridley, J., J. Gregory, P. Huybrechts, and J. Lowe: Committed sea level thresholds from the Greenland ice sheet.

149. Simpson, M. J. R., G.A. Milne, and P. Huybrechts: The influence of non-Greenland ice mass loss on sea-level change around Greenland over the last deglaciation: Implications for Greenland ice sheet (GrIS) evolution.

BNCGG Annual Assembly, Brussel (B), 21 January 2010:

150. Huybrechts, P.: Overview of cryospheric reseach in Belgium.

ice2sea Open Forum Meeting, Krakow (PL), 17-18 March 2010:

151. Goelzer, H., J.J. Fürst, O. Rybak, P. Huybrechts, Improvememts in a large-scale model of the Greenland ice sheet.

ISSI Workshop on Cryosphere and Sea Level Change, Bern (CH), 22-26 March 2010:

152. Huybrechts, P.: The role of ice dynamics in the current and future response of the polar ice sheets.

NICE Third Annual Meeting, Bristol (UK), 8-9 April 2010:

153. Fürst, J., and P. Huybrechts: Dynamic response of the Greenland ice sheet.

European Geosciences Union General Assembly, Vienna (Austria), 2-7 May 2010.

154. Crespin, E., H. Goosse, Y. Sallaz-Damaz, and T. Fichefet, 2010: Constraining the evolution of the intensity of the meridional overturning circulation using a particle filter. Geophysical Research Abstract, 11, Vol. 12, EGU2010-1688, USB.
155. Fürst, J. J., H. Goelzer, O. Rybak, F. De Ridder, and P. Huybrechts: The control of ice-marginal processes on the transient response of the Greenland Ice Sheet. Geophysical Research Abstract, 11, Vol. 12, EGU2010-13910, USB.
156. Goelzer, H., F. De Ridder, J. Fürst, and P. Huybrechts: Initialization of large-scale ice sheet models for future sea-level change projections. Geophysical Research Abstract, 11, Vol. 12, EGU2010-13421, USB.
157. Goelzer, H., P. Huybrechts, M.F. Loutre, H. Goosse, T. Fichefet, and A. Mouchet, 2010 : Impact of Greenland and Antarctic ice sheet interactions on model climate sensitivity. Geophysical Research Abstract, 11, Vol. 12, EGU2010-10510, USB.
158. Goosse, H., O. Arzel, C.M. Bitz, A. de Montety, and M. Vancoppenolle 2010: Increased variability of the Arctic summer ice extent in a warmer climate. Geophysical Research Abstract, 11, Vol. 12, EGU2010-1612, USB.
159. Goosse, H., E. Crespin, Y. Sallaz-Damaz, and M. Crucifix, 2010: Testing a data assimilation method devoted to reconstruct the climate of the past millennium. Geophysical Research Abstract, 11, Vol. 12, EGU2010-1713, USB.
160. Goosse, H., D.M. Roche, and A. Timmermann, 2010: Response of the meridional overturning circulation to a cooling: can we understand the difference between simulations of the LGM? Geophysical Research Abstract, 11, Vol. 12, EGU2010-1716, USB.
161. Renssen, H., H. Goosse, X. Crosta, and D. M. Roche, 2010: Early Holocene Laurentide Icesheet deglaciation causes cooling in the high-latitude Southern Hemisphere through oceanic teleconnection. Geophysical Research Abstract, 11, Vol. 12, EGU2010-2310, USB.
162. Ridley, J., J. Gregory, P. Huybrechts, and J. Lowe, 2010: Thresholds for irreversible decline of the Greenland ice sheet. Geophysical Research Abstract, 11, Vol. 12, EGU2010-14154, USB.
163. Roche, D.M., C. Dumas, C. Ritz, and H. Goosse, 2010: Transient simulation of the last inception (128 to 115ka BP) with a coupled climate - cryosphere model. Geophysical Research Abstract, 11, Vol. 12, EGU2010-12632, USB.
164. Simpson, M., L. Wake, G. Milne, and P. Huybrechts: The influence of mantle viscosity structure and past decadal to millennial-scale ice mass changes on present-day land motion in Greenland. Geophysical Research Abstract, 11, Vol. 12, EGU2010-12884, USB.
165. Widmann, M., H. Goosse, G. van der Schrier, and R. Schnur, 2010: Constraining simulated atmospheric states by sparse empirical information. Geophysical Research Abstract, 11, Vol. 12, EGU2010-11785, USB.

Belgian International Polar Year Symposium, Brussels (Belgium), 26 May 2010.

166. Goelzer, H., P. Huybrechts, M.F. Loutre, H. Goosse, T. Fichefet, and A. Mouchet: Earth and sea-level change projections with the Earth system model of intermediate complexity LOVECLIM.
167. Huybrechts, P., J. Fürst, H. Goelzer, J. Gregory, G. Milne, J. Ridley, and M. Simpson: Modeling the evolution and stability of the Greenland ice sheet.

Dag van de doctorandi, VUB, Brussel, 28 May 2010.

168. Fürst, J.J., H. Goelzer, O. Rybak, and P. Huybrechts, 2010: The ice sheet margin: Greenland's sore spot to future climate evolution.

International Polar Year Oslo Science Conference, Oslo (Norway), 8-12 June 2010.

169. Goelzer, H., P. Huybrechts, M.F. Loutre, H. Goosse, T. Fichefet, and A. Mouchet: Earth and sea-level change projections with the Earth system model of intermediate complexity LOVECLIM

Clivar Southern Ocean Panel Meeting, Southampton (UK), 14-17 Kune 2010.

170. Goosse, H. : Climate modelling status – goals.

IPCC WGI Workshop on Sea Level Rise and Ice Sheet Instabilities, Kuala Lumpur (Malaysia), 21-24 June 2010.

171. Huybrechts, P., H. Goelzer, J. Fürst, F. De Ridder, O. Rybak, and I. Janssens: Response of the polar ice sheets on centennial to millennial time scales from improved 3-D whole ice-sheet models.

International Symposium on Earth's Disappearing Ice: Drivers, Reponses and Impacts; A celebration of the 50th Anniversary of Byrd Polar Research Center, Columbus (USA), 16-20 August 2010.

172. Wake, L. M., G. A. Milne, A. J. Long, S. A. Woodroffe, P. Huybrechts, M. J. R. Simpson, and S. J. Marshall: Constraining changes in the Greenland ice sheet over century timescales.

Fourth Belgian Geography Days, Leuven (B), 22-23 October 2010.

173. Loutre, M.F., A. Mouchet, T. Fichefet, H. Goosse, H. Goelzer, and P. Huybrechts: Assessment of modelling uncertainties in long-term climate projections: the ASTER project.
174. Goelzer, H., P. Huybrechts, M.F. Loutre, H. Goosse, T. Fichefet, and A. Mouchet: Ice and sea level change projections with the Earth system model of intermediate complexity LOVECLIM.
175. Goelzer, H., P. Huybrechts, M.F. Loutre, H. Goosse, T. Fichefet, and A. Mouchet: Impact of Greenland and Antarctic ice sheet interactions on model climate sensitivity.

5. PUBLICATIONS

A. ASTER publications

1. Peer reviewed

1. Driesschaert, E., Fichefet, T., Goosse, H., Huybrechts, P., Janssens, I., Mouchet, A., Munhoven, G., Brovkin, V. and Weber, S.L. (2007). Modeling the influence of Greenland ice sheet melting on the Atlantic meridional overturning circulation. Geophys. Res. Lett., 34, L10707, doi: 10.1029/2007GL029516.
2. Goelzer, H., Huybrechts, P., Loutre, M. F., Goosse, H., Fichefet, T. and Mouchet, A. (2010). Impact of Greenland and Antarctic ice sheet interactions on climate sensitivity. Clim. Dyn., doi: 10.1007/s00382-010-0885-0
3. Goosse H., Driesschaert E., Fichefet T., and Loutre M.F., (2007). Information on the early Holocene climate constrain the summer sea-ice projections for the 21st century, Clim. Past, 3, 683-692.
4. Goosse, H., Brovkin, V., Fichefet, T., Haarsma, R., Jongma, J., Huybrechts, P., Mouchet, Selten, F.M., Barriat, P-Y., Campin, J-M., Deleersnijder, E., Driesschaert, E., Goelzer, H., Janssens, I., Loutre, M-F., Morales Maqueda, M. A., Opsteegh, T., Mathieu, P-P., Munhoven, G., Pettersson, E.J., Renssen, H., Roche, D., Schaeffer, M., Severijns, C., Tartinville, B., Timmermann, A. and Weber, N. (2010). Description of the Earth system model of intermediate complexity LOVECLIM version 1.2, Geosci. Model Dev. Discuss., 3, 309-390, http://www.geosci-model-dev-discuss.net/3/309/2010/gmdd-3-309-2010.html
5. Loutre, M. F., Mouchet, A., Fichefet, T., Goosse, H., Goelzer, H. and Huybrechts, P. (2010). Evaluating climate model performance with various parameter sets using observations over the last centuries. Clim. Past Discuss., 6, 711-765.
6. Plattner, G.-K., Knutti, R., Joos, F., Stocker, T.F., Brovkin, V., Driesschaert, E., Dutkiewicz, S., Eby, M., Edwards, N.R., Fichefet, T., Jones, C., Loutre, M.F., Matthews, H. D., Mouchet, A., Müller, S.A., Nawrath, S., Sokolov, A., Strassmann, K. and Weaver, A. (2008). Long-term projections of climate change commitment. J. Clim., 21, 2721–2751, doi: 10.1175/2007JCLI1905.1.
7. Swingedouw, D., Fichefet, T., Huybrechts, P., Driesschaert, E., Goosse, H. and Loutre, M.F. (2008). Antarctic ice-sheet melting provides negative feedbacks on future global warming. Geophys. Res. Lett., 35, L17705, doi: 10.1029/2008GL034410.

2. Others

1. Goelzer, H., Huybrechts, P., Loutre, M. F., Goosse, H., Fichefet, T. and Mouchet, A. (2010). Ice and sea-level change projections with the Earth system model of intermediate complexity LOVECLIM. Proceedings of the Belgium IPY Symposium 2010.

3. In preparation

1. Goelzer, H., Nemec, J., Janssens, I. and Huybrechts, P. (2010). A dynamic continental runoff routing model applied to the last Northern Hemisphere deglaciation.

2. Goelzer, H., Huybrechts, P., Loutre, M. F., Goosse, H., Fichefet, T. and Mouchet, A. Ice and sea level change projections with the Earth system model of intermediate complexity LOVECLIM.
3. Huybrechts, P., Goelzer, H., Janssens, I., Driesschaert, E., Fichefet, T., Goosse, H., Loutre, M. F., Mouchet, A., Munhoven, G. (2010). Response of fully interactive Greenland and Antarctic ice sheets to a multi-millennial greenhouse warming in an Earth system model of intermediate complexity.
4. Huybrechts, P., Goelzer, H., Janssens, I., Raper, S. C. B., Driesschaert, E., Fichefet, T., Goosse, H., Loutre, M. F., Mouchet, A., Munhoven, G. (2010). Land ice and global sea level changes over the next millennium simulated by the Earth system model of intermediate complexity LOVECLIM.
5. Mouchet, A., Fichefet, T., Goelzer, H., Goosse, H., Huybrechts, P. and Loutre, M.F. (2010). Model sensitivities and future carbon cycle-climate feedbacks: a study with an Earth system model.
6. Mouchet, A., Fichefet, T., Goelzer H., Goosse H., Huybrechts P., Loutre, M.F. and Timmermann, A. (2010). Climate sensitivity and model response to freshwater perturbation: impacts on the North Pacific circulation and the global carbon cycle.

B. ASTER-related publications

1. Peer reviewed

1. Alley, R., Clark, P. U., Huybrechts, P. and Joughin, I. (2005). Ice sheets and sea-level change, Science, 310, 456-460.
2. Cao, L., Eby, M., Ridgwell, A., Caldeira, K., Archer, D., Ishida, A., Joos, F., Matsumoto, K., Mikolajewicz, U., Mouchet, A., Orr, J. C., Plattner, G.-K., Schlitzer, R., Tokos, K., Totterdell, I., Tschumi, T., Yamanaka, Y. and Yool, A. (2009). The role of ocean transport in the uptake of anthropogenic CO_2, Biogeosciences, 6, 375-390 (1726-4189/bg/2009-6-375).
3. Crespin E., Goosse, H., Fichefet, T., Mann, M. E. (2009). The 15th century Arctic warming in coupled model simulations with data assimilation. Clim. Past, 5 (3), 389-401
4. Fettweis, X., Hanna, E., Gallée, H., Huybrechts, P. and Erpicum, M. (2008). Estimation of the Greenland ice sheet surface mass balance for the 20th and 21st centuries, The Cryosphere, 2, 117-129.
5. Friedrich, T., Timmermann, T., Menviel, L., Timm, O., Mouchet, A. and Roche, D. M. (2009). Orbital modulation of millennial-scale climate variability in an earth system model of intermediate complexity. Clim. Past Discuss., 5, 2019-2051.
6. Friedrich, T., Timmermann, T., Menviel, L., Timm, O., Mouchet, A. and Roche, D. M. (2010). Internally generated millennial-scale climate variability in an earth system model of intermediate complexity: sensitivity to ocean bathymetry and orbital forcing. Geosci. Model Dev. Discuss., 3, 273-307.
7. Goosse H., Arzel, O., Luterbacher, J., Mann, M. E., Renssen, H., Riedwyl, N., Timmermann, A., Xoplaki, E. and Wanner, H. (2006). The origin of the European "Medieval Warm Period". Clim. Past, 2, 99-113.
8. Goosse H., Arzel, O., Bitz, C.M., de Montety, A. and Vancoppenolle, M. (2009). Increased variability of the Arctic summer ice extent in a warmer climate. Geophys. Res. Lett., 36, L23702, doi :10.1029/2009GL040546.

9. Goosse H., Crespin, E., de Montety, A., Mann, M.E., Renssen, H. and Timmermann, A. (2010). Reconstructing surface odelling e changes over the past 600 years using climate model simulations with data assimilation. J. Geophys. Res., 115, D09108, doi : 10.1029/2009JD012737.
10. Goosse H., Lefebvre, W., de Montety, A., Crespin, E. and Orsi, A. (2009). Consistent past half-century trends in the atmosphere, the sea ice and the ocean at high southern latitudes. Clim. Dyn., doi: 10.1007/s00382-008-0500-9.
11. Goosse H., Crespin, E., de Montety, A., Mann, M.E., Renssen, H. and Timmermann, A. (2010). Reconstructing surface temperature changes over the past 600 years using climate model simulations with data assimilation. J. Geophys. Res., 115, D09108, doi:10.1029/2009JD012737.
12. Gregory, J. and Huybrechts, P. (2006). Ice-sheet contributions to future sea-level change, Philosophical Transactions of the Royal Society of London A, 364, 1709-1731, doi: 10.1098/rsta.2006.1796.
13. Gregory, J.M., Dixon, K. W., Stouffer, R. J., Weaver, A. J., Driesschaert, E., Eby, M., Fichefet, T., Hasumi, H., Hu, A., Jungclaus, J. H., Kamenkovich, I. V., Levermann, A., Montoya, M. Murakami, S., Nawrath, S., Oka, A., Sokolov, A. P. and Thorpe, R. B. (2005). A model intercomparison of changes in the Atlantic thermohaline circulation in response to increasing atmospheric CO_2 concentration, Geophys. Res. Lett., 32, L12703, doi: 10.1029/ 2005GL023209.
14. Gruber. N., Gloor, M., Mikaloff, S. E., Fletcher, Takahashi, T., Doney, S. C., Gerber, M., Jacobson, A. R., Lindsay, K., Menemenlis, D., Mouchet, A. and Sarmiento, J. L. (2009). Toward consistent estimates of the oceanic sources and sinks for atmospheric CO_2, Global Biogeochem. Cy., 23, GB1005, doi : 10.1029/2008GB003349.
15. Hanna, E., Huybrechts, P., Steffen, K., Cappelen, J., Huff, R., Shuman, C., Irvine-Fynn, T., Wise, S. and Griffiths, M. (2008). Increased runoff from melt from the Greenland Ice Sheet: a response to global warming, J. Climate, 21(2), 331-341.
16. Hanna, E., Cappelen, J., Fettweis, X., Huybrechts, P., Luckman, A. and Ribergaard, M.H. (2009). Hydrologic response of the Greenland ice sheet: the role of oceanographic warming. Hydrol. Process., 23, 7-30.
17. Huybrechts, P. (2006). Numerical modelling of ice sheets through time, In: Knight, P.G. (ed.): Glacier Science and Environmental Change, Blackwell Publishing (Oxford), 406-412.
18. Huybrechts, P. (2007). Ice sheet modelling, In B. Riffenburgh (ed): Encyclopedia of the Antarctic, Routledge, New York, 514-517.
19. Huybrechts, P. (2008). The Greenland ice sheet, In: D. Cuff and A. Goudie (eds.), The Oxford Companion to Global Change, Oxford University Press (USA), 310-316.
20. Huybrechts, P. (2008). Cryosphere, in Gornitz, V. (ed.): Encyclopedia of Paleoclimatology and Ancient Environments, Encyclopaedia of Earth Science Series, Springer Verlag (Berlin, Heidelberg, New York), 221-226.
21. Jongma, J.I., Driesschaert, E., Fichefet, T., Goosse, H. and Renssen, H. (2009). The effect of dynamic-thermodynamic icebergs on the Southern Ocean climate in a three-dimensional model. Ocean Modell., 26, 104–113, doi: 10.1016/j.ocemod.2008.09.007.
22. Lowe, J.A, Gregory, J.M., Ridley, J., Huybrechts, P., Nicholls, R.J. and Collins, M. (2006). The role of sea-level rise and the Greenland ice sheet in dangerous climate change: implications for the stabilisation of climate, In: Schellnhuber,

J., W. Cramer, N. Nakicenovic, T.Wigley and G. Yohe (eds.): Avoiding Dangerous Climate Change, Cambridge University Press (Cambridge), 29-36.
23. Menviel, L., Timmermann, A., Mouchet, A. and Timm, O. (2008). Meridional reorganizations of marine and terrestrial productivity during Heinrich events, Paleoceanography, 23, PA1203, doi: 10.1029/2007PA001445.
24. Menviel, L., Timmermann, A., Mouchet, A. and Timm, O. (2008). Climate and marine carbon cycle response to changes in the strength of the Southern Hemispheric westerlies, Paleoceanography, 23, PA4201, doi: 10.1029/2008PA001604.
25. Menviel, L., Timmermann, A., Mouchet, A. and Tim, O. (2010) Climate and biogeochemical response to a rapid melting of the West-Antarctic ice sheet: Implications for future climate, Paleoceanography, submitted.
26. Menviel, L., Timmermann, A., Timm, O., Mouchet, A., Abe-Ouchi, A., Chikamoto, M.O., Harada, N., Ohgaito, R. and Okazaki, Y. (2010). The Pacific meridional overturning circulation and its impact on global climate and the carbon cycle: idealized modeling experiments. Deep-Sea Res., submitted.
27. Mikaloff Fletcher, S. E., Gruber, N., Jacobson, A. R., Doney, S. C., Dutkiewicz, S., Gerber, M., Follows, M., Joos, F., Lindsay, K., Menemenlis, D., Mouchet, A., Müller, S. A. and Sarmiento, J. L. (2006). Inverse estimates of anthropogenic CO_2 uptake, transport, and storage by the ocean, Global Biogeochem. Cycles, 20, doi : 10.1029/2005GB002530.
28. Mikaloff Fletcher, S. E., Gruber, N., Jacobson, A. R., Doney, S. C., Dutkiewicz, S., Gerber, M., Gloor, M., Follows, M., Joos, F., Lindsay, K., Menemenlis, D., Mouchet, A., Müller, S. A. and Sarmiento, J. L. (2007). Inverse estimates of the oceanic sources and sinks of natural CO_2 and their implied oceanic transport, Global Biogeochem. Cycles, 21, GB1010, doi : 10.1029/2006GB002751.
29. Mouchet, A. and Deleersnijder, E. (2008). The leaky funnel model, a metaphor of the ventilation of the World Ocean as simulated in an OGCM, Tellus, 60A, 761–774, doi: 10.1111/j.1600-0870.2008.00322.x.
30. Najjar, R. G., Jin, X., Louanchi, F., Aumont, O., Caldeira, K., Doney, S. C., Dutay, J.-C., Follows, M., Gruber, N., Joos, F., Lindsay, K., Maier-Reimer, E., Matear, R. J., Matsumoto, K., Mouchet, A., Orr, J. C., Plattner, G-K., Sarmiento, J. L., Schlitzer, R., Weirig, M. F., Yamanaka, Y. and Yool, A. (2007). Impact of circulation on export production, dissolved organic matter, and dissolved oxygen in the ocean: Results from Phase II of the Ocean Carbon-Cycle Model Intercomparison Project (OCMIP-2), Global Biogeochem. Cycles, 21, GB3007, doi : 10.1029/2006GB002857.
31. Okazaki, Y., Timmermann, A., Menviel, L., Harada, N., Abe-Ouchi, A., Chikamoto, M. O., Mouchet, A. and Asahi, H. (2010). Deep water formation in the North Pacific during the Last Glacial Termination, Science, 329(5988), 200-204, doi: 10.1126/science.1190612.
32. Renssen, H., Driesschaert, E., Loutre, M.F. and Fichefet, T. (2006). On the importance of initial conditions for simulations of the Mid-Holocene climate. Clim. Past, 2, 91-97.
33. Renssen H., Goosse, H. and Muscheler, R. (2006). Coupled climate model simulation of Holocene cooling events: oceanic feedback amplifies solar forcing. Clim. Past, 2, 79-90.

34. Renssen, H., Seppä, H., Heiri, O., Roche, D. M., Goosse, H. and Fichefet, T. (2009). The spatial and temporal complexity of the Holocene thermal maximum. Nature Geoscience, 2, 411-414, doi:10.1038/ngeo513.
35. Ridley, J., Gregory, J., Huybrechts, P. and Lowe, J. (2010). Thresholds for irreversible decline of the Greenland ice sheet, Climate Dynamics, published online, doi: 10.1007/s00382-009-0646-0.
36. Roberts, D.H., Long, A.J., Schnabel, C., Davies, B.J., Xu, S., Simpson, M.R. and Huybrechts, P. (2009). Ice sheet extent and early deglacial history of the southwestern sector of the Greenland ice sheet, Quaternary Sci. Rev., 28(25-26), 2760-2773.
37. Simpson, M.J.R, Milne, G.A., Huybrechts, P. and Long, A.J. (2009). Calibrating a glaciological model of the Greenland ice sheet from the last glacial maximum to present-day using field observations of relative sea level and ice extent, Quaternary Sci. Rev., 28, 1631-1657.
38. Steffen, K., Thomas, R., Rignot, E., Cogley, G., Dyurgerov, M., Raper, S. and Huybrechts, P. (2009). Cryospheric contributions to sea-level rise and variability, In: J. Church, P. Woodworth, T. Aarup and S. Wilson (eds.): Understanding Sea-level Rise and Variability, Blackwell Publishing, in press.
39. Swingedouw, D., Fichefet, T., Goosse, H. and Loutre, M.F. (2009). Impact of transient freshwater releases in the Southern Ocean on the AMOC and climate. Clim. Dyn., 33, 2-3, doi: 10.1007/s00382-008-0496-1.
40. Wake, L.M., Huybrechts, P., Box, J.E., Hanna, E., Janssens, I. and Milne, G.A. (2008). Surface mass-balance changes of the Greenland ice sheet since 1866, Ann. Glaciol., 50, 178-184.
41. Widman M., Goosse, H., van der Schrier, G., Schnur, R. and Barkmeijer, J. (2009). Using data assimilation to study extratropical Northern Hemisphere climate over the last millennium. Clim. Past (in press).

2. Others

1. Fichefet, T., Driesschaert, E., Goosse, H., Huybrechts, P., Janssens, I., Mouchet, A. and Munhoven, G. (2004). Modelling the climate and sea level during the third millennium (MILMO), In: M. Vanderstraeten (ed.): Final Reports of the Scientific Support Plan for a Sustainable Development Policy, Belgian Science Policy, 121 p.
2. Fichefet, T., Driesschaert, E., Goosse, H., Huybrechts, P., Janssens, I., Mouchet, A. and Munhoven, G. (2007). Modelling the climate and sea level during the third milennium (MILMO), Scientific Support Plan for a Sustainable Development Policy, Belgian Science Policy, 131 p.
3. Hanna, E., Box, J. and Huybrechts, P. (2007). Recent changes in Greenland ice sheet mass balance, State of Arctic Report 2007. http://www.arctic.noaa.gov/reportcard/essay_hanna.html.

6. ACKNOWLEDGEMENTS

We thank Pierre Yves Barriat for developments on the computer code. H. Goosse. is Research Associate with the Fonds National de la Recherche Scientifique (Belgium). Computer time was partly made available by UCL (Fonds spéciaux de recherche) and FNRS (Fonds de la recherche fondamentale collective) FRFC N°2.4502.05 : "Simulation numérique. Application en physique de l'état solide, océanographie et dynamique des fluides". We also thank the CISM-team.

7. REFERENCES

1. Alley, R.B., Mayewski, P.A., Sowers, T., Stuiver, M., Taylor, K.C. and Clark, P.U. (1997). Holocene climatic instability: a prominent, widespread event 8,200 yr ago. Geology, 25 (6), 483-6.
2. Alley, R.B. and Ágústsdóttir, A.M. (2005). The 8k event: cause and consequences of a major Holocene abrupt climate change. Quaternary Sci. Rev., 24 (10-11), 1123–49.
3. Andres, R.J., Boden, T.A. and Marland, G. (2009). Annual Fossil-Fuel CO_2 Emissions: Global Stable Carbon Isotopic Signature. Carbon Dioxide Information Analysis Center, Oak Ridge National Laboratory, U.S. Department of Energy, OakRidge, Tenn., U.S.A. doi: 10.3334/CDIAC/ffe.db1013.2009
4. Archer, D. (2003). Biological fluxes in the ocean and atmospheric CO_2. In : H. Elderfield (ed), Treatise on Geochemistry, Volume 6, The Oceans and Marine Geochemistry.
5. Barnola, J.-M., Anklin, M., Porcheron, J., Raynaud, D., Schwander, J. and Stauffer, B. (1995). CO_2 evolution during the last millennium as recorded from Antarctica and Greenland ice. Tellus, 47B, 264-272.
6. Beckmann, A. and Goosse, H. (2003). A parameterization of ice shelf-ocean interactions for climate models. Ocean Modell., 5(2), 157-170.
7. Berger, A.L. (1978). Long-term variations of daily insolation and Quaternary climatic changes, J. Atmos. Sci., 35, 2363-2367.
8. Bidle, K.D., Manganalli, M. and Azam, F. (2002). Regulation of oceanic silicon and carbon preservation by temperature control on bacteria, Science, 298, 1980-1984.
9. Bindschadler, R.A. (1998). Future of the west Antarctic ice sheet. Science, 282 (5388), 428-429.
10. Boyer, T.P., Antonov, J.I., Garcia, H.E., Johnson, D.R., Locarnini, R.A., Mishonov, A.V., Pitcher, M.T., Baranova, O.K. and Smolyar, I.V. (2006). World Ocean Database 2005. In: S. Levitus (Ed.), NOAA Atlas NESDIS 60, U.S. Government Printing Office, Washington, D.C., 190 p., DVDs.
11. Braconnot, P., Loutre, M.F., Dong, B., Joussaume, S. and Valdes, P. (2002). How the simulated change in monsoon at 6 ka BP is related to the simulation of the modern climate: results from the Paleoclimate Modeling Intercomparison Project. Clim. Dyn., 19, 107-121.
12. Braconnot, P., Otto-Bliesner, B., Harrison, S., Joussaume, S., Peterschmitt, J.-Y., Abe-Ouchi, A., Crucifix, M., Driesschaert, E., Fichefet, T., Hewitt, C.D., Kageyama, M., Kitoh, A., Loutre, M.F., Marti, O., Merkel, U., Ramstein, G., Valdes, P., Weber, S.L., Yu, Y. and Zhao, Y. (2007). Results of PMIP2 coupled simulations of the mid-Holocene and Last Glacial Maximum. Part 1: Experiments and large-scale features, Clim. Past, 3, 261-277.
13. Braithwaite, R.J., Zhang, Y. and Raper, S.C.B. (2002). Temperature sensitivity of the mass balance of mountain glaciers and ice caps as a climatological characteristic. Zeitschrift für Gletscherkunde und Glazialgeologie, 38, 35-61.
14. Briffa, K.R. (2000). Annual climate variability in the Holocene: interpreting the message of ancient trees. Quat. Sci. Rev., 19(1-5), 87-105.
15. Briffa, K.R., Osborn, T., Schweingruber, F., Harris, I., Jones, P., Shiyatov, S. and Vaganov, E. (2001). Low-frequency temperature variations from a northern tree ring density network. J. Geophys. Res., 106(D3), 2929-2941.

16. Briffa, K.R., Osborn, T.J. and Schweingruber, F.H. (2004). Large-scale temperature inferences from tree rings: a review. Global Planet. Change, 40(1-2), 11-26.
17. Broecker, W.S. and Maier-Reimer, E. (1992). The influence of air and sea exchange on the carbon isotope distribution in the sea. Global Biogeochem. Cycles, 6, 315-320, doi:10.1029/92GB01672.
18. Brohan, P, Kennedy, J. J., Harris, I., Tett, S. F. B. and Jones, P. D. (2006). Uncertainty estimates in regional and global observed temperature changes: a new dataset from 1850, J. Geophys. Res., 11(D12), D12106, doi:10.1029/2005JD006548.
19. Brohan, P, Kennedy, J.J., Harris, I., Tett, S.F.B. and Jones, P.D. (2009). Uncertainty estimates in regional and global observed temperature changes: a new dataset from 1850. J. Geophys. Res., 11 (D12), D12106, doi: 10.1029/2005JD006548.
20. Brovkin, V., Bendsten, J., Claussen, M., Ganopolski, A., Kubatzki, C., Petoukhov, V. and Andreev, A. (2002). Carbon cycle, vegetation and climate dynamics in the Holocene: experiment with the CLIMBER-2 model. Global Biogeochem. Cycles, 16.
21. Bryan, K. and Lewis, L.J. (1979). A water mass model of the World Ocean. J. Geophys. Res., 84 (C5), 2503-2517.
22. Campin, J.M. and Goosse, H. (1999). Parameterization of density-driven downsloping flow for a coarse-resolution ocean model in z-coordinate. Tellus, 51A, 412-430.
23. Charlson, R.J., Langner, J., Rodhe, H., Leovy, C.B. and Warren, S.G. (1991). Perturbation of the Northern Hemisphere radiative balance by backscattering from anthropogenic sulfate aerosols. Tellus, 43 AB, 152-163.
24. Chou, C. and Neelin, J.D. (1996). Linearization of a long-wave radiation scheme for intermediate tropical atmospheric model. J. Geophys. Res., 101 (D10), 15129-15145.
25. Clarke, G.K.C., Leverington, D.W., Teller, J.T. and Dyke, A.S. (2004). Paleohydraulics of the last outburst flood from glacial lake Agassiz and the 8200 BP cold event. Quaternary Sci. Rev., 23, 389-407.
26. Comiso, J.C. and Nishio, F. (2008). Trends in the sea ice cover using enhanced and compatible AMSR-E, SSM/I, and SMMR data. J. Geophys. Res., 113, C02S07, doi: 10.1029/2007JC004257.
27. Cook, E.R., Esper, J. and D'Arrigo, R.D. (2004) Extra-tropical Northern Hemisphere land temperature variability over the past 1000 years. Quaternary Sci. Rev., 23(20-22), 2063-2074.
28. Covey, C., AchutaRao, K.M., Lambert, S.J. and Taylor, K.E. (2000). Intercomparison of present and future climates simulated by coupled ocean-atmosphere GCMs. PCMDI Report 66, Program for Climate Diagnosis and Intercomparison, Lawrence Livermore National Laboratory, University of California, Livermore, CA.
29. Cox, P., Betts, R., Jones, C., Spall, S. and Totterdell, I. (2000). Acceleration of global warming due to carbon-cycle feedbacks in a coupled climate model. Nature, 408, 184-187.
30. Crowley, T. (2000). Causes of climate change over the past 1000 years. Science, 289,270-277.

31. Crowley, T.J., Baum, S.K., Kim, K.Y., Hegerl, G.C. and Hyde, W.T. (2003). Modeling ocean heat content changes during the last millennium, Geophys.Res. Lett., 30, 1932.
32. Cubasch, U., Meehl, G.A., Boer, G.J., Stouffer, R.J., Dix, M., Noda, A., Senior, C.A., Raper, S. and Yap, K.S. (2001). Projections of future climate change. In: Houghton, J.T., Ding, Y., Griggs, D.J., Noguer, M., van der Linden, P.J., Dai, X., Maskell, K. and Johnson, C.A. (eds) Climate change 2001. The Scientific Basis. Contribution of Working Group I to the Third Assessment Report of the Intergovernmental Panel on Climate Change. Cambridge University Press, Cambridge, UK, 525-582.
33. D'Arrigo, R., Wilson, R. and Jacoby, G. (2006). On the long-term context for late twentieth century warming. J. Geophys. Res., 111(D3), doi: 10.1029/ 2005JD006352.
34. Deleersnijder, E. and Campin, J.M. (1995). On the computation of the barotropic mode of a free-surface World Ocean model. Annales Geophysicae, 13, 675-688.
35. Dixon, K. and Lanzante, J. (1999). Global mean surface air temperature and North Atlantic overturning in a suite of coupled GCM climate change experiments. Geophys. Res. Lett., 26, 1885-1888.
36. Domingues, C. M., Church, J. A., White, N. J., Gleckler, P. J., Wijffels, S. E., Barker, P. M. and Dunn, J. R. (2008). Improved estimates of upper-ocean warming and multi-decadal sea-level rise, Nature, 453, 1090-1093, doi:10.1038/nature07080.
37. Driesschaert, E. (1995). Climate change over the next millennia using LOVECLIM, a new Earth system model including the polar ice sheets. PhD thesis, Unversité catholique de Louvain, Louvain-la-Neuve, Belgium.
38. Driesschaert, E., Fichefet, T., Goosse, H., Huybrechts, P., Janssens, I., Mouchet, A., Munhoven, G., Brovkin, V. and Weber, S.L. (2007). Modeling the influence of Greenland ice sheet melting on the meridional overturning circulation during the next millennia. Geophys. Res. Lett., L10707, doi: 10.1029/2007GL029516.
39. Ducoudré, N.I., Laval, K. and Perrier, A. (1993). SECHIBA, a new set of parameterizations of the hydrologic exchanges at the land atmosphere interface within the LMD atmospheric general-circulation model, J. Clim., 6(2), 248-273.
40. Dutay, J.-C., Jean-Baptiste, P., Campin, J.-M., Ishida, A., Maier-Reimer, E., Matear, R.J., Mouchet, A., Totterdell, I.J., Yamanaka, Y., Rodgers, K., Madec, G. and Orr, J.C. (2004). Evaluation of OCMIP-2 ocean models' deep circulation with mantle Helium-3. J. Mar. Systems, 48, 15-36, doi: 10.1016/j.jmarsys.2003.05.010.
41. England, M.H. (1995). The age of water and ventilation time-scales in a global ocean model. J. Phys. Oceanogr., 25, 2756-2777.
42. Enting, I. G., Wigley, T. M. L. and Heimann, M. (1994). Future Emissions and Concentrations of Carbon Dioxide: Key Ocean/Atmosphere/Land Analyses, CSIRO Aust. Div. Atmos. Res., 739 Tech. Pap., 31, 1-118.
43. Esper, J., Cook, E.R. and Schweingruber, F.H. (2002). Low-frequency signals in long tree-ring chronologies for reconvariability. Science, 295(5563), 2250-2253.
44. Etheridge, D.M., Steele, L.P., Langenfelds, R.L., Francey, R.J., Barnola, J.-M. and Morgan, V.I. (1998). Historical CO_2 records from the Law Dome DE08,

DE08-2, and DSS ice cores. In Trends: A Compendium of Data on Global Change. Carbon Dioxide Information Analysis Center, Oak Ridge National Laboratory, U.S. Department of Energy, Oak Ridge, Tenn., USA.

45. ETOPO5 (1988). Data Announcement 88-MGG-02, Digital Relief of the Surface of the Earth. NOAA, National Geophysical Data Center, Boulder, Colorado, http://www.ngdc.noaa.gov/mgg/global/etopo5.HTML.
46. Fichefet, T. and Morales Maqueda, M. (1997). Sensitivity of a global sea ice model to the treatment of ice thermodynamics and dynamics. J. Geophys. Res., 102(C6), 12,609-12,646.
47. Fichefet, T., Poncin, C., Goosse, H., Huybrechts, P., Janssens, I. and Le Treut, H. (2003). Implications of changes in freshwater flux from the Greenland ice sheet for the climate of the 21st century. Geophys. Res. Lett., 30, 1911, doi: 10.1029/2003GL017826.
48. Fichefet, T., Driesschaert, E., Goosse, H., Huybrechts, P., Janssens, I., Mouchet, A. and Munhoven, G. (2007). Modelling the climate and sea level during the third milennium (MILMO), Scientific Support Plan for a Sustainable Development Policy, Belgian Science Policy, 131 p.
49. Forster, P., Ramaswamy, V., Artaxo, P., Berntsen, T., Betts, R., Fahey, D.W., Haywood, J., Lean, J., Lowe, D.C., Myhre, G., Nganga, J., Prinn, R., Raga, G., Schulz, M. and Van Dorland, R. (2007). Changes in atmospheric constituents and in radiative forcing. In: Climate Change 2007: The Physical Science Basis. Contribution of Working Group I to the Fourth Assessment Report of the Intergovernmental Panel on Climate Change [Solomon, S., D. Qin, M. Manning, Z. Chen, M. Marquis, K.B. Averyt, M.Tignor and H.L. Miller (eds.)]. Cambridge University Press, Cambridge, United Kingdom and New York, NY, USA, 129-234.
50. Foukal, P., Frölich, C., Spruit, H. and Wigley, T.M.L. (2006). Variations in solar luminosity and their effect on the Earth's climate, Nature, 443, 161-166.
51. Francey, R.J., Allison, C.E., Etheridge, D.M., Trudinger, C.M., Enting, I.G., Leuenberger, M., Langenfelds, R.L., Michel, E. and Steele, L.P. (1999). A 1000-year high precision record of $\delta^{13}C$ in atmospheric CO_2. Tellus, 51B, 170-193.
52. Frank, D.C, Esper, J., Raible, C.C., Büntgen, U., Trouet, V., Stocker, B. and Joos, F. (2010). Ensemble reconstruction constraints on the global carbon cycle sensitivity to climate. Nature, 463, 527-532, doi:10.1038/nature08769.
53. Friedlingstein, P., Bopp, L., Ciais, P., Dufresne, J.-L., Faihead, L., Le Treut, H., Monfray, P. and Orr, J. (2001). Positive feedback between future climate change and the carbon cycle. Geophys. Res. Lett., 28, 1543-1546.
54. Friedlingstein, P., Dufresne, J.-L., Cox, P. M. and Rayner, P. (2003). How positive is the feedback between climate change and the carbon cycle?, Tellus, 55B, 692-700.
55. Friedlingstein, P., Cox, P., Betts, R., Bopp, L., von Bloh, W., Brovkin, V., Cadule, P., Doney, S., Eby, M., Fung, I., Bala, G., John, J., Jones, C., Joos, F., Kato, T., Kawamiya, M., Knorr, W., Lindsay, K., Matthews, H. D., Raddatz, T., Rayner, P., Reick, C., Roeckner, E., Schnitzler, K.-G., Schnur, R., Strassmann, K., Weaver, A. J., Yoshikawa, C. and Zeng, N. (2006). Climate–carbon cycle feedback analysis: results from the C4MIP model intercomparison. J. Clim., 19, 3337-3353.

56. Fujii, M. and Chai, F. (2005). Effects of biogenic silica dissolution on silicon cycling and export production, Geophys. Res. Lett., 32, L05617, doi: 10.1029/2004GL022054.
57. Ganachaud, A. and Wunsch, C. (2000). Improved estimates of global ocean circulation, heat transport and mixing from hydrographic data. Nature, 408, 453-457.
58. Gent, P. (2001). Will the North Atlantic Ocean thermohaline circulation weaken during the 21st century? Geophys. Res. Lett., 28,1023-1026.
59. Gent, P. and McWilliams, J. (1990). Isopycnal mixing in ocean general circulation model. J. Phys. Oceanogr., 20, 150-155.
60. GLOBALVIEW-CO2 (2006). Cooperative Atmospheric Data Integration Project - Carbon Dioxide. CD-ROM, NOAA GMD, Boulder, Colorado, also available on internet via anonymous FTP to ftp.cmdl.noaa.gov, Path: ccg/co2/GLOBALVIEW.
61. Gnanadesikan, A. (1999). A global model of silicon cycling: sensitivity to eddy parameterization and dissolution. Global Biogeochem. Cycles, 13, 199-220.
62. Goosse, H., Deleersnijder, E., Fichefet, T. and England, M.H. (1999). Sensitivity of a global coupled ocean-sea ice model to the parameterization of vertical mixing. J. Geophys. Res. 104(C6), 13681-13695.
63. Goosse, H. and Fichefet, T. (1999). Importance of ice-ocean interactions for the global ocean circulation: a model study. J. Geophys. Res., 104, 23,337-23,355.
64. Goosse, H., Selten, F.M., Haarsma, R.J. and Opsteegh, J.D. (2001). Decadal variability in high northern latitudes as simulated by an intermediate complexity climate model. Ann. Glaciol., 33, 525-532.
65. Goosse, H., Renssen, H. Timmermann, A. and Bradley, R.S. (2005). Internal and forced climate variability during the last millennium: a model-data comparison using ensemble simulations. Quateranry Sci. Rev., 24, 1345-1360.
66. Goosse, H., Driesschaert, E., Fichefet, T. and Loutre, M.F. (2007). Information on the early Holocene climate constrains the summer sea ice projections for the 21st century. Clim. Past, 3, 683-692.
67. Goosse, H., Brovkin, V., Fichefet, T., Haarsma, R., Jongma, J., Huybrechts, P., Mouchet, Selten, F.M., Barriat, P-Y., Campin, J-M., Deleersnijder, E., Driesschaert, E., Goelzer, H., Janssens, I., Loutre, M-F., Morales Maqueda, M. A., Opsteegh, T., Mathieu, P-P., Munhoven, G., Pettersson, E.J., Renssen, H., Roche, D., Schaeffer, M., Severijns,C., Tartinville, B., Timmermann, A. and Weber, N. (2010). Description of the Earth system model of intermediate complexity LOVECLIM version 1.2, Geosci. Model Dev. Discuss., 3, 309-390, http://www.geosci-model-dev-discuss.net/3/309/2010/gmdd-3-309-2010.html
68. Gregory, J.M. and Oerlemans, J. (1998). Simulated future sea-level rise due to glacier melt based on regionally and seasonally resolved temperature changes. Nature, 391, 474-476.
69. Gregory, J.M., Stouffer, R.J., Raper, S.C.B., Stott, P.A. and Rayner, N.A. (2002). An observationally based estimate of the climate sensitivity. J. Clim., 15, 3117-3121.
70. Gregory, J.M., Huybrechts, P. and Raper, S.C.B. (2004). Threatened loss of the Greenland ice sheet. Nature, 428, 616.
71. Gregory, J.M., Dixon, K.W., Stouffer, R.J., Weaver, A.J., Driesschaert, E., Eby, M., Fichefet, T., Hasumi, H., Hu, A., Jungclaus, J.H., Kamenkovich, I.V.,

Levermann, A., Montoya, M., Murakami, S., Nawrath, S., Oka, A., Sokolov, A. P. and Thorpe, R.B. (2005). A model intercomparison of changes in the Atlantic thermohaline circulation in response to increasing atmospheric CO_2 concentration. Geophys. Res. Lett., 32, L12703, doi: 10.1029/2005GL023209.

72. Gregory, J. and Huybrechts, P. (2006). Ice-sheet contributions to future sea-level change. Philosophical Transactions of the Royal Society of London A, 364, 1709-1731, doi: 10.1098/rsta.2006.1796.
73. Haarsma, R.J., Selten, F.M., Opsteegh, J.D., Lenderink, G. and Liu, Q. (1996). ECBilt, a coupled atmosphere ocean sea-ice model for climate predictability studies. KNMI, De Bilt, The Netherlands, 31 pp.
74. Hegerl, G.C., Crowley, T.J., Hyde, W.T. and Frame, D.J. (2006). Climate sensitivity constrained by temperature reconstructions over the past seven centuries. Nature, 440, 1029-1032.
75. Heinze, C. (2004). Simulating oceanic $CaCO_3$ export production in the greenhouse. Geophys. Res. Lett., 31, L16308, doi: 10.1029/2004GL020613.
76. Hinga, K.R., Arthur, M.A., Pilson, M.E.Q. and Whitaker, D. (1994). Carbon isotope fractionation by marine phytoplankton in culture: the effects of CO_2 concentration, pH, temperature, and species. Global Biogeochem. Cycles, 8, 91-102.
77. Hoefs, J. (1997). Stable Isotope Geochemistry. Springer, Berlin. 4th edition. 201pp.
78. Holland, M.M. and Bitz, C.M. (2003). Polar amplification of climate change in the coupled model intercomparison project. Clim. Dyn., 21, 221-232.
79. Houghton, R.A. (2003). Revised estimates of the annual net flux of carbon to the atmosphere from changes in land use and land management 1850-2000. Tellus, 55B(2), 378-390.
80. Houghton, R.A. and Hackler, J.L. (2002). Carbon Flux to the Atmosphere from Land-Use Changes. In Trends: A Compendium of Data on Global Change. Carbon Dioxide Information Analysis Center, Oak Ridge National Laboratory, U.S. Department of Energy, OakRidge, Tenn., U.S.A.
81. Houghton, J.T., Ding, Y., Griggs, D.J., Noguer, M., van der Linden, P.J., Dai, X., Maskell, K. and Johnson, C.A. (2001). Climate Change 2001: The Scientific Basis. Contribution of Working Group I to the Third Assessment Report of the Intergovernmental Panel on Climate Change. Cambridge University Press, 881 p.
82. Huybrechts, P. and de Wolde, J. (1999). The dynamic response of the Greenland and Antarctic ice sheets to multiple-century climatic warming. J. Clim., 12 (8), 2169-2188.
83. Huybrechts, P. (2002). Sea-level changes at the LGM from ice-dynamic reconstructions of the Greenland and Antarctic ice sheets during the glacial cycles. Quaternary Sci. Rev., 21, 203-231.
84. Indermühle, A., Stocker, T.F., Joos, F., Fischer, H., Smith, H.J., Wahlen, M., Deck, B., Mastroianni, D. Tschumi, J., Blunier, T., Meyer, R. and Stauffer, B. (1999). Holocene carbon-cycle dynamics based on CO_2 trapped in ice at Taylor Dome, Antarctica. Nature 398, 121-126.
85. International GEWEX Project Office: GSWP-2 (2002). The Second Global Soil Wetness Project Science and Implementation Plan. IGPO Publication Series No. 37, 65 pp.

86. IPCC (2000). Emissions Scenarios [Nebojsa Nakicenovic and Rob Swart (eds.)]. Cambridge University Press, Cambridge, United Kingdom and New York, NY, USA. 570 pp.
87. IPCC (2007). Climate Change 2007: The Physical Science Basis. Contribution of Working Group I to the Fourth Assessment Report of the Intergovernmental Panel on Climate Change [Solomon, S., D. Qin, M. Manning, Z. Chen, M. Marquis, K.B. Averyt, M. Tignor and H.L. Miller (eds.)]. Cambridge University Press, Cambridge, United Kingdom and New York, NY, USA, 996 p.
88. Janssens, I. and Huybrechts, P. (2000). The treatment of meltwater retention in mass-balance parameterizations of the Greenland ice sheet. Ann. Glaciol., 31, 133-140.
89. Jasper, J.P., Hayes, J.M., Mix, A.C. and Prahl, F.G. (1994). Photosynthetic fractionation of 13C and concentrations of dissolved CO2 in the central equatorial Pacific during the last 255,000 years. Paleoceanogr., 9, 781-798.
90. Jolly, D., Prentice, I.C., Bonnefille, R., Ballouche, A., Bengo, M., Brenac, P., Buchet, G., Burney, D., Cazet, J.-P., Cheddadi, R., Edorh, T., Elenga, H., Elmoutaki, S., Guiot, J., Laarif, F., Lamb, H., Lezine, A.-M., Maley, J., Mbenza, M., Peyron, O., Reille, M., Reynaud-Farrera, I., Riollet, G., Ritchie, J.C., Roche, E., Scott, L., Ssemmanda, I., Straka, H., Umer, M., Van Campo, E., Vilimumbalo, S., Vincent, A. and Waller, M. (1998). Biome reconstruction from pollen and plant macrofossil data for Africa and the Arabian peninsula at 0 and 6ka, J. Biogeogr., 25, 1007-1027.
91. Jones, P.D., Briffa, K.R., Barnett, T.P. and Tett, S.F.B. (1998). High-resolution palaeoclimatic records for the last millennium: interpretation, integration and comparison with General Circulation Model control-run temperatures. The Holocene, 8(4), 455-471.
92. Jones, P.D., Osborn, T.J. and Briffa, K.R. (2001). The evolution of climate over the last millennium. Science, 292(5517), 662-667.
93. Joos, F., Meyer, R., Bruno, M. and Leuenberger, M. (1999). The variability in the carbon sinks as reconstructed for the last 1000 years. Geophys. Res. Lett., 26, 1437-1440.
94. Kalnay, E., Kanamitsu, M., Kistler, R., Collins, W., Deaven, D., Gandin, L., Iredell, M., Saha, S., White, G., Woollen, J., Zhu, Y., Chelliah, M., Ebisuzaki, W., Higgins, W., Janowiak, J., Mo, K.C., Ropelewski, C., Wang , J., Leetmaa, A., Reynolds, R., Jenne, R. and Joseph, D. (1996). The NCEP/NCAR 40-year reanalysis project., Bull. Amer. Meteor. Soc., 77, 437-471.
95. Keeling, R.F., Piper, S.C., Bollenbacher, A.F. and Walker, S.J. (2010). Monthly atmospheric 13C/12C isotopic ratios for 11 SIO stations. In Trends: A Compendium of Data on Global Change. Carbon Dioxide Information Analysis Center, Oak Ridge National Laboratory, U.S. Department of Energy, Oak Ridge, Tenn., U.S.A.
96. Klaas, C. and Archer, D.E. (2002). Association of sinking organic matter with various types of mineral ballast in the deep sea: Implications for the rain ratio. Global Biogeochem. Cycles, 4, 1116.
97. Lean, J.L., Wang, Y.-M. and Sheeley, N.R. (2002). The effect of increasing solar activity on the Sun's total and open magnetic flux during multiple cycles: implications for solar forcing of climate, Geophys. Res. Lett., 29 (24), 2224.
98. Levitus, S., Antonov, J.I., Boyer, T.P. Locarnini, R.A., Garcia, H.E. and Mishonov, A.V. (2009). Global ocean heat content 1955-2008 in light of recently revealed instrumentation problems. Geophys. Res. Lett., 36, L07608.

99. Loutre, M.F., Mouchet, A., Fichefet, T., Goosse, H., Goelzer, H. and Huybrechts, P. (2010). Evaluating climate model performance with various parameter sets using observations over the last centuries. Clim. Past Discuss., 6, 711-765.
100. Lunt, D., de Noblet-Ducoudré, N. and Charbit, S. (2004). Effects of a melted Greenland ice sheet on climate, vegetation, and the cryosphere. Clim. Dyn., 23, 679-694.
101. Maier-Reimer, E., Mikolajewicz, U. and Winguth, A. (1996). Future ocean uptake of CO_2: interaction between ocean circulation and biology. Clim. Dyn., 12, 711-721.
102. Mann, M.E., Bradley, R.S. and Hughes, M.K. (1999). Northern Hemisphere temperatures during the past millennium: Inferences, uncertainties, and limitations. Geophys. Res. Lett., 26(6), 759–762.
103. Mann, M.E. and Jones, P.D. (2003). Global surface temperatures over the past two millennia. Geophys. Res. Lett., 30(15), 1820, doi: 10.1029/ 2003GL017814.
104. Marland, G., Boden, T. and Andres, R. (2003). Global, regional, and national annual CO_2 emissions from fossil-fuel burning, cement production, and gas flaring: 1751-2000. In: Trends: A Compendium of Data on Global Change, published by Carbon Dioxide Information Analysis Center, Oak Ridge, Tennessee.
105. Martin, J.H., Knauer, G.A., Karl, D.M. and Broenkow, W.W. (1987). VERTEX: carbon cycling in the northeast Pacific. Deep Sea Res., 34, 267-285.
106. Mikolajewicz, U., Crowley, T.J., Schiller, A. and Voss, R. (1997). Modelling teleconnections between the North Atlantic and North Pacific during the Younger Dryas, Nature 387, 384-387.
107. Milly, P.C.D. and Shmakin, A.B. (2002). Global modeling of land water and energy balances. Part II: Land-characteristic contributions to spatial variability. J. Hydrometeor., 3(3), 301-310.
108. Moberg, A., Sonechkin, D.M., Holmgren, K., Datsenko, N.M. and Karlén, W. (2005). Highly variable Northern Hemisphere temperatures reconstructed from low- and high-resolution proxy data. Nature, 433(7026), 613-617.
109. Mook, W.G., Bommerson, J.C. and Staverman, W.H. (1974). Carbon isotope fractionation between dissolved bicarbonate and gaseous carbon dioxide. Earth Planet. Sc. Lett., 22, 169-176.
110. Mouchet, A. and François, L.M. (1996). Sensitivity of a global oceanic carbon cycle model to the circulation and to the fate of organic matter: preliminary results. Phys. Chem. Earth, 21, 511-516.
111. Munhoven G. (2007). Glacial-interglacial rain ratio changes: implications for atmospheric CO_2 and ocean-sediment interaction. Deep Sea Res., 54, 722-746.
112. Murphy, J.M. (1995). Transient response of the Hadley Centre coupled ocean-atmosphere model to increasing carbon dioxide. Part III: analysis of global-mean response using simple models. J. Clim., 8, 496-514.
113. Murphy, J.M., Sexton, D.M.H., Barnett, D.N., Jones, G.S., Webb, M.J., Collins, M. and Stainforth, D.A. (2004). Quantification of modelling uncertainties in a large ensemble of climate change simulations. Nature, 430, 768-772.
114. Muscheler, R., Joos, F., Beer, J., Muller, S.A., Vonmoos, M. and Snowball, I. (2007). Solar activity during the last 1000 yr inferred from radionuclide records. Quaternary Sci. Rev., 26 (1-2), 82-97.

115. Najjar, R.G., Jin, X., Louanchi, F., Aumont, O., Caldeira, K., Doney, S.C., Dutay, J.-C., Follows, M., Gruber, N., Joos, F., Lindsay, K., Maier-Reimer, E., Matear, R.J., Matsumoto, K., Mouchet, A., Orr, J.C., Plattner, G.-K., Sarmiento, J.L., Schlitzer, R., Weirig, M.F., Yamanaka, Y. and Yool, A. (2007). Impact of circulation on export production, dissolved organic matter and dissolved oxygen in the ocean: results from OCMIP-2. Global Biogeochem. Cycles, 21 (3), GB3007.
116. Neftel, A., Friedli, H., Moor, E., Lotscher, H., Oeschger, H., Siegenthaler, U. and Stauffer, B. (1994). Historic CO_2 record from the Siple Station ice core. In: T.A.Boden, D.P. Kaiser, R.J. Sepanski, and F.W. Stoss (eds), Trends '93: A Compendium of Data on Global Change. ORNL/CDIAC-65. Carbon Dioxide Information Analysis Center, Oak Ridge National Laboratory, OakRidge, Tenn., USA, pp11-14.
117. Nelson, D.M., Tréguer, P., Brzezinski, M.A., Leynaert, A. and Quéguiner, B. (1995). Production and dissolution of biogenic silica in the ocean: revised global estimates, comparison with regional data and relationship to biogenic sedimentation. Global Biogeochem. Cycles, 9, 359-372.
118. NOAA ESRL (2009). www.esrl.noaa.gov/gmd/ccgg/trends/; last access: 13 July 2009
119. Oppenheimer, M. (1998). Global warming and the stability of the West Antarctic Ice Sheet. Nature, 393(6683), 325-332.
120. Opsteegh J.D., Haarsma, R.J., Selten, F.M. and Kattenberg, A. (1998). ECBilt: a dynamic alternative to mixed boundary conditions in ocean models. Tellus, 50A, 348-367.
121. Orr, J.C., Fabry, V.J, Aumont, O., Bopp, L., Doney, S.C., Feely, R.M., Gnanadesikan, A., Gruber, N., Ishida, A., Joos, F., Key, R.M., Lindsay, K., Maier-Reimer, E., Matear, R., Monfray, P., Mouchet, A., Najjar, R.G., Plattner, G.-K., Rodgers, K.B., Sabine, C.L., Sarmiento, J.L., Schlitzer, R., Slater, R.D., Totterdell, I., Weirig, M.F., Yamanaka, Y. and Yool, A. (2005). Anthropogenic ocean acidification over the 21st century and its impact on marine calcifying organisms. Nature, 437 (7059), 681-686.
122. Peltier, W.R. (1994). Ice age paleotopography. Science, 265, 195-201.
123. Petit-Maire, N. and Guo, Z. (1996). Mise en évidence de variations climatiques holocènes rapides, en phase dans les déserts actuels de Chine et du Nord de l'Afrique, Sciences de la Terre et des Planètes, 322, 847-851.
124. Pitman, A.J. and Stouffer, R.J. (2006). Abrupt change in climate and climate models. Hydrology and Earth System Sciences, 10, 903-912.
125. Plattner, G.-K., Knutti, R., Joos, F., Stocker, T.F., Brovkin, V., Driesschaert, E. Dutkiewicz, S., Eby, M., Edwards, N.R., Fichefet, T., Jones, C., Loutre, M.F., Matthews, H.D., Mouchet, A., Müller, S.A., Nawrath, S., Sokolov, A., Strassmann, K. and Weaver, A. (2008). Long-term projections of climate change commitment. J. Clim., 21, 2721-2751, doi: 10.1175/2007JCLI1905.1.
126. Pollack, H.N. and Smerdon, J.E. (2004). Borehole climate reconstructions: Spatial structure and hemispheric averages. J. Geophys. Res., 109(D11), D11106, doi: 10.1029/2003JD004163.
127. Pongratz, J., Reick, C., Raddatz, T. and Claussen, M. (2008). A reconstruction of global agricultural areas and land cover for the last millennium. Global Biogeochem. Cycles, 22, GB3018, doi: 10.1029/2007GB003153.
128. Rahmstorf, S., Crucifix, M., Ganopolski, A., Goosse, H., Kamenkovich, I., Knutti, R., Lohmann, G., Marsh, B., Mysak, L., Wang, Z. and Weaver, A.

(2005). Thermohaline circulation hysteresis: a model intercomparison. Geophys. Res. Lett., 32, L23605, doi: 10.1029/2005GL23655.
129. Ramankutty, N. and Foley, J. A. (1999). Estimating historical changes in global land cover : croplands from 1700 to 1992. Global Biogeochem. Cycles, 13(4), 997-1027.
130. Randall, D.A., Wood, R.A., Bony, S., Colman, R., Fichefet, T., Fyfe, J., Kattsov, V., Pitman, A., Shukla, J., Srinivasan, J., Stouffer, R.J., Sumi, A. and Taylor, K.E. (2007). Cilmate models and their evaluation. In: Climate Change 2007: The Physical Science Basis. Contribution of Working Group I to the Fourth Assessment Report of the Intergovernmental Panel on Climate Change [Solomon, S., D. Qin, M. Manning, Z. Chen, M. Marquis, K.B. Averyt, M.Tignor and H.L. Miller (eds.)]. Cambridge University Press, Cambridge, United Kingdom and New York, NY, USA, 589-662.
131. Raper, S.C.B. and Braithwaite, R.J. (2006). Low sea level rise projections from mountain glaciers and icecaps under global warming. Nature, 439, 311-313.
132. Rau, G.H., Riebesell, U. and Wolf-Gladrow, D. (1997). CO_{2aq}-dependent photosynthetic ^{13}C fractionation in the ocean: a model versus measurements. Global Biogeochem. Cycles, 11, 267-278.
133. Rayner, N.A., Parker, D.E., Horton, E.B., Folland, C.K., Alexander, L.V., Rowell, D.P., Kent, E.C. and Kaplan, A. (2003). Global analyses of sea surface temperature, sea ice, and nigh marine air temperature since the late nineteenth century. J. Geophys. Res., 108 (D14): 4407, doi:10.1029/2002JD002670.
134. Raynaud, D., Barnola, J.-M., Chappellaz, J., Blunier, T., Indermühle, A. and Stauffer, B. (2000). The ice record of greenhouse gases: a view in the context of future changes. Quaternary Sci. Rev., 19, 9–17.
135. Reich, P.B., Hobbie, S.E., Lee, T., Ellsworth, Da. S., West, J.B., Tilman, D., Knops, J.M.H., Naeem, S. and Trost, J. (2006). Nitrogen limitation constrains sustainability of ecosystem response to CO_2. Nature, 440, 922-925, doi: 10.1038/nature04486.
136. Reifen, C. and Toumi, R. (2009). Climate projections: past performance no guarantee of future skill? Geophys. Res. Lett., 36, L13704.
137. Renssen, H., Goosse, H. and Fichefet, T. (2002). Modeling the effect of freshwater pulses on the early Holocene climate: the influence of high-frequency climate variability. Paleoceanogr., 17.
138. Renssen, H., Goosse, H., Fichefet, T., Brovkin, V., Driesschaert,E. and Wolk, F. (2005). Simulating the Holocene climate evolution at northern high latitudes using a coupled atmosphere-sea ice-ocean-vegetation mode, Clim. Dyn., 24, 23-43.
139. Ridley, J., Gregory, J., Huybrechts, P. and Lowe, J. (2010). Thresholds for irreversible decline of the Greenland ice sheet. Clim. Dyn., published online, doi: 10.1007/s00382-009-0646-0.
140. Rignot, E.J. and Jacobs, S.J. (2002). Rapid bottom melting widespread near Antarctic ice sheet grounding lines. Science, 296, 2020-2023.
141. Rohling, E.J, Marsh, R., Wells, N.C., Siddall, M. and Edwards, N.R. (2004). Similar meltwater contributions to glacial sea level changes from Antarctic and northern ice sheets. Nature, 430, 1016-1021.
142. Rutherford, S., Mann, M.E., Osborn, T.J., Bradley, R.S., Briffa, K.R., Hughes, M.K. and Jones, P.D. (2005). Proxy-based Northern Hemisphere surface

temperature reconstructions: sensitivity to method, predictor network, target season, and target domain. J. Clim., 18(13), 2308–2329.
143. Sarmiento, J.L., Hughes, T.M., Stouffer, R.J. and Manabe, S. (1998). Simulated response of the ocean carbon cycle to anthropogenic climate warming. Nature, 393, 245-249.
144. Schaeffer, M., Selten, F.M. and van Dorland, R. (1998). Linking Image and ECBilt. National Institute for Public Health and the Environment (RIVM), Bilthoven, The Netherlands, Report no 4815008008.
145. Schmittner, A. (2005). Decline of the marine ecosystem caused by a reduction in the Atlantic overturning circulation. Nature, 434, 628-633.
146. Shine, K.P. and Henderson-Sellers, A. (1985). The sensitivity of a thermodynamic sea ice model to changes in surface albedo parameterization. J. Geophys. Res., 90(D1), 2243-2250.
147. Siegenthaler, U., Monnin, E., Kawamura, K., Spahni, R., Schwander, J., Stauffer, B., Stocker, T.F., Barnola, J.-M. and Fischer, H. (2005). Supporting evidence from the EPICA Dronning Maud Land ice core for atmospheric CO_2 changes during the past millennium. Tellus, 57B, 51-57(7), doi: 10.1111/j.1600-0889.2005.00131.x.
148. Siegenthaler, U. and Münnich, K.O. (1981). $^{13}C/^{12}C$ fractionation during CO_2 transfer from air to sea. In: Carbon Cycle Modelling. Ed. Bolin, B. John Wiley & Sons, New-York, 249-257.
149. Smith, H.J., Fischer, H., Wahlen, M., Mastroianni, D. and Deck, B. (1999). Dual modes of the carbon cycle since the Last Glacial Maximum. Nature, 400, 248-250, doi: 10.1038/22291.
150. Stainforth, D.A., Aina, T., Christensen, C., Collins, M., Faull, N., Frame, D.J., Kettleborough, J.A., Knight, S., Martin, A., Murphy, J.M., Piani, C., Sexton, D., Smith, L.A., Spicer, R.A., Thorpe, A.J. and Allen, M.R. (2005). Uncertainty in predictions of the climate response to rising levels of greenhouse gases. Nature, 433, 403-406.
151. Swingedouw D., Fichefet T., Huybrechts P., Driesschaert M., Goosse H. and Loutre, M.F. (2008). Antarctic ice-sheet melting provides negative feedbacks on future global warming. Geophys. Res. Lett., 35, L17705.
152. Swingedouw, D., Fichefet, T. Goosse, H. and Loutre, M.F. (2009). Impact of transient freshwater releases in the Southern Ocean on the AMOC and climate. Clim. Dyn., 33, 2-3, doi: 10.1007/s00382-008-0496-1.
153. Tarasov, L. and Peltier, W.R. (2005). Arctic freshwater forcing of the Younger Dryas cold reversal. Nature, 435, 662-665.
154. Tartinville, B., Campin, J., Fichefet, T. and Goosse, H. (2001). Realistic representation of the surface freshwater fux in an ice-ocean general circulation model. Ocean Modell., 3, 95-108.
155. Taylor, K.E. (2001). Summarizing multiple aspects of model performance in a single diagram. J. Geophys. Res., 106, 7183-7192.
156. Thompson, S.T., Govindasamy, B., Mirin, A., Caldeira, K., Delire, C., Milovich, J., Wickett, M. and Erickson, D. (2004). Quantifying the effects of CO_2-fertilized vegetation on future global climate and carbon dynamics. Geophys. Res. Lett., 31, L23211, doi: 10.1029/2004GL021239.
157. Toniazzo, T., Gregory, J.M. and Huybrechts, P. (2004). Climatic impact of a Greenland deglaciation and its possible irreversibility. J. Clim., 17, 21-33.

158. Tsunogai, S. and Noriki, S. (1991). Particulate fluxes of carbonate and organic carbon in the ocean. Is the marine biological activity working as a sink of the atmospheric carbon? Tellus, 43, 256-266.
159. van de Wal, R.S.W. and Wild, M. (2001). Modelling the response of glaciers to climate change by applying volume-area scaling in combination with a high resolution GCM. Clim. Dyn., 18, 359-366.
160. van Geen, A., Fairbanks, R.G., Dartnell, P., McGann, M., Gardner, J.V. and Kashgarian, M. (1996). Ventilation changes in the northeast Pacific during the last deglaciation. Paleoceanogr., 11 (5), 519-528.
161. Van Vuuren, D.P., Meinshausen, M., Plattner, G.-K., Joos, F., Strassmann, K. M., Smith, S.J., Wigley, T.M.L., Raper, S.C.B., Riahi, K., de la Chesnaye, F., den Elzen, M.G.J., Fujino, J., Jiang, K., Nakicenovic, N., Paltsev, S. and Reilly, J.M. (2008). Temperature increase of 21st century mitigation scenarios. PNAS, 105 (40), 15258-15262.
162. Vaughan, D.G. and Spouge, J. (2002). Risk estimation of collapse of the West Antarctic ice sheet. Climatic Change, 52, 65-91.
163. Vaughan, D.G. and Arthern, R. (2007). Why is it hard to predict the future of ice sheets? Science, 315 (5818), 1503-1504.
164. Warner, R.C. and Budd, W.F. (1998). Modelling the long-term response of the Antarctic ice sheet to global warming. Ann. Glaciol., 27, 161-168.
165. Weaver, A.J., Saenko, O.A., Clark, P.U. and Mitrovica, J.X. (2003). Meltwater pulse 1A from Antarctica as a trigger of the Bolling-Allerod warm interval. Science, 299, 1709-1713.
166. Weber, S.L., Drijfhout, S.S., Abe-Ouchi, A., Crucifix, M., Eby, M., Ganopolski, A., Murakami, S., Otto-Bliesner, B. and Peltier, W.R. (2007). The modern and glacial overturning circulation in the Atlantic ocean in PMIP coupled model simulations. Clim. Past, 3, 51-64.
167. Wiersma, A.P. and Renssen, H. (2006). Model-data comparison for the 8.2 ka BP event: confirmation of a forcing mechanism by catastrophic drainage of Laurentide Lakes. Quaternary Sci. Rev., 25(1-2), 63-88.
168. Wiersma, A.P., Renssen, H., Goosse, H. and Fichefet, T. (2006). Evaluation of different freshwater forcing scenarios for the 8.2 ka BP event in a coupled climate model. Clim. Dyn., 27, 831-849, doi : 10.1007/s00382-006-0166-0.
169. Xie, P.P. and Arkin, P.A. (1996). Analyses of global monthly precipitation using gauge observations, satellite estimates and numerical model predictions, J. Clim., 9, 840-858.
170. Xie, P. P. and Arkin P. A. (1997). Global precipitation: A 17-year monthly analysis based on gauge observations, satellite estimates, and numerical model outputs, Bull. Am. Meteorol. Soc., 78(1), 2539-2558.
171. Zhao, Y., Braconnot, P., Marti, O., Harrison, S.P., Hewitt, C.D., Kitoh, A., Liu, Z., Mikolajewicz, U., Otto-Bliesner, B. and Weber, S.L. (2005). A multi-model analysis of ocean feedbacks on the African and Indian monsoon during the mid-Holocene. Clim. Dyn., 25, 777-800.
172. Zheng, Y., van Geen, A., Anderson, R.F., Gardner, J.V. and Dean, W.E. (2000). Intensification of the Northeast Pacific Oxygen Minimum Zone During the Bölling-Alleröd Warm Period. Paleoceanogr., 15(5), 528-536.
173. Zondervan, I., Zeebe, R., Rost, B. and Riebesell, U. (2001). Decreasing marine biogenic calcification: a negative feedback on rising atmospheric pCO_2. Global Biogeochem. Cycles, 15, 507-516.

174. Zweck, C. and Huybrechts, P. (2005). Northern Hemisphere ice sheet modeling of the last glacial cycle and glaciological sensitivity. J. Geophys. Res., 110, D07103, doi: 10.1029/2004JD005489.